

1990

# Investigations of the effect of ultra-rapid heating on the softening of a cold rolled low-carbon steel

Shi Hua

*University of Wollongong*

---

## Recommended Citation

Hua, Shi, Investigations of the effect of ultra-rapid heating on the softening of a cold rolled low-carbon steel, Doctor of Philosophy thesis, Department of Materials Engineering, University of Wollongong, 1990. <http://ro.uow.edu.au/theses/1505>

## **NOTE**

This online version of the thesis may have different page formatting and pagination from the paper copy held in the University of Wollongong Library.

## **UNIVERSITY OF WOLLONGONG**

### **COPYRIGHT WARNING**

You may print or download ONE copy of this document for the purpose of your own research or study. The University does not authorise you to copy, communicate or otherwise make available electronically to any other person any copyright material contained on this site. You are reminded of the following:

Copyright owners are entitled to take legal action against persons who infringe their copyright. A reproduction of material that is protected by copyright may be a copyright infringement. A court may impose penalties and award damages in relation to offences and infringements relating to copyright material. Higher penalties may apply, and higher damages may be awarded, for offences and infringements involving the conversion of material into digital or electronic form.

**INVESTIGATIONS OF THE EFFECT OF  
ULTRA-RAPID HEATING ON THE SOFTENING  
OF A COLD ROLLED LOW-CARBON STEEL**

A thesis submitted in fulfilment of the requirements for  
the award of the degree of

**DOCTOR OF PHILOSOPHY**

from

**THE UNIVERSITY OF WOLLONGONG**

by

**HUA SHI, B. Sc., M. Sc.**

**DEPARTMENT OF MATERIALS ENGINEERING**

**1990**

## **CANDIDATE'S CERTIFICATE**

This is to certify that the work presented in this thesis was original and carried out by the candidate in the Department of Materials Engineering at the University of Wollongong and has not been submitted to any other university for a higher degree.

.....



# TABLE OF CONTENTS

ACKNOWLEDGEMENTS.....	i
SYNOPSIS.....	iii
LIST OF FIGURE CAPTIONS.....	vi
CHAPTER 1. INTRODUCTION.....	1
CHAPTER 2. LITERATURE SURVEY.....	4
<u>2.1 INTRODUCTION</u> .....	5
<u>2.2 ANNEALING OF COLD WORKED METALS</u> .....	6
2.2.1 Softening Phenomena.....	6
2.2.2 Annealing Processes .....	7
2.2.2.1 Release of stored energy of deformation.....	7
2.2.2.2 Recovery.....	11
2.2.2.3 Recrystallization.....	11
2.2.2.4 Interaction of recovery and recrystallization .....	12
2.2.2.5 Recrystallization and the softening point.....	16
2.2.3 Property Changes during Annealing .....	18
2.2.3.1 Electrical resistivity and density changes.....	18
2.2.3.2 Mechanical property changes.....	21
2.2.4 Factors which Influence Softening .....	22
2.2.4.1 Cold deformation .....	22

2.2.4.2	Texture and plastic anisotropy.....	23
2.2.4.3	Chemical composition.....	25
2.2.5	Microstructural Changes during Annealing.....	26
2.2.5.1	Changes in microstructure during recovery.....	26
2.2.5.2	Microstructure at the beginning of recrystallization.....	30
2.2.5.3	Changes in microstructure during recrystallization .....	37
2.2.6	Mechanisms of Nucleation during Recrystallization.....	40
2.2.6.1	Classical theory .....	40
2.2.6.2	The "block" theories.....	40
2.2.6.3	Nucleation by migration of low-angle boundaries .....	41
2.2.6.4	Polygonization .....	42
2.2.6.5	Subgrain coalescence by rotation .....	43
2.2.6.6	Nucleation by grain-boundary bulging.....	46
2.2.7	Kinetics of Softening.....	49
2.2.7.1	Recovery kinetics .....	49
2.2.7.2	Recrystallization kinetics.....	51
2.2.8	The Effect of Chemical Compositions on Softening .....	53
<b>2.3</b>	<b><u>SOFTENING PROCESSES IN IRON AND LOW-CARBON STEELS.....</u></b>	<b>56</b>
2.3.1	Studies of Nucleation in Ferrous Alloys.....	56
2.3.2	Studies of Growth of Recrystallized Grains.....	57
<b>2.4</b>	<b><u>AGEING SUSCEPTIBILITY OF LOW-CARBON STEELS .....</u></b>	<b>60</b>

## 2.5 RAPID AND ULTRA-RAPID ANNEALING OF IRON AND

<u>LOW-CARBON STEELS</u> .....	62
2.5.1 Methods of Heating .....	62
2.5.2 Development of the Continuous Annealing Process .....	63
2.5.3 Laboratory Investigation of the Rapid and Ultra-rapid Annealing Process.....	66
2.5.4 Influence of Heating Rate on Softening.....	67
2.5.5 Structure and Mechanical Properties Resulting from Rapid Annealing.....	75

## 2.6 TEMPERATURE MEASUREMENT..... 82

2.6.1 Thermocouples.....	82
2.6.2 Three-wire Thermocouples.....	84
2.6.3 Detection of Rapid Temperature Changes in Small Size Specimens .....	87

## 2.7 HEAT TRANSFER..... 93

2.7.1 Introduction .....	93
2.7.2 Heat Transfer by Conduction .....	94
2.7.3 Heat Transfer by Radiation.....	101
2.7.4 Heat Transfer by Convection.....	102
2.7.5 Variation of Physical Properties with Temperature .....	105
2.7.6 Application of Heat Transfer Calculations to Resistance Heating ....	110

<b>CHAPTER 3. SCOPE OF THE PRESENT WORK.....</b>	<b>114</b>
<b>CHAPTER 4. EXPERIMENTAL INVESTIGATION METHODS.....</b>	<b>118</b>
<u>4.1 MATERIAL.....</u>	<u>121</u>
<u>4.2 HEAT TREATMENT PROGRAMME.....</u>	<u>124</u>
4.2.1 Ultra-rapid Annealing .....	124
4.2.2 Batch Annealing .....	126
4.2.3 Ultra-rapid Annealing with Prior Recovery .....	126
<u>4.3 EXPERIMENTAL PROCEDURES AND TECHNIQUES .....</u>	<u>127</u>
4.3.1 Resistance Heating .....	127
4.3.1.1 Apparatus.....	127
(1) General description .....	127
(2) Electrical system .....	127
(3) Controlling system.....	131
(4) Quenching system .....	134
4.3.1.2 Temperature Measurement.....	131
(1) General principles.....	131
(2) Practical problems .....	134
4.3.2 Computer Modelling of Temperature Profile in a Resistance Heated Specimen .....	136
4.3.2.1 Advantages of computer modelling.....	136
4.3.2.2 Development of model .....	136
4.3.2.3 Test piece design.....	138

4.3.3	Mechanical Testing .....	139
4.3.3.1	Hardness.....	139
4.3.3.2	Tensile tests.....	140
(1)	General description .....	140
(2)	Extensometer .....	140
(3)	Data processing .....	141
4.3.4	Microstructural Examination .....	143
4.3.4.1	Optical microscopy .....	143
4.3.4.2	Measurement of grain size distributions.....	143
4.3.4.4	Transmission electron microscopy.....	144
<b>CHAPTER 5.</b>	<b>COMPUTER MODELLING.....</b>	<b>145</b>
<u>5.1</u>	<u>INTRODUCTION.....</u>	<u>146</u>
<u>5.2</u>	<u>NOMENCLATURE.....</u>	<u>147</u>
<u>5.3</u>	<u>TEMPERATURE EQUATION .....</u>	<u>149</u>
<u>5.4</u>	<u>BOUNDARY CONDITIONS.....</u>	<u>153</u>
5.4.1	At Center and Edges.....	153
5.4.2	Curved Parts of a Specimen.....	153
<u>5.5</u>	<u>VARIATION OF THE PHYSICAL PROPERTIES WITH</u>	
<u>TEMPERATURE</u>	<u>.....</u>	<u>155</u>
<u>5.6</u>	<u>COMPARISON WITH THE EQUATIONS OF THE EXPLICIT</u>	
<u>METHOD</u>	<u>.....</u>	<u>157</u>

5.6.1	Stability .....	157
5.6.2	Convergence .....	160
5.6	<u>RESULTS AND DISCUSSION</u> .....	162
<b>CHAPTER 6.</b>	<b>RESULTS</b> .....	165
6.1	<u>INTRODUCTION</u> .....	166
6.2	<u>CALIBRATIONS OF THE RESISTANCE HEATING APPARATUS</u> .....	167
6.2.1	The Heating Rate and the Maximum Temperature during the First Heating .....	167
6.2.2	Effect of Second Voltage $V_2$ on Thermal Profile .....	172
6.2.3	The Soak Time .....	177
6.2.4	The Heating Rate .....	177
6.2.5	The Maximum Temperature .....	181
6.2.6	The Cross-sectional Area of the Specimen .....	181
6.3	<u>EXAMINATION OF SOFTENING BEHAVIOUR</u> .....	184
6.3.1	Ultra-rapid Annealing .....	184
6.3.1.1	Annealed 70% cold reduced samples .....	184
6.3.1.2	Influence of cold reduction .....	184
6.3.2	Batch Annealing .....	187
6.3.2.1	Annealed 70% cold reduced samples .....	187
6.3.2.2	Influence of cold reduction .....	187
6.3.3	Ultra-rapid Annealed Samples with Prior Recovery .....	190
6.3.3.1	Annealed 70% cold reduced samples .....	190

6.3.3.2	Influence of cold reduction .....	192
<u>6.4</u>	<u>HARDNESS DISTRIBUTIONS</u> .....	194
6.4.1	Ultra-rapid Annealed Samples .....	194
6.4.1.1	Annealed 70% cold reduced samples.....	194
6.4.1.2	Influence of cold reduction .....	194
6.4.2	Batch Annealed Samples.....	197
6.4.2.1	Annealed 70% cold reduced samples.....	197
6.4.2.2	Influence of cold reduction .....	197
6.4.3	Ultra-rapid Annealing with Prior Recovery .....	197
<u>6.5</u>	<u>TENSILE PROPERTIES</u> .....	201
6.5.1	Ultra-rapid Annealed Samples .....	201
6.5.1.1	Annealed 70% cold reduced samples.....	201
6.5.1.2	Influence of cold reduction on ductility .....	201
6.5.2	Batch Annealed Samples.....	204
6.5.2.1	Annealed 70% cold reduced samples.....	204
6.5.2.2	Influence of cold reduction .....	204
<u>6.6</u>	<u>MICROSTRUCTURAL EXAMINATION</u> .....	207
6.6.1	Optical Microscopy.....	207
6.6.1.1	Ultra-rapid annealing .....	207
(a)	$t_1 = 0.2$ seconds.....	207
(b)	$t_1 = 0.5$ seconds.....	212
(c)	Influence of cold reduction on structures .....	212

6.6.1.2	Batch annealing .....	219
6.6.2	Measurements of Grain Size Distributions .....	219
6.6.2.1	Grain size distributions of ultra-rapid annealed samples .....	219
(a)	Annealed 70% cold reduced samples.....	219
(b)	Influence of cold reduction .....	222
6.6.2.2	Grain size distributions of batch annealed samples .....	223
6.6.3	Transmission Electron Microscopy.....	224
6.6.3.1	Cold rolled structures.....	224
6.6.3.2	Ultra-rapid annealed structures.....	224
(a)	Annealed 70% cold reduced samples.....	224
(b)	Influence of cold reduction .....	231
6.6.3.3	Batch annealed structures .....	231
<b>CHAPTER 7.</b>	<b>DISCUSSION.....</b>	<b>237</b>
<u>7.1</u>	<u>INTRODUCTION.....</u>	<u>238</u>
<u>7.2</u>	<u>INFLUENCE OF HEATING RATES ON RECRYSTALLIZATION</u>	
	<u>TEMPERATURE RANGES .....</u>	<u>239</u>
<u>7.3</u>	<u>KINETICS.....</u>	<u>247</u>
<u>7.4</u>	<u>NUCLEATION MECHANISMS FOR ULTRA-RAPID ANNEALING.....</u>	<u>253</u>
7.4.1	Electron Microscopical Observations.....	253
<u>7.5</u>	<u>MICRO-HARDNESS AND METALLOGRAPHIC STUDIES OF</u>	
	<u>SOFTENING BY ULTRA-RAPID HEATING.....</u>	<u>257</u>



7.5.1	Variations in Hardness and Microstructure with Annealing	
	Conditions .....	258
7.5.2	Micro-hardness Distributions .....	261
7.5.3	Recrystallization Grain Size and Grain Size Distributions.....	262
<b>7.6</b>	<b><u>INFLUENCE OF COLD REDUCTION</u></b> .....	<b>265</b>
7.6.1	The Softening Behaviour .....	265
7.6.2	Micro-Hardness Distributions.....	269
<b>7.7</b>	<b><u>THE MECHANISM OF SOFTENING DURING ULTRA-RAPID</u></b>	
	<b><u>ANNEALING</u></b> .....	<b>270</b>
7.7.1	Effect of Type of Heating Method.....	273
<b>7.8</b>	<b><u>TENSILE PROPERTIES OF ULTRA-RAPID ANNEALING</u></b> .....	<b>274</b>
7.8.1	Yield Stress and Tensile Strength.....	274
7.8.2	Ductility.....	275
7.8.3	Toughness.....	276
7.8.4	Plastic Strain Ratio - R.....	277
<b>CHAPTER 8.</b>	<b>CONCLUSIONS</b> .....	<b>280</b>
<b>APPENDIX</b>	.....	<b>283</b>
A.	Computer Programme of Implicit Method .....	284
B.	Publications.....	295
<b>REFERENCES</b>	.....	<b>318</b>

## ACKNOWLEDGEMENTS

The research work reported in this thesis was carried out in the laboratories of the Department of Materials Engineering at the University of Wollongong under the supervision of Associate Professor D. P. Dunne and Mr. M. Atkinson.

My gratitude is first due to Mr. M. Atkinson for his patient , encouraging and inspiring guidance, invaluable criticisms and for introducing me into the field of ultra-rapid annealing. My deep gratitude is due to Associate Prof. D. P. Dunne for his consistent support, enlightening advice and helpful assistance during the writing of the thesis. I am grateful to Associate Professor N. F. Kennon for his continued encouragement, personal assistance and skilful guidance during the study leave of Mr. M. Atkinson and Dr. D. P. Dunne.

I am indebted to past and present chairmen of the Department, Assoc. Prof. N. F. Kennon and Prof. W. J. Plumbridge for the provision of laboratory facilities and a University scholarship to enable this research programme to be conducted on a full-time basis.

I would like to express my thanks to F. Groves and G. Hamilton for their significant help in the experimental process and computer programming of tensile tests. My thanks are also due to Dr. R. Smith and R. De Jong for their assistance in TEM and setting up resistance heating apparatus. I am grateful to Ms. A. Webb, Ms. M. Standen, Ms. L. Middleton, G. Tillman, N. Mackie and other staff in the department for their assistance and concerns about my research.

My special thanks are due to Drs. J. S. H. Lake and D. Willis at the Research and Technology Center, Coated Products Division of BHP for providing some of the material and two opportunities to gain work experience in their labatory. My thanks are also due

to the Department of Metals Technology of Wollongong Technical College for access to their rolling mill for cold rolling the steel used in the investigation.

Finally, I would like to express my special gratitude and respect to my husband Kenong for his continuous support, encouragement, patience and love. My grateful acknowledgement is extended to my mother and my sister who have given me many encouragements throughout the course of the investigation.

## SYNOPSIS

Ultra-rapid annealing deals with softening of a metal or alloy by using heating rates greater than about 500°C/second. Electrical resistance heating was used in the present investigation to heat specimens at rates in the range of 1000 to 5000°C/second, and it has been confirmed that very rapid softening ("ultra-rapid annealing") can be obtained in cold reduced low carbon steels in heat treatment times of a fraction of a second.

The resistance heating apparatus was designed originally by A. Pearce and developed over a number of years in the Department of Materials Engineering at the University of Wollongong. It basically consists of a controller, an electrical system and a water quench device. Tensile shaped specimens can be heated to temperatures in the range of 500 to 1100°C in a fraction of a second. A three-wire thermocouple arrangement was applied in the present investigation to measure the specimen temperature accurately and reproducibly. A computer model has been established using an implicit method to predict the temperature profile and to design the optimum shape of the specimen for ultra-rapid annealing. Less than 1% discrepancy was found between thermocouple measurements and computer predictions .

A decarburized low carbon steel was cold rolled with reductions in the range 40 to 80%. The deformed material was ultra-rapid heated to study the effect of heating rates on softening temperature range. It was found that for heating rates between ~1000 to 5000°C/second, the softening process is enhanced or accelerated as the heating rate increases. This result confirms, for resistance heating and for higher heating rates, results reported previously for salt bath and induction heating.

Batch annealing in the softening temperature ranges of ultra-rapid annealing was applied to the same material to draw comparison with ultra-rapid annealing in a study of the recrystallization kinetics and mechanisms. The results suggest that recrystallization

during ultra-rapid annealing is controlled by nucleation, while recrystallization during batch annealing depends on both nucleation and grain growth. Compared with the batch annealed case, partially restored ultra-rapid annealed samples showed less tendency to form a well developed subgrain structure and greater structural heterogeneity. Despite these difference and a remarkable acceleration in the rates of recovery and recrystallization, there was little evidence of any novel mechanisms for restoration during ultra-rapid annealing.

Both recovery and recrystallization were accelerated, with recovery being promoted relative to recrystallization. These findings are inconsistent with a proposal that enhanced softening occurs by very rapid recrystallization due to suppression of recovery.

The enhancement of softening by ultra-rapid heating could be restricted by a prior recovery treatment at 100°C, but the rate of softening was still high relative to that characteristic of batch annealing and the rate increased sharply as the heating rate increased.

The observations are consistent with a suppressed solution model in which dissolution of carbon and/or nitrogen is restricted by very rapid heating, thus allowing restoration to occur freely without the retarding effects of significant concentrations of interstitial solutes.

Tensile tests were conducted on the annealed materials. The ultra-rapid heating rates resulted in an increase in ductility and toughness, compared with the batch annealing treatment. Ultra-rapid annealing also resulted in a decrease in yield stress and tensile strength and increase in ductility, toughness and plastic strain ratio (R) as the temperature and the amount of recrystallization increased.

The major original contributions of the present investigation are (1) establishing a reproducible resistance heating method for ultra-rapid annealing; (2) developing a computer model to accurately predict the specimen temperature profile during ultra-rapid

heating; (3) demonstrating that ultra-rapid annealing by resistance heating results in a substantial acceleration of the rate of softening of a cold rolled low carbon steel; and (4) showing that the phenomenon of enhanced softening is not due to suppressed recovery, but is consistent with suppressed solution of carbon and/or nitrogen atoms.

LIST OF FIGURE CAPTIONS

2-1 Effect of heating rate. [ref. 8]..... 8

2-2 Effect of heating rate (Summary). [ref. 8]..... 8

2-3 Rate of energy release as a function of time during isothermal annealing at 189.7°C for 99.999% pure copper deformed by tension to two strains. [ref. 78]..... 10

2-4 The effect of the amount of deformation on the recovery and recrystallization temperatures for a metal with a high stacking fault energy (curve A) and a metal with a low stacking energy (curve B). [ref. 60]..... 13

2-5 The assessment of 50% primary recrystallization by means of hardness testing after isothermal annealing: (a) hardness vs. annealing temperature; (b) rate of change of hardness with annealing temperature vs. annealing temperature. \*Metal 1 softens slightly prior to primary recrystallization. \*\*Metal 2 softens entirely during primary recrystallization. [ref. 59] ..... 15

2-6 Schematic representation of the annealing temperatures corresponding to 50% primary recrystallization for (a) a metal which softens entirely by primary recrystallization, and (b) a metal which softens prior to, as well as during , primary recrystallization. [ref. 205]..... 17

2-7 Power difference ( $\Delta P$ ), increment in electrical resistivity ( $\Delta \rho$ ), and change in density ( $\Delta D$ ), as a function of temperature, for 99.85% purity nickel after 70% compression at room temperature; heating rate 6°C/min. [ref. 70] ..... 19

2-8 Power difference ( $\Delta P$ ) and increment in electrical resistivity ( $\Delta \rho$ ) as a function of temperature for 99.98% purity copper wire drawn to an effective elongation of 54% at 78°K; heating rate 2°C/min. [ref. 49] ..... 20

2-9	Electron transmission micrographs showing the change in microstructure upon annealing the (001)[110] crystal. (a) after 80 min. at 200°C, (b) after 1280 min. at 200°C. [ref. 132].....	27
2-10	Electron transmission micrographs showing the change in microstructure upon annealing the (001)[110] crystal. (a) after 20 min. at 400°C, (b) after 1280 min. at 400°C. [ref. 132].....	27
2-11	Electron transmission micrographs showing the change in microstructure upon annealing the (001)[110] crystal. (a) after 5 min. at 600°C, (b) after 1280 min. at 600°C. [ref. 132].....	28
2-12	Electron transmission micrographs showing the change in microstructure upon annealing the (001)[110] crystal. (a) after 1 min. at 800°C, (b) after 5 min. at 800°C. [ref. 132] .....	28
2-13	Recovery of diamond pyramid hardness of the (001)[110] crystal, measured with 1 kg load. Experimental points represent the average of 10 measurements for each specimen, and the probable error limits are indicated. Note that complete softening without recrystallization is obtained in the specimen annealed for 1280 minutes at 600°C. Solid circle represents a specimen which was completely recrystallized. [ref. 132].....	29
2-14	Optical micrographs of a specimen of the (001)[100] crystal annealed for 25 minutes at 600°C, showing recrystallized grains formed along the boundary between matrix deformation bands. The variation in size of these recrystallized grains indicates that their growth rates are different, which, in turn, suggests that their orientations are different. Nital etch, 500x. [ref. 132].....	31
2-15	Electron transmission micrographs showing the growth of subgrains within a microband region. Many subgrain boundaries appear to be gradually eliminated by the removal of dislocations from these boundaries, suggesting that subgrain "growth" occurs largely by coalescence. A few of these boundaries that have not yet been completely eliminated are indicated by arrows. (001)[100] crystal annealed 125 minutes at 600°C. [ref. 132] .....	32



2-16 Electron transmission micrographs showing the growth of subgrains within a microband region. Features similar to those described in Fig. 2-17 are shown. (001)[100] crystal annealed 125 minutes at 600°C. [ref. 132] ..... 32

2-17 Electron transmission micrographs showing the growth of subgrains within a microband region. Features similar to those described in Fig. 2-17 are shown. (001)[100] crystal annealed 125 minutes at 600°C. [ref. 132] ..... 33

2-18 Electron transmission micrographs showing the growth of subgrains within a microband region. Spherical and elongated shapes develop side by side. The coalescence nature of subgrain "growth" is suggested by those boundaries. [ref. 132]..... 33

2-19 Electron transmission micrographs showing the growth of subgrains within a microband region. A general growth of the subgrains is shown in this area. The coalescence nature of subgrain growth is suggested by those boundaries indicated by arrows. (001)[100] crystal annealed 125 minutes at 600°C. [ref. 132] ..... 34

2-20 Carbon-shadowed replica electron micrographs taken from the transverse cross section of the (001)[100] crystal, after the specimen was annealed at 600°C for 5 minutes showing that (a) the microband segments consist of thin sheets on edge extending through the thickness of the specimen, and (b) that growth of the microband segments has taken place in another area. Note that the growth occurs within the microband, and proceeds largely by eliminating the boundaries between the microband segments, as indicated by the arrows. [ref. 132] ..... 35

2-21 Electron transmission micrographs showing the formation of a crystallized grain through the growth of subgrains within a microband region. The orientation of this recrystallized grain is shown by the selected-area diffraction pattern. (001)[100] crystal annealed 125 minutes at 600°C. [ref. 132]..... 36

2-22	Electron transmission micrographs showing two recrystallized grains that have successfully grown into the matrix region. No subgrains formation is as yet evident in the matrix band region. The selected-area diffraction pattern shows the orientation of one of those two crystallized grains G superimposed upon the orientation of the matrix M. Circle on the micrograph indicates the size and location of the electron beam used for obtaining the diffraction pattern. The orientation relationship between G and M corresponds to a rotation of $36^\circ$ around [001] normal to specimen plane. (001)[100] crystal annealed 125 minutes at $600^\circ\text{C}$ . [ref. 132] .....	38
2-23	The structure of Armco iron cold rolled 96% and annealed for 2 hours at $450^\circ\text{C}$ . 20,400x. [ref. 127] .....	39
2-24	Dislocation structure of Armco iron after cold rolled 96%. 20,400x.[ref. 127] .....	39
2-25	The structure of Armco iron cold rolled 96% and annealed for 2 hours at $550^\circ\text{C}$ . 20,400x. [ref. 127] .....	39
2-26	Micrograph showing etch pits in polygonized aluminium. 75x. [ref. 182] .....	44
2-27	Schematic representation of the polygonization process: (a) random arrangement of edge dislocations, and (b) alignment of edge dislocations to form walls. [ref. 184] .....	44
2-28	Schematic representation of edge dislocations at a tilt boundary triple point. [ref. 184] .....	45
2-29	Schematic representation of subgrain coalescence by subgrain rotation. [ref. 27] .....	47
2-30	Schematic representation of the formation of a primary recrystallization nucleus by subgrain coalescence. [ref. 156] .....	47
2-31	Schematic representation of primary recrystallization by strain-induced grain-boundary migration. [ref. 188].....	48

2-32	Recovery kinetics for the flow stress of iron at various annealing temperature: (1-R) represents the fraction of the flow stress increment which remains after annealing. [ref. 194].....	50
2-33	Recovery kinetics for the electrical resistivity of copper at various annealing temperature. [ref. 198].....	50
2-34	The characteristic form of the progress of primary recrystallization during isothermal annealing. [ref. 207].....	52
2-35	Effect of alloy addition on softening of iron at 595°C. [ref. 215 & 216] .....	55
2-36	Initiation of recrystallization at a grain boundary, showing migration of a high angle boundary into a grain with fine cell structure. From left to right: 2,600x, 5,200x, 10,400x. [ref. 194] .....	58
2-37	Nonuniform distribution of dislocations in three grains at a junction. Fe-3.25%Si, quenched from 775°C. Electron transmission, 20,000x. [ref. 192] .....	58
2-38	Typical heat cycle of continuous annealing. [ref. 2] .....	65
2-39	Effect of maximum temperature on hardness. [ref. 9].....	68
2-40	Effect of heating rate on recrystallization temperature range. [ref. 6] .....	69
2-41	Elevation of critical temperatures with heating rate for a 0.086%C steel with a coarse carbide distribution. [ref. 293].....	71
2-42	Effect of heating rate on the eutectoid temperature of a 0.79%C steel. [ref. 293].....	71
2-43	Elevation of the $A_{c1}$ and $A_{c3}$ with heating rate for a 0.086%C steel with fine spheroidal carbide structure. [ref. 293] .....	72
2-44	Effect of heating rate on the allotropic transformation temperature of BISRA pure iron. [ref. 293].....	72

2-45	Schematic representation of the process rate of both recrystallization and recovery with temperature. Note the cross point is $T_x$ . [ref. 6].....	74
2-46	Effect of grain size and cold reduction on the ultimate tensile strength of gauge mild steel. [ref. 288].....	76
2-47	Effect of grain size and cold reduction on hardness of gauge mild steel. [ref. 288].....	77
2-48	Effect of grain size and cold reduction on lower yield points of gauge mild steel. [ref. 288].....	77
2-49	Effect of cold reductions on mechanical properties of gauge mild steel (Summary). [ref. 288].....	78
2-50	The results of a microhardness survey carried out on a material heated at 915°C/sec. (to 625°C) and brine quenched. [ref. 6].....	80
2-51	Comparison of the overaged hardness of rolled material with pre-recovered material, showing that recrystallization processes are significant retarded when low temperature recovery is allowed to proceed unsuppressed. [ref. 6].....	81
2-52	The mechanical properties of 0.088% rimmed steel resistance heated at 208°C.sec. to 1000°C, quenched in brine. [ref. 306].....	81
2-53	Temperature versus emf curves. Reference junction, 32°F. [ref. 329] .....	85
2-54	(a) Conventional Wheatstone electric bridge. [ref. 331] (b) The equivalent Wheatstone bridge circuit with three-wire ( $l_1$ , $l_2$ and $l_3$ ) thermocouple. ....	86
2-55	Intrinsic thermocouple attached normal to semi-infinite body. [ref. 332] .....	89
2-56	Sketch showing direction of heat flow. [ref. 335] .....	96
2-57	Elemental volume for one-dimensional heat-conduction analysis. [ref. 351] .....	96

2-58	Temperature distribution in the semi-infinite solid. [ref. 335].....	99
2-59	Nomenclature for numerical solution of one-dimensional unsteady-state conduction. [ref. 294].....	99
2-60	Heisler's chart for the temperature-time history at the center of an infinitely long cylinder at temperature $t_i$ and placed in a medium at $t_f$ . [ref. 341].....	104
2-61	Variation of emissivity with temperature and condition of ferrous materials. [ref. 336].....	106
2-62	The effect of temperature and composition on the thermal conductivity of steel. [ref. 342] .....	107
2-63	Variation of the resistance ratio with temperature for pure metals. From data of ref. 344. ....	109
2-64	Variation of specific heat of iron with temperature. From data of ref. 345. ....	109
2-65	Effect of parameter $\alpha\Delta t/(\Delta X)^2$ on the stability of finite-difference solution of one-dimensional heat flow problem. [ref. 295].....	112
3-1	Diagram showing the planned approach used to carry out the research. The numbers indicate the stages and the sequence of the work. ....	116
4-1	Standard tensile test piece used in the investigation. ....	123
4-2	Schematic diagram of ultra-rapid annealing apparatus. ....	128
4-3	Photograph showing the ultra-rapid annealing apparatus.....	129
4-4	Diagram showing the electrical system of the ultra-rapid annealing apparatus.....	130
4-5	Diagram showing (a) the control unit of the ultra-rapid annealing apparatus; (b) the functions of the control unit.....	132

4-6	Diagram showing (a) three wire thermocouple as wired to the specimen; (b) the equivalent Wheatstone bridge circuit of a three wire thermocouple.....	133
4-7	Temperature recorder traces showing reproducibility of the thermal cycle. ....	135
4-8	The prototype extensometer in use testing a sample after ultra-rapid annealing (arrowed). ....	142
5-1	Schematic diagram of one-dimensional system. ....	151
5-2	Position of P and its adjacent points.....	151
5-3	The curved part of a specimen. ....	154
5-4	The temperatures predicted by the explicit method under conditions of $t_1 = 0.2$ sec., $t_2 = 0.3$ sec. and $V_1 = 130$ V, showing that the values are not stable as the time interval changes. ....	158
5-5	The temperatures predicted by the implicit method under conditions of $t_1 = 0.2$ sec., $t_2 = 0.3$ sec. and $V_1 = 130$ V, showing that the values are very stable no matter what the time interval is. ....	158
5-6	The temperatures predicted by the explicit method under conditions of $t_1 = 0.2$ sec., $t_2 = 0.3$ sec. and $V_1 = 150$ V, showing that the values do not convergence to a stable one.....	161
5-7	The temperatures predicted by the implicit method under conditions of $t_1 = 0.2$ sec., $t_2 = 0.3$ sec. and $V_1 = 150$ V, showing that the values do convergence to a stable one no matter what the number of elements.....	161
5-8	Comparison of the temperatures (a) experimentally measured and (b) predicted by the computer modelling using an implicit method. ....	163

5-9	The temperature profiles predicted by an computer modelling using the implicit method during ultra-rapid annealing at $t_1 = 0.2$ , $t_2 = 1.8$ sec. and $V_1 = 220$ V. (the time interval for plotting the curve is 0.05 sec.).....	164
5-10	Comparison of the temperatures experimentally measured and predicted by the computer modelling using an implicit method at various input voltages.....	164
6-1	Experimental curves showing the temperature variation with time for several first heating voltages in a sample with 70% cold reduction. ( $t_1 = 0.2$ and $t_2 = 0.1$ sec.).....	168
6-2	The relationship between the maximum temperature at the end of the first heating and the first heating voltage for $t_1 = 0.2, 0.3$ and $0.5$ seconds. ( $t_2 = 0.1$ seconds) .....	169
6-3	Maximum temperature contours for various first heating voltages and heating times ( $t_2 = 0.1$ sec.).....	170
6-4	The relationship between the heating rate and the first heating voltage with $t_1 = 0.2, 0.3$ and $0.5$ sec. ( $t_2 = 0.1$ sec.).....	171
6-5	Some of the experimental heating cycles obtained as a function of second heating voltage $V_2$ for a sample with 70% cold reduction and $V_1 = 150$ V, $t_1 = 0.2$ and $t_2 = 6.0$ sec.....	173
6-6	Temperature variations for different second heating voltages during the second heating under $V_1 = 160$ V and $V_1 = 240$ V, respectively. ( $t_1 = 0.2$ sec.).....	174
6-7	Temperature profiles for different combinations of $V_1$ and $V_2$ which brought about a constant sample temperature. ( $t_1 = 0.2$ and $t_2 = 6.0$ sec.).....	175
6-8	The relationship between the first heating voltage and the second heating voltage $V_{2c}$ for $t_1 = 0.2$ and $0.3$ sec., respectively.....	176
6-9	The relationship between the second heating voltage $V_{2c}$ and the constant temperature $T_c$ . ( $t_2 = 0.1$ sec., $V_1 = \text{variable}$ ).....	178

6-10	The influence of the soak time on hardness. ( $T_c = 685^\circ\text{C}$ and $t_1 = 0.2$ sec.).....	179
6-11	The influence of the heating rate on softening at $T_c = 685^\circ\text{C}$ . ( $t_2 = 0.1$ sec.).....	180
6-12	Effect of the maximum temperature on softening of 70% cold reduced samples.for a heating rate of $\sim 1600^\circ\text{C}/\text{sec}$ . and $t_2 = 0.1$ sec. ....	182
6-13	The effect of the sample width ( at constant length and thickness) on softening. ( $V_1 = 240$ V, $t_1 = 0.2$ sec., $V_2 = 112$ V and $t_2 = 0.1$ sec.) .....	183
6-14	The softening behaviour of a sample with 70% cold reduction after ultra-rapid annealing. ( $t_2 = 0.1$ sec.) .....	185
6-15	The softening behaviour after ultra-rapid annealing in samples with different cold reductions. ( $t_1 = 0.3$ and $t_2 = 0.1$ sec.).....	186
6-16	The softening behaviour in a sample with 70% cold reduction after batch annealing at different temperatures for 30 minutes. ....	188
6-17	Influence of cold reduction on the softening behaviour after batch annealing at various temperatures for 30 minutes.....	189
6-18	Effect of prior recovery on softening behaviour in samples with 70% cold reduction ultra-rapid annealed at heating rates of 3500, 2333 and $1400^\circ\text{C}/\text{second}$ ( $t_1 = 0.3$ sec., $T_c = 700^\circ\text{C}$ ). ....	191
6-19	Hardness versus the total heating time for samples with 40% and 70% cold reductions subjected to prior recovery annealing at $100^\circ\text{C}$ for 1.5, 3, 5 and 10 hours followed by ultra-rapid annealing. ( $t_1 = 0.3$ seconds, $T_c = 700^\circ\text{C}$ ) .....	193
6-20	The distributions of hardness measurements in samples with 70% cold reduction after ultra-rapid annealing at $T_c = 520, 600, 667$ and $820^\circ\text{C}$ , corresponding to 0, 13, 50 and 100% softening. ( $t_1 = 0.3$ and $t_2 = 0.1$ sec.) .....	195



6-21	The distributions of hardness measurements in samples with different cold reductions after ultra-rapid annealing at $T_c = 650^\circ\text{C}$ , $t_1 = 0.3$ and $t_2 = 0.1$ sec. (see Fig. 6-15) .....	196
6-22	The distributions of hardness measurements in samples with 70% cold reduction after batch annealing at 450, 500 and $650^\circ\text{C}$ for 30 minutes, corresponding to 0, 50 and 100% softening. (see Fig. 6-16) .....	198
6-23	The distributions of hardness measurements in samples with different cold reductions after batch annealing at $500^\circ\text{C}$ for 30 minutes. (see Fig. 6-17) .....	199
6-24	The distributions of hardness in a material with 70% cold reduction after prior recovery at $100^\circ\text{C}$ for 10 hours and ultra-rapid annealing at $667^\circ\text{C}$ for $t_1 = 0.3$ sec. and $t_2 = 0.1$ sec.. .....	200
6-25	Tensile testing results of 70% cold reduced samples after ultra-rapid annealing at $T_c = 630, 667, 700$ and $720^\circ\text{C}$ . ( $t_1 = 0.3$ and $t_2 = 0.1$ sec.) .....	202
6-26	Comparison of the tensile testing results of samples with different cold reductions after ultra-rapid annealing at $T_c = 720^\circ\text{C}$ . ( $t_1 = 0.3$ and $t_2 = 0.1$ sec.) .....	203
6-27	Tensile testing result in a 70% cold reduced sample after batch annealing at $680^\circ\text{C}$ for 30 minutes.....	205
6-28	Comparison of the tensile testing results of 40%, 60%, 70% and 80% cold reduced samples after batch annealing at $680^\circ\text{C}$ for 30 minutes. ....	206
6-29	Microstructures of samples with 70% cold reduction after ultra-rapid annealing with $t_1 = 0.2$ , $t_2 = 0.1$ seconds and with $T_c =$ (a) $450^\circ\text{C}$ ; (b) $510^\circ\text{C}$ ; (c) $530^\circ\text{C}$ ; (d) $550^\circ\text{C}$ ; (e) $650^\circ\text{C}$ ; (f) $700^\circ\text{C}$ and (g) $720^\circ\text{C}$ . (h) is a higher magnification of (g). (see Fig.6-14). ....	208
6-30	Microstructure changes with maximum temperatures and the corresponding hardness for a sample with 70% cold reduction after ultra-rapid annealing with $t_1 = 0.2$ and $t_2 = 0.1$ seconds. ....	211

6-31	Microstructures of a sample with 70% cold reduction after ultra-rapid annealing with $t_1 = 0.5$ , $t_2 = 0.1$ seconds and at $T_c =$ (a) 510°C; (b) 600°C; (c) 650°C; (d) 700°C; (e) 720°C; (f) 750°C; (g) 820°C; (h) 857°C and (i) 912°C. (j) is a higher magnification of (i). (see Fig. 6-14). ....	213
6-32	Microstructure changes with maximum temperatures and the corresponding hardness for a sample with 70% cold reduction after ultra-rapid annealing for $t_1 = 0.5$ and $t_2 = 0.1$ seconds. ....	217
6-33	Microstructures of samples with different cold reductions after ultra-rapid annealing for $t_1 = 0.3$ , $t_2 = 0.1$ seconds and at $T_c =$ 600, 630, 667, 700 and 720°C. ....	218
6-34	Microstructures of samples with different cold reductions after batch annealing at 680°C for 30 minutes. ....	220
6-35	Cold rolled structure found in a sample with 40% cold reduction showing elongated cells or microbands.....	225
6-36	Intersecting dislocation grid in a sample with 40% cold reduction showing (a) intersecting dislocations; (b) the corresponding diffraction pattern close to a $\langle 110 \rangle_{bcc}$ axis.....	226
6-37	Dislocation networks and cell boundaries observed in a sample with 40% cold reduction.....	227
6-38	Subgrains (arrowed) observed in a sample with 70% cold reduction after ultra-rapid annealing at 630°C for $t_1 = 0.3$ and $t_2 = 0.1$ sec.....	228
6-39	Typical microstructure of a sample with 70% cold reduction after ultra-rapid annealing at 650°C for $t_1 = 0.3$ , $t_2 = 0.2$ seconds showing large subgrains.....	228
6-40	Close up of grain "A" in Fig. 6-39.....	229
6-41	High magnification around the point B in Fig. 6-40. ....	229

6-42	Dislocation structures observed in a sample with 70% cold reduction after ultra-rapid annealing at 667°C for $t_1 = 0.3$ and $t_2 = 0.1$ seconds. ....	230
6-43	Dislocation networks found in a sample with 70% cold reduction after ultra-rapid annealing at 667°C for $t_1 = 0.3$ and $t_2 = 0.1$ seconds. ....	230
6-44	Large angle boundaries observed in a sample with 70% cold reduction after ultra-rapid annealing at 700°C for $t_1 = 0.3$ and $t_2 = 0.1$ seconds. ....	232
6-45	Dark field image showing a large angle grain boundary in Fig. 6-44. ....	232
6-46	Completely recrystallized structures observed in a sample with 70% cold reduction after ultra-rapid annealing for $t_1 = 0.3$ , $t_2 = 0.1$ seconds and $T_c = 720^\circ\text{C}$ . ....	233
6-47	The "microbulging" of grain boundaries found in a sample with 40% cold reduction and ultra-rapid annealed at 600°C for $t_1 = 0.3$ and $t_2 = 0.1$ seconds. ....	233
6-48	Grain boundary with different cell structures across the boundary with 60% cold reduction and ultra-rapid annealed at 600°C with $t_1 = 0.3$ and $t_2 = 0.2$ seconds. ....	234
6-49	Grains observed in a sample with 70% cold reduction and batch annealed at 680°C for 30 minutes. ....	235
6-50	Subgrain structures observed in a sample with 70% cold reduction and batch annealed at 450°C for 30 minutes. ....	236
6-51	Close up of point "A" in Fig. 6-50. ....	236
7-1	The softening behaviour of 70% cold rolled samples after ultra-rapid annealing at various heating rates. ....	240
7-2	The effect of heating rate to the indicated temperature on the hardness of 70% cold rolled samples. ....	241

7-3	The effect of heating rate on the start ( $T_S$ ) and finish ( $T_F$ ) temperatures for softening.....	242
7-4	Recrystallization temperature ranges at different heating rates. Zones A and B were reported by Andrews [6] using induction and salt bath heating, respectively. Zone D and C are the predictions by Andrews, of the effect of annealing with and without recovery, respectively. Zone E shows the result of the present investigation for resistance heating of decarburised steel.....	243
7-5	Effect of heating rates on recrystallization temperature ranges obtained by various researchers. Zones 1 and 2 were reported by Andrews [6] and correspond to Zones A and B in Fig. 7-4. Zone 3 is the result by Staüb [40]; Zone 4 by L'vov [38] and Zone 5 by Mohri [39]. Zone 6 , corresponding to Zone E in Fig. 7-4, was obtained in the present investigation.....	244
7-6	Recrystallization kinetics for a sample with 70% cold reduction and ultra-rapid annealed at 630, 667, 700 and 720°C, showing that recrystallization progresses in a sigmoidal manner with respect to time.....	248
7-7	Comparison of recrystallization kinetics for a sample with 70% cold reduction subjected to various heating rates. ....	250
7-8	Plot of value B from Avrami equation versus ultra-rapid annealing temperature.....	252
7-9	Partially recovered cell structure observed in a sample with 70% cold reduction ultra-rapid annealed at 510°C. ....	255
7-10	Transmission electron micrograph showing the deformed structure observed in a sample of 80% cold reduction prior to ultra-rapid annealing.....	255
7-11	Transmission electron micrograph showing a partially recovered cell structure in a sample with 70% cold reduction ultra-rapid annealed at 550°C.....	256

7-12	Transmission electron micrograph showing the partially recrystallized structure observed in a sample with 70% cold reduction after ultra-rapid annealing at 667°C for $t_1 = 0.3$ and $t_2 = 0.1$ seconds .....	256
7-13	Microstructures showing the (a) rolling plane section, (b) transverse section close to the free edge of the test piece, and (c) in the centre of the test piece after ultra-rapid annealed at 667°C for $t_1 = 0.3$ and $t_2 = 0.1$ sec.....	259
7-14	Micrograph showing the microstructure and hardness indentation size of a sample ultra-rapid annealed at 667°C for $t_1 = 0.3$ and $t_2 = 0.1$ sec.....	263
7-15	The effect of cold reduction on softening behaviour after ultra-rapid annealing at 700°C.....	266
7-16	Effects of cold reduction on softening behaviour of a sample subjected to ultra-rapid annealing at 667°C.....	267
7-17	The effects of cold reductions on softening behaviour after batch annealing at 550°C, indicating that more deformation results in shorter softening time. ....	268

# ***CHAPTER 1***

## **INTRODUCTION**

Metal has been worked and then softened by annealing since prehistoric times [1]; but little attempt was made to examine the effect of heating rate on softening behaviour until 1936 when the first continuous annealing line was built. Continuous annealing underwent significant developments in the 1950's, and it became a significant alternative to batch annealing.

The heating rates used in most current continuous annealing processes are still relatively low, in the range of  $10 - 10^5$ °C/hour ( $\leq 30$ °C/sec.) [2] . However, rates up to about  $500$ °C/sec. have been reported [3, 4, 5]. Research work at the Steel Company of Wales in the 1960's [6] resulted in significant progress, by raising the heating rates up to  $1600$ °C/second with the use of salt bath and induction heating methods. These results also showed that recrystallization could be completed within a fraction of a second by using sufficiently high heating rates.

The development of electrical resistance heating methods has significantly made it possible to obtain heating rates in the range of  $1000$  to  $5000$ °C/second [7]. The annealing practice at heating rates  $\geq 500$ °C/sec. is referred to as ultra-rapid annealing. Despite these developments, the influence of the heating rate on recrystallization temperature range and softening behaviour was not systematically studied.

It is widely recognized that a clear understanding of the annealing processes, particularly those related to recrystallization, must be based on analysis of the microstructures of materials. Much work in the past has been carried out on normally annealed materials, i.e., those subjected to heating rates below  $10^5$ °C/hour. There have been no detailed reports of the microstructures of ultra-rapid annealed material.

Similarly, the tensile behaviour of materials is important in engineering applications. Although much research has been conducted to determine the tensile properties of iron and low carbon steels, few experiments have been performed to characterize the tensile behaviour of ultra-rapid annealed materials. This deficiency in the knowledge of the basic

tensile properties and the relationship between these properties and the microstructures after ultra-rapid annealing inhibits the establishment of design criteria and the improvement of processing methods for cold rolled low carbon steel.

The objectives of the present investigation were to systematically examine the ultra-rapid annealing process, to study the kinetics of recrystallization as a function of heating rate, to characterize the microstructure at various stages of ultra-rapid annealing, and to examine other factors, such as percentage of cold reduction and prior recovery, which might affect the softening behaviour.



## *CHAPTER 2*

# LITERATURE SURVEY

## 2.1 INTRODUCTION

It is well known that cold worked metals can be softened by annealing to improve their ductility and drawability and much work has been reported on property changes and restoration mechanisms during annealing. In ferrous alloys, in particular, annealing is an important step in conditioning the material for subsequent cold forming processes. However, conventional batch annealing of coiled steel sheet requires a long process time and therefore, continuous annealing techniques were developed from the 1930s to speed up the process. Although progress since then has been impressive, there are inevitably conflicting results and opinions. The focus issue is still how to reduce the processing costs.

Continuous annealing involves rates  $<500^{\circ}\text{C}/\text{sec.}$  and is commonly referred to as "rapid" annealing. The advent of "ultra-rapid" annealing, which followed in the 1960s, provided a new impetus to research on the rapid softening of low carbon steels[8]. Initially, investigations were carried out using salt bath and induction heating[6]. However, the results were not very satisfactory because of conflicting results and limitations of heating rates ( $\leq 1600^{\circ}\text{C}/\text{sec.}$ ). In the 1980s, an experimental resistance heating method was developed which allows rates of  $1000\text{-}5000^{\circ}\text{C}/\text{sec.}$  [9]. This equipment opens up a new field and intensive investigations are needed to explore and understand the ultra-rapid annealing process and related phenomena.

The following literature survey deals, in general, with restoration processes on annealing of cold worked metals; and, in particular, on the annealing of iron and low-carbon steel. Work reported on rapid and ultra-rapid annealing of iron and low-carbon steel is reviewed in detail. In addition, literature on temperature measurement, heat transfer and computer modeling is examined to provide a background for later chapters on experimental aspects of the investigation.

## 2.2 ANNEALING OF COLD WORKED METAL

### 2.2.1 Softening Phenomena

Softening of cold worked metals can be achieved by annealing. It has been known that metals could be work hardened and then softened by annealing at high temperatures. In 1881 Kalisher [10] postulated that working a metal destroyed its crystal form and that heating recrystallize it. Since then a great deal of effort has been made to observe and explain the changes involved. Becker [11] recognized that the softening phenomenon was due to recovery and recrystallization, and that recrystallization was a result of nucleation and grain growth which consumed the deformed material. The early work on the recovery and recrystallization was reviewed by Czocharlski [12]; and reviews on work up to the 1950s have been presented by several authors [13, 14, 15, 16, 17]. However, these investigations were carried out at a time when the development of knowledge was limited by the absence of high-resolution microscopical techniques. Thus, any theories of the detailed mechanisms of structural changes had to be based on indirect evidence such as mechanical and physical property changes, rather than on direct observations. With the development of advanced techniques ( e.g. microprobe, microbeam x-ray and electron microscopy ) more detailed evidence of the structure of cold worked metals and the changes which it undergoes during annealing [18 to 36] became available. Much of the recent evidence has been summarized by Cahn [37].

Despite the massive volume of work on annealing of cold worked metals, comparatively little attention has been devoted to the effect of heating rate on softening phenomena. Annealing processes can be classified according to heating rate, e.g. batch annealing is associated with a low heating rate; continuous annealing involves a high or rapid heating rate ( $<500^{\circ}\text{C}/\text{sec.}$ ); and ultra-rapid annealing describes processes characterised by a very high heating rate ( $>500^{\circ}\text{C}/\text{sec.}$ ).

In 1966, it was proposed by Andrews and Atkinson [8] that raising the heating rate to between 300 and 1600°C/second could increase the rate of softening and lower the temperature range in which recrystallization occurred, as shown in Fig. 2-1. The decrease in recrystallization temperature with increasing heating rate was termed "accelerated recrystallization" by L'vov [38] and the process was termed "rapid annealing" by Andrews and Atkinson [8]. Mohri [39], Staüb and Cieslak [40] also reported that at high heating rates the temperature range in which the softening occurred decreased (Fig. 2-2). It should be noted that the terms "accelerated recrystallization" and "rapid annealing" were used to distinguish the softening behaviour from that occurring at more conventional rates of  $\leq 500^\circ\text{C}/\text{sec}$ . More recent work by Spunar [9], Vourliotis [41] and Yip [7] showed that raising the heating rate to between 1000 and 5000°C/sec. ("ultra-rapid annealing") further lowered the temperature range in which the softening phenomena occurred. The change in behaviour at very high heating rates might indicate a change in the softening mechanism, and result in the microstructure and mechanical properties of the ultra-rapid annealed metal being distinctly different from those obtained by conventional annealing. Although much work has been done on the softening at normal heating rates [42 to 48] (below 500°C/sec.), very little information is available on softening at very high heating rates. Therefore, the following sections mainly describe conventional annealing processes and the resulting structural and property changes, and serves as a background for this investigation of ultra-rapid annealing.

## 2.2.2 Annealing Processes

### 2.2.2.1 Release of stored energy of deformation

Stored energy created during deformation provides the driving force for both recovery and recrystallization and thus these processes are competitive in consuming this excess energy. One of these two processes may be dominant depending on the strain level, the annealing temperature and the composition.

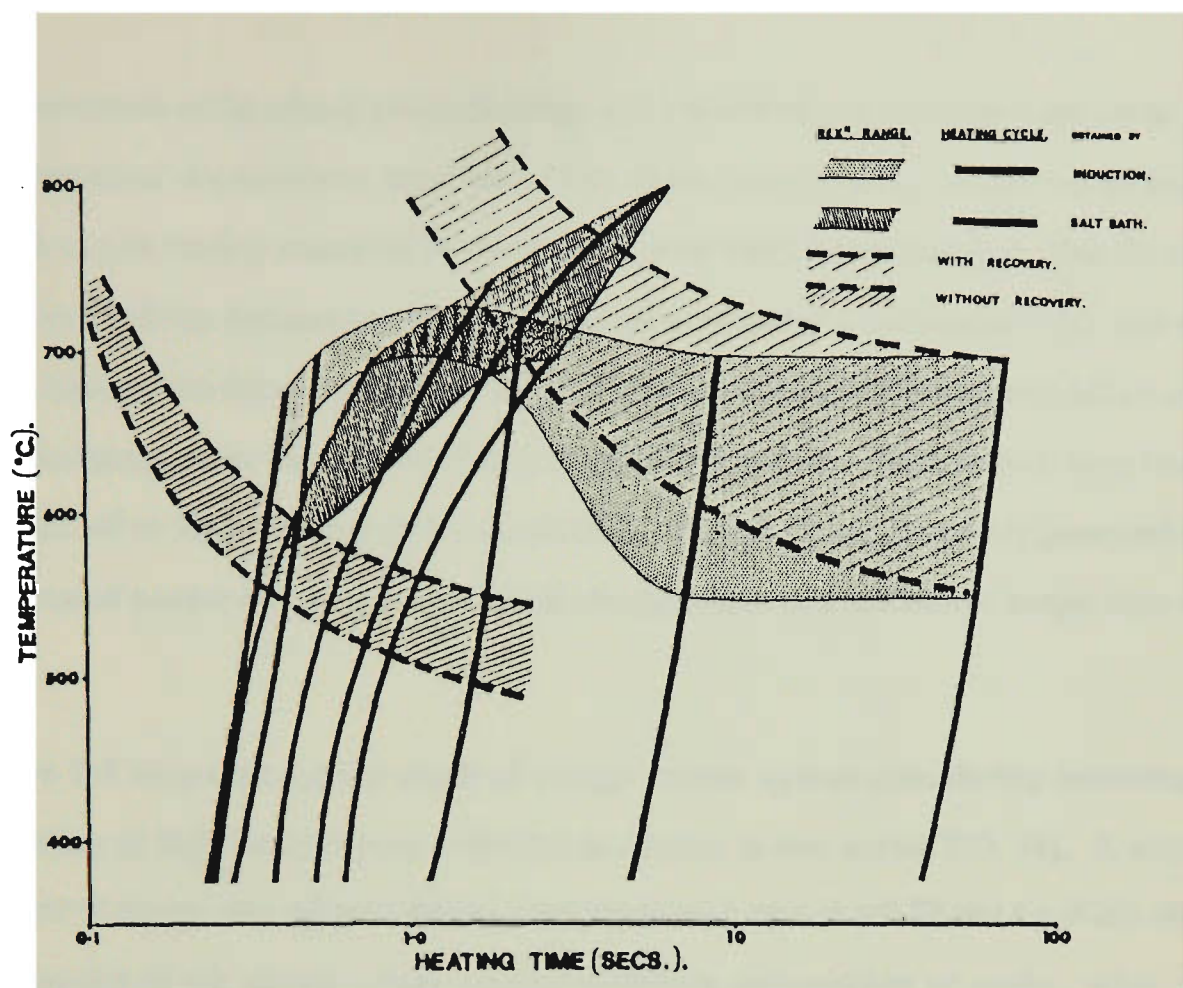


Fig. 2-1 Effect of heating rate [ref. 8]

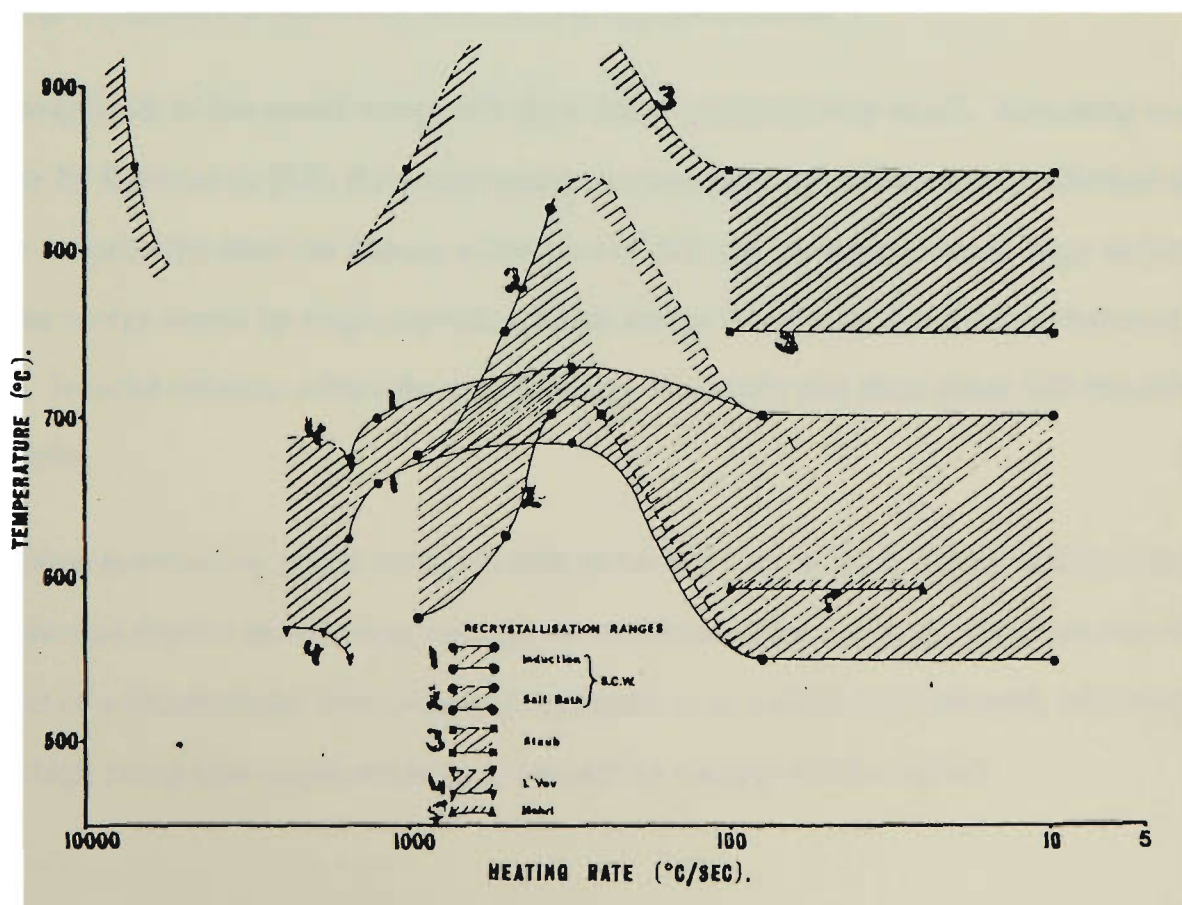


Fig. 2-2 Effect of heating rate ( Summary) [ref. 8]

Measurements of the release of stored energy and a knowledge of its kinetics are useful to understand of the processes involved. Most of the stored energy is released as heat, which can be readily measured in calorimeters with sufficient sensitivity. Usually the samples ( both the deformed and undeformed ) are annealed in a calorimeter either with an fixed heating rate through a selected range of temperature (anisothermal method) or at a constant temperature for a period of time (isothermal method). Such methods have been popular [49 to 55] since Hort [56] invented them. The results are commonly presented in the form of a curve representing the rate of energy release as a function of temperature or time.

Figure 2-3 shows the typical result of energy release against time during isothermal annealing of high purity copper deformed in tension to two strains [50, 51]. A small amount of energy was released during recovery in each case ( $\epsilon = 0.28$  and  $\epsilon = 0.16$ ), and the amount of the stored energy seemed relatively independent of strain. Also, at 189.7°C, the recrystallization peak occurred after shorter times and the rate was high at the beginning and then decreased as annealing time progressed.

The magnitude of the stored energy of cold work, is comparatively small. According to a survey by Bever et al. [57], the stored energy in most polycrystalline metals deformed at room temperature does not exceed a few tens of calories per mole even at large strains and the energy stored by single crystals at small strains is typically less than 5 calories per mole. In solid-solution alloys the stored energy is usually less than about 200 calories per mole.

In relation to release of stored energy in cold rolled low carbon steel, Taylor and Quinney [58] showed that the stored energy at a given amount of deformation decreased as carbon content of a decarburized steel increased compared to an undecarburized steel, indicating that a high purity iron would retain much less of the energy of deformation.

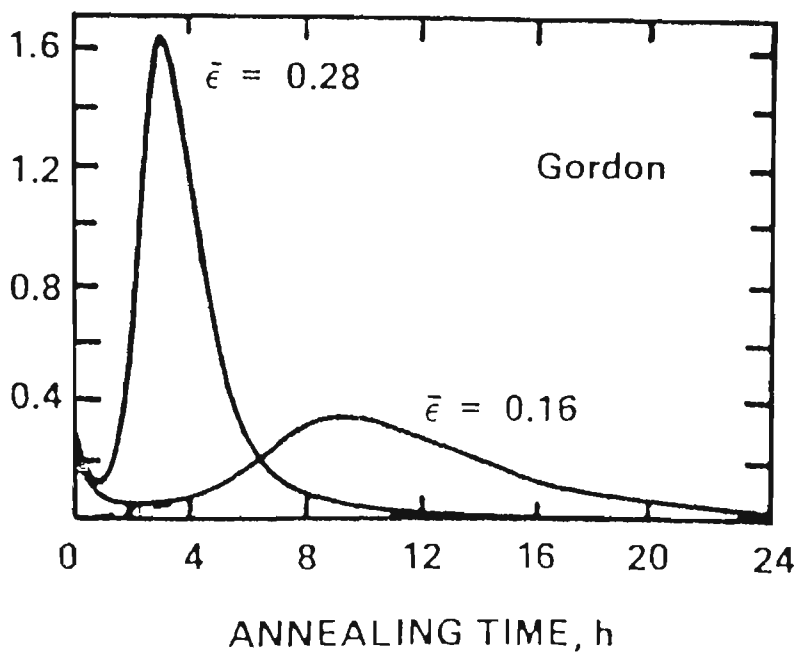


Fig. 2-3 Rate of energy release as a function of time during isothermal annealing at 189.7°C for 99.999% pure copper deformed by tension to two strains. [ref. 78]

In fact, differences in composition, grain size, mode and temperature of deformation give rise to a variation in stored energy, which provides the driving force for recovery and recrystallization during annealing [49, 54, 55].

#### 2.2.2.2 Recovery

Recovery is a restoration process during which the defects from deformation reorganize themselves, resulting in a reduction in strain energy. The defect rearrangement in recovery consists mainly of thermally activated climb of dislocations [54]. In contrast, the most distinctive aspect of recrystallization is the replacement of the deformed structure with new strain-free grains created by migration of high angle boundaries.

The characteristics of the property changes, physical or mechanical, during recovery are of no incubation period and the rate of change decreases sharply initially, then becomes more gradual, and finally approaches zero. Compared with recrystallization, the recovery process is considered homogeneous. The structural changes occur more or less simultaneously throughout the matrix without the formation and growth of a new structure by interface migration.

Generally, recovery results in the release of stored energy as described in 2.2.2.1. The recovery of physical and mechanical properties is outlined in Section 2.2.3.1.

#### 2.2.2.3 Recrystallization

Recrystallization, or primary recrystallization, occurs by the nucleation and growth of new grains at the expense of deformed and recovered matrix. An incubation period usually exists during which nuclei of strain free grains are formed at a number of preferred sites. The driving energy for recrystallization is the portion of the stored energy that has not been released by recovery. This may correspond to 90% of the total stored energy in the deformed material (Fig. 2-3). The driving energy for recrystallization is associated mainly with dislocations in the subgrain boundaries [54].



Three conditions must be satisfied for recrystallization to occur in a deformed matrix [59]:

- (1) the stored energy must be high enough to provide the driving force;
- (2) a steep stored energy gradient should exist to allow local instability to develop;
- (3) lattice curvature should be present to allow a growing nucleus to have a high angle boundary.

These conditions are more likely to be satisfied in some grains of a deformed metal than in others with different orientations, because of anisotropy of the stored energy. These conditions are also more easily satisfied where extensive recovery has not happened. Therefore, static recrystallization occurs more readily in metals and alloys with low stacking fault energy where dislocation rearrangement becomes difficult due to the wider distance between partial dislocations which inhibits easy cross slip.

So far, the mechanism of recrystallization has been studied over a period of many years without the emergence of a satisfactory general mechanism. The significant models of recrystallization are presented in Section 2.2.6.

#### 2.2.2.4 Interaction of recovery and recrystallization

As mentioned before, the stacking-fault energy of a material influences its deformation structure, and thus the extent of recovery. Cross-slip of dislocations in high stacking-fault energy metals can be induced the long-range stress fields of the cell walls on annealing. In other words, it is easier for dislocations to annihilate and rearrange in high stacking-fault energy metals than in low stacking-fault energy. The relative recovery/recrystallization behaviour of metals of different stacking-fault energy was discussed by McLean [60]. The recovery and recrystallization behaviour of two materials, i.e. aluminium with high stacking-fault energy and copper with low stacking-fault energy is shown in Fig. 2-4. In aluminium, recrystallization is favored only at large strains, whereas substantial recovery may prevent recrystallization at low strains (curve A). On the other hand, little energy release occurs prior to recrystallization at any strains

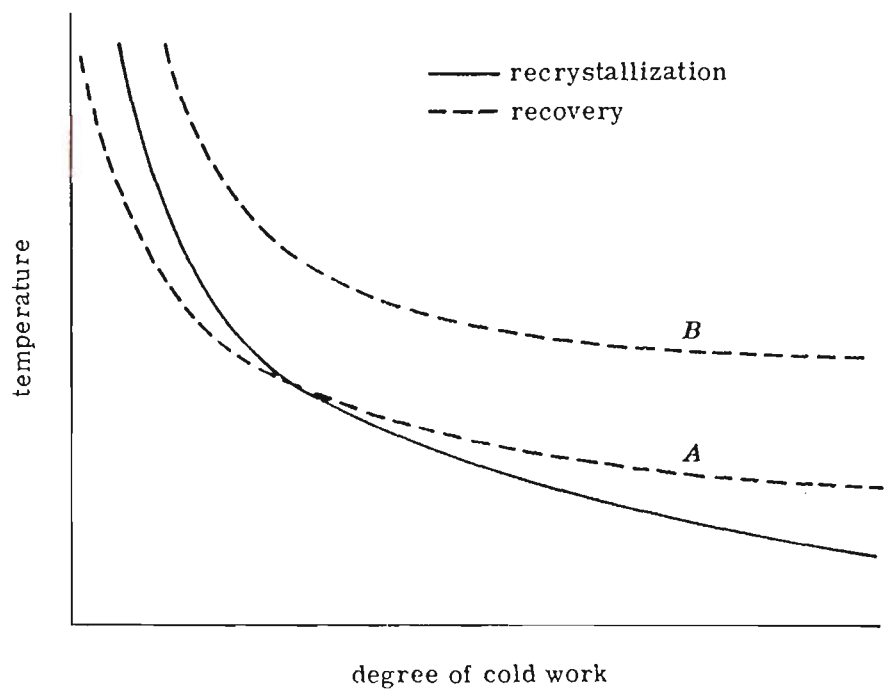


Fig. 2-4 The effect of the amount of deformation on the recovery and recrystallization temperatures for a metal with a high stacking fault energy (curve A) and a metal with a low stacking energy (curve B). [ref. 60]

in copper (curve B). This explains the experimental observation that little mechanical recovery is observed for copper and its alloys prior to recrystallization. In contrast, aluminium recovers considerably its mechanical properties. This is because mechanical properties are sensitive to dislocation density and arrangement, but not point defects.

Using the micro-hardness distribution technique to the isochronally annealed super-purity aluminium, Mould and Cotterill [61] revealed another feature of annealing characteristics of high stacking-fault energy metals. There were two distinct "hardness peaks" at lower annealing temperatures, one corresponding to regions which had recrystallized and the other to the regions which had not. As the annealing temperature increased, the hardness of the unrecrystallized regions continued to decrease slightly. Therefore, at any stage of the annealing process, pre-recrystallization softening continues to occur in the regions which have not been recrystallized.

The coexistence of recovering and recrystallized regions prevents a clear division of a hardness vs annealing temperature curve into regions which are separately considered to correspond to "cold work", "recovery" and "recrystallization". As "recovery" will continue until the entire specimen has been consumed by the recrystallizing grains, the various processes overlap. This effect increases the difficulties in measuring the position of the 50% recrystallization on the basis of 50% softening, which are outlined in Section 2.2.2.5.

To obtain a more meaningful 50% softening point a method similar to differential thermal analysis is used. This procedure involves the measurement of the slope of the conventional hardness versus annealing temperature curve and then plots slope against the annealing temperature, as shown in Fig. 2-5. The rate of change of hardness with annealing temperature changes sharply as the annealing temperature is increased. The annealing temperature at which the maximum rate of change occurs corresponds to the temperature at which the recrystallization fraction is 50%. The determination is supported by metallographic observations [61]. In addition, the temperatures corresponding to the

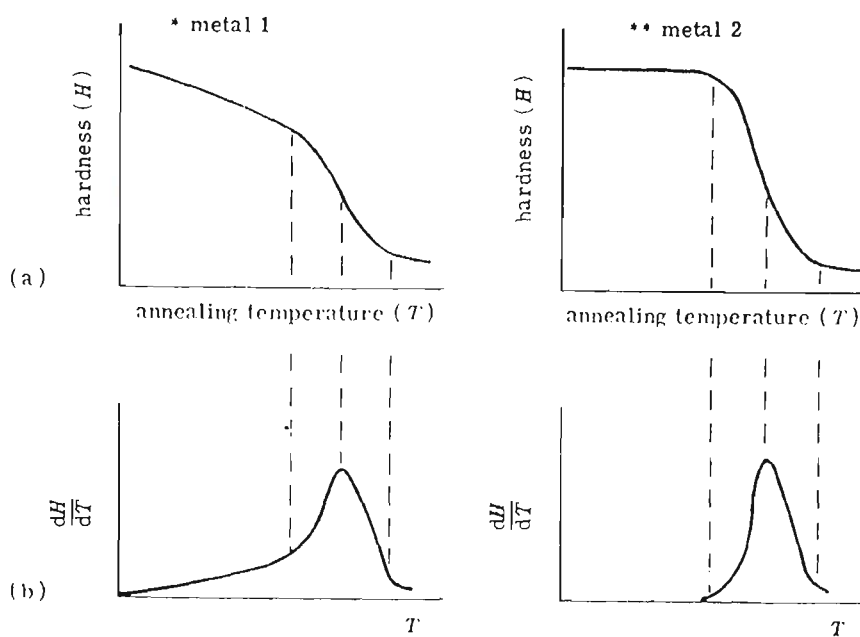


Fig. 2-5 The assessment of 50% primary recrystallization by means of hardness testing after isothermal annealing: (a) hardness versus annealing temperature; (b) rate of change of hardness with annealing temperature vs. annealing temperature. \*Metal 1 softens slightly prior to primary recrystallization. \*\*Metal 2 softens entirely during primary recrystallization. [ref. 59]

start and finish of recrystallization can be obtained more readily from such a curve than from the conventional softening curve.

Further evidence which supports the above description of simultaneous recovery and recrystallization is provided by the work of Vandermeer and Gordon [48].

#### 2.2.2.5 Recrystallization and the softening point

In studying recrystallization, isothermal annealing is used mainly to study the nucleation and growth rates of the process in order to form the basis for interpretation of the basic mechanisms of recrystallization. Isochronal annealing is used primarily to obtain the temperature range over which recrystallization occurs.

Hardness testing is probably the most common technique used to study softening phenomena. However, the conventional techniques of macro-hardness measurement and optical metallography often give different recrystallization temperatures ranges. New grains usually can be observed before any measurable drop of hardness occurs. Consequently, the results of a macro-hardness test often indicate a later start of the recrystallization process than do the results of a metallographic examination. Metallography is therefore more sensitive, but more difficult in providing any quantitative description. Sometimes a point counting technique similar to that of Anderson and Mehl [62] is used. Details of typical metallographic techniques are described by Perryman [63] and Underwood [64].

The determination of the 50% recrystallization temperature (or time) is normally based on evaluating the position of 50% softening. This is only accurate when no recovery occurs. Otherwise, the softening from recovery prior to recrystallization and that from recrystallization needs to be distinguished. Perryman [65] showed that error may be significant if such distinction were not made, as depicted in Fig. 2-6. Obviously, the greater the proportion of softening due to recovery, the bigger the difference between the position of the 50% total softening and the true position of the 50% recrystallization.

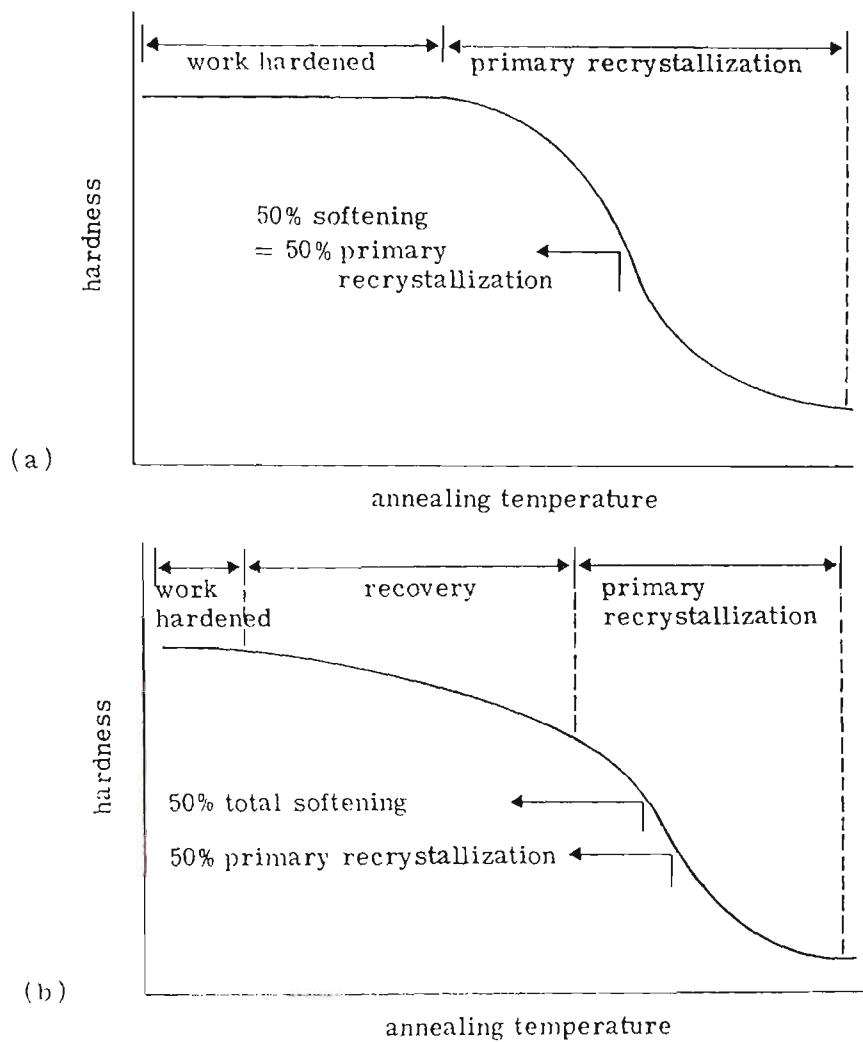


Fig. 2-6 Schematic representation of the annealing temperatures corresponding to 50% primary recrystallization for (a) a metal which softens entirely by primary recrystallization, and (b) a metal which softens prior to, as well as during, primary recrystallization. [ref. 205]

The micro-hardness population count method [66] has been used to the recrystallization of aluminium [67] and copper [68, 69]. It has the advantage that a statistical plot of a large number of indentations can be obtained over a wide area of the specimen. Therefore, errors can be minimized.

Another method to study recrystallization is x-ray diffraction. It is used mainly for texture analysis. Other techniques include calorimetry [70, 71], resistivity [70, 71] and internal friction [72, 73].

### 2.2.3 Property Changes during Annealing

#### 2.2.3.1 Electrical resistivity and density changes

Plastic deformation increases the number of vacancies and dislocations in a material. As a result, the electrical resistivity of the material increases and the density decreases. During annealing resistivity decreases as defects are destroyed. Typical examples of this are shown in Fig. 2-7 and Fig. 2-8 [74]. Figure 2-7 shows curves for 99.85% nickel for which the density and electrical resistivity change significantly in those temperature regions where there is an energy-release peak occurs, and only slightly at other temperatures. In a high-purity copper (Fig. 2-8), the energy release is continuous and correspondingly a continuous change of resistivity is seen, with little change in the temperature region between the energy release prior to recrystallization (i.e. up to 20°C) and that associated with the occurrence of recrystallization (i.e. above 150°C).

Comparison of the neutron-irradiated molybdenum [75] with the cold worked molybdenum [76] shows that the increased resistivity was annealed out at a temperature of about 150°C. Peiffer [77] made similar measurements on cold-worked molybdenum annealed at 145°C and noticed that the recovery of resistivity was nearly complete after 96 hours and that no strain ageing occurred. It was therefore concluded that the resistivity change was not due to the migration of carbon, hydrogen or oxygen, but rather to the annihilation of vacancies. Some evidence for a larger resistivity change after irradiation has been reported but this may not be due only to vacancies [78, 79]. The data on

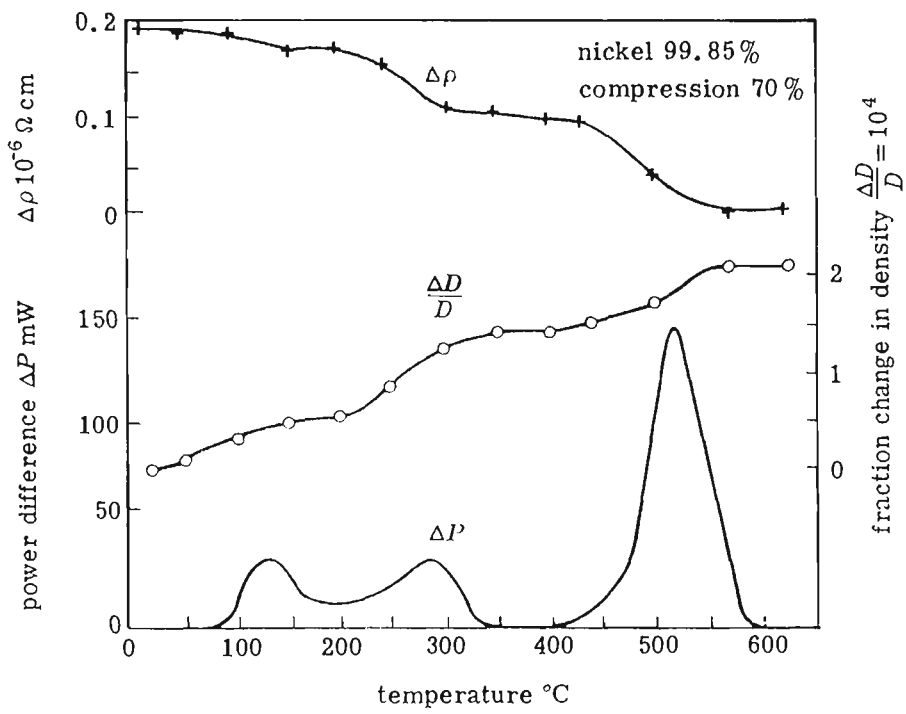


Fig. 2-7 Power difference ( $\Delta P$ ), increment in electrical resistivity ( $\Delta \rho$ ), and change in density ( $\Delta D$ ), as a function of temperature, for 99.85% purity nickel after 70% compression at room temperature; heating rate  $6^{\circ}\text{C}/\text{min}$ . [ref. 70]



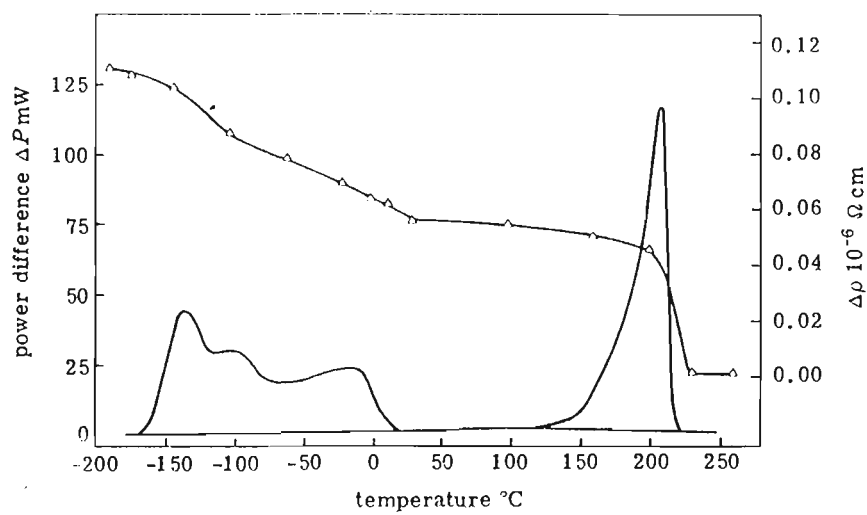


Fig. 2-8 Power difference ( $\Delta P$ ) and increment in electrical resistivity ( $\Delta \rho$ ) as a function of temperature for 99.98% purity copper wire drawn to an effective elongation of 54% at 78 K; heating rate 2°C per min. [ref. 49]

vacancy annealing kinetics in Table 2-1 indicate that vacancies will migrate significantly in body-centred-cubic metals at temperatures greater than about 10-15% of their absolute melting temperature.

Table 2-1 The annealing kinetics of vacancies in several BCC metal

Metals	Melting point $T_M$ , K	Temp. of migration of vacancies $T_m$ , K	Activation energy for vacancy migration ev	$\frac{T_m}{T_M}$	$\frac{ev \cdot 10^8}{T_m}$ (ev K <sup>-1</sup> )	Ref.
Columbium	2740	373	1	0.136	0.365	364
Molybdenum	2895	423	1.16	0.146	0.435	75, 76
Tantalum	3270	383	1.35	0.117	0.413	364
Tungsten	3585	625	1.70	0.174	0.475	75,365

2.2.3.2 Mechanical property changes

According to their different pre-recrystallization changes in mechanical properties, metals can be divided into two groups. The first group of metals, such as copper, nickel, etc, have a low stacking-fault energy and usually show very little change in their mechanical properties on annealing prior to recrystallization. This behaviour is generally assumed to be due to the fact that in such metals dislocation rearrangement processes are extremely difficult. Consequently, stored-energy release occurring prior to recrystallization are associated primarily with vacancy removal which has a much greater effect on properties such as density and electrical resistivity than on mechanical properties.

The second group of metals have a high stacking-fault energy (e.g. aluminium,  $\alpha$ -iron, etc.) and usually soften considerably on annealing even before recrystallization takes place. Dislocation rearrangement can occur relatively readily within the deformed metal

if the temperature is high enough. In such a case, partial softening can occur without the formation of new grains. In general, this pre-recrystallization softening represents only a small proportion. However, in some particular situations, the whole of the work hardening has been recovered without recrystallization, e.g. in aluminium [80], zinc [81], iron-aluminium and iron-silicon [82].

The mechanical properties of deformed metals usually recover monotonically towards the values of the fully annealed materials. However, some copper-based solid solutions show a slight increase in hardness as the result of pre-recrystallization annealing. This is usually considered to be due to the restoration of short-range order ( which was destroyed by deformation) within the solution [83, 84]. Such materials then exhibit full softening, in the normal way, during subsequent recrystallization.

## 2.2.4 Factors which Influence Softening

### 2.2.4.1 Cold deformation

The extent of the deformation in the metal prior to annealing determines the behaviour of primary recrystallization. The driving force for the process is provided by the high internal energy associated with the deformed state. In addition, the details involved in softening are related to the distribution of strain ( or, more specifically, of dislocations ) within the deformed metal. However, thermal energy is needed to activate various processes. This leads to the concept of a "recrystallization limit", which has been defined [85] as "the lowest temperature which produces complete recrystallization for a specific metal and condition". The recrystallization limit of a metal can be related to its deformation conditions. First, there is a minimum strain below which no recrystallization would occur. Second, increasing the strain above this value lowers the recrystallization limit temperature.

Increasing the strain decreases the rate of change in both the recrystallization temperature and the resultant grain size. For example, increasing the strain from 3 to 25% lowered

the recrystallization temperature of copper by over 200°C, whereas increasing the deformation to over 90% only produced a further decrease of less than 100°C [86]. This effect is generally associated with the observation that the kinetics of nucleation and growth are most sensitive to change of strain at low strains. In general, the activation energies for nucleation and growth are approximately equal at strains greater than 15 to 20%. The softening process can then be represented by a single activation energy which decreases with strain [87].

The mechanism of nucleation depends also on strain. Beck [17] pointed out that the strain-induced boundary-migration mechanism is apparently responsible at low to medium deformations and that other mechanisms may dominate in heavily deformed materials where the nucleation sites are often within the deformed grains rather than at the boundaries. Bailey and Hirsh [88, 89, 90] studied heavily deformed single crystals of copper and polycrystalline silver and nickel. They found that rolling reduced 90% produced very high dislocation contents which were distributed in high and low density regions with misorientations of the order of 10°. The ultimate recrystallization took place by grain-boundary migration. However, it was difficult to establish whether the migrating boundaries were the original grain boundaries or were formed by some subgrain dependent process within the grain interiors.

#### 2.2.4.2 Textures and plastic anisotropy

Texture is an important property of sheet metals because it induces plastic anisotropy, which can be beneficial to forming operations [91, 92, 93]. The formability of deep drawing sheet steels can be predicted from the plastic strain ratio  $R$  and it has been known [94 to 100] that this ratio is related to the preferred orientations in the recrystallized steel. For this reason the recrystallization texture of low-carbon steel has received much attention and many attempts have been made to improve the drawing characteristics by enhancing desirable components of the recrystallization texture.

There have been numerous attempts [94, 97 to 100, 101 to 107] to relate  $\bar{R}$  values to the recrystallization texture of low-carbon steel. Generally speaking, strong  $\{111\}\langle uvw \rangle$  texture components and weak  $\{100\}\langle uvw \rangle$  texture components give high  $\bar{R}$  values. Nagashima et al. [104] have calculated theoretical  $\bar{R}$  values for orientations having various directions normal to the sheet, and their results are given in Table 2-2.

Table 2-2

Orientation	$\langle 111 \rangle$	$\langle 332 \rangle$	$\langle 321 \rangle$	$\langle 110 \rangle$	$\langle 211 \rangle$	$\langle 210 \rangle$	$\langle 411 \rangle$	$\langle 310 \rangle$	$\langle 100 \rangle$
$\bar{R}$ value	2.39	2.17	1.38	1.38	1.30	0.71	0.57	0.49	0.33

These results indicate that the ideal texture for deep drawing would be a perfect fibre texture with a  $\langle 111 \rangle$  fibre axis normal to the surface of the sheet. In cubic crystals the  $\langle 111 \rangle$  direction is the direction of maximum flow stress and maximum Young's modulus and this fibre texture imparts both elastic stiffness and high resistance to thinning ( i.e. high  $\bar{R}$  values ) in the sheet normal direction [95, 96].

Although the softening textures of the various steel types are similar in many respects, the variations between individual textures are greater than those for the corresponding cold rolled steels. The major recrystallization texture component,  $\{111\}\langle 110 \rangle$  is found in iron [108,109], rimmed steel [107,110,111], Al-killed steel [108,110] and continuously cast low carbon steel [112].

The primary recrystallization texture is relatively insensitive to both the rate of heating and the annealing temperature [113 to 121]. Nevertheless, minor differences have been detected [107, 113, 115, 116, 119] and attempts have been made to relate these textural variations to the extent of recovery before recrystallization. However, the observed variations are not large and no clear trend is apparent.

#### 2.2.4.3. Chemical composition

Normally, increasing the solid-solution content of a metal leads to a higher recrystallization limit with a reduced sensitivity to strain. Consequently metals which are often considered recrystallizing at elevated temperatures are in fact capable of recrystallizing at room temperature under the combined influence of high purity and heavy deformations. Typical early examples were provided by the work on copper [86] , on silver [122] , on aluminium [123], and on zinc [124]. Demmler [125] found that the softening of pure aluminium was complete after 1.5 hours at room temperature for 90% deformation and after 3 hours for 75% deformation, while Albert, Dimitrov and Le Héricy [126] found that softening could start after 3 hours and be complete in 3 days at -50°C for aluminium containing less than 10 ppm impurities, deformed by 96%.

The latter effect was also found by Talbot in his study of the effects of purity and deformation on the softening of iron [127]. For zone-refined iron ( less than 25 ppm impurities), deformed in tension by amounts up to 20%, annealing produced an extremely stable substructure within the original grains and recrystallization did not occur. This substructure was in stable low-energy state which could not be removed by high temperature annealing and did not fulfil the role of an intermediate state between the cold-worked state and the fully recrystallized one. However, samples of the same material cold reduced by more than 80%, recrystallized in about two hours at 350°C by the formation of nuclei directly from the cold-worked matrix. The specific mechanism of nucleation was not identified, although it clearly occurred within the grains and was not a form of boundary bulging. In contrast to this, iron containing more impurities (e.g. commercial Armco iron) recrystallized after deformations of 3% or more. In this case the recrystallization process was preceded by a sharpening of the deformation cell structure during annealing. Talbot et al. showed that this observation compared very closely with similar effects of purity and deformation in aluminium alloys [128 to 131].

## 2.2.5 Microstructural Changes during Annealing

### 2.2.5.1 Changes in microstructure during recovery

Detailed work on structural changes during recovery was due to Hu [132] who found that in a (001)[110] crystal of Fe-Si alloys, isothermal annealing resulted mainly in a general reduction in dislocation density, followed by the formation of subgrains and the growth of subgrains. Figures 2-9 to 12 show the general changes in microstructure produced by annealing at temperatures from 200 to 800°C. The density of dislocations decreased rather slowly when annealing at low temperatures (200-400°C), as shown in Figs. 2-9 and 10. Subgrain formation began at 500-600°C, and a well-defined subgrain structure was developed after annealing at 600°C ( Fig. 2-11). At still higher temperatures, e.g. 800°C, the average size of the subgrains became larger, as shown in Fig. 2-12(b). After annealing at 800°C for 125 minutes, the specimen was completely softened (see the hardness curves in Fig. 2-13), but no recrystallization and no preferred orientation could be detected.

During recovery, vacancies can migrate or anneal out and dislocations can rearrange themselves. Studies of recovery in iron deformed by irradiation in a reactor [133] showed that excess vacancies anneal out at subzero temperature.

Studies of x-ray line broadening also illustrated the influence of the degree of deformation at a given temperature on the recovery rate. In severely deformed Armco iron [134], x-ray line broadening began to decrease at temperatures as low as 280°C, decreased sharply at about 325°C and became fairly constant at 400-500°C. At about 500°C, there was a second decrease associated with recrystallization. Tetelman et al. [135] deformed vacuum melted iron of reasonable purity to 5% in tension and showed that appreciable line sharpening due to the onset of recovery occurred only in the range 375-475°C. For single crystals of an Fe-Si alloy [132] cold reduced by 80%, the various reflections began to sharpen at 200°C. These observations show that the temperature at the onset of recovery line broadening is a function of the degree of cold work.

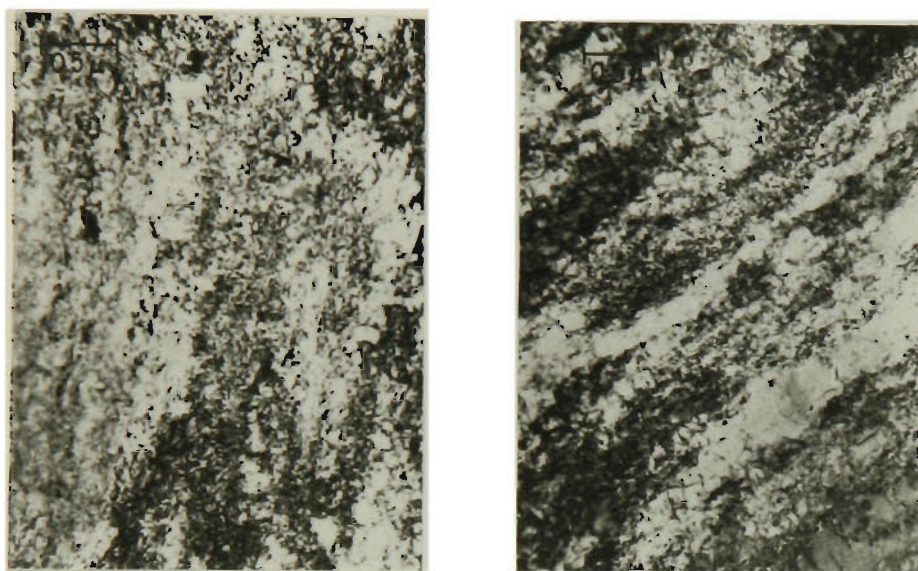


Fig. 2-9 Electron transmission micrographs showing the change in microstructure upon annealing the (001)[110] crystal. (a) after 80 min. at 200°C, (b) after 1280 min. at 200°C. [ref. 132]

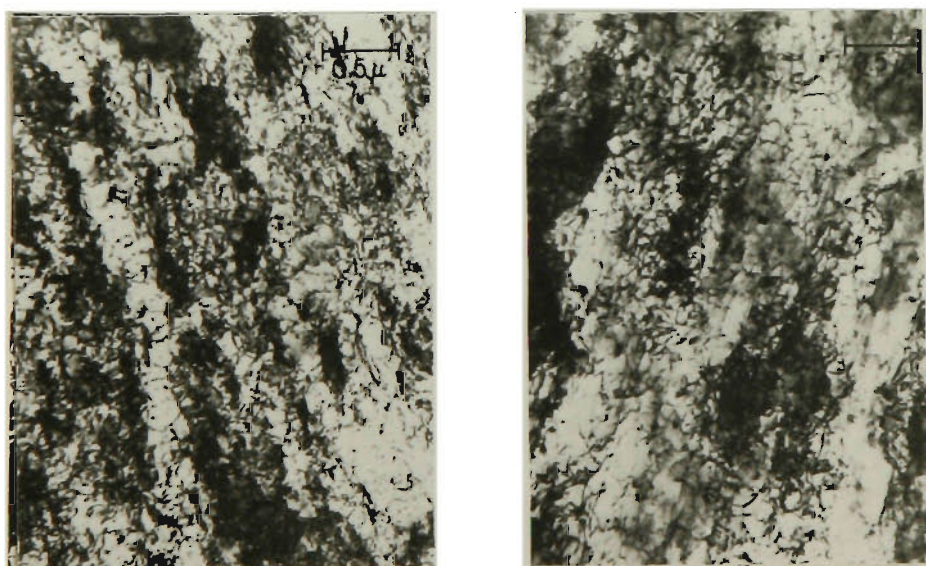


Fig. 2-10 Electron transmission micrographs showing the change in microstructure upon annealing the (001)[110] crystal. (a) after 20 min. at 400°C, (b) after 1280 min. at 400°C. [ref. 132]



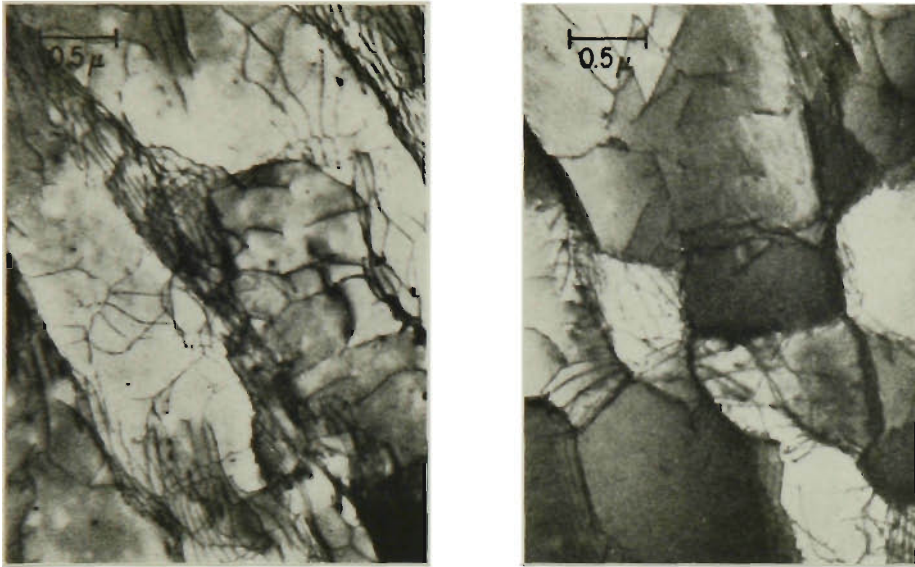


Fig. 2-11 Electron transmission micrographs showing the change in microstructure upon annealing the (001)[110] crystal. (a) after 5 min. at 600°C, (b) after 1280 min. at 600°C. [ref. 132]

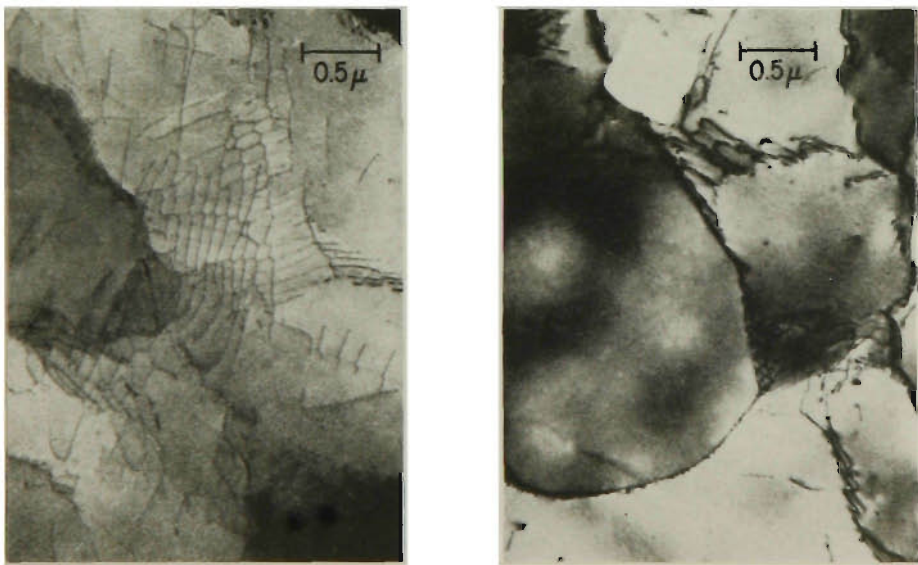


Fig. 2-12 Electron transmission micrographs showing the change in microstructure upon annealing the (001)[110] crystal. (a) after 1 min. at 800°C, (b) after 5 min. at 800°C. [ref. 132]

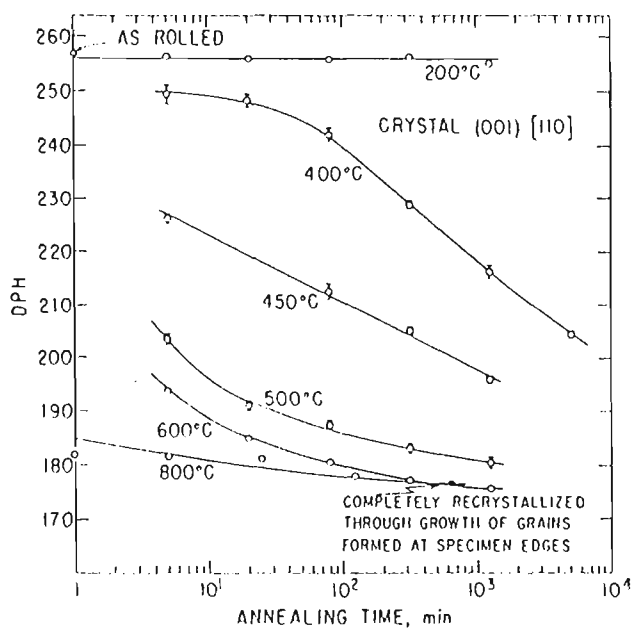


Fig. 2-13 Recovery of diamond pyramid hardness of the (001)[110] crystal, measured with 1 kg load. Experimental points represent the average of 10 measurements for each specimen, and the probable error limits are indicated. Note that complete softening without recrystallization is obtained in the specimen annealed for 1280 min. at 600°C. Solid circle represents a specimen which was completely recrystallized. [ref. 132]

### 2.2.5.2 Microstructure at the beginning of recrystallization

Following recovery, recrystallization takes place by nucleation and growth of new grains at the expense of the recovered matrix. An incubation period may be observed during which viable nuclei are formed at a number of preferred sites. These nuclei of newly formed grains are relatively strain-free, and when reaching the critical size, are surrounded or partially surrounded by high-angle boundaries with high mobilities. They are, then energetically capable of growing into the matrix by the migration of their high-angle boundaries. This effect is shown in Fig. 2-14 [132] which is a conventional optical micrograph of the surface of a deformed Fe-Si (001)[100] crystal. By observing a number of specimens annealed for 125 minutes at 600°C, various transmission electron micrographs were obtained around the microband region, which are shown in Figs. 2-15 to 19. While in some locations only one or two large subgrains were formed, these generally having elongated shapes (Figs. 2-15 and 16), both elongated and large equiaxed subgrains were formed in other regions (Figs. 2-18 and 19). There were also regions where general subgrain growth occurred before a recrystallized grain was formed (Fig. 2-19). However, in all situations, two features were observed to be common: (1) the growth of subgrains always took place among the subgrains within the microband, and the growth of a subgrain in the outermost segment of a microband into the matrix by the migration of the outermost boundary was not observed; and (2) the growth of subgrains occurs largely by the elimination of the boundary between them; i.e. by the coalescence of subgrains [109]. A few such regions, where residual dislocations can still be seen, are indicated by the arrows in Figs. 2-17 to 19. In other cases, some boundary migration may have taken place, as suggested by the curvature of the boundary. Nevertheless, boundary migration is believed to be secondary, as some adjustment of the connecting boundaries at the junction point is necessary after a coalescence event.

In addition, the following observations were made: large subgrains developed within the microband by the coalescence of polygonized segments (Fig. 2-20); growth of large subgrains occurred within the microband (Fig. 2-21); and growth of recrystallized grains

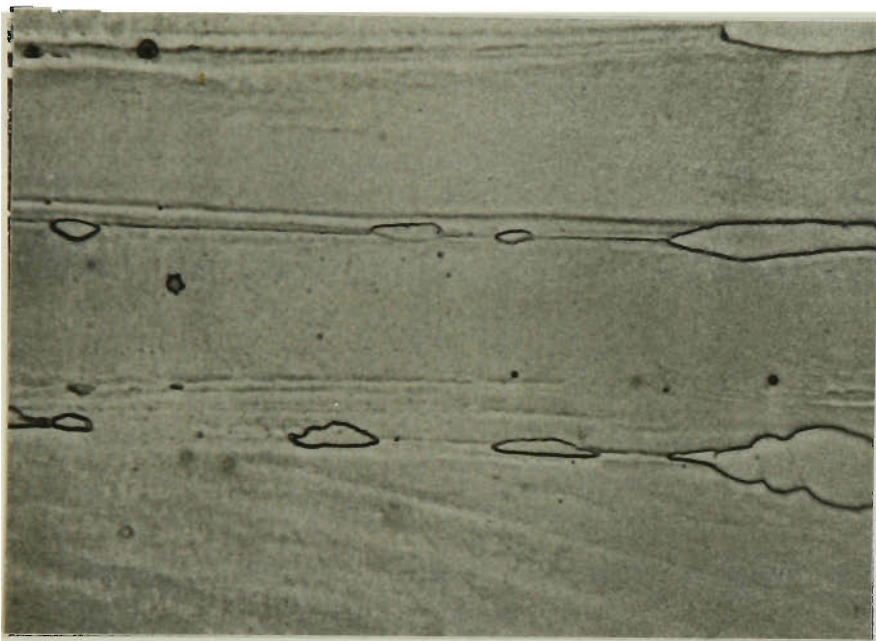


Fig. 2-14 Optical micrographs of a specimen of the (001) [100] crystal annealed for 25 min. at 600°C, showing recrystallized grains formed along the boundary between matrix deformation bands. The variation in size of these recrystallized grain indicates that their growth rates are different, which, in turn, suggests that their orientations are different. Nital etch, 500x. [ref. 132]





Fig. 2-15 Electron transmission micrograph showing the growth of subgrains within a microband region. Many subgrain boundaries appear to be gradually eliminated by the removal of dislocations from these boundaries, suggesting that subgrain "growth" occurs largely by coalescence. A few of these boundaries that have not yet been completely eliminated are indicated by arrows. (001)[100] crystal annealed 125 min. at 600°C. [ref. 132]



Fig. 2-16 Electron transmission micrograph showing the growth of subgrains within a microband region. Features similar to those described in Fig. 2-17 are shown. (001)[100] crystal annealed 125 min. at 600°C. [ref. 132]

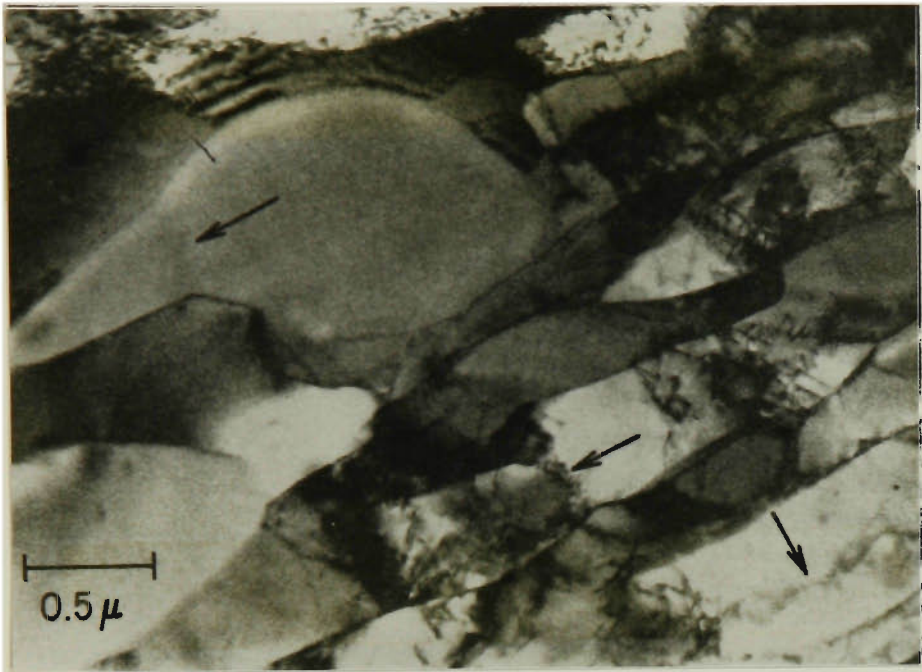


Fig. 2-17 Electron transmission micrograph showing the growth of subgrains within a microband region. Features similar to those described in Fig. 2-17 are shown. (001)[100] crystal annealed 125 min. at 600°C. [ref. 132]



Fig. 2-18 Electron transmission micrograph showing the growth of subgrains within a microband region. Spherical and elongated shapes develop side by side. The coalescence nature of subgrain "growth" is suggested by those boundaries. [ref. 132]

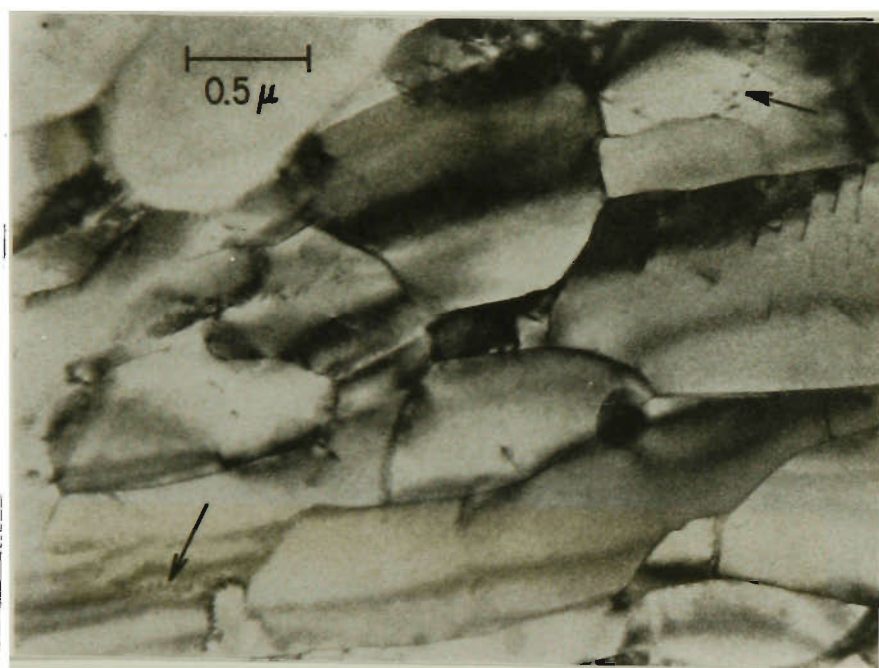
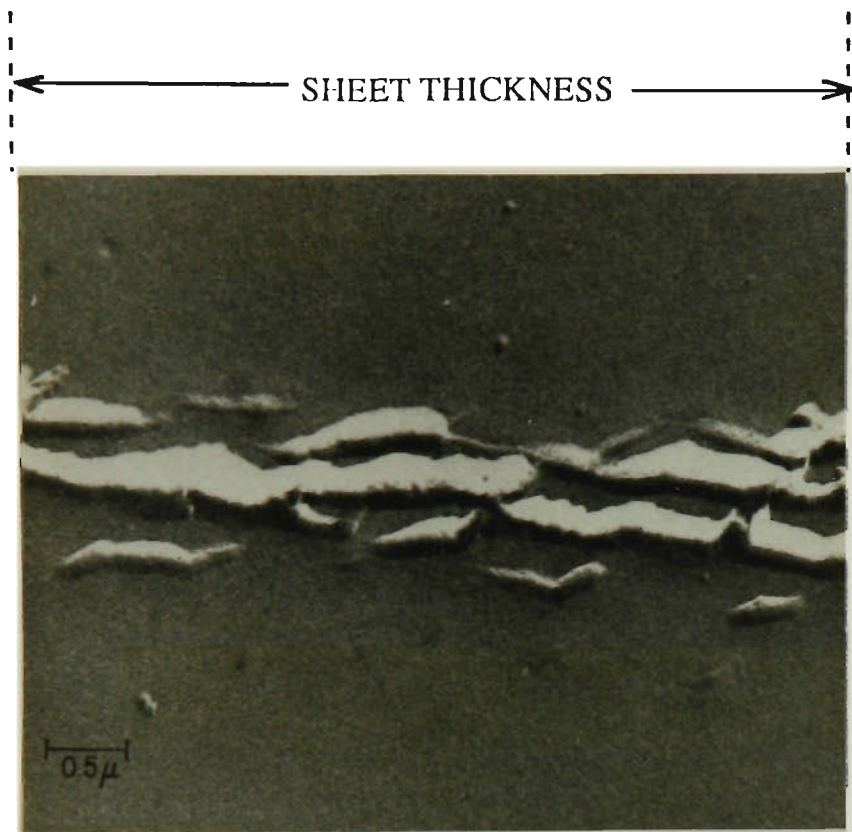
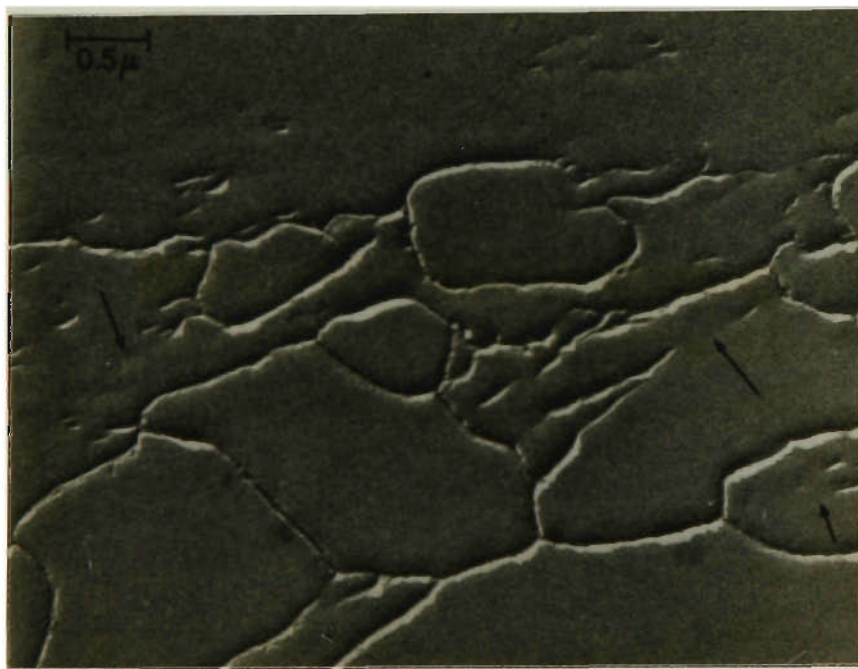


Fig. 2-19 Electron transmission micrograph showing the growth of subgrains within a microband region. A general growth of the subgrains is shown in this area. The coalescence nature of subgrain growth is suggested by those boundaries indicated by arrows. (001)[100] crystal annealed 125 min. at 600°C. [ref. 132]





(a)



(b)

Fig. 2-20 Carbon-shadowed replica electron micrographs taken from the transverse cross section of the (001)[100] crystal, after the specimen was annealed at 600°C for 5 min. showing that (a) the microband segments consist of thin sheets on edge extending through the thickness of the specimen, and (b) that growth of the microband segments has taken place in another area. Note that the growth occurs within the microband, and proceeds largely by eliminating the boundaries between the microband segments, as indicated by the arrows. [ref. 132]



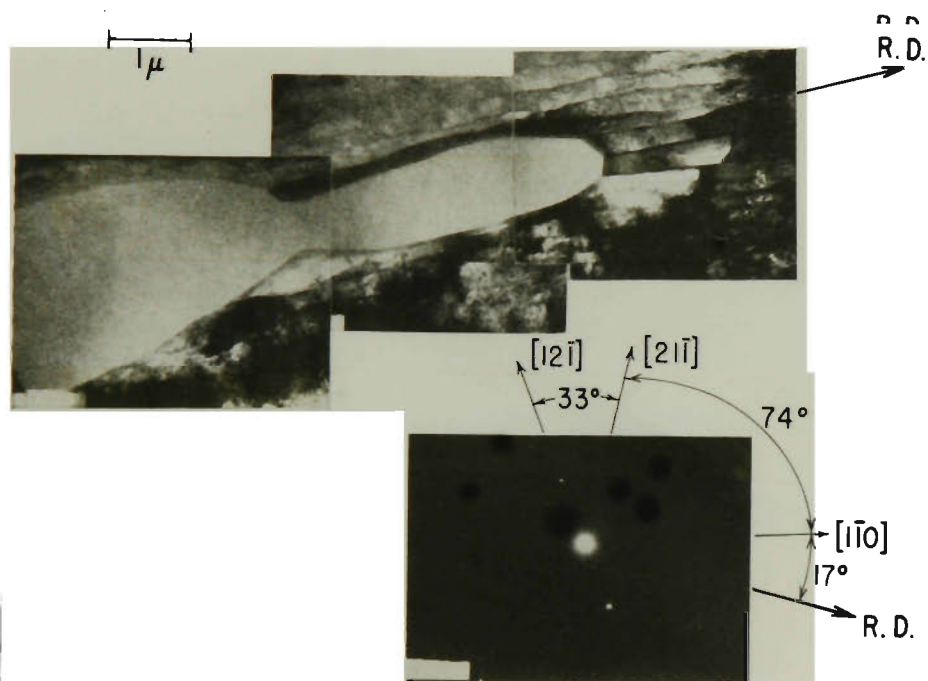


Fig. 2-21 Electron transmission micrograph showing the formation of a crystallized grain through the growth of subgrains within a micro-band region. The orientation of this recrystallized grain is shown by the selected-area diffraction pattern. (001)[100] crystal annealed 125 min. at  $600^\circ\text{C}$ . [ref. 132]

into matrix regions occurred without polygonization (Fig. 2-22) [132]. These observations are in conformity with the results obtained from Talbot's studies [127].

#### 2.2.5.3 Changes in microstructure during recrystallization

No significant changes in the structure of a cold-rolled zone-refined iron were observed before recrystallization [136]. When recrystallization occurred, the nuclei grew directly from the cold-worked matrix. In iron of lower purity no visible change in the structure occurred on annealing at temperatures below 400°C. At 400°C and above, however, some recovery was evident, with certain regions of the specimen becoming "cleaner". The structure of Armco iron (low purity) after severe cold reduction and annealing for 2 hours at 450°C is shown in Fig. 2-23. Compared with the cold rolled structure (Fig. 2-24), the tangled dislocation walls became thinner and sharper. The cells were also cleaner, although they still contained some dislocations. Their relative misorientations, as determined by selected area diffraction, was of the same order as that in the cold-worked state.

Recrystallization proceeded within the recovered structure. A general growth of cells was observed, and, after 2 hours at 550°C, the average size was 5 to 6  $\mu\text{m}$ . Figure 2-25 illustrates the growth of a recrystallization nucleus into the recovered matrix.

The investigation of Messenger and Dimitrov [137,138,139] at Vitry showed that cold-worked high-purity iron and aluminium behaved in a similar manner on annealing. However, the structure of cold-worked, impure aluminium was altered due to recovery. Recrystallization of the recovered matrix occurred by growth of cells created during the deformation process.

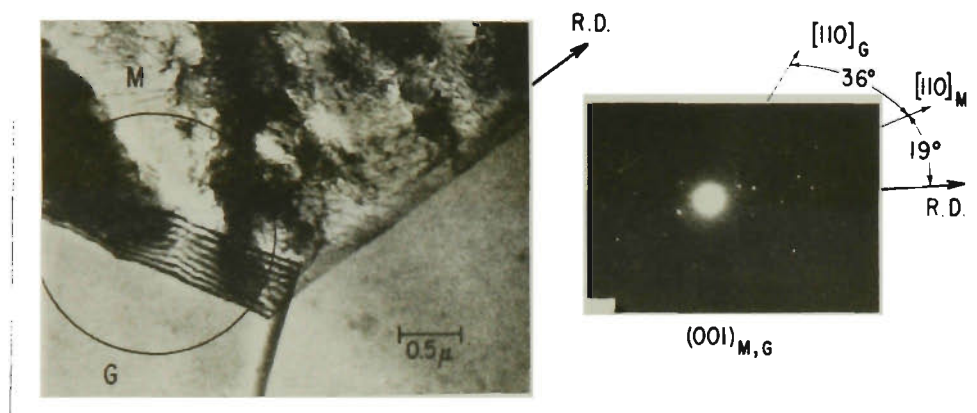


Fig. 2-22 Electron transmission micrograph showing two recrystallized grains that have successfully grown into the matrix region. No subgrain formation is as yet evident in the matrix band region. The selected-area diffraction pattern shows the orientation of one of those two recrystallized grains G superimposed upon the orientation of the matrix M. Circle on the micrograph indicates the size and location of the electron beam used for obtaining the diffraction pattern. The orientation relationship between G and M corresponds to a rotation of 36° around [001] normal to specimen plane. (001)[100] crystal annealed 125 min. at 600°C. [ref. 132]



Fig. 2-23 The structure of Armco iron cold rolled 96% and annealed for 2 hr at 450°C. 20,400x. [ref. 127]



Fig. 2-24 Dislocation structure of Armco iron after cold rolled 96% . 20,400x. [ref. 127]



Fig. 2-25 The structure of Armco iron cold rolled 96% and annealed for 2 hr at 550°C. 20,400x. [ref. 127]

## 2.2.6 Mechanisms of Nucleation during Recrystallization

### 2.2.6.1 Classical theory

Because of the similarities between the recrystallization and phase transformations, many efforts have been made to apply classical nucleation theory to the early stages of recrystallization. However, when reasonable assumptions were made about the values of the grain boundary energy and the bulk free energy difference between the deformed and recrystallized states, the predicted activation energy was higher by several orders of magnitude than expected. Burgers [140] pointed out that deformation is not uniform on a microscopic scale and that high local values of stored energy of cold worked should exist. He calculated that the experimentally observed activation energy for nucleation would require a local increase of ~30-fold in the stored energy of cold work; such an increase is most improbable.

Another "prediction" of the theory is that the new grains should form with low misfit angles relative to the deformed matrix in order to have low interfacial-energy values, since a high interfacial energy leads to a large critical embryo radius. However, it is often found that the orientation of the new grain differs considerably from that of cold-worked "parent" region.

The application of the classical theory to softening requires also that the cold-worked state is metastable with respect to the strain-free state. Oriani [141], however, found that the cold-worked metal was actually unstable and that nucleation in the classical sense was not a necessary step in recrystallization. Therefore, many models and mechanisms of nucleation during softening have been proposed since the classical one is very limited.

### 2.2.6.2 The "Block" theories

In these theories it is proposed that a nucleus block, sufficiently large to grow, already exists within the deformed matrix or can be formed by recovery processes. Two theories have been put forward: the "High Energy Block Theory" in which the block is considered

to be a region of higher than average strain; and the " Low Energy Block Theory" in which the block is envisaged as a region that has remained essentially strain-free during formation [142].

In the high energy theory, some blocks are considered to become nuclei by a gradual healing of the distorted lattice until they obtain the thermodynamic ability to grow. Cahn [143] proposed that the necessary dislocation removal occurred by polygonization, as was confirmed in aluminium and its alloys [144 to 146], iron [147], copper [148] and nickel [149, 150]. Cottrell [151] pointed out that, in these regions, nuclei had a greater opportunity for growth since they could more readily develop the necessary mobile high-angle boundaries.

The stage envisaged in the low energy block theory proposed by Nielson [152] in 1954 is actually the initial polygonization of the deformed lattice in regions of strong curvature, followed by a period of fast subgrain growth caused by the rapid movement of low-angle boundaries between subgrains. Eventually, some of the subgrains reach a size where part of their periphery contains a high-angle boundary which can then migrate rapidly and consume the neighbouring material. Electron microscopy has provided some supporting evidence during recovery and recrystallization of aluminium alloys [146, 153, 154, 155], iron-silicon alloys [156 to 162] and titanium [163]. Subgrains have also been found to act as important nucleation sites in chromium [164], although the precise mechanism involved is not clear.

#### 2.2.6.3 Nucleation by migration of low-angle boundaries

Since Shockley and Read established the equation to calculate the boundary energy [165], many attempts have been made to explain the phenomenon of boundary migration. Data have been published for iron-silicon alloys [166, 167], tin [168], lead [169], silver [170] and silver chloride [171]. The results show that the Read-Shockley equation is obeyed up to misorientations of about 25°. However, there were not sufficient data at very low

misorientations ( $\leq 6^\circ$ ) to check the theory in the misorientation region for which it is most likely to be valid.

Later, the detailed measurements by Gjostein and Rhines [172, 173] showed that the Read-Shockley curve rose more steeply and reached a maximum at lower misorientations than that drawn through data involving high misorientations. In particular, Gjostein and Rhines [172] demonstrated that the boundary energy of low-angle [100] tilt boundaries in copper reaches a maximum at a misorientation of the order of  $\sim 8^\circ$ .

The migration of low-angle boundaries, of both the tilt and twist types, has been studied in a wide range of metals [174 to 180]. It can be summarized into two characteristics: (1) the migration rate is relatively high initially and decreases as growth proceeds; and (2) if the boundary is able to change its form to that characteristic of a high-angle grain boundary the reverse trend in rate would occur. The conclusions seem to support Cottrell's contention [181] that, in order to form a viable nucleus in a region of deformed metal containing subgrains, the boundary around the appropriate "block" of metal must change from a dislocation array, to a conventional grain boundary having a higher migration rate.

#### 2.2.6.4 Polygonization

Polygonization model proposed by Cahn [182] and Beck [183], independently, follows as a result of dislocation climb.

Initially, this process was found in a bent aluminium crystal, as shown in Fig. 2-26. Cahn proposed that polygonization was due to the formation of walls of dislocations at right angles to the planes which had been active (as glide plane) during the original bending. Such walls, if composed of similar edge dislocations would form a tilt boundary having a lower overall strain energy than the more random dislocation arrangement. The driving force for this process was provided by this reduction in strain energy. Both climb and short-range glide of edge dislocations were required to form the

new walls. A schematic representation of the polygonization process is shown in Fig. 2-27 [184]. Edge dislocations forming a tilt boundary triple point are shown in Fig. 2-28 [185].

The basic differences between the formation of a substructure by polygonization during annealing and the formation of subgrains during cold-working have been summarized by Byrne [186] as follows:

- (1) In polygonization an excess of one type of dislocation is required --- such as edge dislocations produced on bending;
- (2) Polygonization is not produced directly during low-temperature cold-working, whereas subgrains, or at least tangled cell walls ( which are their forerunners ) do originate during cold-working.
- (3) Polygonization requires either an elevated temperature anneal, or concurrent creep, or deformation at an elevated temperature; whereas deformation cell formation does not;
- (4) The size of the polygonized substructure is often an order of magnitude larger than that of a typical cell formed during cold-working.

#### 2.2.6.5 Subgrain coalescence by rotation

This theory was developed by Hu [156, 157, 158] during an examination of subgrain growth in cold rolled Fe-Si single crystals using hot stage electron microscopy. In many cases the boundaries between neighbouring subgrains gradually disappeared and the contrast between relevant subgrains decreased. Hu proposed that growth had occurred by coalescence rather than by boundary migration. A coalescence process of this kind would require subgrain rotation leading to the development of identical orientations in adjacent subgrains.

A mechanism for coalescence was proposed subsequently by Li [27] and this is shown schematically in Fig. 2-29. The gradual disappearance of a common boundary occurs by



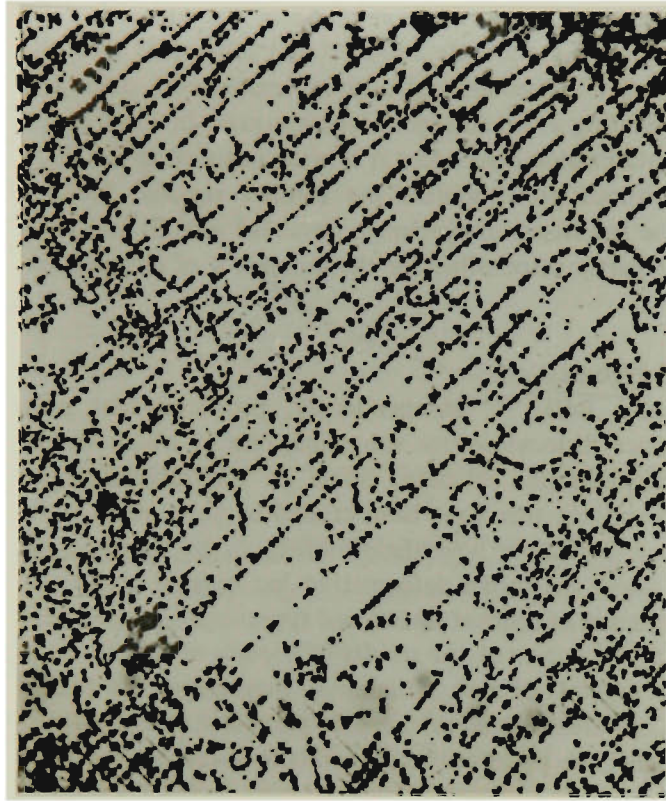


Fig. 2-26 Micrograph showing etch pits in polygonized aluminium. 75x. [ref. 182]

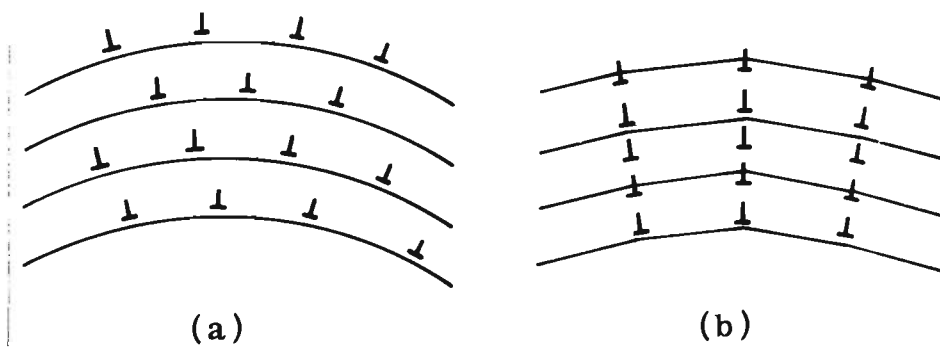


Fig. 2-27 Schematic representation of the polygonization process: (a) random arrangement of edge dislocations, and (b) alignment of edge dislocations to form walls. [ref. 184]

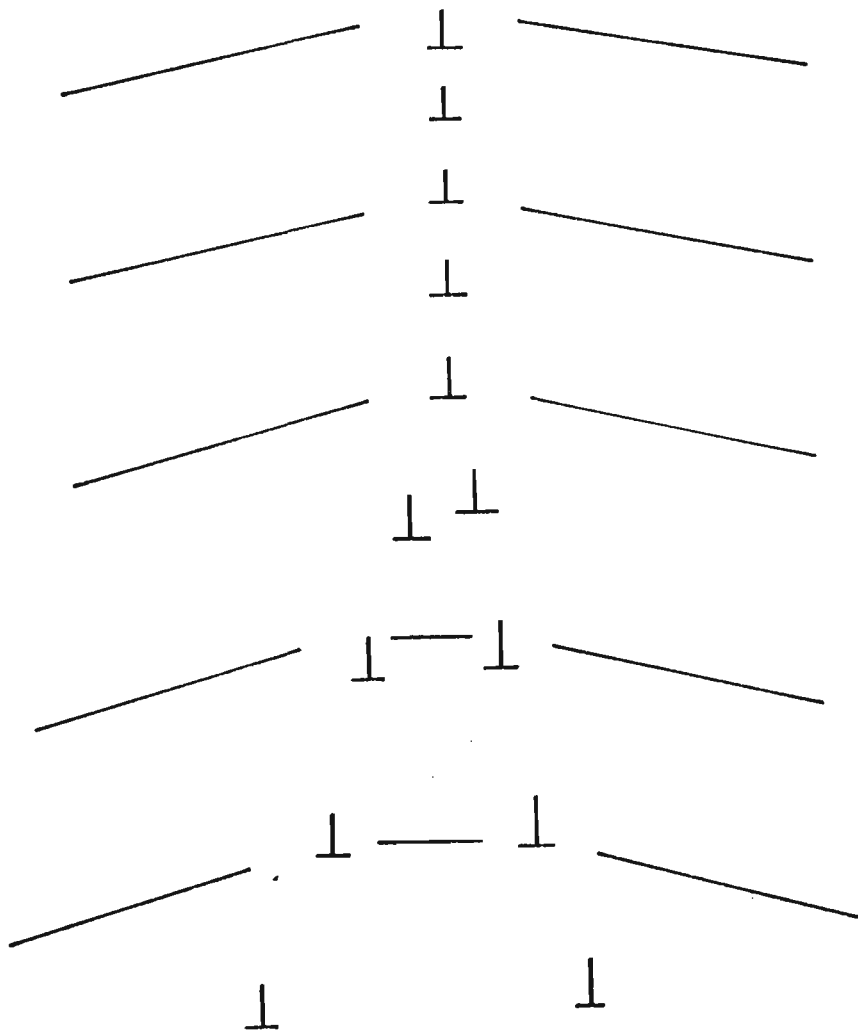


Fig. 2-28 Schematic representation of edge dislocations at a tilt boundary triple point. [ref. 184]

the movement of dislocations from the disappearing boundary into the connecting boundaries around the subgrains. This involves dislocation climb along the disappearing boundary and a rotation of the lattice orientation and requires movement of some of the atoms around the subgrains. Li demonstrated that a process of this nature is feasible, both energetically and kinetically.

The formation of a nucleus by subgrain coalescence is shown schematically in Fig. 2-30. The orientation of the subgrain changes as a result of the elimination of the sub-boundary and in this sense subgrain coalescence differs from the "geometric coalescence" proposed earlier by Neilson [187].

#### 2.2.6.6 Nucleation by grain-boundary bulging

Nucleation by grain-boundary bulging or strain induced boundary migration (SIBM) actually is a migration of a grain-boundary which makes a system more stable by moving a boundary from the higher strain state to a lower one.

This mechanism, postulated by Beck and Sperry [188], is shown schematically in Fig. 2-31. It is assumed, firstly, that the boundary is capable of high mobility by virtue of a large misorientation between the two grains ( A and B in Fig. 2-31 ) which it separates, and, secondly, that there is a significant strain difference ( grain A in Fig. 2-31 is of lower strain than grain B as indicated by the larger subgrain size). In these circumstances the boundary migration is said to be initiated by that part of its length which forms a boundary to one of the large subgrains (S) in the lower strain grain (A). The direction of migration is then away from this grain into the more heavily strained grain B. This leads to a reduction in internal energy which is equivalent to the difference between the stored energy released in the consumed region and the energy required to extend the length of the migrating boundary.

Tiedema [189] observed by x-ray studies that when recrystallization was complete the main portion of a recrystallized grain often consisted of two or more slightly misoriented

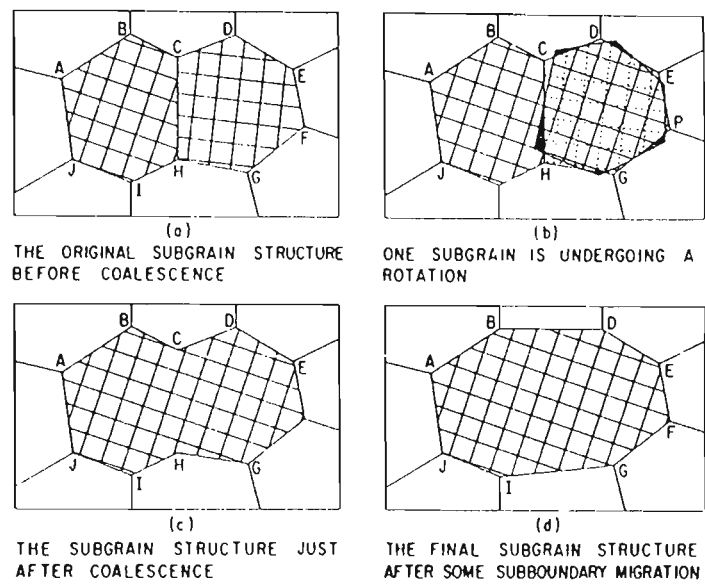


Fig. 2-29 Schematic representation of subgrain coalescence by subgrain rotation. [ref. 27]

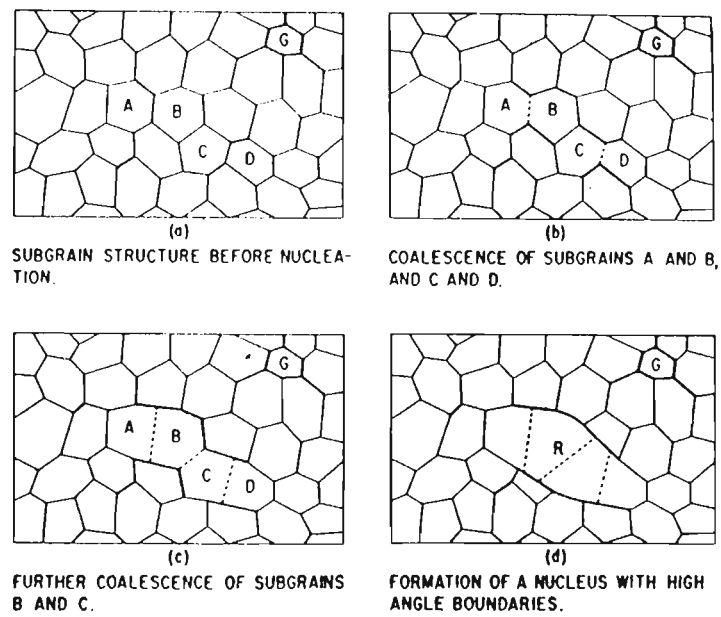


Fig. 2-30 Schematic representation of the formation of a primary recrystallization nucleus by subgrain coalescence. [ref. 156]

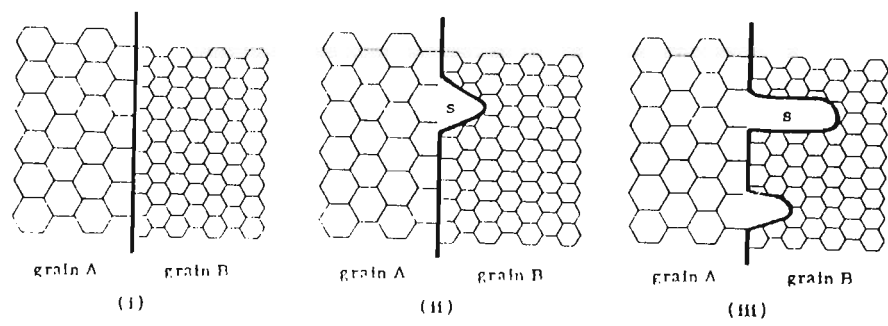


Fig. 2-31 Schematic representation of primary recrystallization by strain-induced grain-boundary migration. [ref. 188]

domains . Crussard [190] and Aust and Dunn [191] confirmed this observation by revealing sub-boundaries, in Fe-Si, on both sides of a grain boundary which was in the process of strain-induced migration. Other support for the bulge mechanism can be found in the work of Vandermeer and Gordon [48, 192] and Bailey and Hirsh [88, 89, 193].

## 2.2.7 Kinetics of Softening

A review of the annealing characteristics of cold-worked materials has been presented in section 2.2. In this section the kinetics of softening will be addressed.

### 2.2.7.1 Recovery kinetics

The detailed nature of the property changes, the associated mechanisms and their kinetics have been due to the work of Leslie [194], Perryman [195], Bever [196] and Li [197]. The following is a brief review of their work on the classical features of recovery kinetics.

Leslie et al. [194] found that in an isothermal annealing treatment the rate of change of a property prior to recrystallization was initially high and decreased continuously as the annealing time continued, as shown in Figs. 2-32 [194] and 2-33 [198]. The same characteristic was found for the release of stored energy in copper ( see Fig. 2-3 in section 2.2.2.1).

The relationship between the activation energy  $Q$  and the annealing time  $t$  can be expressed as follows [199]:

$$A = k t e^{-Q/RT} \quad (2-1)$$

or

$$\ln t = \ln A + \frac{Q}{RT} - \ln k \quad (2-2)$$

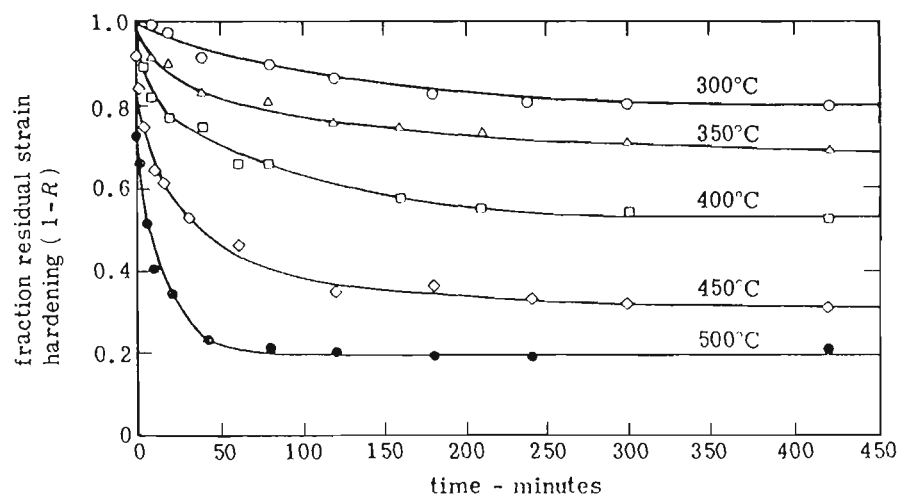


Fig. 2-32 Recovery kinetics for the flow stress of iron at various annealing temperature:  $(1-R)$  represents the fraction of the flow stress increment which remains after annealing. [ref. 197]

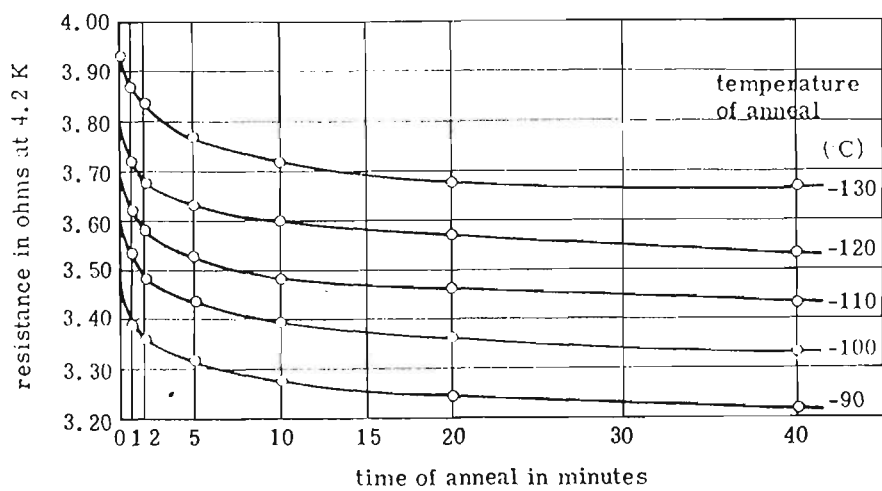


Fig. 2-33 Recovery kinetics for the electrical resistivity of copper at various annealing temperatures. [ref. 198]

where  $A$  is an unknown function of  $(\sigma_m - \sigma_r)$  where  $\sigma_m$  is the flow stress after deformation,  $\sigma_r$  is the flow stress after recovery,  $R$  is the gas constant and  $T$  is the absolute temperature.

Equation (2-2) is valid only when the activation energy has a constant value. However, this is not always the case during recovery. Compared with the work by Leslie [194] and that by Michalak and Paxton [200] it was indicated that the activation energy varies during recovery, close to that for vacancy migration at the start of recovery and to that for self-diffusion in the later stages [201].

Kuhlman-Wilsdorf [202] proposed that activation energy depends on the instantaneous value of the recovering property :

$$\frac{dY}{dt} = -k \exp \left( - \frac{(Q_0 - bY)}{RT} \right) \quad (2-3)$$

where  $Y$  --- the instantaneous value of the recovering property;

$Q_0$  --- activation energy relevant to the final stage of recovery;

$k, b$  --- constants.

#### 2.2.7.2 Recrystallization kinetics

An incubation period during which no recrystallization occurs is followed by a rate of recrystallization which is initially slow, then accelerates and, finally slows down again as the process nears completion. This process is schematically shown in Fig. 2-34; and contrasts with the continuously decreasing rate of change during pre-recrystallization recovery.

The kinetics of recrystallization can be described in terms of the recrystallized fraction per volume and/or the number of nuclei.



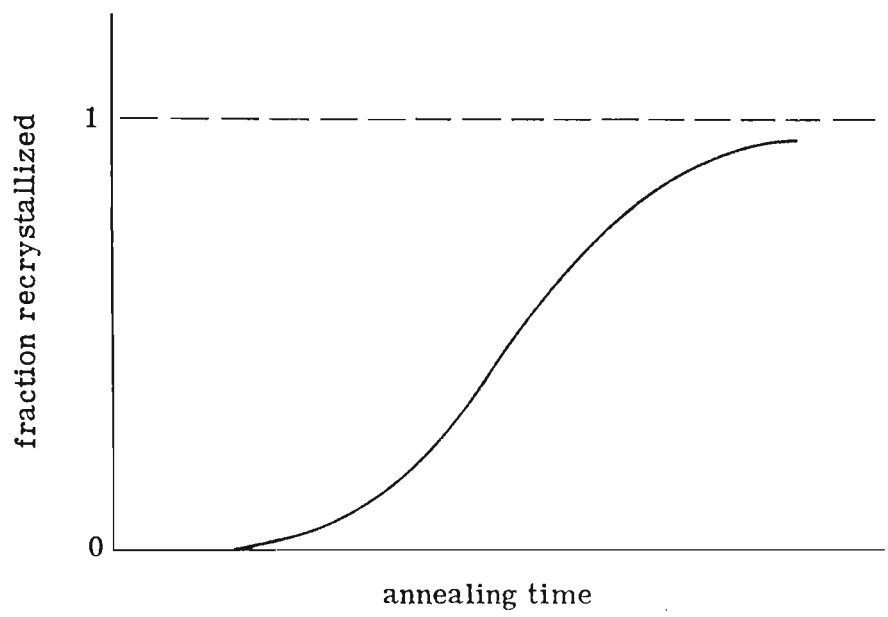


Fig. 2-34 The characteristic form of the progress of primary recrystallization during isothermal annealing. [ref. 207]

Formulations based on recrystallized fraction have been presented by Burke and Turnbull [16], reviewed by Byrne [201] and modified by Johnson and Mehl [202] and also by Avrami [204, 205, 206]. The Avrami relationship between the recrystallized fraction (X) and the annealing time (t) is:

$$1-X = e^{-Bt^k} \quad (2-4)$$

where B and k are constants,  $k = 3$  or  $4$  for three-dimensional recrystallization;  $k = 2$  or  $3$  for two-dimensional recrystallization; and  $k = 1$  or  $2$  for one-dimensional recrystallization.

One example of a kinetic formula based on number of nuclei is [207]:

$$\dot{N} = a e^{-bt} \quad (2-5)$$

where  $\dot{N}$  --- nucleation frequency; a,b --- constants; t --- annealing time.

This relationship between the nucleation frequency ( $\dot{N} = \frac{dN}{dt}$ ) and annealing time t was based on studies of aluminium, previously deformed 3.1% in tension.

Equation 2-5 indicates that the nucleation frequency decreases exponentially with increasing annealing time.

### 2.2.8 The Effect of Chemical Composition on Softening

Several investigators have reported the influence of impurities on the recovery of various properties, but no general effect is apparent. Impurities are also important in establishing the cold-worked state. The hardness, line boardening, and electrical resistivity of Al-Mg alloys were found to increase with increasing magnesium content for a given strain [208] and the subgrain size after deformation decreased as the magnesium content increased. Another investigation showed that the addition of cobalt or titanium to nickel increased the initial flow stress, but not the strain hardening rate, and decreased the cell size for a fixed tensile strain [209]. In the case of iron alloys, manganese increases the as-annealed and

as-cold-rolled hardness of zone-melted iron [210], and alloy hardening of cold deformed ferrite has been reported [211, 212].

Niemark and Swalin [213] demonstrated that the presence of impurities ( $<0.001\%$  K,  $<0.002\%$  Al,  $<0.0003\%$  O, trace Si) in tungsten retarded the recovery of electrical resistivity, particularly at lower temperatures. The activation energy for recovery was increased from 1.7 to 2.3 eV by the impurity content. Strong interactions between point defects and impurity atoms could be responsible.

The work of Kimura et al [214] showed that iron with a enough purity was softened by hydrogen addition at temperatures between 190 and 300K, and hardened below 180K. The softening is due to the enhanced mobility of screw dislocations through the reduction of the Peierls potential. Carbon, and nitrogen, cause softening and hardening in temperature ranges similar to those for hydrogen. The softening is considered to be due to the reduction in the energy for the double kink formation.

Addition of approximate 0.30 atomic-% manganese or molybdenum retarded the softening of high purity iron after 60% cold reduction and annealing [215, 216]. The plot of percentage softening versus percentage of recrystallization for pure iron, Fe-0.31% Mn, Fe-0.315%Mo shown in Fig. 2-35 illustrates that recovery occurs simultaneously with recrystallization and that the total softening at a given amount of recrystallization decreases in the order of Fe, Fe-Mn and Fe-Mo. The difference in fraction of softening for a given fraction of recrystallization must be due to differences in the softening resulting from recovery.

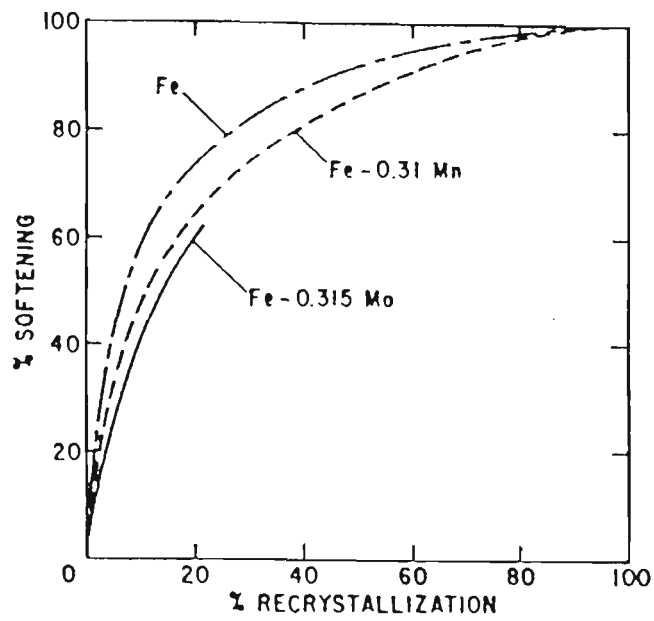


Fig. 2-35 Effect of alloy addition on softening of iron at 595°C. [ref. 215 & 216]

## 2.3 SOFTENING PROCESSES IN IRON AND LOW-CARBON STEELS

The kinetics of softening reviewed in Section 2.2.7 indicate that recrystallization is a growth-controlled process, nucleation does not occur randomly and formation of nuclei by thermal fluctuations does not occur. These conclusions have general applicability and describe that nature of recrystallization in iron and low-carbon steels. The main nucleation mechanisms, which involve the growth of subgrains to the point at which high angle boundaries are formed, have been outlined in 2.2.5 on the basis of references 134, 143, 196, 219, 221 to 231. Again these models are general and apply to ferrous alloys.

### 2.3.1 Studies of Nucleation in Ferrous Alloys

For high purity iron, the growth of subgrains during the incubation period of recrystallization can occur at three types of sites [194]: (1) in the interior of a ferrite crystal; (2) at a high angle boundary; and (3) at an inclusion or a second phase particle.

The nature of subgrains growing within ferrite grains has been analysed by Leslie [194]. The following evidence was provided based on electron microscopy and x-ray examination: (a) subgrains grew in a region in which the misorientation measured in the rolling plane was only  $\sim \pm 2^\circ$ ; (b) the recrystallized grains and the matrix grains had a common [110] direction in zone-melted iron cold rolled 60%, treated at  $450^\circ\text{C}$  for 2 minutes; (c) subgrain growth was driven by the decrease in volume free energy taking account of the increase in surface free energy [217 to 220], giving a critical radius for growth of

$$R < \frac{2\sigma}{\Delta F_v} \quad (2-6)$$

where  $\sigma$  is the surface free energy per unit area and  $\Delta F_v$  is the difference in volume free energy per unit volume. The larger the misorientation between neighbouring cells, the greater the free energy difference due to the local strain gradient, resulting in a smaller critical radius and greater growth rate.

Figure 2-36 shows a recrystallized grain at a high angle boundary in an Fe-0.8%Cu alloy [194]. This situation appears to be identical with that observed by Dunn and Daniels [221] and discussed by Beck [222] (Fig. 2-31) for the migration of high angle boundaries by the growth of a grain with large cells into a neighbouring grain comprised of smaller cells. Fig. 2-37 shows a difference in dislocation density between three grains meeting at a junction. Such differences in dislocation density can lead to growth of the most "clean" grain, giving rise to the type of edge-nucleated recrystallization observed by Vandermeer and Gordon [194].

The third type of site is at inclusions or second phase particles. Although this phenomenon was reported many years ago [223 to 225], it has not received the attention it deserves. A recent investigation [226] confirmed that increasing the number of inclusions can increase the rate of isothermal recrystallization.

### 2.3.2. Studies of Growth of Recrystallized Grains

The Avrami growth rate equation of recrystallization [204 to 206] can be expressed as:

$$X = 1 - \exp (-Bt^n) \quad (2-7)$$

where  $X$  is the fraction recrystallized,  $t$  is the annealing time, and  $B, n$  are constants. This equation has often been used to describe the kinetics of isothermal recrystallization. If the conditions for applicability of this equation are fulfilled, plots of  $\ln \ln(\frac{1}{1-X})$  vs  $\log$  time should produce straight lines of slopes equal to  $n$ . One requirement for use of the Avrami equation is that growth rates be independent of time. Since this condition is not generally fulfilled, it is not surprising that straight lines were not obtained in  $\ln \ln(\frac{1}{1-X})$  vs  $\ln$  time plots for recrystallization of iron [194] and aluminium-copper alloys [227].

Using an impure iron cold rolled to 97% reduction in thickness, Michalak and Hibbard [228] found that growth rate decreased with time at constant temperature and that rate of growth was greater in the length direction than in the thickness direction of the sheet.

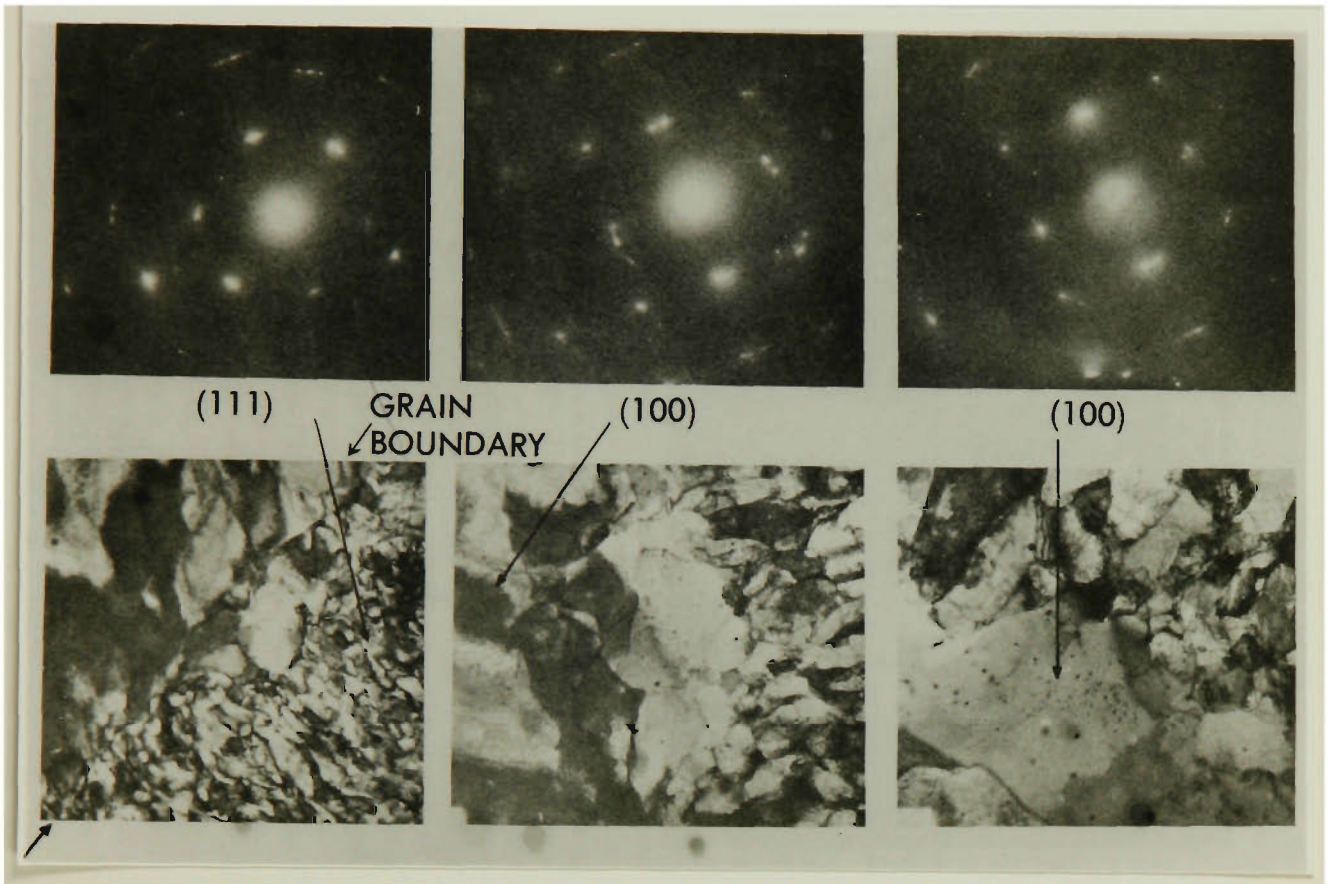


Fig. 2-36 Initiation of recrystallization at a grain boundary, showing migration of a high angle boundary into a grain with fine cell structure. From left to right: 2,600x, 5,200x, and 10,400x. [ref. 194]

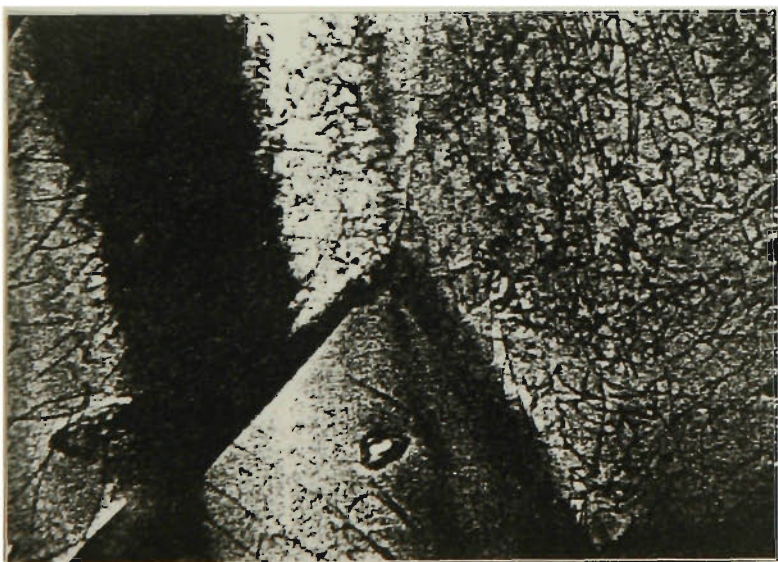


Fig. 2-37 Nonuniform distribution of dislocations in three grains at a junction. Fe-3.25%Si, quenched from 775°C. Electron transmission, 20,000x. [ref. 192]

Despite the much higher reduction used in their work, the initial rates of growth of recrystallized grains were only  $\sim 1/100$  of the rate observed in zone-melted iron [213].

The observation that rate of growth of recrystallized grains in heavily cold-worked iron or aluminium decreases rapidly as a function of annealing time is not necessarily in conflict with the earlier observations that rate of growth in lightly worked iron and aluminium is constant. In a cold-worked metal, recovery and recrystallization are both driven by the stored energy of cold work and, as has been pointed out in the 2.2.2.1. Their relative rates will depend upon the amount and type of deformation, the grain size, cleanliness and purity of the metal, the orientation of the grains with respect to the plastic strain, and the annealing temperature. Thus, after small strains, recovery can be substantially complete before recrystallization begins, leaving a constant driving force for recrystallization and producing a constant rate of growth.



## 2.4 AGEING SUSCEPTIBILITY OF LOW-CARBON STEELS

Strain ageing is an important problem in production of low-carbon deep drawing steels by continuous annealing. In general, strain ageing is due to the existence of solute carbon and nitrogen in steel. Many studies have been carried out on ageing phenomena [229 to 258], including Andrew [229] on rimmed steel, Brun et al. [230] on HSLA steels, Yang et al. [242] on dual-phase steel and Kurihara et al. [256] on steels of different chemical compositions. Little information is available on ageing of decarburized iron after annealing, or ultra-rapid annealing.

Work by Brun et al. has shown that for the continuous annealing of HSLA steels: (1) strain-ageing is reduced in the temperature range of 30 to 200°C when the manganese content of the steels increases or when niobium is added as a micro-alloying element; (2) for Al-killed steels, the residual nitrogen in solid solution is practically zero at the end of the annealing cycle which implies that strain-ageing in these steels is essentially due to residual carbon in solid solution; (3) the absence of intragranular precipitation after strain-ageing at 100°C for 4 hours indicates that the residual unbound carbon concentrations are very low in both the niobium and niobium-free steels.

In another investigation [242], intercritically annealed specimens were aged at room temperature, 70, 120 and 170°C for times up to 7560 hours and the effects of ageing were evaluated by measuring mechanical properties and changes in the stress-strain curves at low strains. The results indicated that intercritical annealing of cold-rolled C-Mn-Si steel produced a much finer dispersion of martensite than does intercritical annealing of normalized microstructures; the ageing at temperature below 100°C results in the precipitation of fine carbide on from dislocations in the retained ferrite matrix, while precipitation does not occur in the epitaxial ferrite immediately adjacent to martensite; the ageing at above 100°C results in the precipitation of cementite on dislocations and a reduction in dislocation density in the dual-phase steel; long time ageing at room temperature decreases ductility but ageing at higher temperatures increases ductility;

ultimate tensile strength goes through a maximum and yield strength continuously increases with ageing time at ageing temperatures up to 170°C; ageing of intercritically annealed steels causes the development of increasing Lüders strain with time as reflected in the inflections in stress-strain curves at low strains; cold rolling prior to intercritically annealing accelerates ageing by producing finer dispersions of martensite.

One way of improving the anti-ageing property is by an overageing treatment, as discussed by Andrews [229] and Kurihara et al. [256]. They found that the anti-ageing property could be improved by decreasing solute carbon via carbide precipitation. Chemical composition affects carbide precipitation and is therefore important in the reduction of solute carbon. The effect of chemical composition and heat treatment conditions on the precipitation rate can be summarised as follows:

- (1) the rate of precipitation of carbide is affected by silicon, manganese, phosphorus and sulphur but not by carbon and solute Al: the rate decreases with an increase in silicon, manganese, and phosphorus content, but it increases with an increase in sulphur content;
- (2) the effect of sulphur can be associated with a change in solute Mn: a decrease in solute Mn leads to an increase in the precipitation rate;
- (3) the relationship between overageing temperature and precipitation rate is established for steels with various solute carbon content after rapid cooling;
- (4) the carbide dispersion and distribution changes with variation in steel chemistry and/or cooling condition; For high precipitation rates, carbide has in a high distribution density.

## 2.5 RAPID AND ULTRA-RAPID ANNEALING OF IRON AND LOW-CARBON STEELS

In general, the maximum heating rate associated with rapid annealing is about 500°C/sec. and commercial continuous annealing processes commonly operate at rates lower than this. Ultra-rapid annealing refers to processes with rates in excess of about 500°C/sec. The following sections cover the development of rapid and ultra-rapid annealing methods by discussing heating methods (2.5.1), the development of the continuous annealing process (2.5.2), laboratory investigations (2.5.3), the influence of heating rate (2.5.4) and the structure and mechanical properties of steels after rapid annealing (2.5.5).

A basic problem in rapid and ultra-rapid heating is the accurate recording of the true sample temperature which is influenced by the heating method and the heat transfer geometry of the system. Temperature measurement and distribution and heat transfer geometry will be discussed in detail in Sections 2.6 and 2.7.

### 2.5.1 Methods of Heating

Factors that must be considered in the selection of the heating method include (1) the desired operating temperature; (2) the principal mode of heat transfer, i.e., radiation, conduction or convection of both source and sink; (3) the heating rate; (4) the uniformity of temperature or achievement of desired temperature gradient; (5) the allowable variation in sample temperature; (6) furnace atmosphere, chemistry and pressure; (7) convenience, life of use, ease of repair and cost.

The heating methods most frequently used [259] are (1) indirect heating with a metallic or conductive refractory element, including a salt bath; (2) direct resistance heating of the metal in wire, rod or sheet form; (3) induction heating; (4) electron beam; (5) arc or heat source imaging; (6) fluid bed heating and cooling techniques; (7) plasma techniques.

Research by Bakish et al. [260 to 261] on these heating methods indicated that the heating rate is limited by the allowable thermal stress in the part for electron beam heating, while arc or heat source imaging furnaces are normally used in melting and high temperature property determination of refractory metals and non-metallic refractory compounds. In the latter type of equipment, the temperature and the heating rate are very difficult to control. Fluid bed heating and the high intensity or plasma arc heating cannot achieve very high heating rate and generally they are used for purposes other than rapid heating.

Work by Andrews [6] showed that increasing the heating rate up to  $1600^{\circ}\text{C}/\text{sec}$ . by using salt bath and induction heating methods raised the rate of softening and lowered the recrystallization temperature range of cold rolled steel.

More recently, Spunar [9] showed that heating rates between  $1000$  and  $5000^{\circ}\text{C}/\text{sec}$ . could be obtained by resistance heating. He also stated that higher heating rates up to  $10,000^{\circ}\text{C}/\text{sec}$  were possible.

### 2.5.2. Development of the Continuous Annealing Process

There are currently two commercial processes for annealing of cold-rolled metals: batch annealing and continuous annealing. Particular attention has been given to the continuous annealing process because of the high productivity and variety of products.

The first commercial continuous annealing facility was commenced in 1936 to produce cold-rolled steels for tin plate. The output of tin plate produced by continuous annealing increased rapidly between 1955 and 1965 [263]. Continuous annealing is also used to produce galvanized sheet steels [264] and deep drawing steels [265]. However, those products are not normally characterized by high ductility and formability and batch annealing is still used for the production of highly ductile steels.

In 1972, new technology was developed in Japan which combined continuous annealing with an overageing treatment for production of sheet steels of similar quality to batch

annealed products [266, 267]. Since then, several developments in continuous annealing technology have occurred, and many continuous annealing lines have been constructed [268 to 278].

The continuous annealing thermal cycle for mild steel has two metallurgical objectives. Figure 2-38 shows that the rapid heating and soaking steps aim at obtaining a desired grain structure after recrystallization and grain growth, and also an appropriate annealing texture for good deep drawability. The rapid cooling and overageing steps, subsequent to annealing, serve to promote the precipitation of solute carbon dissolved during the preceding steps and to control the distribution and size of the cementite particles [2, 279 to 282]. In batch annealing, the coil is furnace cooled at a very slow rate after annealing, which allows carbon to precipitate during cooling. Therefore, the overageing treatment peculiar to continuous annealing plays a role equivalent to furnace cooling in batch annealing.

The metallurgical background of continuous annealing was discussed in the Met. Soc. AIME symposium on Metallurgy of Continuous Annealed Sheet Steels in 1982 [283], and later in 1984 [284]. The discussions led to two definite conclusions: one is that new continuous annealing technology has wide implications for steels treated by newly developed refining technologies (to reduce impurity elements) and for proper hot- and cold-rolling practice. The other is that although different continuous annealing lines may employ radically different cooling mechanisms, reducing the solution of carbon during annealing remains important and alternative process mechanisms are desirable.

One possible approach is the suggestion by Andrews and Atkinson [8] that recrystallization can be completed before the occurrence of carbon solution by using very high heating rates, typical of those associated with ultra-rapid annealing.

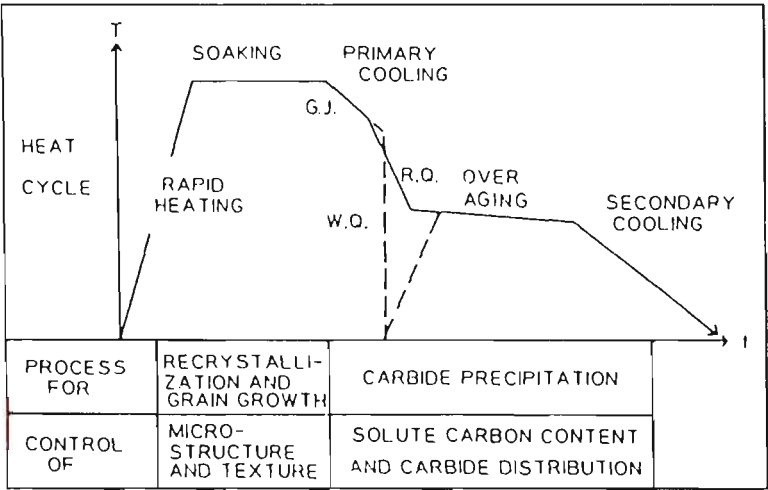


Fig. 2-38 Typical heat cycle of continuous annealing. [ref. 2]

### 2.5.3 Laboratory Investigations of the Rapid and Ultra-rapid Annealing Process

Laboratory investigations of ultra-rapid annealing have been reported by Andrews and Atkinson [6, 8, 285, 286], L'vov [38], Cieslak [287], Dewsnap [288] Williams [289, 290] and Garber et al. [291 to 293]. All of these investigations used salt bath and induction heating methods, which can provide heating rates up to 1600°C/sec. Ultra-rapid annealing investigations, involving resistance heating, were commenced in the 1980's. Research has been carried out by using a resistance heating method [7, 9, 41, 294 to 296], but there is little published information.

Investigations into the ultra-rapid annealing of steel strip by L'vov [38] and Staüb and Cieslak [287] by using salt bath and induction heating methods proved that it was possible to completely recrystallize steel in a fraction of a second if high heating rates were used. However, the short soak time and rapid cooling characteristic of these treatments resulted in a fine grain size because of limited grain growth. Quench age hardening was also a problem due to the ferrite becoming supersaturated with carbon on cooling to room temperature. Another problem with cycles of quick heating and rapid cooling in Al-killed steels is that the heating time available is not sufficient to obtain very fine precipitates of AlN which lead to the development of the {111} recrystallization texture desirable for quality drawing steels sheets. All these mechanisms lead to a reduction in the drawability of the steel.

The solutions usually used to overcome the three problems mentioned above are: (1) to promote grain growth by minimizing the precipitates which pin the growing grain boundaries, by controlling the chemistry or by raising the temperature; and (2) to prevent an increase in solution of carbon in ferrite. The amount of carbon dissolved can be minimized by using a low annealing temperature and minimum holding time at the recrystallization temperature. The use of decarburized steel satisfies both of these requirements.

Work done by Spunar et al [7, 9, 41] showed that the greater the heating rate between 1000 and 5000°C/sec. used in ultra-rapid annealing, the lower the recrystallization temperature ( shown in Fig. 2-39). The change in behaviour at such high heating rates may indicate a change in the softening mechanism. But, unfortunately, these workers only paid attention to the temperature measurement, and not structural aspects of the phenomenon. This "accelerated recrystallization" could result in the microstructure, physical and mechanical properties of ultra-rapid annealed materials being different from those resulting from conventional annealing.

#### 2.5.4 Influence of Heating Rate on Softening

The relationship between heating rate and temperature determined by Andrews and Atkinson [6, 8] using both salt bath and induction heating of rimmed steels, cold reduced 68% is shown in Fig. 2-40. The data in Fig. 2-40 indicate that varying the heating rate in the range 10 to 80°C/sec. had no significant effect on recrystallization, which started at ~550°C and was finished at ~700°C. When the heating rate was increased to 300°C/sec., however, apparent softening due to recrystallization was not detected until the temperature exceeded 700°C, i.e. the recrystallization temperature was raised as the heating rate increased. Further increasing the heating rates above 300°C/sec. up to the maximum of 1600°C/sec. caused a lowering of the recrystallization temperature to the extent so that, at the fastest heating rate of 1600°C/sec. softening was essentially complete when the specimens reached 675°C. Therefore, the recrystallization temperature underwent a maximum value at ~300°C/sec. It should be pointed out that Andrew and Atkinson only paid attention to the lowering of recrystallization temperature period after 300°C/sec. and did not discuss nor attempt to explain the phenomenon of the recrystallization temperature peak at ~300°C/sec.

Other data have been reported by Mohri [297] for heating rates in the range 25 to 100°C/sec. Mohri concluded that changes in heating rate in this range had no effect on the recrystallization behaviour of an 80% cold reduction low carbon steel. He observed



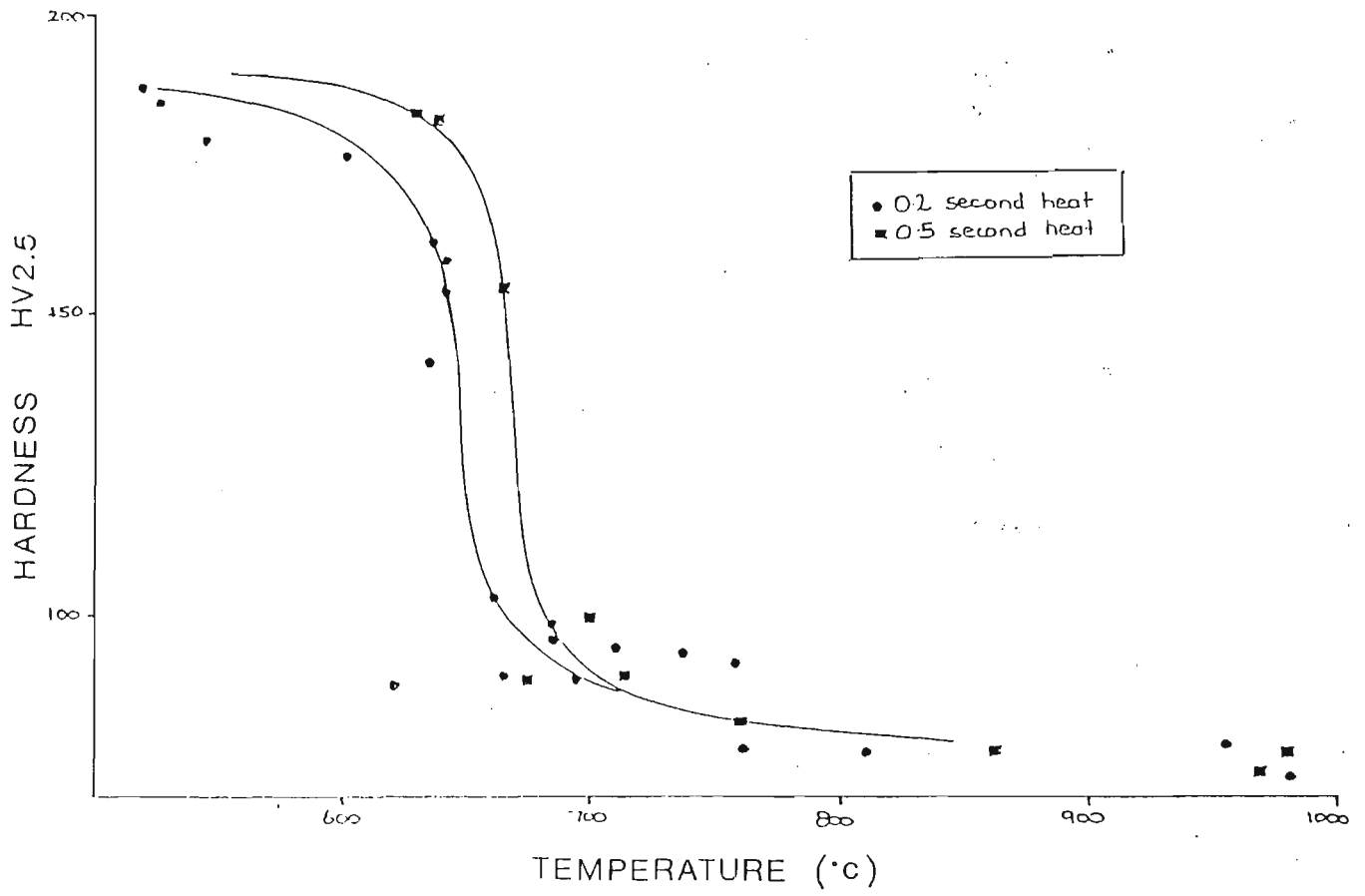


Fig. 2-39 Effect of maximum temperature on hardness. [ref. 9]

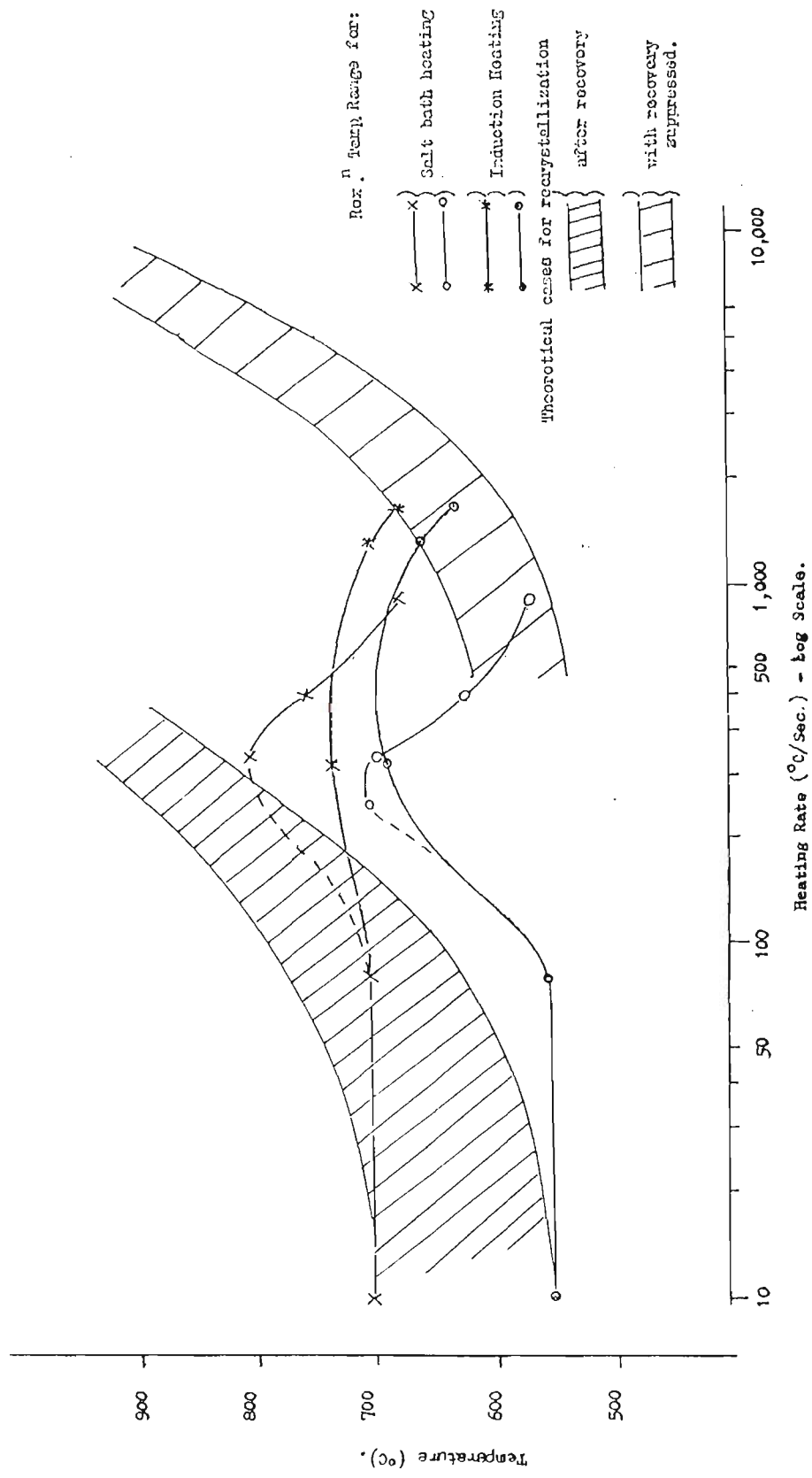


Fig. 2-40 Effect of heating rate on recrystallization temperature range. [ref. 6]

that, irrespective of heating rate, new strain free grains were formed in this material at 595°C and that recrystallization was not completed until a considerable time (normally > 25 seconds) had been spent above this temperature. Mohri's findings were not confirmed, however, in the work conducted by Williams [298], who observed that complete recrystallization could be obtained by heating the specimens to 700°C for 1 second. The accelerated recrystallization reported by Williams was detected by L'vov [299], who found that specimens heated to 675°C at a heating rate of 1250°C/sec. were completely recrystallized.

The effect of heating rates on recrystallization has also been investigated by Staüb and Cieslak [300], who metallographically examined specimens of an 80% cold reduced low carbon steel quenched from 850°C and observed a completely recrystallized structure after heating at rates in the range of 7 to 100°C/sec. Higher rates between 1000 and 5400°C/sec. resulted in only partial recrystallization.

The heating rate also has an effect on  $\alpha$ - $\gamma$  transformation. A study by Albutt and Garber [293] showed that for a 0.086%C steel with a fine spheroidal carbide dispersion and a eutectoid steel,  $A_{c1}$  rose linearly with logarithmic heating rate ( Figs. 2-41 and 2-42) at moderate rates of heating up to ~100°C/sec. At higher heating rates, this linear relationship became apparent with the fine carbide distribution steel (Fig. 2-43) and with the eutectoid steel (Fig. 2-42). The effect of heating rate on the allotropic transformation temperature in pure iron is illustrated in Fig. 2-44, which shows that the starting temperature of the  $\alpha$ - $\gamma$  transformation is insensitive to heating rate over the range plotted. There does appear, however, to be a time-dependent component of the reaction which prevents complete transformation at one temperature. The independence of the transformation start temperature of the heating rate is inconsistent with the theory of nucleation and growth [293].

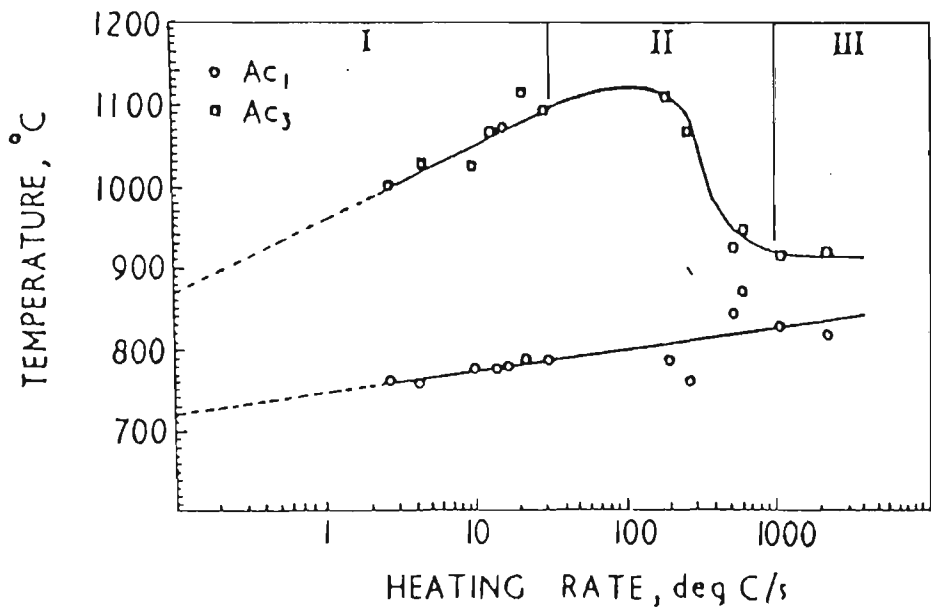


Fig. 2-41 Elevation of critical temperatures with heating rate for a 0.086%C steel with a coarse carbide distribution. [ref. 293]

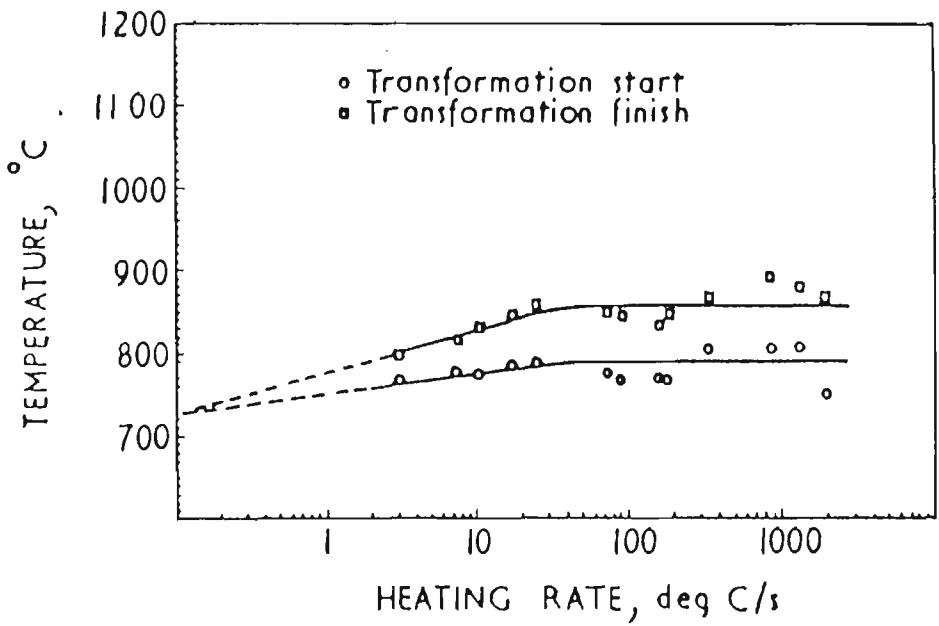


Fig. 2-42 Effect of heating rate on the eutectoid temperature of a 0.79%C steel. [ref. 293]

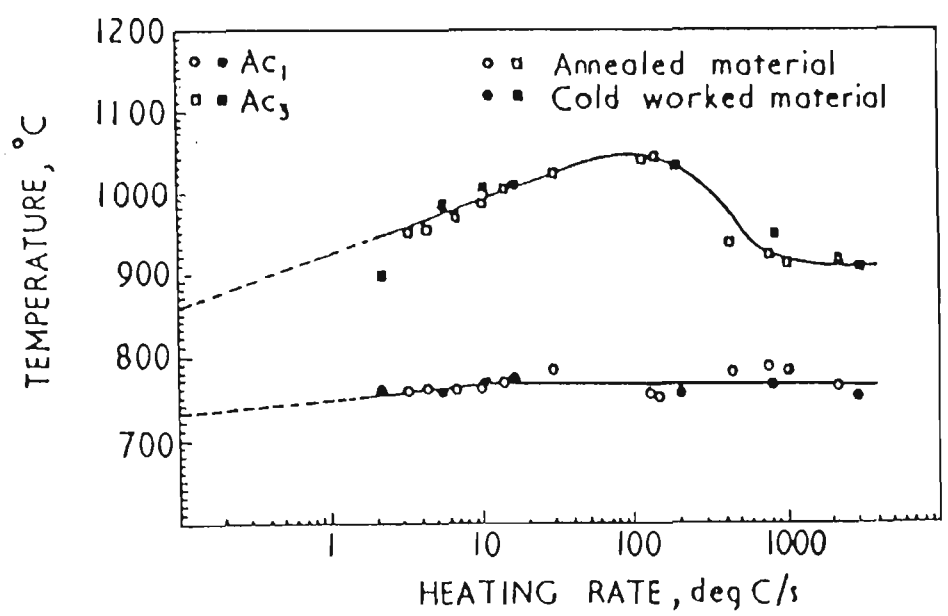


Fig. 2-43 Elevation of the Ac<sub>1</sub> and Ac<sub>3</sub> with heating rate for a 0.086%C steel with fine spheroidal carbide structure. [ref. 293]

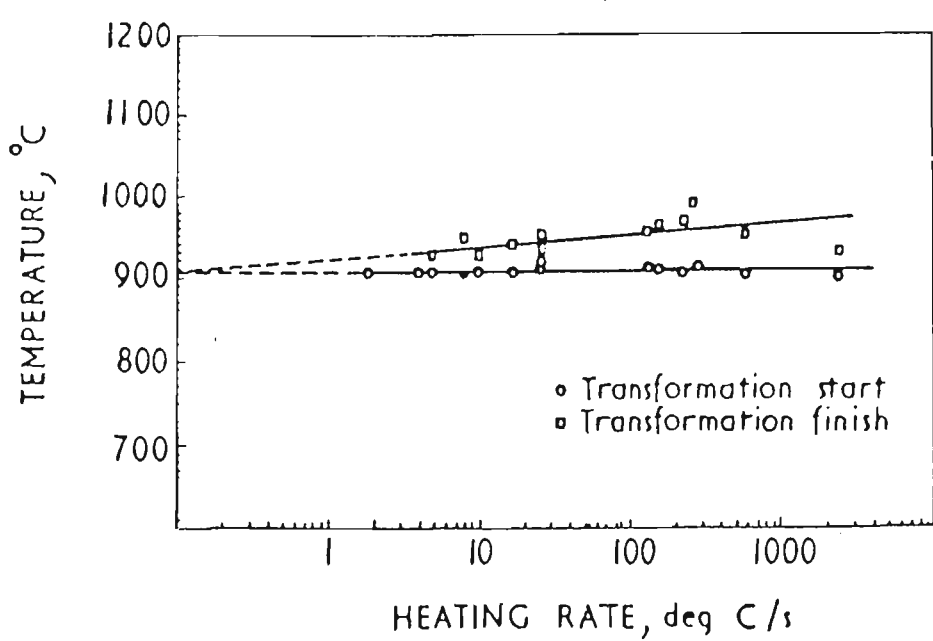


Fig. 2-44 Effect of heating rate on the allotropic transformation temperature of BISRA pure iron. [ref. 293]

The phenomenon of accelerated recrystallization is difficult to explain from the available information, but two tentative explanations can be drawn from the literature: the "recovery-suppressed" mechanism and the "hot-working" mechanism.

The "recovery-suppressed" mechanism [6] assumes that the normal sequence of changes in structure and properties during annealing is consistent with that in recovery processes at low temperatures and that in recrystallization processes at high temperatures. Raising the temperature of the system will result in accelerated processes but, according to Blanter et al. [301], differences in the process rate for recrystallization and recovery, shown schematically in Fig. 2-45 will determine which process dominates. The cross point is  $T_x$ . At temperatures below  $T_x$ , the recovery process is kinetically more favoured than recrystallization, while above  $T_x$  the reverse is true. It is therefore feasible that by very rapid heating to a temperature above  $T_x$ , recrystallization might develop more intensively than recovery, leading to the retention of sub-microscopic imperfections up to the temperatures at which recrystallization is possible, and thereby, increasing the driving force for nucleation.

The "hot working" mechanism was proposed by Andrews [6] with reference to Stüwe's idea [302] which showed that the use of very rapid heating rates to high temperatures can create conditions which may be likened to those existing during hot working where softening is believed to occur simultaneously with deformation. Stüwe [302] proposed that softening during hot working occurs not by recrystallization, but by recovery processes characterised by homogeneous softening throughout the matrix. Recrystallization, on the other hand, involves the growth of new grains at the expense of deformed structures to form a new matrix. Under these conditions and at any given time during the process of recrystallization, there are local areas in the metal that have already softened and others that have not.

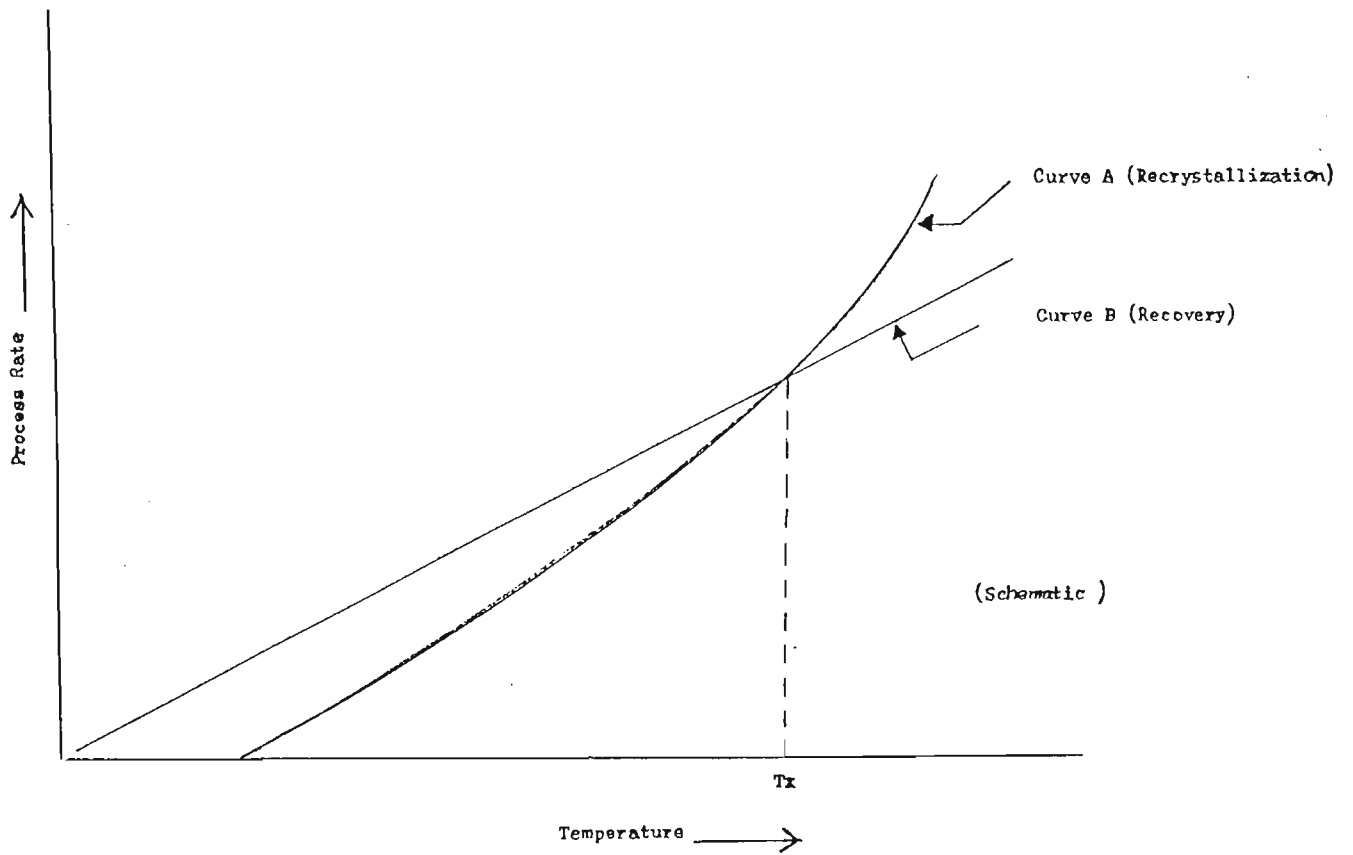


Fig. 2-45 Schematic representation of the process rate of both recrystallization and recovery with temperature. Note the cross point is  $T_x$ . [ref. 6]

2.5.5 Structures and Mechanical Properties Resulting from Rapid and Ultra-rapid Annealing

Normally, short heat treatment involved in the continuous annealing process results in a product that is too hard and lacks sufficient ductility for forming uses in gauge products, mainly because the fast heating results in a finer grain size, as compared with batch annealed products. While L'vov [38] and Ivanov and Osipov [303] claimed that the recrystallization proceeds more rapidly with increasing heating rate, Niebch [304] pointed out the importance of cold reduction and annealing temperature, which are directly related to the structures and mechanical properties of materials.

Dewsnap [305] studied the effect of grain size and cold reduction on strength properties of batch annealed materials, as shown in Figs. 2-46, 47, 48, and 49. It was reported that the initial grain size and cold reduction exert a larger effect on yield point than on the UTS of rimmed steels. In this connection Cracknell and Petch [305] have shown that the lower yield point of mild steel is proportional to  $d^{-1/2}$ , where d = grain diameter. As demonstrated by other workers [303, 306], the effect of cold reduction has a strong influence on the yield point after annealing for both relatively slow and rapid annealing cycles, because of reduced ferrite grain size. In terms of U.T.S (Fig. 2-46) and lower yield stress (Fig. 2-49), the 40% cold reduced sample compared well with a similar grade after batch annealing (see Table 2-3).

Table 2-3 Mechanical properties of commercial batch annealed materials (refer to [276])

Qualities	Yield Stress (MPa)	U.T.S (MPa)	Total Elongation on 2 in. (%)	Rockwell hardness 'B'
Extra deep drawing	183.92	319.20	39	48
Deep drawing	203.68	338.96	37	52
Drawing	224.20	360.24	35	55



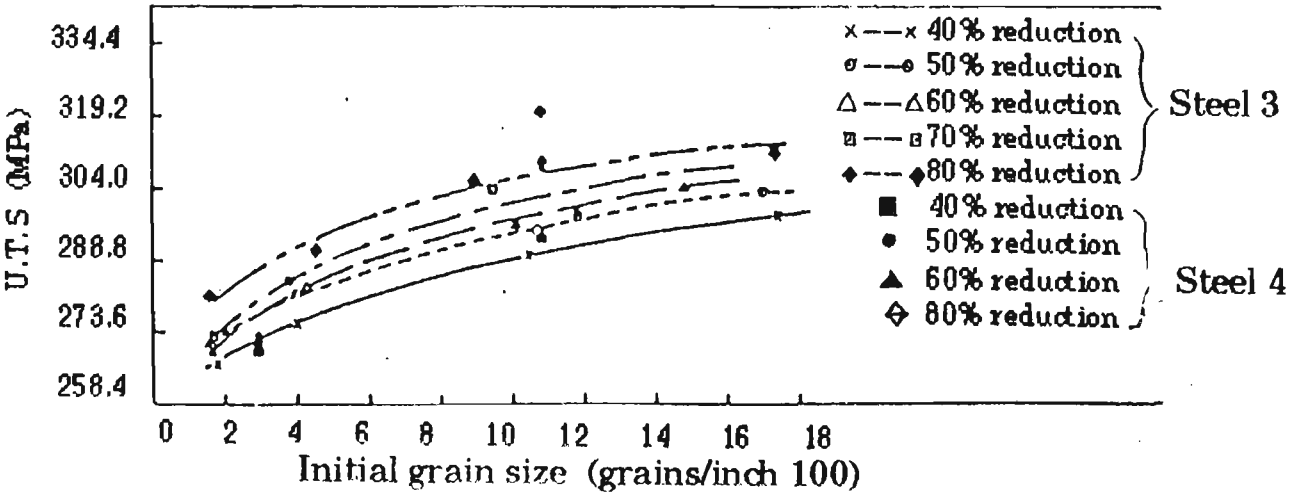


Fig. 2-46 Effect of grain size and cold reduction on the ultimate tensile strength of gauge mild steel. [ref. 288]

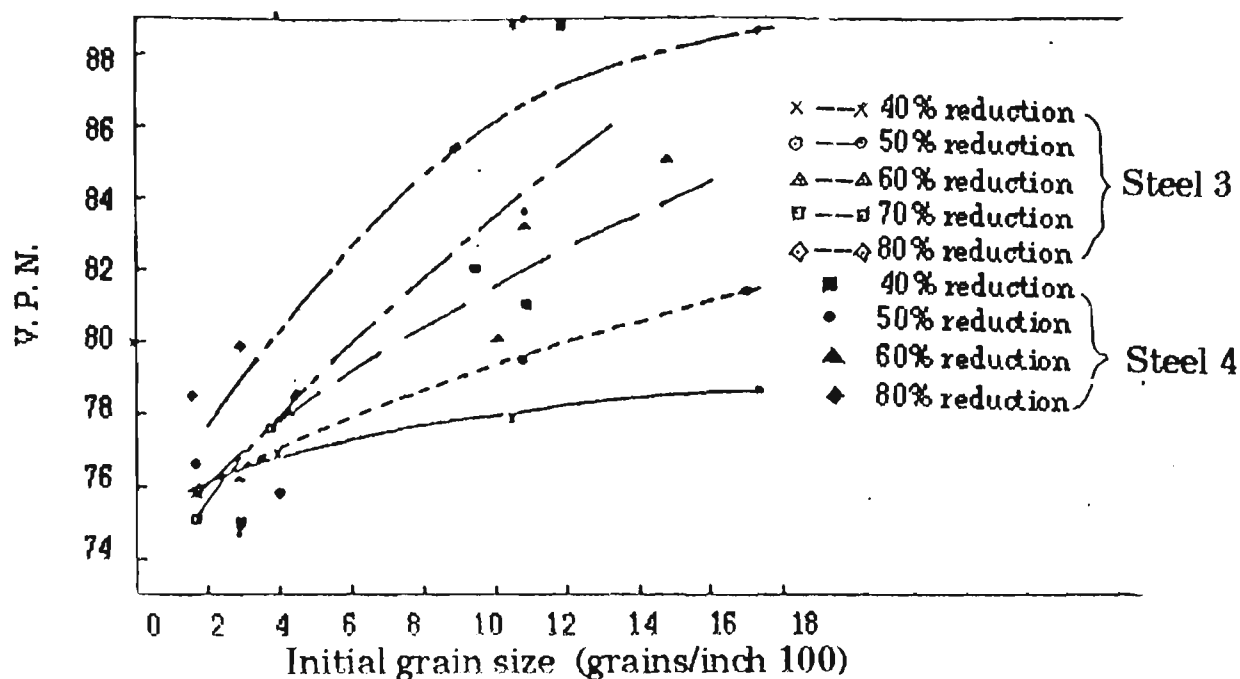


Fig. 2-47 Effect of grain size and cold reduction on hardness of gauge mild steel. [ref. 288]

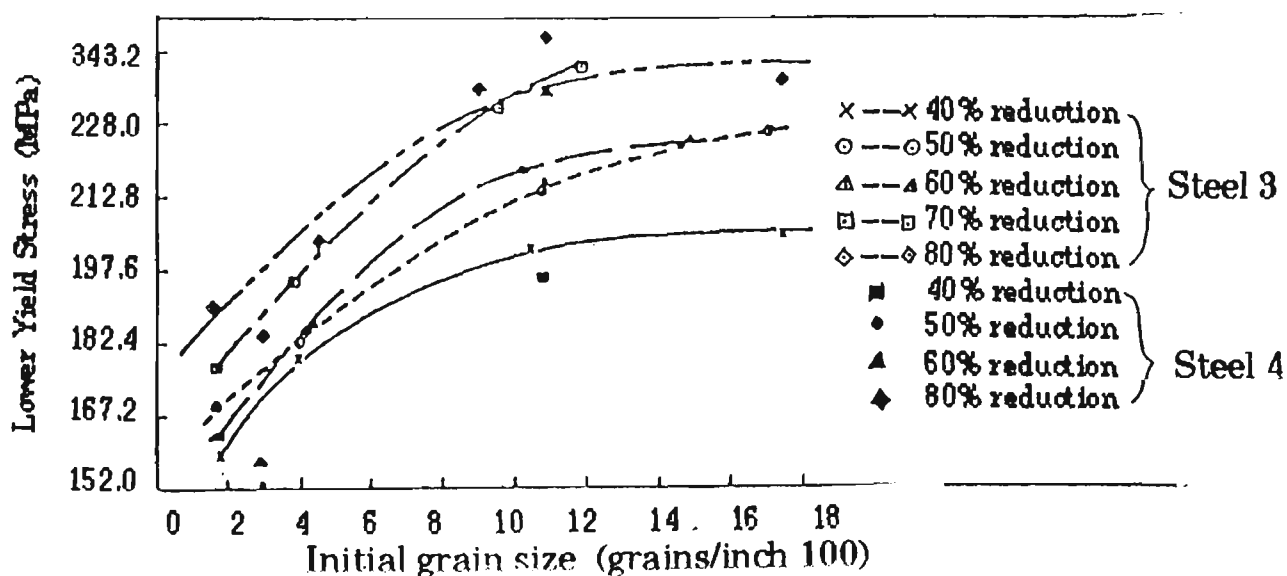


Fig. 2-48 Effect of grain size and cold reduction on lower yield point of gauge mild steel. [ref. 288]

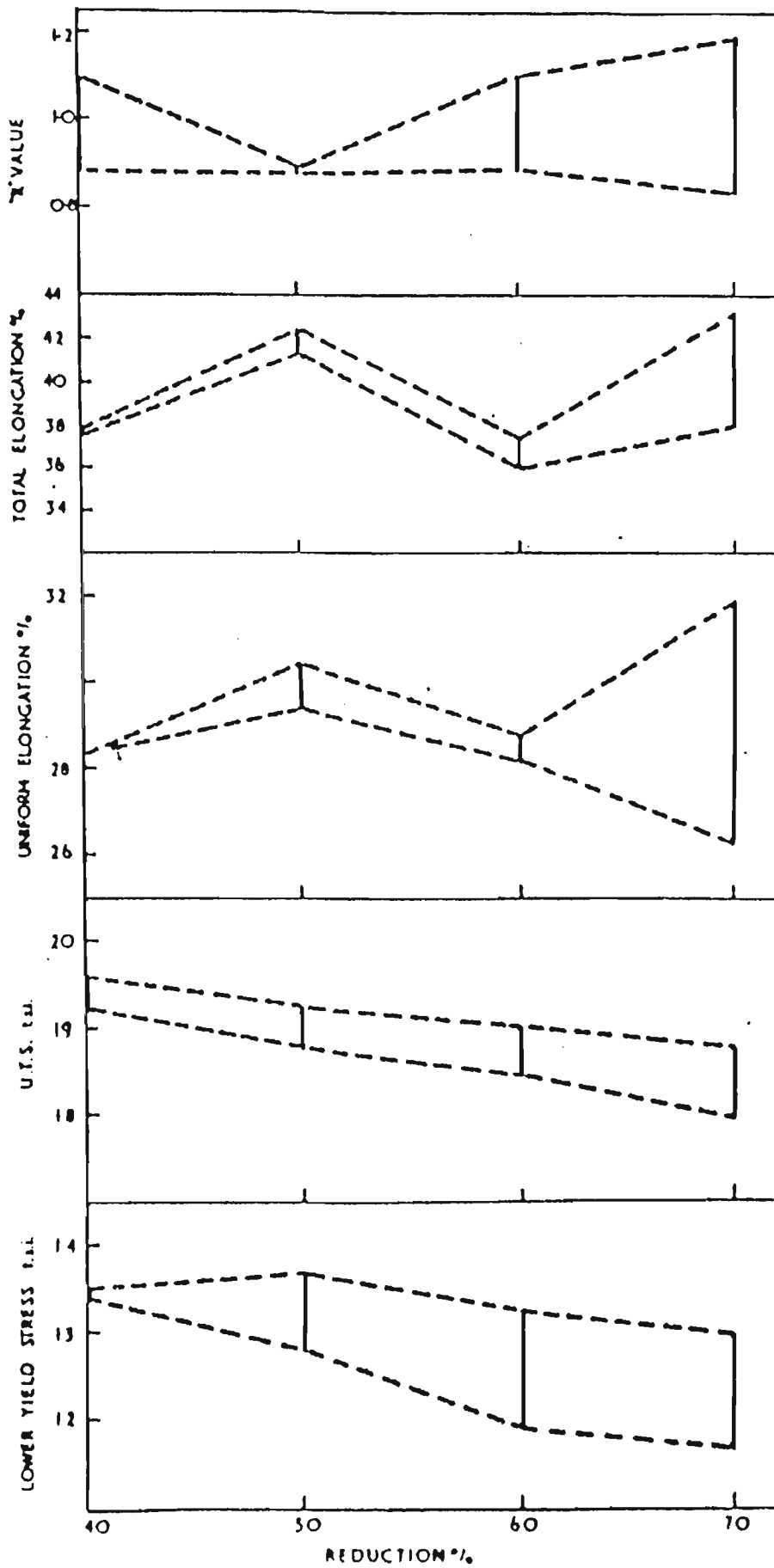


Fig. 2-49 Effect of cold reduction on mechanical properties of gauge rimmed mild steel. ( Summary). [ref. 288]

Hardness is another important mechanical property during the investigation of rapid annealing. Figure 2-50 illustrates the results of a micro-hardness survey carried out on a material heated at  $915^{\circ}\text{C}/\text{sec.}$  (to  $625^{\circ}\text{C}$ ) and brine quenched (before the completion of softening ) [6] and shows that there exist two definite hardness peaks suggestive of softening due to recrystallization. Furthermore, specimens subjected to a low temperature heat treatment ( 1 hour at  $480^{\circ}\text{C}$  ) to ensure that considerable recovery had occurred prior to anisothermal recrystallization ( carried out in a salt bath set at  $900^{\circ}\text{C}$  ) exhibited a softening curve which is compared in Fig. 2-51 with other specimens of the same material which had not been subjected to the low temperature heat treatment. The results presented in Fig. 2-51 indicate that when low temperature recovery is allowed to proceed unsuppressed, recrystallization processes are significantly retarded.

The ultra-rapid annealing of iron and low-carbon steel by Spunar et al.[7, 9, 41] using resistance heating did not yield satisfactory results and explanations of the effect of microstructure on mechanical properties. The only reported work appears to be that due to Garber and Albutt [306] who made a brief study of the properties obtained in a 0.088% C rimmed steel of gauge 0.006-0.04 in., resistance heated at  $200^{\circ}\text{C}/\text{sec.}$  to  $1000^{\circ}\text{C}$  and immediately quenched in agitated brine. The results of that investigation are presented in Fig. 2-52, from which it can be seen that combinations of strength and ductility can be produced, even in the 0.04 in. thick material.

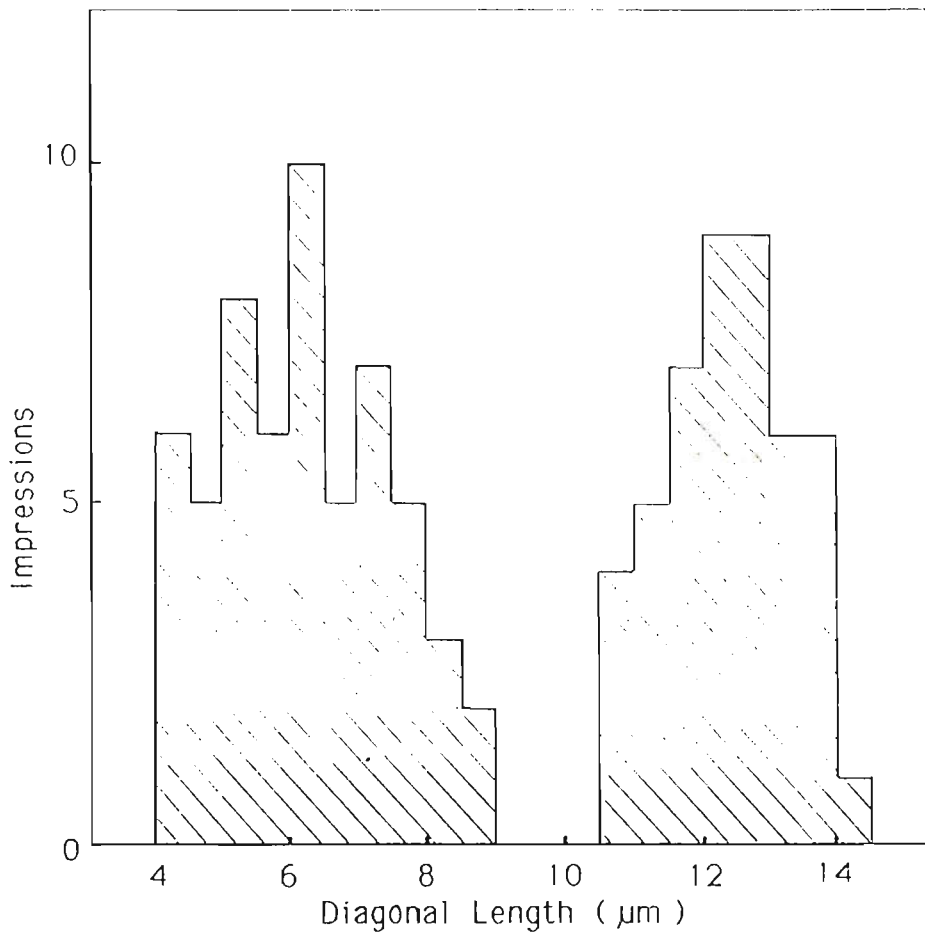


Fig. 2-50 The results of a microhardness survey carried out on sample heated at 915°C/sec. (to 625°C) and brine quenched. [ref. 6]

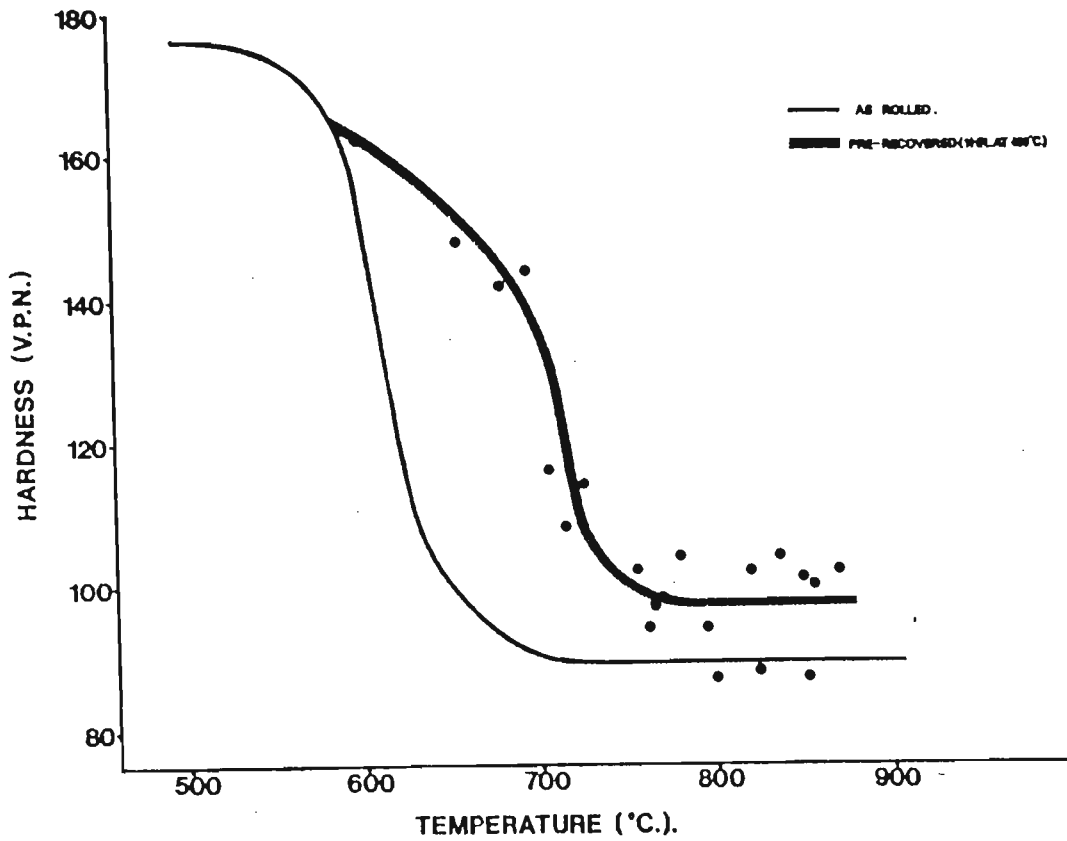


Fig. 2-51 Comparison of the overaged hardnesses of rolled material with pre-recovered material, showing that recrystallization processes are significantly retarded when low temperature recovery is allowed to proceed unsuppressed. [ref. 6]

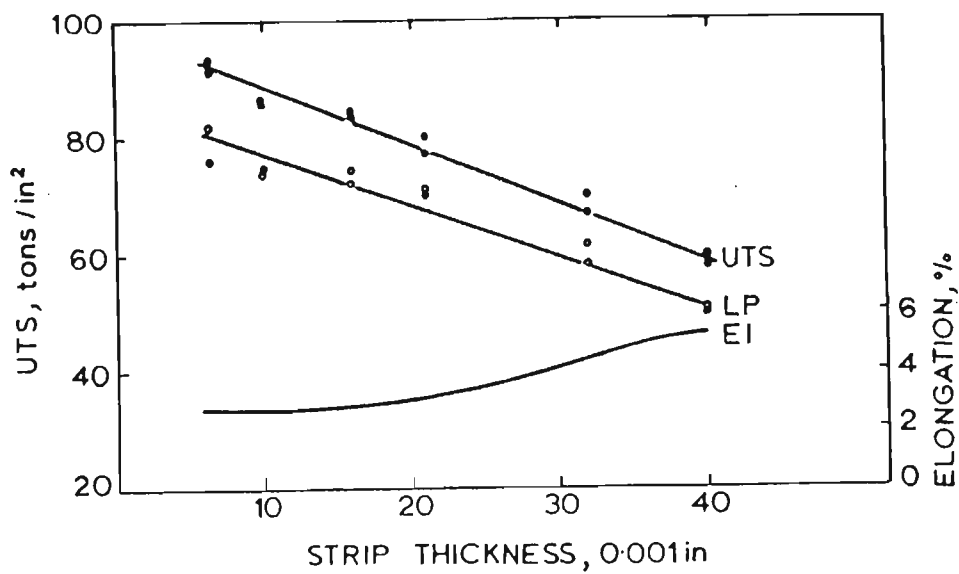


Fig. 2-52 The mechanical properties of 0.088% rimming steel resistance heated at 208°C/s. to 1000°C, quenched in brine. [ref. 306]

## 2.5 TEMPERATURE MEASUREMENT

Throughout industry and research, temperature measurement is an important field, and the thermocouple is one of the most used devices for temperature measurement. However, it is also probably the least understood: a situation that frequently leads to serious error as described in Bentley's paper [307]. Such a misunderstanding often arises from the apparent simplicity of the thermocouple itself, being just a pair of wires with no hint as to its *modus operandi*. Other electrical forms of temperature detection such as those utilizing resistance elements, thermistor pellets, IC chips and transistors, consist, in each case, of a clearly defined sensor attached to a set of leads. The sensor produces the desired signal and the leads convey the information to an instrument. Although many efforts have been made to regard the thermocouple tip as being the source of the observed emf (electromotive force) [308, 309], the modern attitude toward thermocouples is based on the realization that it is the leads rather than tip that generate emf. Therefore, better understanding of thermocouples is essential for accurate temperature measurement .

### 2.6.1 Thermocouples

The principle upon which the thermocouple depends was discovered in 1821 by Seebeck [310], who found that when two wires of different metals are joined in a closed circuit and the two junctions are at different temperatures an electric current will flow. For example, if a copper wire and an iron wire are joined together at each end and one junction is heated, an electric current will flow from the copper to the iron at hot junction, which is known as 'Seebeck effect'. Peltier [311] discovered the so-called 'Peltier effect' in which that the emf produced by heat energy at the junction of two metals was reversible and depended for its value on the nature of the metals and the temperature employed. Lord Kelvin ( then Sir William Thomson ) [312 to 319] found that in a homogeneous metal wire a small emf was produced when parts of the wire were at different temperatures , an effect which is called the 'Thomson effect' and its value also

varies with different metals. Thus, the emf produced in a thermocouple is the sum of the values from the Peltier effect and the Thomson effect, consideration being given to the algebraic signs of the respective values.

Talbot [316] suggested, however, that the electronic theory of metals provides a more complete explanation of thermo-electricity. A metal wire may be regarded as possessing conduction electrons having one degree of freedom of motion in the metal. In different metals, electrons have different concentrations and different average velocities of thermal agitation. If two metals are placed in contact, there is a diffusion of electrons across the interface. If the circuit is completed and the two junctions are kept at the same temperature, the thermal emfs at the junctions are equal and opposite and no flow of electrons occurs. If, however, the junctions are maintained at different temperatures, the electron concentrations differ and a steady flow occurs. In this way, heat energy is transferred into electrical energy.

Following Seebeck's discovery, Becqueral [317] in 1826 used the couple of platinum/palladium. Pouillet [318] in 1836 used the iron/platinum thermocouple and Tait [319] in 1872 used iridium/platinum alloys. Le Chatelier [320,321] investigated a 10% rhodium-platinum/platinum thermocouple for temperature measurement. Barus [322] published a comprehensive survey of the development of the use of thermocouples and other methods of temperature measurement up to the year 1889 and gave the results of his own experiments on platinum, iridium/platinum, platinum/palladium and platinum/nickel couples which he calibrated at the boiling points of mercury, zinc and various organic substances. Later, Burgess [323], Hatfield [324], Wenzl and Morawe [325] and Schofield et al. [326, 327] all made contributions to the development in the use of thermocouples.

Today, we have a large family of thermocouples available depending on the need and accuracy required. The advent of BS 4937 has provided a partial range of thermocouples to meet the requirements of most applications. Chromel/alumel is one of them [328].



Figure 2-53 shows the relationship between the emf output and temperature for various thermoelements with respect to platinum 67 (a standard maintained at the National Bureau of Standards). Chromel/alumel type thermocouples are used to generate values of voltage as a function of temperature from 0 to 1372°C. The inverse relation provides reference temperatures accurate to  $\pm 0.02^\circ\text{C}$  from 400 to 1100°C [329], which is ideal for the present investigation.

The thermocouples so far discussed consist of two wires of two dissimilar metals. A variation of this type of thermocouple, i.e. the one used in the present investigation, consists of three wires of two dissimilar metals. The three-wire thermocouple arrangement has the advantage of being able to be balanced so that the emf generated by a current flow in the specimen can be cancelled [329].

### 2.6.2 Three-wire Thermocouples

This type of thermocouple was adopted by Pearce [330], as a mean of measuring temperature in a rapid resistance heating apparatus built at the University of Wollongong in 1982. The first effort was made in the three-wire thermocouple of two dissimilar metals was spot welded to the center of a specimen. The thermocouple output was recorded on a Houston instrument chart recorder with a chart speed of 50 cm/min. Maximum temperatures were then obtained by using the appropriate emf conversion table.

The three-wire thermocouple arrangement is equivalent to a Wheatstone bridge circuit, as shown in Fig. 2-54(a) [331]. The points A and C are connected to a battery, while B and D are connected to a galvanometer. The resistance values of the arms of the bridge are adjusted until no current flows through the galvanometer.

Under balance conditions:

$$\text{Potential at B} = \text{Potential at D}$$

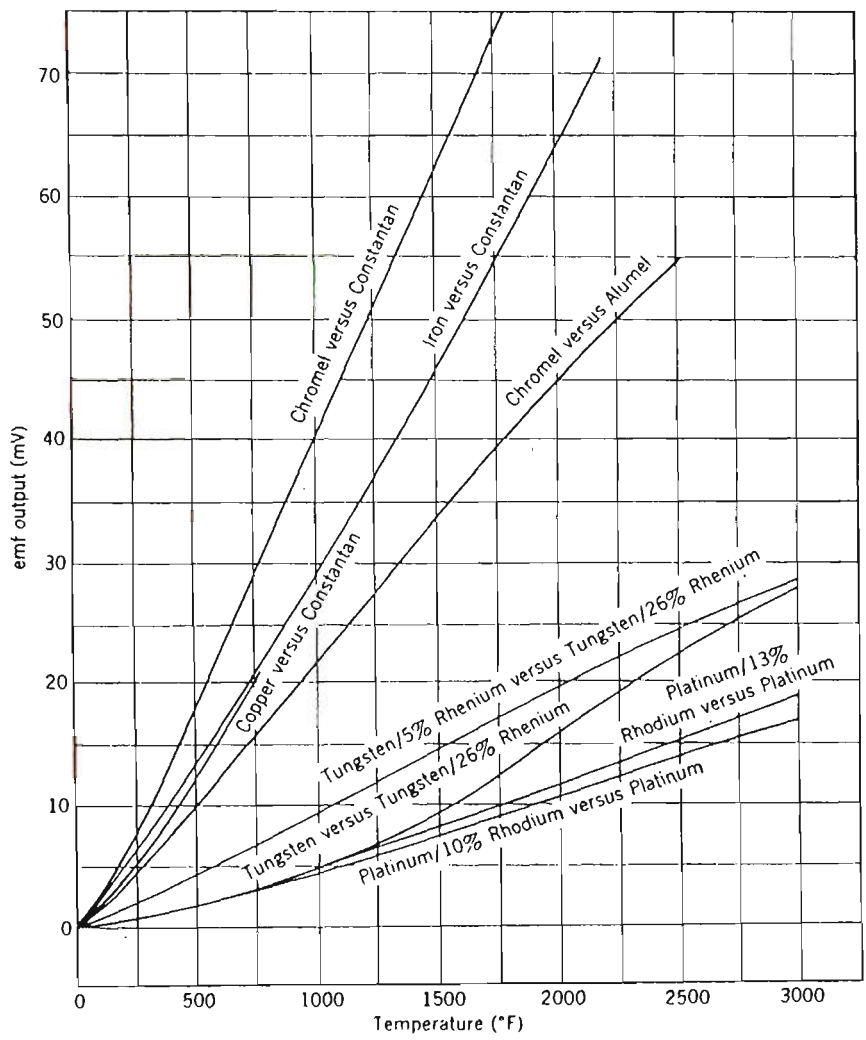


Fig. 2-53 Temperature versus emf curves. Reference junction, 32°F. [ref. 329]

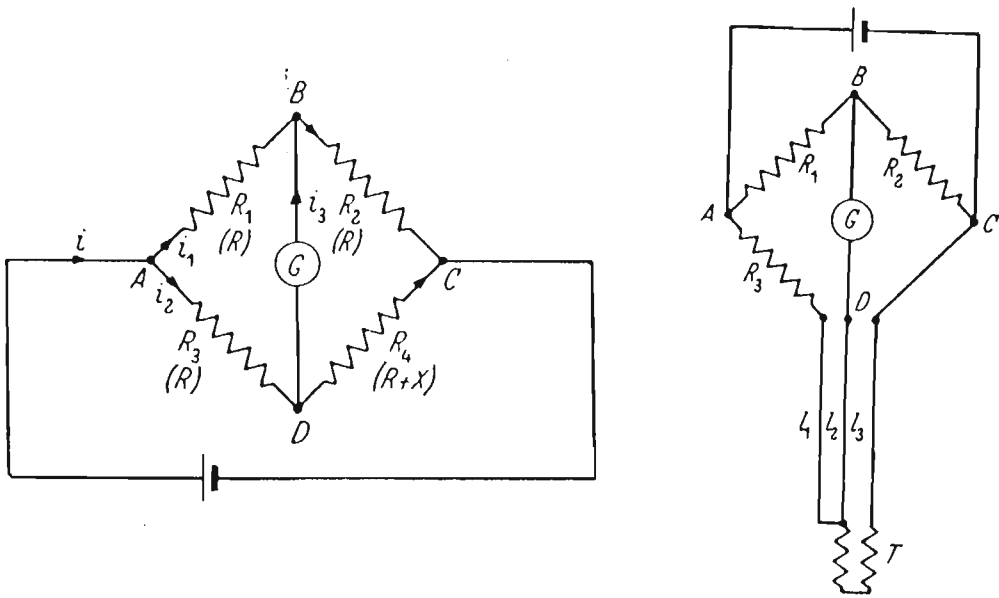


Fig. 2-54 (a) Conventional Wheatstone electric bridge circuit.  
[ref. 331] (b) The equivalent Wheatstone bridge circuit with  
three-wire ( $l_1$ ,  $l_2$  and  $l_3$ ) thermocouple.

i.e. Potential drop in AB = Potential drop in AD

$$i_1 R_1 = i_2 R_3 \quad (2-8)$$

Also Potential drop in BC = Potential drop in DC

$$i_1 R_2 = i_2 R_4 \quad (2-9)$$

Dividing equation (2-8) by equation (2-9):

$$\frac{i_1 R_1}{i_1 R_2} = \frac{i_2 R_3}{i_2 R_4} \quad \text{or} \quad \frac{R_1}{R_2} = \frac{R_3}{R_4} \quad (2-10)$$

that is:  $R_4 = \frac{R_1}{R_2} R_3 \quad (2-11)$

Therefore,  $R_4$  is determined by the fixed ratio  $\frac{R_1}{R_2}$  and the variable  $R_3$ , which can be obtained from the calibrated scale. When balanced, the emf recorded by the chart recorder is that generated solely by the temperature of the specimen.

In practice, three-wire thermocouple  $l_1$ ,  $l_2$  and  $l_3$  are connected to a specimen and a bridge circuit shown in Fig. 2-54(b). It is found that if  $l_1$  and  $l_3$  are made of identical wire and have the same length, they will have equal resistances and changes of ambient temperature will affect both thermocouples equally. If  $R_1 = R_2$  (by setting same distances between each thermocouple wire), the bridge will remain balanced all the times during the resistance heating of the specimen.

### 2.6.3 Detection of Rapid Temperature Changes in Small Size Specimens

With the advent of rapid annealing treatment, a new class of experiments had to be designed to investigate material structures and properties resulting from the rapid heating. The annealing devices impart extremely large amounts of energy in very short times to a small test specimen, resulting in sharp temperature increases. Therefore, the monitoring of temperature changes during ultra-rapid annealing necessitates the employment of temperature detectors with very fast response.

Looking over the literature, perhaps the fastest instrument for measuring the temperature of a test specimen is the infrared detector [332]. A number of these detectors are commercially available which are capable of responding in less than one microsecond. However, all of these detectors employ an optical system and must be carefully calibrated to measure temperature accurately. The small size and varying surface emissivity of test specimens, as well as variations in experiment conditions, may make it exceedingly difficult to use infrared detector in most applications.

A thermocouple overcomes all of the objectionable problems associated with infrared detectors. However, it should be mentioned that the thermocouple cannot measure temperature as rapidly as do infrared detectors because it has a finite mass. By optimizing the geometry and selecting proper thermocouple materials and arrangement, a satisfactory rapid temperature response can be obtained.

Research done by Henning et al. [332] shows that in an intrinsic thermocouple installation, both wires are independently attached to the metallic substrate whose temperature is to be monitored ( shown in Fig. 2-55 ). At a given temperature, the algebraic sum of the emf generated at both junctions between the dissimilar thermocouple wires and the substrate is identical to that produced by directly joining the two thermocouple wires, according to the law of intermediate metals [333]. When this disjointed configuration is used, there is less mass associated with the thermocouple junction, which must be heated or cooled when temperature changes of the substrate are being followed, and then a faster transient response can be expected.

Of the many physical effects present in thermocouple wire, the Seebeck effect is by far the most important. The emf so produced is a function of the thermoelectric properties of the two dissimilar conductors and the temperature present at their interface. Thus the time-emf response of a thermocouple is directly related to the time-temperature response of the thermocouple junction. Accordingly, the transient response of an intrinsic thermocouple is analogous to the transient temperature response of an infinite pin attached

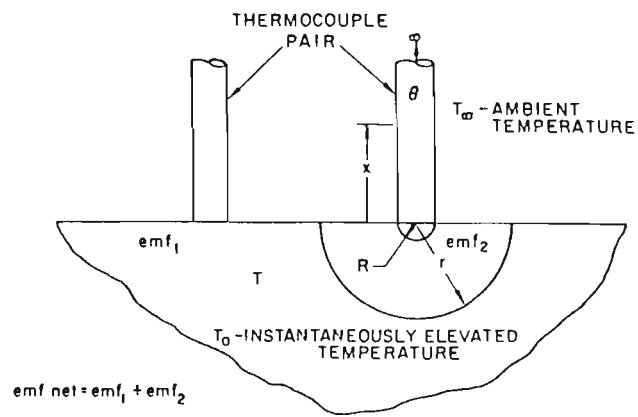


Fig. 2-55 Intrinsic thermocouple attached normal to semi-infinite body. [ref. 332]

normal to the surface of a semi-infinite body which has been subjected to a rapid temperature change.

The major point of interest is the transient temperature response of the thermocouple junction. For each junction the transient response can be accurately described by the following equation [332]:

$$\frac{\theta - T_{\infty}}{T_0 - T_{\infty}} = 1 - (1 - a) e^{a^2 t^*} \text{Erfc}(a\sqrt{t^*}) \quad (2-12)$$

Where a suitable value of a can be:

$$a = \frac{1}{\left(1 + (1/1.5) \sqrt{\frac{k_T}{k}}\right)} \quad (2-13)$$

where  $\theta$  --- temperature in thermocouple, °C

$T_{\infty}$  --- ambient temperature, °C

$T_0$  --- instantaneously elevated temperature in substrate, °C

$t^*$  --- dimensionless time,  $\alpha t/R^2$

$\alpha$  --- thermal diffusivity of substrate,  $\text{cm}^2/\text{sec}$ .

$t$  --- time, sec.

$R$  --- radius of thermocouple wire, cm

$k_T$  --- thermal conductivity of thermocouple wire,  $\text{cal/sec.-cm-}^\circ\text{C}$

$k$  --- thermal conductivity of substrate,  $\text{cal/sec.-cm-}^\circ\text{C}$ .

The elapsed time necessary for an intrinsic thermocouple junction to reach 95% of the steady state emf can be estimated by expanding the complementary error function in equation (2-12) with an asymptotic series given by Jahnke and Emde [334]:

$$t_{95\%} = \frac{25(D^2)k_T}{\pi(\alpha)k} \quad (2-14)$$

where  $D$  is the diameter of the thermocouple wire,  $\alpha$  is the thermal diffusivity of the substrate,  $k_T$  and  $k$  are the thermal conductivities of thermocouple wire and substrate, respectively.

The response of both junctions between the dissimilar wires and the substrate, which compose an intrinsic thermocouple, must be evaluated, since the net emf will be an algebraic sum of the emf's produced at the individual junctions. Because of thermoelectric properties, nearly all the emf's may be produced at just one junction. Obviously, this junction will dominate the transient emf produced by the thermocouple, the response of the other junction being unimportant.

In general, a thermocouple wire of small diameter and low thermal conductivity will produce the fastest response and a small size of specimen is better to use in the fast heating practice for uniformity. If a three-wire thermocouple with two dissimilar materials is applied, reliable experimental results can be obtained. For example, in the work done by Conran et al. [294 to 296] two Chromel wires and one Alumel wire of  $\sim 0.1$  mm in diameter were spot welded onto the center of a specimen and the free ends of the thermocouple wires were connected to a Wheatstone bridge circuit which can be balanced by adjusting the potentiometer on the control unit ( see 2.5.2 ). The use of a three-wire Chromel/Alumel thermocouple arrangement was found to give a reproducible maximum temperature even at a heating rate of  $5400^\circ\text{C}/\text{sec}$ .

The increase in temperature due to resistance heating causes an emf to be induced in the thermocouple wire which can then be recorded on a suitable recording instrument. This emf is summed with the emf produced by the thermocouple at room temperature; hence, the maximum specimen temperature may be found by using the standard emf to temperature conversion chart for a Chromel/Alumel thermocouple.



During the investigation of temperature measurement in a rapid heating process, an attempt had been made to record the maximum temperature profile using a data-logger [296]. This attempt to obtain a more precise measurement of temperature was to aim at checking a calculated sample temperature profile. However, accurate temperatures could not be determined due to the form of the electrical signal flowing along the thermocouple wire during heating of a specimen. The signal recorded using a data-logger showed a portion of the heating voltage superimposed upon the emf from the thermocouple bridge. As the emf from the thermocouple bridge could not be determined by examining these results, a chart recorder was again utilized for recording temperature.

## 2.7 HEAT TRANSFER

### 2.7.1 Introduction

As mentioned above, temperature is a very important factor during the investigation of ultra-rapid annealing. Once there is a temperature difference in the sample, heat transfer will occur. Heat transfer is a science that seeks to predict the energy transfer which takes place between material bodies as a result of a temperature gradient. It seeks not only to explain how heat energy may be transferred, but also to predict the rate at which the exchange will take place under certain specified conditions.

Generally speaking, there are three modes of heat transfer, i.e. conduction, radiation and convection. Conduction heat transfer will happen whenever a temperature gradient exists; radiation is electromagnetic energy transport and the energy travels through space via radiation; and convection heat transfer describes the process in which heat is carried away by flowing air or liquid. These three modes of heat transfer can exist simultaneously. Sometimes, however, only one or two of them occur depending upon the environmental situation. The study of the processes can be used to predict the final equilibrium temperature of a system.

In practice, the annealing by resistance heating actually is a heat transfer process, which involves the conduction, radiation and convection effects. It is feasible to establish a mathematical model based on heat transfer theory to imitate the heating process. Research by Kelly et al. [7, 294 to 296] showed that a study of heat transfer is very helpful in establishing a mathematical modelling during ultra-rapid annealing. It can also predict the temperature profile for a certain heating practice. With the help of the computer, it is possible to utilize the model to vary the heating conditions of the specimen or the specimen shape itself and produce a temperature profile which indicates what effect these variations have on the temperature profile and conduction leading to a uniformly heat

treated test piece. Therefore, heat transfer theory is a basic requirement in establishing the computer model and thus to achieve optimum results in ultra-rapid annealing.

### 2.7.2 Heat Transfer by Conduction

When a temperature gradient exists in a body, molecular transport of heat occurs from a region of higher temperature to a region of lower temperature. It is said that the energy is transferred by conduction and the heat transfer rate per unit area is proportional to the normal temperature gradient [335], i.e.:  $\frac{q}{A} \propto \frac{\partial T}{\partial X}$ , and when the proportionality constant is inserted:

$$q = -kA \frac{\partial T}{\partial X} \quad (2-15)$$

where  $q$  --- the heat transfer rate (energy transfer per unit time);

$\frac{\partial T}{\partial X}$  --- the temperature gradient in the direction of heat flow;

$A$  --- cross sectional area;

$k$  --- thermal conductivity of the material.

The minus sign inserted means that heat must flow downhill on the temperature scale, as shown in Fig. 2-56.

Equation (2-15) is called the Fourier's law of heat conduction. Integrating equation (2-15) for a one dimensional steady state system, we have:

$$q = -kA \frac{T_2 - T_1}{X_2 - X_1} \quad (2-16)$$

If the temperature of a solid is changing with time or if there are heat sources within the solid then the situation, and hence the equations, are more complex.

Considering the one dimensional system shown in Fig. 2-57 and given that temperature is changing with time and there is also a heat source within the body, for the element of thickness  $dX$  the following energy balance can be made:

Energy conducted into the left face + Heat generated within the element

= Change in internal energy + Energy conducted out of the right face

These can be expressed as:

$$\text{Energy conducted into the left face} = q_x = -kA \frac{\partial T}{\partial X}$$

$$\text{Energy generated within element} = \dot{q}AdX$$

$$\text{Change in internal energy} = \rho C_p A \frac{\partial T}{\partial X} dX$$

$$\text{Energy out of the right face} = -A \left[ k \frac{\partial T}{\partial X} + \frac{\partial}{\partial X} \left( k \frac{\partial T}{\partial X} \right) dX \right]$$

where:  $\dot{q}$  --- energy generated / unit volume,  $W/m^3$ ;

$C_p$  --- specific heat,  $J/kg \cdot ^\circ C$ ;

$\rho$  --- density,  $kg/m^3$ .

Combining the above equations gives:

$$\frac{\partial}{\partial X} \left( k \frac{\partial T}{\partial X} \right) + \dot{q} = \rho C_p \frac{\partial T}{\partial t} \quad (2-17)$$

which is a one dimensional heat conduction equation.

The above equations, (2-15) and (2-17), can be modified to deal with more than one dimension. In the specified conditions, equations (2-15) and (2-17) can be expressed as follows:

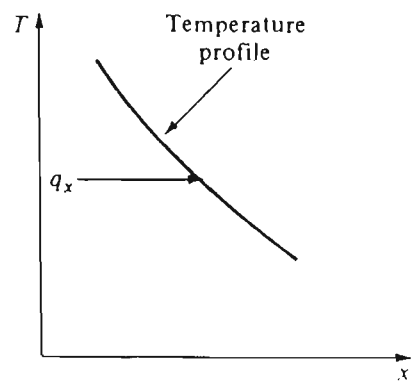


Fig. 2-56 Sketch showing direction of heat flow. [ref.335]

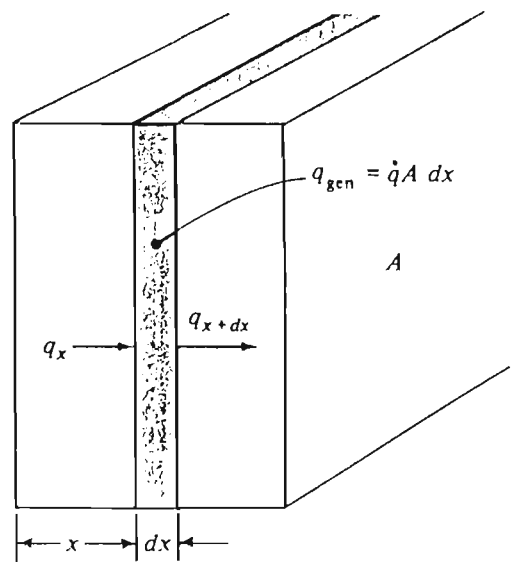


Fig. 2-57 Elemental volume for one-dimensional heat-conduction analysis. [ref. 336]

(1) steady state one dimensional heat flow ( no generation ):

$$\frac{\partial^2 T}{\partial X^2} = 0 \quad (2-18)$$

(2) steady state one dimensional heat flow with internal generation:

$$\frac{\partial^2 T}{\partial X^2} + \frac{\dot{q}}{k} = 0 \quad (2-19)$$

The steady state condition, as described above, applies when the material has reached an equilibrium temperature condition. Before the body has reached the equilibrium temperature it would undergo some heating or cooling. In this period of transient heating or cooling , the analysis must be modified to take into account the temperature variation not only with position in space but also with time at any position. This leads to a number of complex solutions, some of which can only be used in specified condition [336, 337, 338].

The general differential equation for transient heat transfer is of:

$$\frac{\partial^2 T}{\partial X^2} = \frac{1}{\alpha} \frac{\partial T}{\partial t} \quad (2-20)$$

$\alpha = \frac{k}{\rho C_p}$  is called the thermal diffusivity of the material. The larger the value of  $\alpha$ , the faster heat will diffuse through the material.

To solve equation (2-20) one initial condition and two boundary conditions are needed. For example, for a semi-infinite solid system maintained at an initial temperature  $T_i$ , if the temperature is lowered to  $T_o$  and maintained at  $T_o$  at one end, then it is necessary to consider the change of the temperature distribution with time and the equation can be used to calculate the heat flow at any position in the solid as a function of time. Assuming constant properties , the boundary and initial conditions for equation (2-20) are:

$$T(X,0) = T_i \quad (2-21)$$

$$T(0,t) = T_0 \quad \text{for } t > 0 \quad (2-22)$$

Given conditions (2-21) and (2-22), equation (2-20) can be solved by Laplace transform technique and is given as [338]:

$$\frac{T(X,t) - T_0}{T_i - T_0} = \operatorname{erf} \frac{X}{2\sqrt{\alpha t}} \quad (2-23)$$

where  $\operatorname{erf} \frac{X}{2\sqrt{\alpha t}}$  is the Gaussian error function and is defined as:

$$\operatorname{erf} \frac{X}{2\sqrt{\alpha t}} = \frac{2}{\sqrt{\pi}} \int_0^{\frac{X}{2\sqrt{\alpha t}}} e^{-\eta^2} d\eta \quad (2-24)$$

The heat flow at any position  $X$  can be obtained from:

$$q_x = -kA \frac{\partial T}{\partial X} \quad (2-25)$$

where

$$\frac{\partial T}{\partial X} = \frac{T_i - T_0}{\sqrt{\pi \alpha t}} e^{-X^2/4\alpha t} \quad (2-26)$$

Therefore, the heat flow is given by :

$$q_x = \frac{-kA(T_i - T_0)}{\sqrt{\pi \alpha t}} e^{-X^2/4\alpha t} \quad (2-27)$$

A plot of temperature distribution for the semi-infinite solid is shown in Fig. 2-58.

Consider a one dimensional body divided into increments as shown in Fig. 2-59. Within the solid body, the differential equation which governs heat flow can be expressed as equation (2-20), i. e.,  $a \frac{\partial^2 T}{\partial X^2} = \frac{\partial T}{\partial t}$ . The partial derivatives may be approximated to:

$$\frac{\partial^2 T}{\partial X^2} = \frac{T(X+\Delta X,t) + T(X-\Delta X,t) - 2T(X,t)}{(\Delta X)^2} \quad (2-28)$$

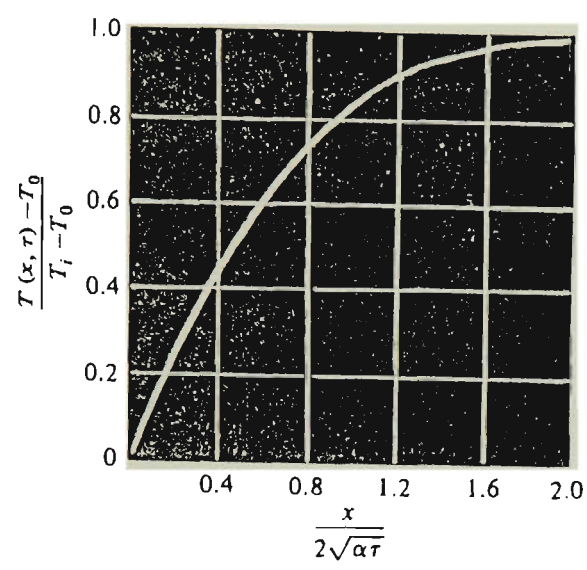


Fig. 2-58 Temperature distribution in the semi-infinite solid. [ref. 335]

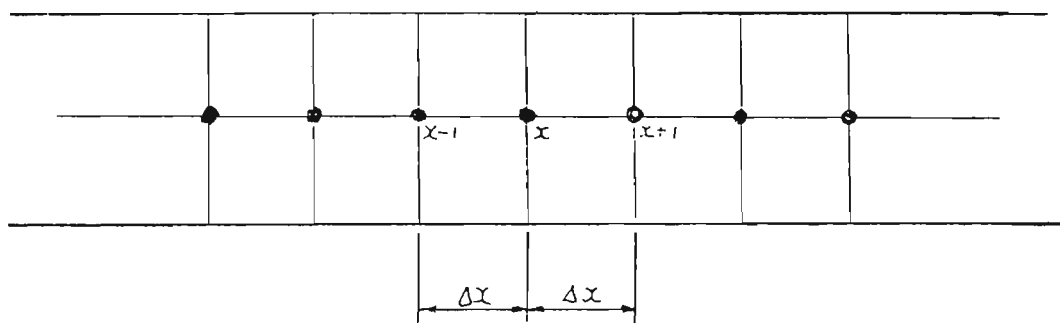


Fig. 2-59 Nomenclature for numerical solution of one-dimensional unsteady-state conduction. [ref. 294]



$$\frac{\partial T}{\partial t} = \frac{T(X,t+\Delta t) - T(X,t)}{\Delta t} \quad (2-29)$$

therefore equation (2-20) can be rewritten as:

$$T(X,t+\Delta t) = \frac{\alpha \Delta t}{(\Delta X)^2} (T(X+\Delta X,t) + T(X-\Delta X,t)) + \left(1 - \frac{2\alpha \Delta t}{(\Delta X)^2}\right) T(X,t) \quad (2-30)$$

$$\text{if } M = \frac{(\Delta X)^2}{\alpha \Delta t}$$

then the final equation is:

$$T(X,t+\Delta t) = \frac{T(X+\Delta X,t) + T(X-\Delta X,t) + (M-2) T(X,t)}{M} \quad (2-31)$$

There is one restriction to the above case, i.e.  $M \geq 2$ . If  $M < 2$ , the coefficient of  $T(X,t)$  becomes negative and a condition is generated that violates the second law of thermodynamics in that there would be an "uphill" heat flow to adjoining temperature nodes.

The equations above have been developed on a forward difference technique, in that the temperature of a node at a further increment is expressed in terms of the surrounding nodal temperatures at the beginning of the time increment. These equations (2-30 and 2-31) are called explicit equations because it is possible to calculate the temperature at  $T(X,t+\Delta t)$  explicitly in terms of the previous temperature  $T(X,t)$ .

The explicit method results in a set of simple algebraic relations which can be easily solved with a digital computer. However, stability considerations have restricted the size of the time increment for a given distance step. If the time increment size becomes small compared to the distance size then computational problems become important. In such a case, implicit method is better to be used.

Considering equation (2-20), the finite-difference expression for equation (2-20) using the Crank and Nicholson implicit method [339] can be expressed as follows:

$$\frac{T(X, t+\Delta t) - T(X, t)}{\Delta t} = \frac{1}{2} \alpha \left( \frac{T(X-\Delta X, t+\Delta t) + T(X+\Delta X, t+\Delta t) - 2T(X, t+\Delta t)}{(\Delta X)^2} + \frac{T(X-\Delta X, t) + T(X+\Delta X, t) - 2T(X, t)}{(\Delta X)^2} \right) \quad (2-32)$$

The Crank-Nicholson equation (2-32) requires a simultaneous solution of all equations for each time increment. It is stable for all values of  $M$ . Therefore, the implicit method was selected for the present development of computer model (Chapter 5).

### 2.7.3 Heat Transfer by Radiation

Thermal radiation is electromagnetic radiation that is propagated as a result of a temperature difference. Thermodynamic considerations show that an ideal thermal radiator, or black body, will emit energy at a rate proportional to the fourth power of the absolute temperature of the body and directly proportional to its surface area [340]. That is:

$$q_r = \sigma A T^4 \quad (2-33)$$

where  $q_r$  --- energy emitted by black body;

$\sigma$  --- Stefan-Boltzmann constant, with the value of  $5.669 \times 10^{-8} \text{ W/m}^2 \cdot \text{K}^4$ ;

$A$  --- surface area of radiation body,  $\text{m}^2$ ;

$T$  --- absolute temperature, K.

Equation (2-33) is called the Stefan-Boltzmann law of thermal radiation, and it applies only to black body.

Equation (2-33) can be modified for real bodies between the energy absorbed and the energy emitted situation by introducing the fraction of energy of a black body emitted with a real body which is called the emissivity  $e$ , and equation (2-33) can be rewritten as:

$$q_r = \sigma \epsilon A (T_1^4 - T_2^4) \quad (2-34)$$

where  $\epsilon$  --- the emissivity of material,

$T_1$  --- temperature of the emitting body,

$T_2$  --- temperature of the surrounds,

$A$  --- surface area of the body which is emitting and absorbing.

The amount of heat energy transferred by radiation is dependent upon many factors such as absorptivity of the real body, emissivity of the real body and the fact that radiant energy being transferred is not monochromatic ( as assumed in the Stefan-Boltzmann equation ) but rather consists of a range of wavelengths characteristic of the temperature of emission.

#### 2.7.4 Heat Transfer by Convection

It is well known that a hot body will cool faster when placed in front of a fan than exposed to still air. This process of carrying heat by flow air or liquid is termed as convection heat transfer [340].

Considering a convection heat transfer from a hot plate in air, Newton's cooling law can be used to express the overall effect of convection as:

$$q_c = hA (T_w - T_\infty) \quad (2-35)$$

where  $q_c$  --- energy transferred by convection;

$h$  --- convection heat transfer coefficient;

$A$  --- surface area;

$T_w$  --- temperature of plate;

$T_\infty$  --- ambient temperature.

Here the heat transfer rate is related to the overall temperature difference between the plate and fluid and the surface area. In fact, convection heat transfer will have a dependence on the viscosity of the fluid in addition to its dependence on the thermal properties of the fluid ( such as thermal conductivity, specific heat, density, etc. ).

Usually, heat transfer involves not only conduction but also convection. For the semi-infinite solid system described in 2.6.2, the differential equation including convection is expressed as:

$$hA (T_{\infty} - T)_{x=0} = -kA \left( \frac{\partial T}{\partial X} \right)_{x=0} \quad (2-36)$$

The solution to equation (2-36) has been worked out in detail by Schneider [338]. The result is:

$$\frac{T - T_i}{T_{\infty} - T_i} = 1 - \operatorname{erf} X - \left( \operatorname{erf} \frac{hx}{k} + \frac{h^2 \alpha t}{k^2} \right) \left( 1 - \operatorname{erf} \left( X + \frac{h \sqrt{\alpha t}}{k} \right) \right) \quad (2-37)$$

where  $X = \frac{x}{2\sqrt{\alpha t}}$ ,  $T_i$  is the initial temperature of the solid, and  $T_{\infty}$  is the environment temperature.

Solutions to equation (2-37) have been worked out for different geometries and the results of analysis for these geometries have been presented in graphical form by Heisler [341] shown in Fig. 2-60.

The Heisler charts are very useful for calculating temperatures in a regular shaped solid under transient heat-flow conditions. Many geometric shapes of practical interest are not regular in shape and appropriate boundary conditions have to be used. In these instances, the problem is best handled by a numerical technique.

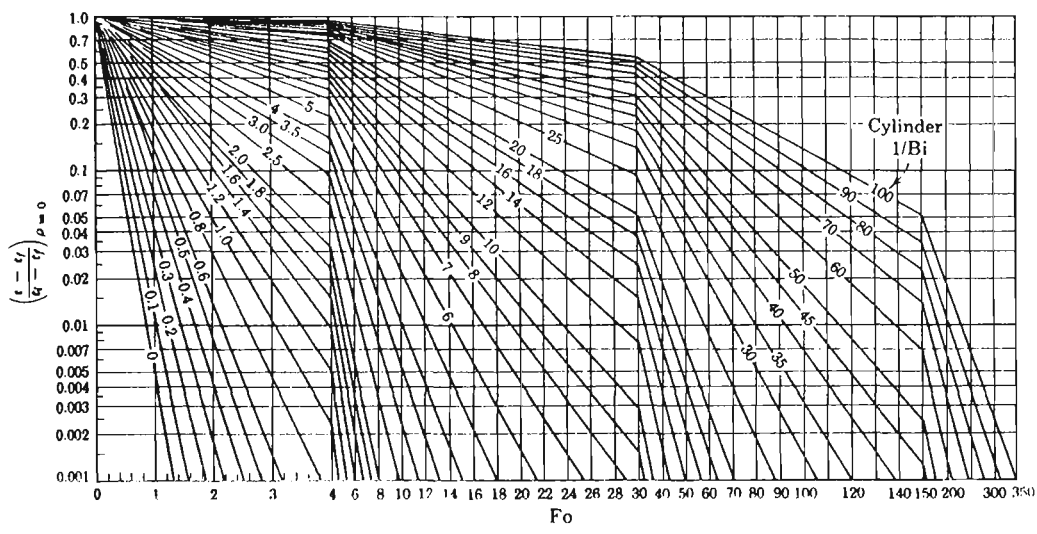


Fig. 2-60 Heisler's chart for the temperature-time history at the center of an infinitely long cylinder at temperature  $t_i$  and placed in a medium at  $t_f$ . [ref. 341]

### 2.7.5 Variation of Physical Properties with Temperature

A number of physical properties including emissivity, thermal conductivity, specific heat and resistivity, vary with temperature. It is necessary to know the relationship between each of the above properties and temperature when establishing a computer model. The following graphs show how these properties vary as temperature increases.

Figure 2-61 shows the effects of temperature and surface condition on emissivity of ferrous materials. Emissivity is very sensitive to surface conditions, especially in metals for which the emitted radiation is generated very close to the surface.

It can be seen from Fig. 2-61 that the more smooth the surface of specimen, the lower the emissivity value. As temperature increases, the emissivity increases, too, and is nearly proportional to  $T^{1/2}$  [336].

Figure 2-62 shows the effect of temperature on thermal conductivity [342]. It is found for pure iron that as temperature increases, the thermal conductivity decreases and hence conduction will be less effective at higher temperatures.

In the theory of electrical conduction, resistivity (also called the specific resistance) is defined as a proportionality factor characteristic of different substance and is equal to the resistance that a centimeter cube of the substance offers to the passage of electrical current being perpendicular to two parallel faces [343]. Resistance is therefore given by the equation:

$$R = \rho_r \frac{l}{A} \quad (2-38)$$

where  $R$  --- resistance of a uniform conductor;

$l$  --- length;

$A$  --- cross sectional area;

$\rho_r$  --- resistivity.

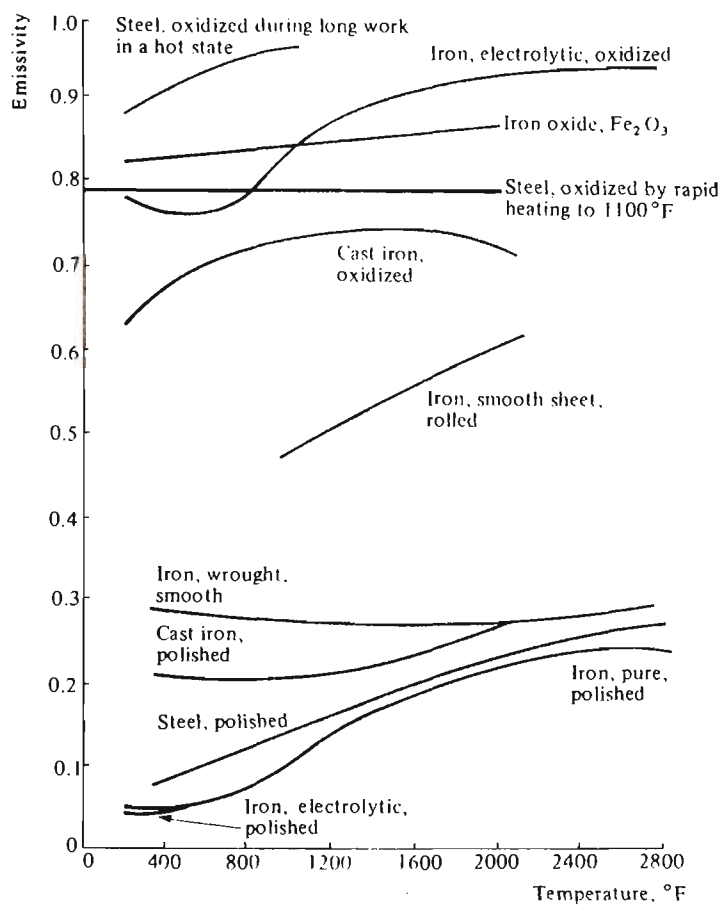


Fig. 2-61 Variation of emissivity with temperature and condition of ferrous materials. [ref. 336]

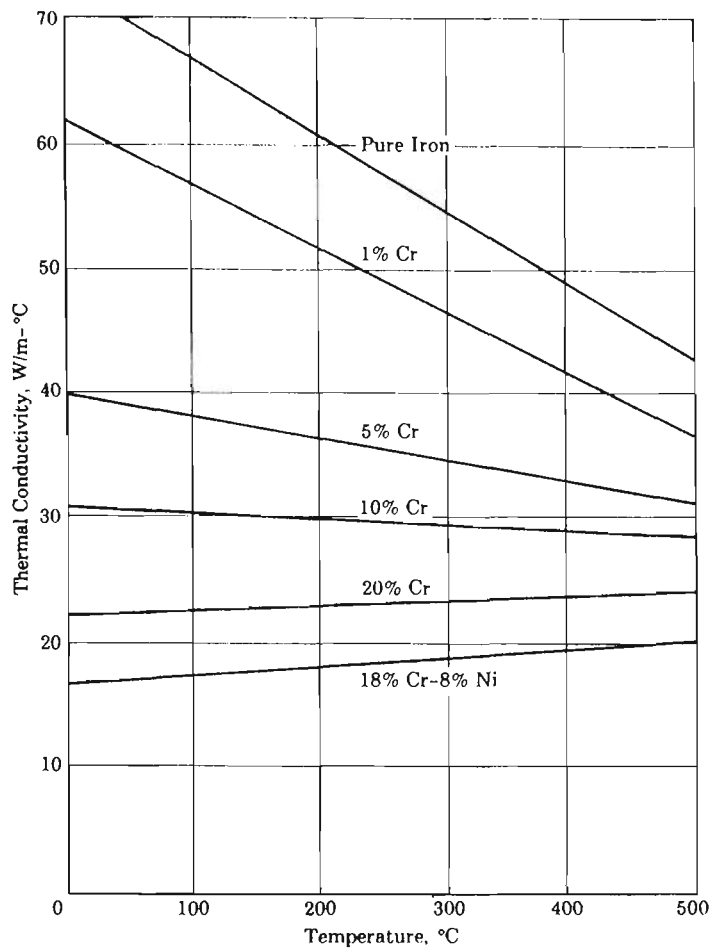


Fig. 2-62 The effect of temperature and composition on the thermal conductivity of steel. [ref. 342]



As illustrated in Fig. 2-63 [344], the resistivity of iron increases markedly with increasing temperature and so affects the heat generated in an electrical conductor. When a current is passed through a body power is generated according to:

$$P = I^2R \quad (2-39)$$

where  $P$  --- power, W;

$I$  --- current, A;

$R$  --- resistance, ohm.

Therefore, as the temperature increases, resistivity increases and so does resistance. Power generated in the form of heat energy increases too, and hence the body heats more rapidly. This is one of the reasons why resistance heating can provide such a high heating rate during annealing.

The specific heat increases with temperature as shown in Fig. 2-64 [345]. Thus the rate of change of temperature will decrease with a constant rate of heat input.

When a body is exposed to ambient air without an external source of motion, a movement of the air would be experienced as a result of the density gradients near the body, which is called free convection. The free convection heat transfer often occurs in normal life. The approximate ranges of free convection heat transfer coefficients are indicated in Table 2-4 [346].

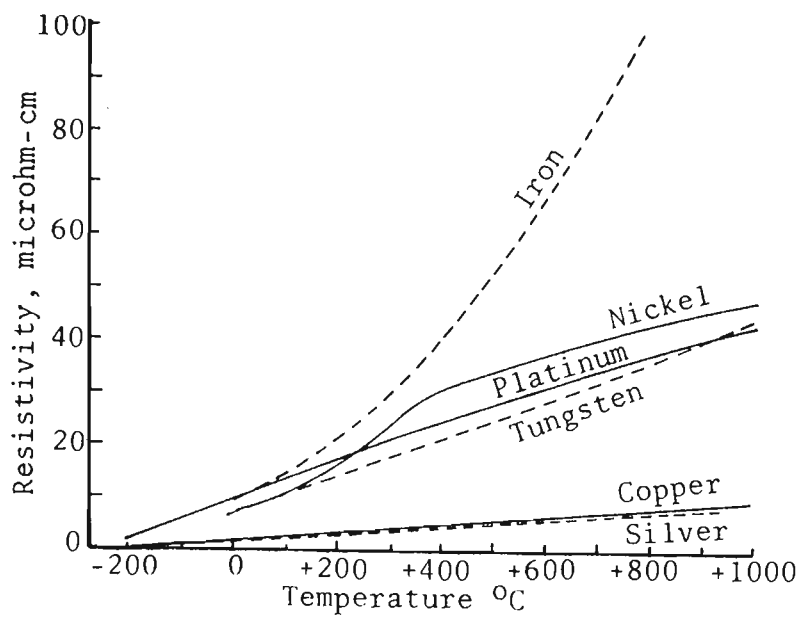


Fig. 2-63 Variation of the resistance ratio with temperature for pure metals. From data of ref. 344.

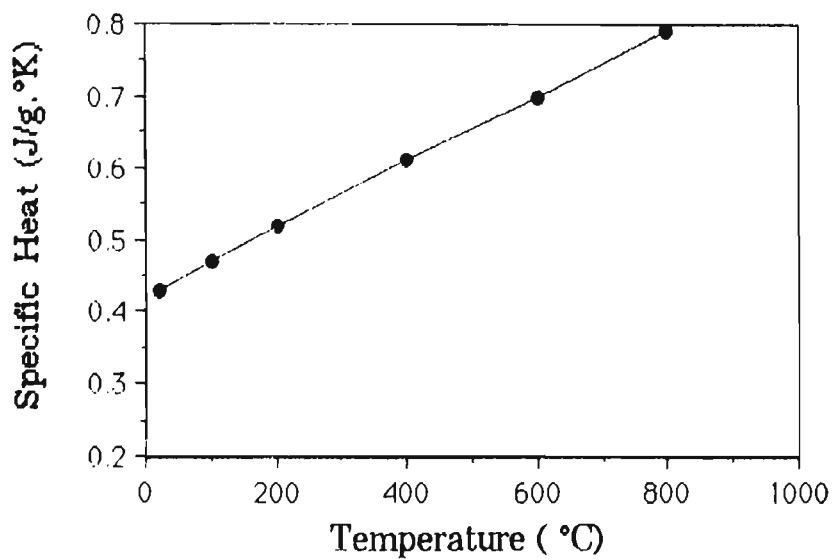


Fig. 2-64 Variation of specific heat of iron with temperature. From data of ref. 345.

Table 2-4 Approximate values of free convection heat transfer coefficient  
(  $\Delta T = 30^{\circ}\text{C}$  )

Mode	h	
	W/m <sup>2</sup> .°C	Btu/h·ft <sup>2</sup> .°F
Vertical plate 0.3 m (1ft) high in air	4.5	0.79
Horizontal cylinder, 5-cm dia. in air	6.5	1.14
Horizontal cylinder, 2-cm dia. in water	890	157

In summary, as the resistivity increases there is an increase in the heat generated by a passing electrical current and, although the decrease of thermal conductivity and the increase of heat lost by radiation are opposed to each other, the increasing loss by radiation is more important because radiation loss is proportional to  $T^4$  and the emissivity also increases.

2.7.6 Application of Heat Transfer Calculations to Resistance Heating

Heat transfer is very important in engineering design. There are many applications which are related to heat transfer [347 to 362]. Resistance heating is one of the fields to which the finite difference method can be applied to predict the temperature profile during a heating process.

As described above, the solution of heat conduction equations is complicated by concurrent lateral radiation and convection and by variations in material properties due to temperature changes. Under these circumstance, the finite difference approximations are normally applied and it is necessary to use a computer to carry out the extensive calculations.

The usefulness of the heat transfer analysis in resistance heating is in the production of a temperature profile for a system, illustrating the flow of heat. This is basically achieved by dividing the system into a number of finite elements and approximating the temperature in a certain element using the temperatures in the surrounding elements as a guide, such as the explicit method described previously. However, the accuracy of such an approximation can be increased by choosing  $\Delta X$  and  $\Delta t$  as small as possible. At each stage in the calculation, no matter how small, some roundoff errors are introduced. When heat transfer is applied to the resistance heating problem, stability and convergence must be taken into account in addition to the roundoff errors for the explicit method.

Stability consideration is important in the solution of the differential equation with finite differences. The finite-difference solution to the differential equation of heat conduction is:

$$T(X, t+\Delta t) = \frac{\alpha \Delta t}{(\Delta X)^2} (T(X+\Delta X, t) + T(X-\Delta X, t)) + \left(1 - \frac{2\alpha \Delta t}{(\Delta X)^2}\right) T(X, t) \quad (2-30)$$

The important term to note in equation (2-30) is the  $\frac{\alpha \Delta t}{(\Delta X)^2}$  term, i.e.  $\frac{1}{M}$ , and as mentioned before, equation (2-30) is only stable when  $M \geq 2$ , i.e.  $\frac{1}{M} \leq 0.5$ . If  $\frac{1}{M}$  is larger than 0.5 then equation (2-30) describes heat transferring from a colder to a hotter region, which is of course impossible. This relationship becomes the stability criteria for one dimensional solution of the finite difference.

This stability condition introduces a limit to the maximum size of time steps that can be chosen for a fixed  $X$ . Figure 2-65 illustrates what happens to the numerical solution when the stability criteria is violated. It must be pointed out that the stability criteria given above can not be generalized for other systems [363]. Further, when the problems are non-linear there is no general method that can be used effectively to determine the stability of the resulting finite-difference equation.

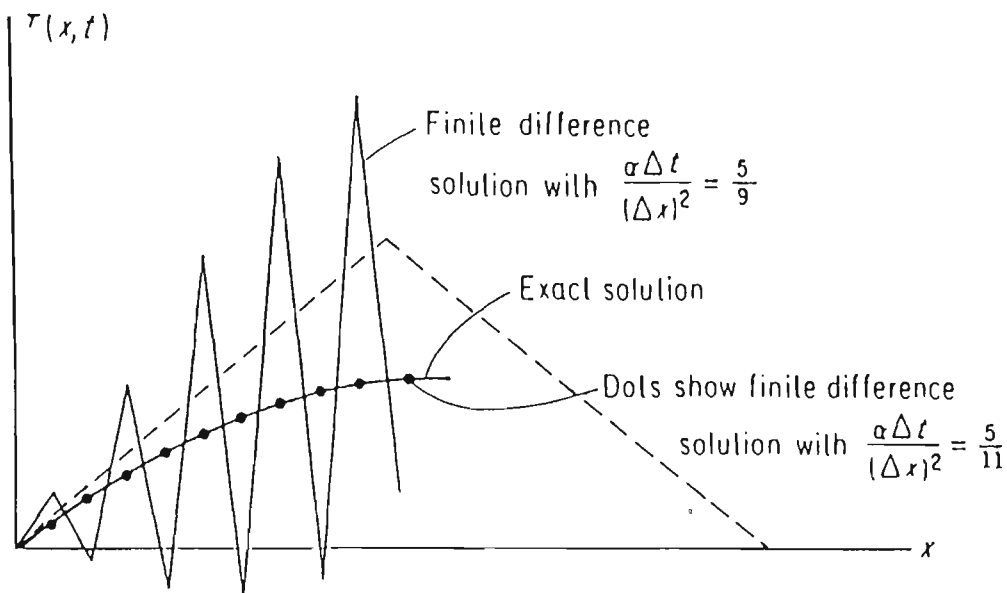


Fig. 2-65 Effect of parameter  $\Delta t/(\Delta X)$  on the stability of finite-difference solution of one-dimensional heat flow problem.

[ref. 295]

The finite-difference equations for one dimensional heat transfer will converge at faster rates to the correct solution if the truncation error is as close to zero as possible. The truncation error is equal to zero and convergence will be fastest when following equation is established [295]:

$$\frac{\alpha \Delta t}{(\Delta X)^2} = \frac{1}{6} \quad (2-40)$$

The computer models of resistance heating during ultra-rapid annealing developed by Yip [7], Howes [294] and Kelly [295] to explain the resistance heating process contain an explicit expression for the relationship of temperature of finite elements. However, stability and convergence considerations restrict the size of the time increment for a particular distance step, and there are also some other deficiencies in their models which will be discussed in section 3.3.1.3. Therefore, an implicit method of finite difference is superior as it will be stable and converge for all values of the parameter  $\frac{\alpha \Delta t}{(\Delta X)^2}$  [339].

## ***CHAPTER 3***

### **SCOPE OF THE PRESENT WORK**

The specific aims of the ultra-rapid annealing investigation were to elucidate the effect of heating rate on softening of cold worked low carbon steel and to produce a uniformly heat treated specimen which could be used as a tensile test piece. Despite the abundance of research on annealing of cold rolled iron and low carbon steels, there is a shortage of information on, and limited understanding of the ultra-rapid annealing processes. Therefore, a systematic study of ultra-rapid annealing has been undertaken in an attempt to elucidate the effect of very high heating rates on the structure and properties of cold rolled, low carbon steels.

The present investigation is summarized schematically in Fig. 3-1. A decarburized steel was used and ultra-rapid annealing was achieved by a resistance heating apparatus. The apparatus was specially designed to heat a cold rolled specimen very quickly at rates of  $\sim 1000$  to  $5000^\circ\text{C}/\text{sec}$ . Furthermore, careful calibrations of the equipment were carried out to ensure accurate and reproducible results.

In particular, accurate temperature measurement is a vital factor in monitoring the thermal cycle and in determining the softening temperature range. A three wire thermocouple system which constitutes a Wheatstone electrical bridge was used for this purpose. This technique has been proved to be accurate and reproducible [9] and so it was adopted in the present investigation. However, a large number of temperature measurements at various specimen positions is needed to obtain the temperature distribution and hence to establish the uniformly heated zone. A computer model based on heat transfer theory was therefore employed to overcome these experimental difficulties. A new model was established by using an implicit method to predict the variations of temperatures during the ultra-rapid heating cycle. This computer model was also used to give the overall temperature profile and to assist in the design of the optimum shape of the specimen.



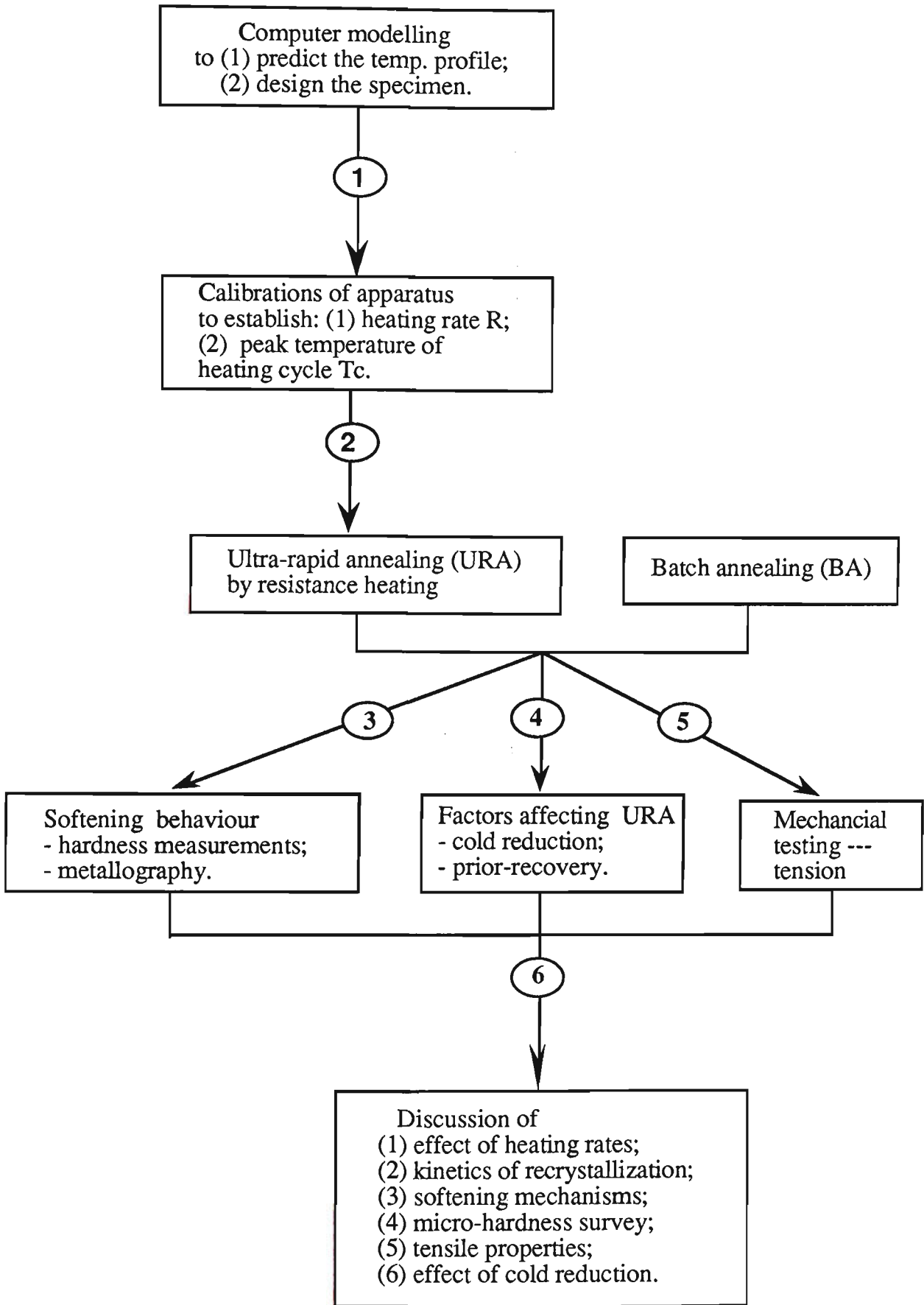


Fig. 3-1 Diagram showing the planned approach used to carry out the research. The numbers indicate the stages and the sequence of the work.

It has been proposed by Andrews and Atkinson [99] that raising the heating rate to between 300 to 1600°C/sec. increases the rate of softening and lowers the temperature range in which recrystallization occurs. The present investigation was designed to check the hypothesis and to further increase heating rates and elucidate the effect of heating rate on the recrystallization temperature ranges. In addition, other factors which might influence the softening behaviour of cold rolled material, such as degree of cold reduction and prior-recovery, were considered.

Mechanical properties are of most concern in engineering applications. Tension tests were conducted after ultra-rapid annealing to characterize yield stress, tensile strength, ductility, toughness and plastic strain ratio.

Batch annealing was used as a basis for comparison with the structures and properties developed on the ultra-rapid annealing.

In summary, conducting the research according to the plan in Fig. 3-1, it was intended to establish a new computer model to predict the temperature profile and to design the specimen; to study systematically the ultra-rapid annealing process by relating the heating rates to the softening temperature ranges; and to analyse the kinetics and mechanisms of recrystallization at different heating rates. Other objectives were to examine the resultant mechanical properties and to investigate other factors that might affect the softening behaviour of the material, such as the extent of cold reduction and prior recovery.

## ***CHAPTER 4***

# **EXPERIMENTAL INVESTIGATION METHODS**

## NOMENCLATURE

The following symbols will be used in Chapter 4.

$R_p$  = potentiometer setting (ohm)

$T_n^{p+1}$  = temperature at time (p+1) of the element n ( $^{\circ}\text{K}$ )

$\Delta t$  = time interval (sec.)

$\rho$  = density ( $\text{g}/\text{m}^3$ )

$C_p$  = specific heat ( $\text{J}/\text{g}\cdot^{\circ}\text{K}$ )

$I$  = current ( amps)

$R$  = resistance (ohm)

$K$  = thermal conductivity ( $\text{J}/\text{sm}^{\circ}\text{K}$ )

$\Delta X$  = length of the element (m)

$A$  = cross area of a test piece ( $\text{m}^2$ )

$\eta$  = emissivity

$\beta$  = Stefan-Boltzmann constant ( $\text{J}/\text{sm}^2 \cdot \text{K}^4$ )

$V$  = volume ( $\text{m}^3$ )

$T_{\infty}$  = environmental temperature ( $^{\circ}\text{K}$ )

$T_{\text{center}}$  = the temperature at center of the specimen ( $^{\circ}\text{K}$ )

$T_0$  = the temperature at edge of the specimen ( $^{\circ}\text{K}$ )

$a_W$  = a coefficient in an implicit temperature equation at left side of unknown point p.

$a_E$  = a coefficient in an implicit temperature equation at right side of unknown point p.

$a_p$  = a coefficient at point p in the implicit computer modelling; it related to  $a_W$  and  $a_E$ .

$b$  = a parameter during producing the temperature equation; it often related to the material physical properties.

$T_p$  = the temperature at point p ( $^{\circ}\text{K}$ )

$T_W$  = the temperature at left side of point p ( $^{\circ}\text{K}$ )

$T_E$  = the temperature at right side of point p ( $^{\circ}\text{K}$ )

$k$  = a constant in a power equation describing the stress-strain relationship; often termed the "strain hardening coefficient"

$n$  = a constant in a power equation; often termed the "strain hardening index"

$\epsilon$  = "true plastic strain";  $\epsilon = \ln(l/l_0)$

$\sigma$  = true stress ( $\text{kg/m}^2$ )

$\sigma_0$  = a constant in a stress-strain equation; often described as a "threshold stress" and loosely related to the "yield stress".

$\gamma$  = skewness

$\bar{D}$  = arithmetic mean grain diameter.

$D_i$  = grain diameter

$N_i$  = number of grains in the interval represented by diameter  $D_i$ .

$\sigma_v$  = standard deviation.

$D_g$  = the geometric mean diameter.

$\sigma_g$  = the geometric standard deviation.

$\mu_1, \mu_2, \mu_3$  = the first, second and third central moments, they are related respectively to the average size, the deviation from the average and the skewness.

#### 4.1 MATERIALS

The material used was decarburized iron supplied by John Lysaght, BHP International Group. As received, the steel was a capped grade (ingot route) steel which is no longer made by BHP Slab and Plate Products Division (SPPD). The hot band from SPPD was 4.5 mm thick. It was pickled and then cold rolled to 1.56 mm followed by open coil annealing to decarburize and denitride to 0.005 and 0.0006 levels, respectively. The denitridding was designed to limit the susceptibility to strain aging. Decarburizing is carried out at 680°C in a H<sub>2</sub>, N<sub>2</sub>, H<sub>2</sub>O atmosphere and denitridding at a lower temperature of ~550°C with an adjusted mixture. The steel was given a skin pass of ~1% after annealing and it is normally recommended that it be drawn within six weeks of temper rolling to prevent discontinuous yielding at the surface.

The structure of the steel after processing consisted of equiaxed grains of ferrite with an average intercept length of 50 µm. A small amount of non metallic inclusions was present together with a very small volume fraction of grain boundary carbide. This steel grade is principally for processing and enamelling of bath tubs.

The sheets of 1.56 mm thickness were unidirectionally cold rolled using a "Hille" rolling mill to total reductions of 40%, 60%, 70% and 80% at Wollongong Technical College. In order to limit recovery occurring during cold rolling, care was taken to ensure that the cold rolled strip remained cool by using small rolling reductions (less than 5% per pass) and rapid water quenching after each pass. Details of the chemical composition of the sheet are given in Table 4-1.

Table 4-1 Chemical composition of material

Element	C	P	Mn	Si	S	Ni	Cr	Mo
Wt %	.005	.015	.40	<.005	.010	.023	.016	.003
Element	Ca	Sn	Ti	V	N <sub>2</sub>	O <sub>2</sub>	sol. Al	
Wt %	.021	.003	<.002	<.002	.0006	.0375	.010	

The cold reduced sheets were machined into the tensile test pieces shown in Fig.4-1 after cold rolling and they were carefully milled to prevent recovery due to heat generation. For reference, the central reduced section of the test piece was called the "gauge", and the outer wide section called the "flag". The length of the test piece was governed by the distance between the sample holders of the apparatus; and the area of the cross section of test pieces was kept constant for samples with different cold reductions. Details of the test pieces are given in Table 4-2.

Table 4-2 Sample sizes for different cold reductions

test piece dimension	half length (mm)		width	thickness
cold reduction	flag	gauge	(mm)	(mm)
40%	20.0	15.0	3.09	0.94
60%	20.0	15.0	4.47	0.65
70%	20.0	15.0	6.17	0.47
80%	20.0	15.0	9.26	0.31

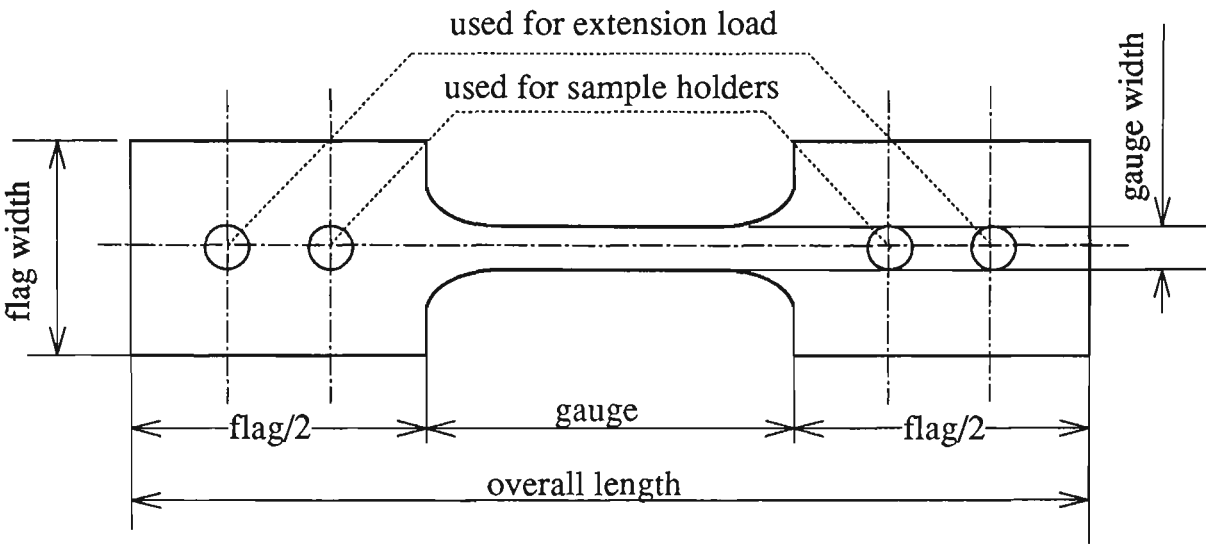


Fig.4-1 Standard tensile test piece used in the ultra-rapid annealing investigation



4.2 HEAT TREATMENT PROGRAMME

4.2.1 Ultra-rapid Annealing

Laboratory ultra-rapid annealing was realized by a resistance heating apparatus, which is described in 4.3.1.1.

The details of ultra-rapid annealing experiments designed to calibrate the equipment and define process conditions are given in Table 4-3.

Table 4-3 Description of annealing experiments

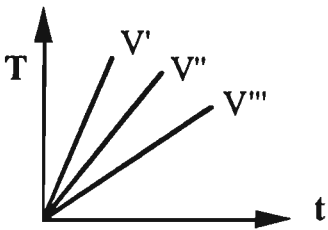
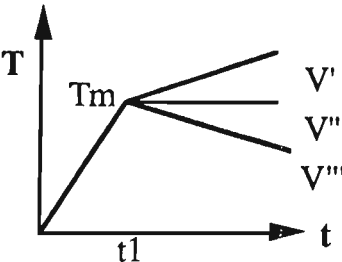
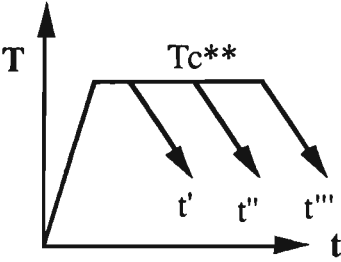
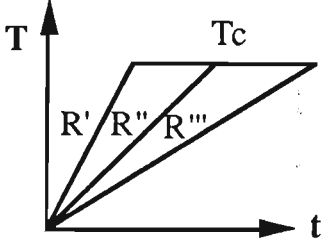
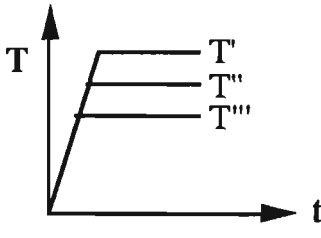
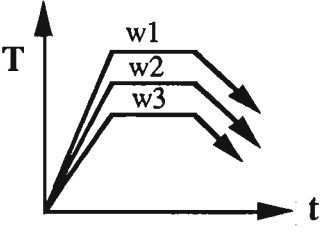
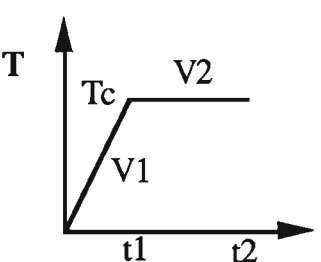
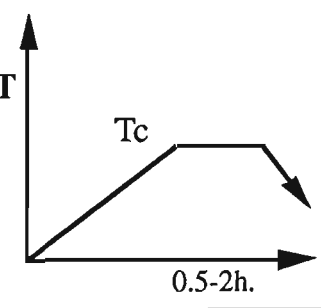
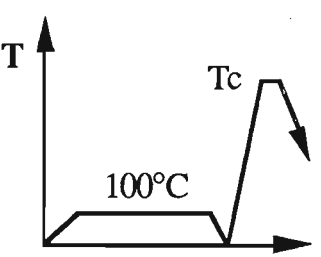
Experiment	Sample	Schematic representation of the process	Action	Objective
1	Steel 70%*		change the first heating voltage $V_1$	determine the heating rate at $V_1$
2	Steel 70%		change the second heating voltage $V_2$	determine the maximum hold temperature $T_c$
3	Steel 70%		change the soak time $t_2$ at same $V_1 V_2$	study the effect of soak time on softening

Table 4-3 Description of annealing experiments (continued)

Experiment	Sample	Schematic representation of the process	Action	Objective
4	Steel 70%		change the heating rate R at same temperature T	study the effect of heating rate on softening
5	Steel 70%		change the hold temperature T	study the effect of softening at various T
6	Steel 70%		change the width of samples	observe the size effect on softening
7	Steel 40% 60% 70% 80%		change the cold reduction of samples	study the effect of cold reduction on softening
8 Batch annealing	Steel 40% 60% 70% 80%		reduce the heating rate and lengthen holding time	compare the results with ultra-rapid annealing
9 URA with prior-recovery	Steel 70% 40%		anneal at 100°C for various time before URA***	study the effect of prior recovery on softening

\* 70% cold reduction.

\*\*\* Ultra-rapid annealing

\*\* Tc is the maximum (constant) temperature.

Experiment 1 was designed to determine the heating rate at a given input voltage. Experiment 2 defines the second heating voltage required to produce a constant hold temperature; this constant temperature is denoted as  $T_c$ . Experiment 3 was conducted to study the effect of soak time on softening; the "soak time" refers to the duration of the hold temperature. Experiment 4 was designed to determine the influence of different heating rates on softening at a common hold temperature. Experiment 5 was used to investigate the softening behaviour at different hold temperatures. Experiment 6 was designed to observe the size effect of samples on heating and on subsequent softening. Experiment 7 was used to investigate the effect of cold reduction on softening; it was important in this case to keep the area of the cross section of the specimens constant to maintain the same heating rate.

#### 4.2.2 Batch Annealing

Experiment 8 in Table 4-3 describes the batch annealing treatment with the temperature  $T_c$  and holding time  $t$ . Samples with 40%, 60%, 70% and 80% cold reduction were batch annealed in this way and hardness tested to assess the difference between samples which were ultra-rapid annealed and those subjected to conventional batch annealing.

Several samples with 70% cold reduction were annealed for various times at both 450° and 680°C to establish the relationship between hardness and annealing time.

#### 4.2.3 Ultra-rapid Annealing with Prior Recovery

Experiment 9 in Table 4-3 was designed to study ultra-rapid annealing with prior recovery. Samples with 70% cold reduction were annealed at 100°C for 1.5, 3, 5 and 10 hours, respectively, before ultra-rapid annealing at various heating rates to investigate the effect of prior recovery on softening. Samples with 40% cold reduction were also treated in the same way to study the effect of degree of deformation.

### 4.3 EXPERIMENTAL PROCEDURES AND TECHNIQUES

#### 4.3.1 Resistance Heating

##### 4.3.1.1 Apparatus

##### (1) General description

Resistance heating was achieved in an apparatus designed originally by A. Pearce and developed over a number of years in the Department of Materials Engineering at the University of Wollongong. The heating unit consisted basically of a controller, an electrical system, a specimen and a water quench device, linked as shown schematically in Fig. 4-2.

Figure 4-3 shows a photograph of the apparatus. The test piece in the form of a tensile profile was used both for fixing onto hangers and the clamping of electrical leads at either end. A tensile load of ~200 grams was applied at one end to prevent the specimen from buckling during heating. Water was chosen as the quench medium and was efficient enough to rapidly cool the specimen. The softening produced by these heat treatments was then investigated by hardness testing.

##### (2) Electrical System

A schematic diagram of the resistance heating circuit is given in Figure 4-4. Heating was effected in two stages - initial heating to peak temperature and an isothermal hold at this temperature. The first heating stage was accomplished by a variac autotransformer (A in Figure 4-4) which supplied an input voltage  $V_i$  between 0 and 240 volts to the step-down transformer and determined the specimen heating rate. A second transformer (B in Figure 4-4) supplied a voltage that produced the isothermal hold. Voltage  $V_2$  from transformer B varied from 0 to ~93 volts and was obtained by 3:1 reduction of the input voltage of 0 to 280 volts. The durations of the first and second stages of heating were determined by setting the timer in the control system.

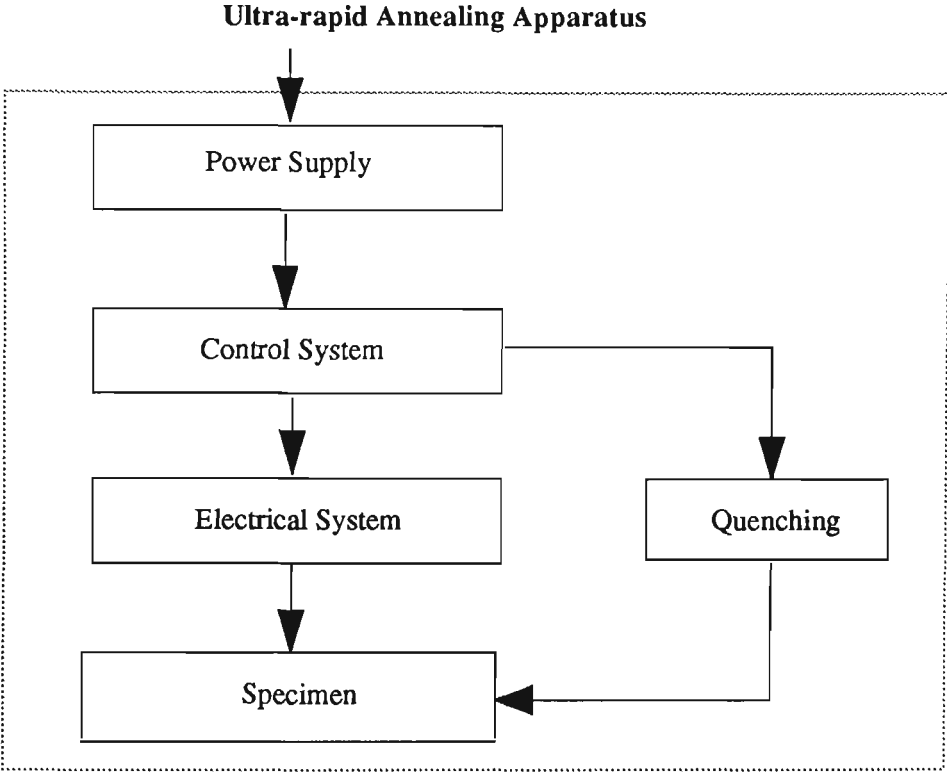


Fig. 4-2 Schematic diagram of ultra-rapid annealing apparatus.

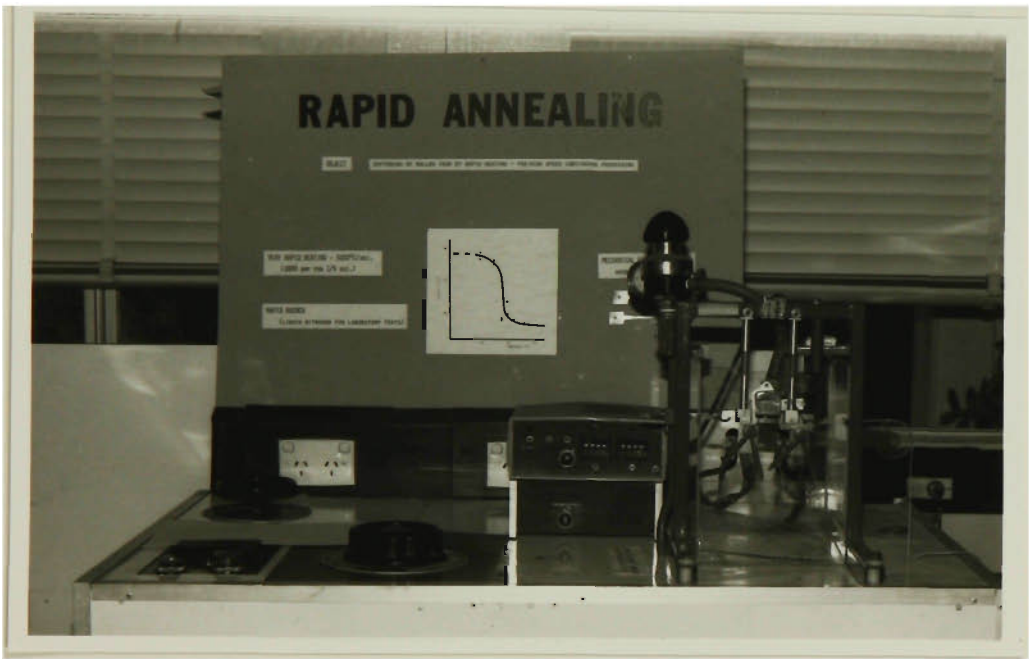


Fig. 4-3 Photograph showing the ultra-rapid annealing apparatus.

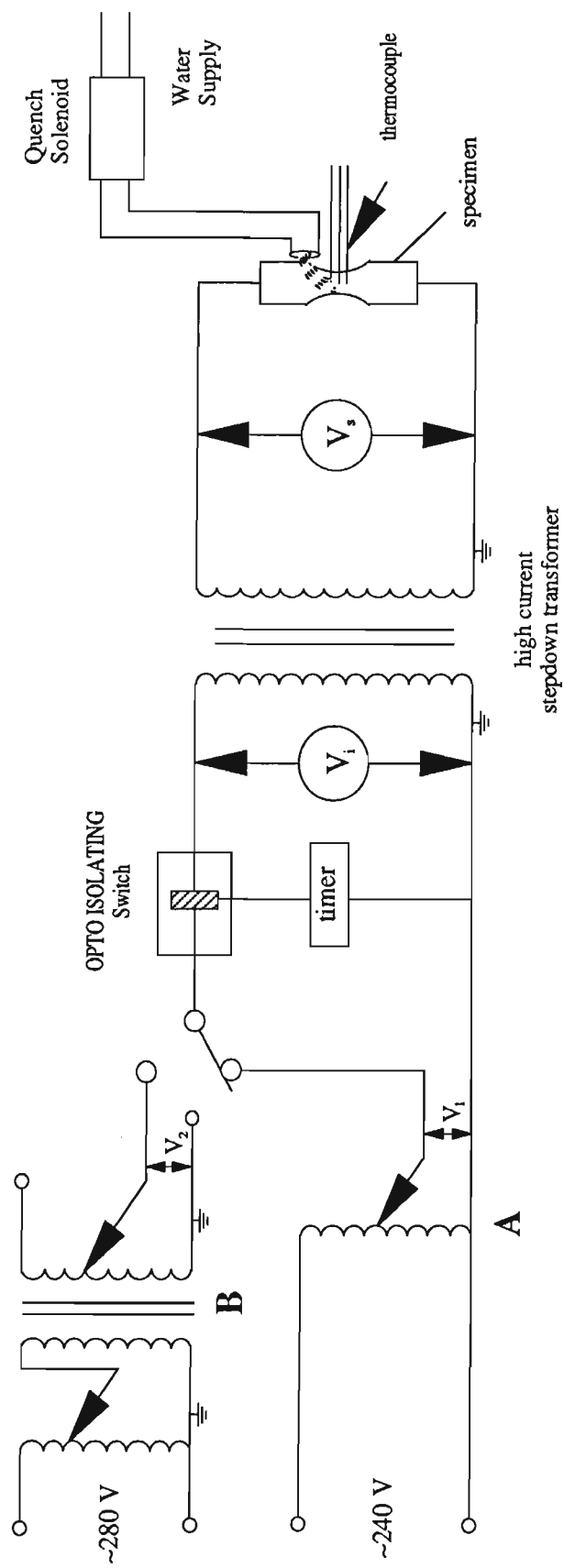


Fig. 4-4 Diagram showing the electrical system of the ultra-rapid annealing apparatus.

### (3) Control System

The control system consisted of a logic unit, a timer and a zero crossing switch, as schematically shown in Figure 4-5. The logic unit controlled the start of the first and second heating stages as well as the start of quenching. The timer was used to set the duration of the first heating stage  $t_1$  and the total heating time ( $t_1+t_2$ ). The zero crossing detector monitored the voltage waveform from the combination of the logic unit and the timer, and switched on or off the appropriate electrical circuit. The duration of heating was measured by counting the number of half cycles of alternating current.

### (4) Quenching System

Quenching was accomplished by spraying the test piece with water. A nozzle connected to a water supply was installed above the test piece and was activated after a present time by the control unit.

#### 4.3.1.2 Temperature Measurement

##### (1) General principles

Accurate temperature measurements are essential in quantifying both the heating rate and peak temperatures obtained in the thermal cycle. A three wire Chromel/Alumel thermocouple arrangement was used to construct a Wheatstone electrical bridge to measure specimen temperature. The three thermocouple wires were spot welded to the center part of the specimen at spacings of approximately 2.5 mm, with the Alumel wire in the middle flanked by two Chromel wires. The thermocouple output from one of the Chromel/Alumel pair was monitored on a Houston instrument chart recorder.

A three wire thermocouple arrangement has the advantage of being able to be balanced so that the emf generated by the current flowing in the test piece can be cancelled [366]. Balancing was achieved via a Wheatstone bridge consisting of a thermocouple trim potentiometer ( $RX_1$  and  $RX_2$ ) in Figure 4-6, which had a total resistance of  $100\Omega$ , and



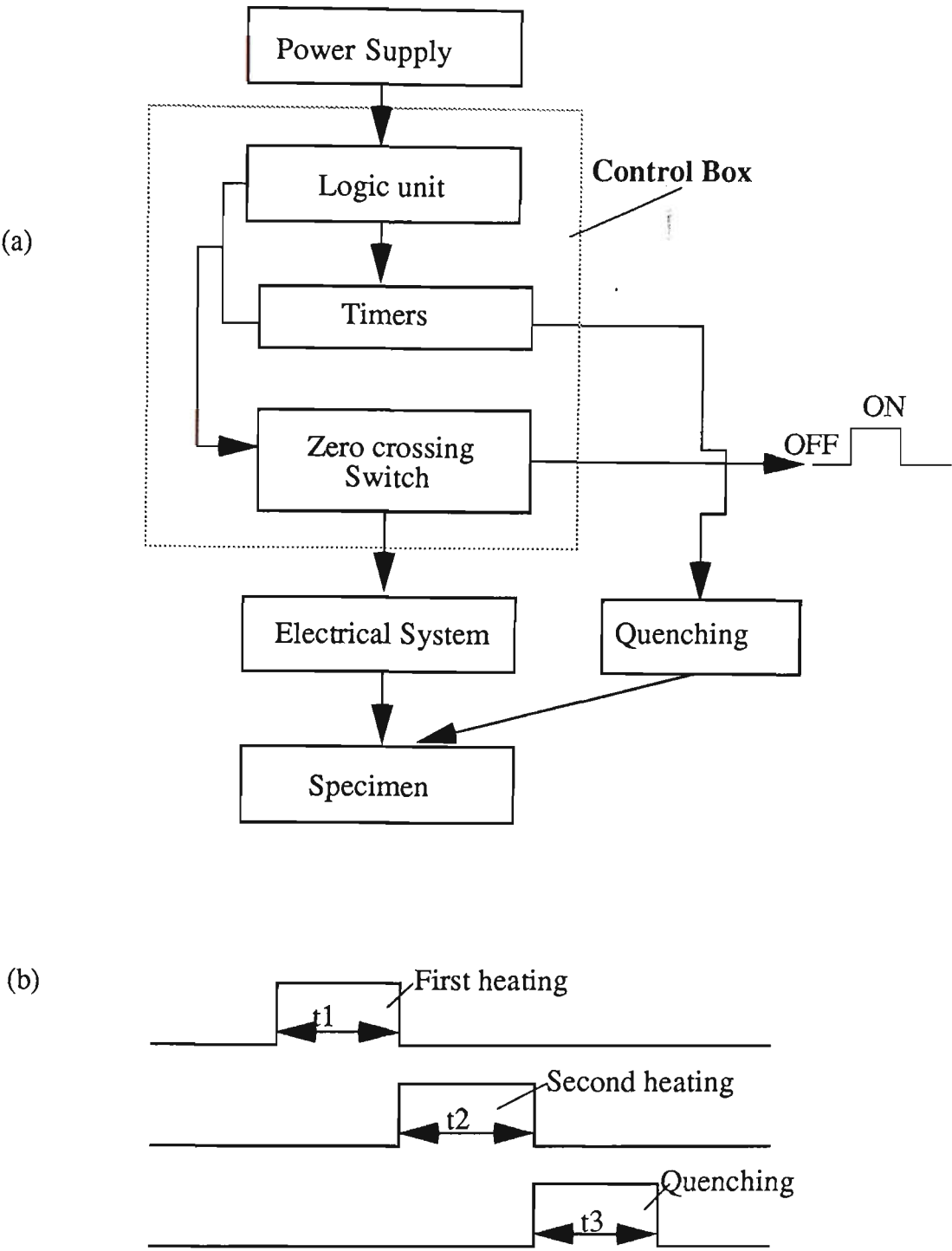


Fig. 4-5 Diagram showing (a) the control unit of ultra-rapid annealing apparatus; (b) the sequences of the control unit.

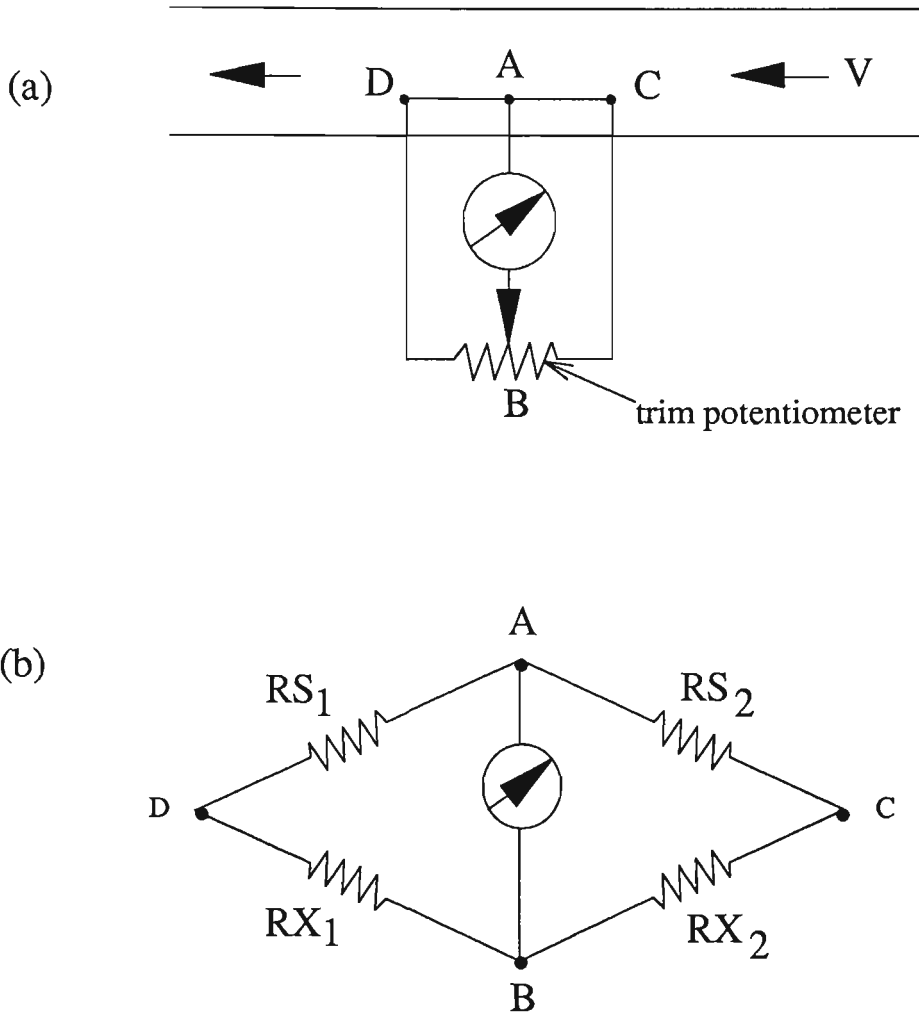


Fig. 4-6 Diagram showing (a) three wire thermocouple as wired to the specimen; (b) the equivalent Wheatstone bridge circuit of a three wire thermocouple.

the specimen resistances  $RS_1$  and  $RS_2$  between C and D (Figure 4-6). The emf.'s generated in sections AD and AC (between the thermocouples on the specimen) when a current is flowing, are determined by the specimen resistance  $RS_1$  and  $RS_2$ . If the material is uniform, then  $\frac{RS_1}{RS_2} = \frac{AD}{AC}$ . The lengths AD and AC were accurately measured using a travelling microscope and for the Wheatstone bridge to be balanced:

$$\frac{RX_1}{RX_2} = \frac{RS_1}{RS_2} = \frac{AD}{AC} \dots\dots\dots(4-1)$$

Since  $RX_1+RX_2 = 100 \Omega$  (the total potentiometer resistance) it follows that,

$$RX_2 = 100 \frac{AC}{AC+AD} \dots\dots\dots(4-2)$$

For this resistance, the bridge is balanced and the recorder receives an emf which is determined solely by the temperature of the specimen.

Temperature measurements obtained during a rapid annealing cycle are shown in Figure 4-7 for three specimens subjected to the same heating conditions. The peak temperatures varied by only 1°C, establishing that the measurements of peak temperature are reproducible.

(2) Practical problems

Several practical problems arose in determining experimentally the temperature profile.

- (a) There was a need for a large number of temperature measurements in various places on the test piece and for a variety of heating conditions because of a temperature gradient along the gauge length of the specimen. This gave rise to an extensive experimental programme.
- (b) The Wheatstone bridge had to be balanced for each specimen to account for differences in the distance of each of the two outside thermocouples from the central thermocouple.

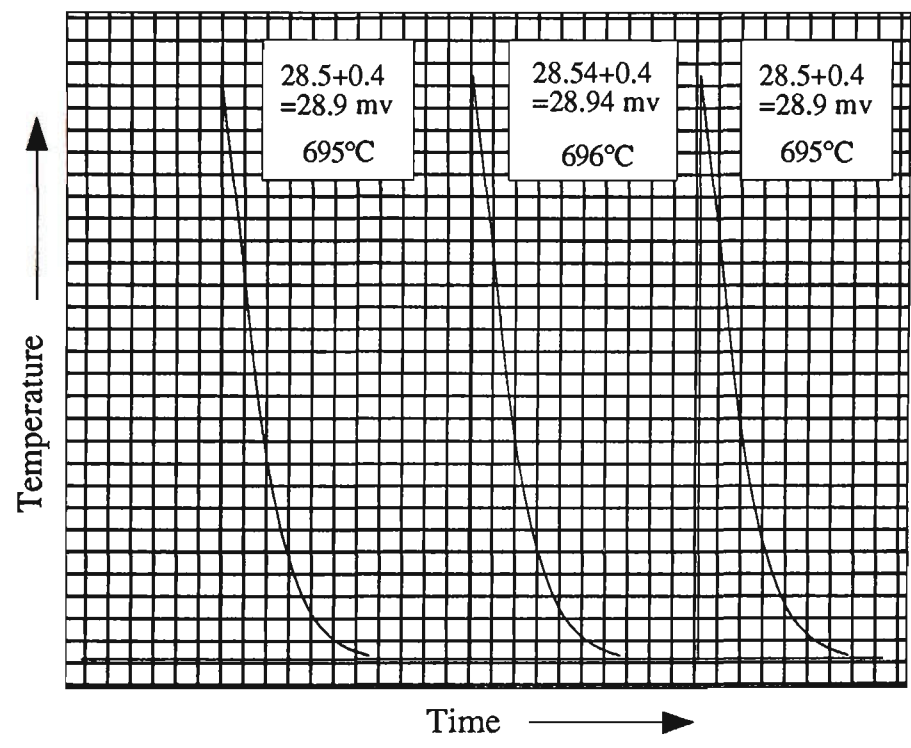


Fig. 4-7 Temperature recorder traces showing reproducibility of the thermal cycle.

(c) The welding of thermocouples to the specimen has an effect on the local microstructure.

Some of these problems can be avoided by applying a computer model.

#### 4.3.2 Computer Modelling of Temperature Profile in a Resistance Heated Specimen

##### 4.3.2.1 Advantages of Computer Modelling

The computer modelling of the ultra-rapid annealing process is an optimum way to determine the temperature profile. The model of the heating process, which is established on the basis of heat transfer, can be used to predict the temperature profile in the specimen within the range of conditions used and to evaluate the uniform heating zone. With the help of the computer model, it is possible to vary the heating conditions and the specimen shape to produce corresponding temperature profiles. Consequently, optimum heating conditions can be determined to establish a desired temperature profile which will lead to a uniformly heat treated tensile test piece.

##### 4.3.2.2 Development of Models

Research by Yip [7] revealed a number of deficiencies in the computer modelling of resistance heating investigated by Howes [294]. These deficiencies were :

- (1) all temperature dependent variables were assumed to be constant (including the specimen resistivity), while they were not;
- (2) electric current remained constant during heating, while it varied;
- (3) the temperature gradient was ignored between the gauge length and the flag length of the specimen ;
- (4) heat convection effect was not considered; and

(5) the predicted temperature increased as the number of the elements in the finite difference model increased.

Consequently, Yip redetermined the relationship between temperature and material properties in this model to account for change in heating current due to change in test piece resistance. Yip also established the existence of a temperature gradient in the test piece and determined an optimum number of elements to be used in the model in its modified form.

The equation used to describe the temperature profile of the test piece after completion of resistance heating was of the form:

$$T_n^{p+1} = T_n^p + \frac{\Delta t}{\rho C_p} \left( \frac{I^2 R - \eta \beta A (T_n^4 - T_\infty^4)}{V} + \frac{K}{\rho C_p} \frac{T_{n+1}^p - 2T_n^p + T_{n-1}^p}{\Delta X^2} \right) \quad \text{.....(4-3)}$$

with boundary conditions defined by:

$$T_{\text{center}}^{p+1} = T_n^p + \frac{\Delta t}{\rho C_p} \left( \frac{I^2 R - \eta \beta A (T_{\text{center}}^4 - T_\infty^4)}{V} + K \frac{T_{n+1}^p - 2T_n^p + T_{n-1}^p}{\Delta X^2} \right) \quad \text{.....(4-4)}$$

and

$$T_o^{p+1} = T_o^p + \frac{\Delta t}{\rho C_p} \left( \frac{I^2 R - \eta \beta A (T_o^4 - T_\infty^4)}{V} + K \frac{T_1 - T_o}{\Delta X^2} \right) \quad \text{.....(4-5)}$$

This is an explicit method, i.e. the new temperature at time (p+1) is determined by the temperature at the previous time p.

Subsequent improvements of the computer modelling carried out by Kelly [295] were principally confined to use of a specimen configuration which took into account the curved section between the "flag" and the "gauge" and allowed for analysis of materials other than iron by introducing variable coefficients in the material property equations.

However, Kelly's program did not converge very well and failed to include the heat convection effect. Therefore, it was necessary to establish a new computer model.

On the basis of heat transfer, an implicit finite difference method was used in the present investigation to obtain a temperature distribution which converges more readily than in the explicit method (see Chapter 5).

The implicit computer model program is listed in Appendix.

#### 4.3.2.3 Test piece design

A standard tensile profile 30 mm long by 5 mm wide central section and larger ends was found to heat up more in the center of the narrow section than at the ends. Therefore, the first task was to find a suitable size and shape of the test piece in an attempt to increase the uniformly heated area. Initially, several modifications of the standard tensile shape were investigated [9, 41], where the size of the uniformly heated area was gauged by visual estimation of the red hot area. In the present study, with the development of computer modelling, the size and shape of the specimen can be predicted which will provide the maximum uniformly heated area.

Given the conditions: first heating time  $t_1$ , soak time  $t_2$ , the heating rate controlled by the first heating voltage  $V_1$  and temperature  $T$ , the computer model determines the optimum sample size, i.e. the width if the length and thickness are known, or the thickness if the length and width are fixed. The overall length of the specimen was governed by the distance between the grips of the sample holder. For example, when the  $t_1 = 0.2$  second,  $t_2 = 0.1$  second,  $V_1 = 240$  volts and  $T = 800^\circ\text{C}$ , the optimum sample size is:  $w = 4.21$  mm,  $L = 30$  mm and  $t = 0.65$  mm.

### 4.3.3 Mechanical Testing

#### 4.3.3.1 Hardness

Two hardness testing machines, a standard Vickers machine and a Leitz low-load micro-hardness tester, each with a Vickers indenter, were used.

The conventional 2.5 kg load on the Vickers hardness tester is too high for the thickness of materials tested in the present investigation [9]. The general rule is that the thickness of the material being tested must be greater than seven times the diagonal length of the indentation. In this project, the maximum diagonal length measured was  $\sim 100\text{ }\mu\text{m}$  which suggest that a lower load than 2.5 kg should be used when testing the material 0.3 to 0.9 mm thick. Therefore, the applied load for both machines was chosen as 1 kg or 1000 grams.

The following techniques for estimating the extent of softening were applied to specimens subjected to ultra-rapid annealing or batch annealing.

(1) Hardness measurements made on a standard Vickers machine using a load of 1 kg with 2/3 in. objective lens. Five values were taken for each specimen and the figures averaged.

(2) Hardness distribution was carried out on a bench micro-hardness tester with a 1000 grams load ( specially machined) and a 4 mm objective lens. Hardness values were taken at  $\sim 0.1\text{ mm}$  intervals across the entire surface of the heating area of the specimen. Thus, for each condition, about 100 hardness values were recorded.

(3) Metallographic analysis was conducted with the specimen etched in a solution of 2% Nital. A Leitz MM6 optical microscope was used to correlate microstructural observations with the results obtained by the hardness survey.



#### 4.3.3.2 Tensile tests

##### (1) General description

A screw-driven "hard" tensile testing machine was used, which was built in collaboration with Vernier Engineering Company in Wollongong.

The annealed test piece was fixed in the sample holders and an electromechanical extensometer was used, which was able to accommodate a short gauge length and fitted between the specimen grips.

A data-logging device was connected to the tensile testing machine to collect data. Before testing, calibrations of force and the extensometer were necessary. A BBC computer was used to display the procedure of tensile testing and process data\*. Normally the start parameters were selected as follows: the original opening of the extensometer ( $E_0$ ) ~14 mm (the full opening is 21 mm); the original force ( $F_0$ ) ~ 5 N (the full scale is 200 N); the data collecting interval, 9/100 second; and the testing speed, 4 mm/min.

##### (2) Extensometer

The extensometer is the most important instrument during the testing of ductility of materials. The prototype instrument was designed by M. Atkinson [367] and was built on 'space frame' principles to combine high stiffness of the component parts with reasonably low mass. This construction allowed each pivot to be provided with widely spaced ball bearings, thus minimizing friction in the designed motion and obviating any other looseness. A tendency for the lower arm to fall was counteracted by fitting a light spring with an appropriate toggle action to maintain a constant balancing force.

Each arm was fitted with an adjustable, lateral, needle point and an opposing pressure pad with adjustable compliant spring. This arrangement is believed to minimize uncertainty

---

\* The programme was written by G.Hamilton, in the Department of Materials Engineering, the University of Wollongong.

about the gauge length by avoiding rolling contact error and any tendency to slip as the grip orientation changes with specimen extension. This view is sustained by experience which confirms that lateral grips operate reliably at very low grip pressure.

This instrument is illustrated in Fig. 4-8. The effective lever arm length is 60 mm and the lever ratio is 3:1.

### (3) Data processing

The changes in gauge length and force during tensile testing were recorded by a BBC microcomputer. Up to 16,000 bytes of information was logged in a test, depending on the ductility of the sample. The data were processed through the following steps:

(a) calculation and plotting of the relationship between strain and stress according to the Hollomon equation [368]:  $\sigma = k\epsilon^n$ ;

(b) calculation and plotting of the relationship between  $\log\left(\frac{d\sigma}{d\epsilon}\right)$  and  $\log \epsilon$  to present the Jaoul [369] equation:  $\log\left(\frac{d\sigma}{d\epsilon}\right) = \log(nk) + (n-1) \log \epsilon$ ;

(c) calculation and plotting of the relationship between  $\sigma \frac{d\epsilon}{d\sigma}$  and strain according to the equation [370]:  $\sigma \frac{d\epsilon}{d\sigma} = \frac{(\epsilon_0 + \epsilon)}{n(1 - \sigma_0/\sigma)}$ ;

(d) calculation and plotting of the relationship between  $\log \sigma$  and  $\log \epsilon$  according to the Voce logarithmic form:  $\log(\sigma - \sigma_0) = \log(k) + n \log(\epsilon + \epsilon_0)$ .

All the processing was carried out by the BBC computer simultaneously with tensile testing.

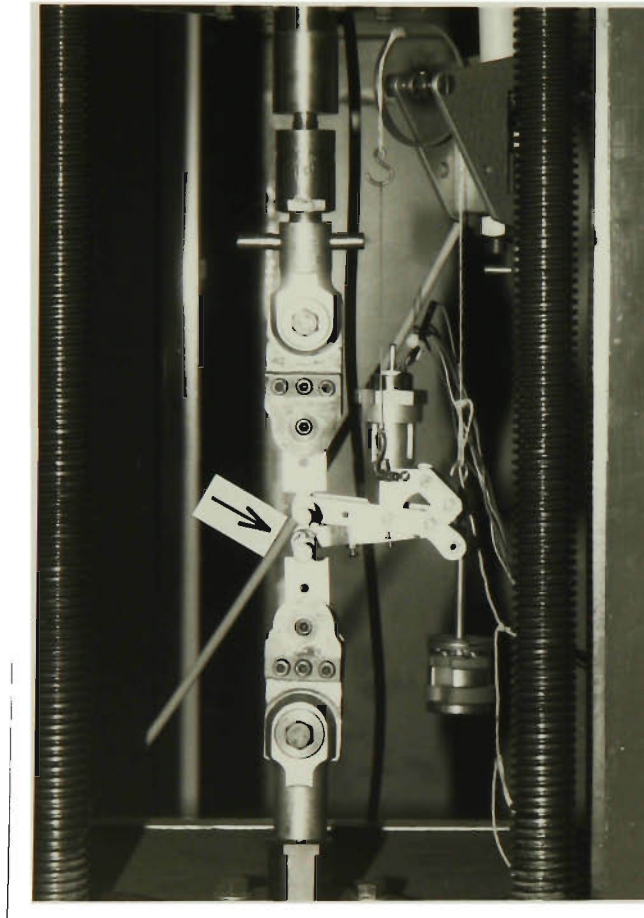


Fig. 4-8 The prototype extensometer in use testing a sample after ultra-rapid annealing (arrowed).

### 4.3.4 Microstructural Examination

#### 4.3.4.1 Optical Microscopy

A Leitz MM6 optical microscope was used in this investigation to examine structural changes associated with the softening process.

Test pieces were cut to expose a longitudinal cross-section which was and mounted into metallographic samples after annealing. Following grinding the sample surfaces were polished and etched for about 10-15 seconds in a solution of 2% Nital.

#### 4.3.4.2 Measurement of Grain Size Distributions

The distribution information obtained was the distribution of grain intercept areas in a two-dimensional section and these data were converted to the distribution of equivalent circle diameters. The more complex problem of determining the spatial distribution of grain diameters was not attempted, as it was assumed that the distribution of equivalent circle diameters reflected the true grain size variation in a given sample and the relative variation between samples. Support for the validity of this assumption is provided by the analysis of Shehata and Boyd [371].

The measured discrete distributions of grain size in both ultra-rapid annealing samples and batch annealing samples were skewed. Without making any assumptions about the form of the distributions, a skewness factor  $\gamma$  can be calculated using the following equations [372]:

$$\bar{D} = \frac{\sum N_i D_i}{\sum N_i} \quad \dots\dots\dots(3-6)$$

$$\sigma = \sqrt{\frac{\sum (D_i - \bar{D})^2}{\sum N_i}} \quad \dots\dots\dots(3-7)$$

$$\gamma = \frac{1}{\sigma^3} \frac{\sum N_i (D_i - \bar{D})^3}{\sum N_i} \quad \dots\dots\dots(3-8)$$

where  $\bar{D}$  is the arithmetic mean diameter,  $N_i$  is the number of grains in the interval represented by diameter  $D_i$ , and  $\sigma_v$  is the standard deviation.

For a distribution which is symmetrical about the mean,  $\gamma = 0$ ; and for an asymmetrical distribution,  $\gamma$  is positive or negative depending on the sense of skew. In the present case the skew was positive, having a pronounced tail which extended to larger grain size than the mean.

#### 4.3.4.3 Transmission Electron Microscopy

Thin foils from the samples subjected to various heating rates and with different cold reductions were examined using a JEM 2000FX (JEOL) Transmission Electron Microscope operating at 200 kV. The foils were produced by jet thinning with a solution of 15% perchloric acid and 85% acetic acid at room temperature under the conditions of 20 V, 200 mA for ~20 seconds.

# ***CHAPTER 5***

## **COMPUTER MODELLING**

## 5.1 INTRODUCTION

The significance of temperature measurements has been addressed in Chapter 4, which demonstrates that computer modelling of the ultra-rapid annealing process is the best way to determine the temperature profile during such a short cycle time. However, ultra-rapid annealing by resistance heating is actually very complicated, and involves many variables that may give errors which are difficult to detect. Also, the temperature equation for the explicit methods has problems in stability and convergence. Therefore, an implicit method has been chosen to imitate the temperature distribution during resistance heating and this method has proven very satisfactory for the present investigation.

The computer programme for the implicit method is given in Appendix A.

## 5.2 NOMENCLATURE

The symbols used in Chapter 5 have the following definitions:

$R_p$  = potentiometer setting (ohms)

$a, b$  = distance between each thermocouple wire (m)

$T_n^{p+1}$  = temperature at (p+1) time of the element n ( $^{\circ}\text{K}$ )

$\Delta t$  = time interval (second)

$\rho$  = density ( $\text{g}/\text{m}^3$ )

$C_p$  = specific heat ( $\text{J}/\text{g}^{\circ}\text{K}$ )

$I$  = current ( amps)

$R$  = resistance (ohm)

$K$  = thermal conductivity ( $\text{W}/\text{m}^{\circ}\text{K}$ )

$\Delta X$  = length of the element (m)

$\epsilon$  = emissivity

$\sigma$  = Stefan-Boltzmann constant (  $\text{J}/\text{m}^2 \text{ }^{\circ}\text{K}^4$  )

$S_r$  = area of radiation ( $\text{m}^2$ )

$V$  = volume ( $\text{m}^3$ )

$T_{\infty}$  = environmental temperature (  $^{\circ}\text{K}$ )

$S_c$  = across area of conduction ( $\text{m}^2$ )

$h$  = heat convection coefficient

$m$  = mass of the element (g)

$q_i$  = heat density at point i ( $\text{J}/\text{m}^2$ )

$\Omega$  = resistivity (ohms\*m)

$RAD$  = radius of connection between flag and gauge of specimen (m)

$NUMX1$  = number of division along gauge length

$NUMX2$  = number of division along flag length

$NUMX3$  = number of division along curved part of specimen



$S$  = thickness of the element (m)

$W$  = width of the element (m)

$Nuf$  = Nusselt number

$x$  = vertical plane width

$g$  = acceleration of gravity ( $m/sec^2$ )

$\mu$  = dynamic viscosity

$\nu$  = kinetic viscosity

$G_{rf}$  = Grashot number

$Pr_f$  = Prandtl number

### 5.3 TEMPERATURE EQUATION

Consider the general case of a one-dimensional system shown in Figure 5-1, where the temperature may change with time and heat sources may be present within the body. For the element of thickness  $dx$  the following energy balance may be made:

Net energy conducted in the element + heat generated within the element – energy lost by radiation – energy lost by convection = temperature change with time [373].

The net energy conducted in the element =  $-S_c(q_{i+1/2} - q_{i-1/2})$

heat generated within the element =  $I^2 R$

energy lost by radiation =  $\epsilon \sigma S_r (T^4 - T_\infty^4)$

energy lost by convection =  $h S_r (T - T_\infty)$

temperature change =  $\rho C_p \frac{\partial T}{\partial t} S_c \Delta X$

That is :

$$-S_c(q_{i+1/2} - q_{i-1/2}) + I^2 R - \epsilon \sigma S_r (T^4 - T_\infty^4) - h S_r (T - T_\infty) = \rho S_c \Delta X C_p \frac{\partial T}{\partial t} \quad \text{.....(5-1)}$$

$$\frac{S_c(q_{i+1/2} - q_{i-1/2})}{S_c \Delta X} + \frac{I^2 R}{S_c \Delta X} - \frac{\epsilon \sigma S_r (T^4 - T_\infty^4)}{S_c \Delta X} - \frac{h S_r (T - T_\infty)}{S_c \Delta X} = \rho C_p \frac{\partial T}{\partial t} \quad \text{.....(5-2)}$$

Since  $S_c = S * W$   $S_r = 2(\Delta X * W + S * \Delta X) = 2\Delta X(S + W)$

$$q = -k \frac{T}{X} \quad R = \Omega \frac{\Delta X}{S_c} = \Omega \frac{\Delta X}{S * W}$$

$$\frac{\partial}{\partial X} \left( k \frac{\partial T}{\partial X} \right) + I^2 R \frac{\Omega}{S * W} * \frac{1}{S * W} - \frac{2\epsilon \sigma (S + W)}{S * W} (T^4 - T_\infty^4) - \frac{2h(S + W)}{S * W} (T - T_\infty) = \rho C_p \frac{\partial T}{\partial t} \quad \text{.....(5-3)}$$

$$\rho C_p \frac{\partial T}{\partial t} = \frac{\partial}{\partial X} \left( k \frac{\partial T}{\partial X} \right) + I^2 \frac{\Omega}{S^2 * W^2} - 2\epsilon \sigma \frac{S + W}{S * W} (T^4 - T_\infty^4) - 2h \frac{S + W}{S * W} (T - T_\infty) \quad \text{.....(5-4)}$$

Now  $A = I^2 \frac{\Omega}{S^2 * W^2}$

$$D = 2\epsilon\sigma \frac{S+W}{S*W}$$

$$F = 2h \frac{S+W}{S*W}$$

$$\rho C_p \frac{\partial T}{\partial t} = \frac{\partial}{\partial X} \left( k \frac{\partial T}{\partial X} \right) + A - D(T_p^4 - T_\infty^4) - F(T - T_\infty) \quad \dots\dots(5-5)$$

Consider point P, whose temperature is  $T_p$ , point W to the left ( $T_w$ ) and point E to the right ( $T_E$ ) (shown in Figure 5-2).

When the time changes from  $t$  to  $t+\Delta t$ , we have

$$\begin{aligned} \int_w^e \int_t^{t+\Delta t} \rho C_p \frac{\partial T}{\partial t} dx dt &= \int_t^{t+\Delta t} \int_e^w \frac{\partial}{\partial X} \left( k \frac{\partial T}{\partial X} \right) dx dt - \int_t^{t+\Delta t} \int_w^e D(T_p^4 - T_\infty^4) dx dt \\ &\quad - \int_t^{t+\Delta t} \int_w^e A dx dt + \int_t^{t+\Delta t} \int_w^e F(T_p - T_\infty) dx dt \\ &= \int_t^{t+\Delta t} \left[ K_E \frac{T_E - T_P}{(\delta X)_E} - K_W \frac{T_P - T_W}{(\delta X)_W} \right] dt - D(T_p^4 - T_\infty^4) \Delta X \Delta t + A \Delta X \Delta t - F \Delta X \Delta t (T_p - T_\infty) \end{aligned} \quad \dots\dots\dots(5-6)$$

$$\begin{aligned} \rho C_p \Delta X (T_p^1 - T_p^0) &= \left[ \frac{K_E (T_E - T_P)}{(\delta X)_E} - \frac{K_W (T_P - T_W)}{(\delta X)_W} \right] \Delta t - D(T_p^4 - T_\infty^4) \Delta X \Delta t \\ &\quad + A \Delta X \Delta t - F \Delta X \Delta t (T_p - T_\infty) \quad \dots\dots\dots(5-7) \end{aligned}$$

$$\begin{aligned} \rho C_p \frac{\Delta X}{\Delta t} (T_p^1 - T_p^0) &= \left[ \frac{K_E (T_E - T_P)}{(\delta X)_E} - \frac{K_W (T_P - T_W)}{(\delta X)_W} \right] - D(T_p^4 - T_\infty^4) \Delta X \Delta t \\ &\quad + A \Delta X \Delta t - F \Delta X \Delta t (T_p - T_\infty) \quad \dots\dots\dots(5-8) \end{aligned}$$

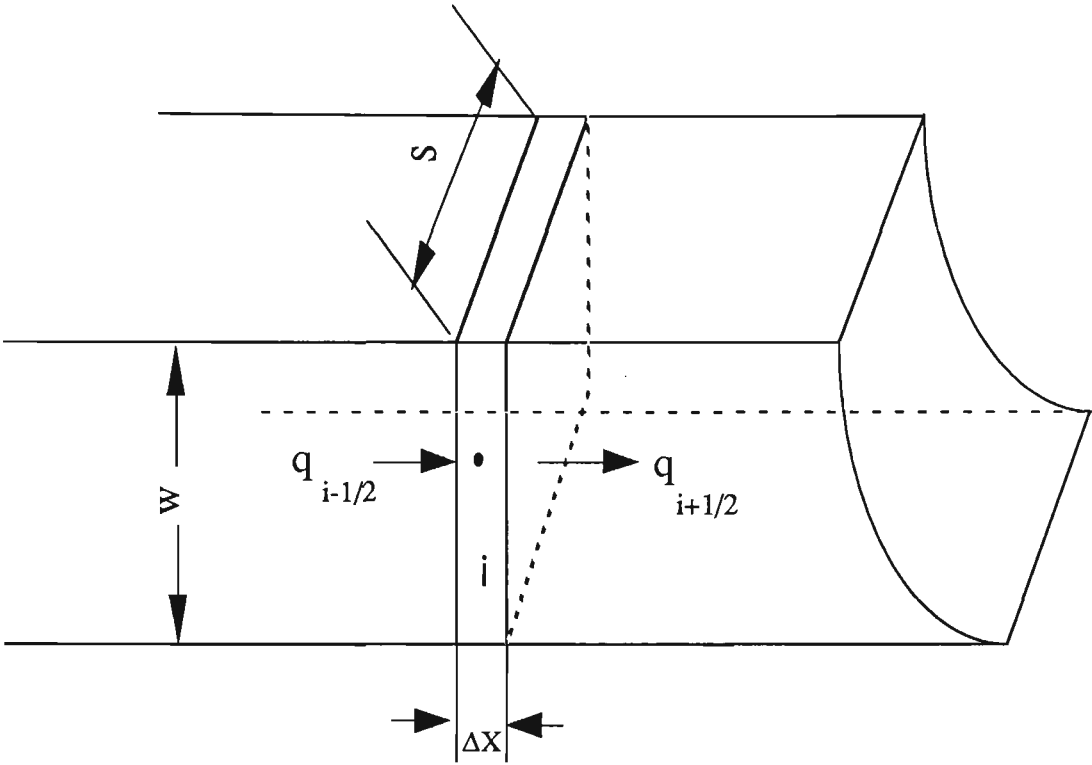


Fig. 5-1 Schematic diagram of one-dimensional system

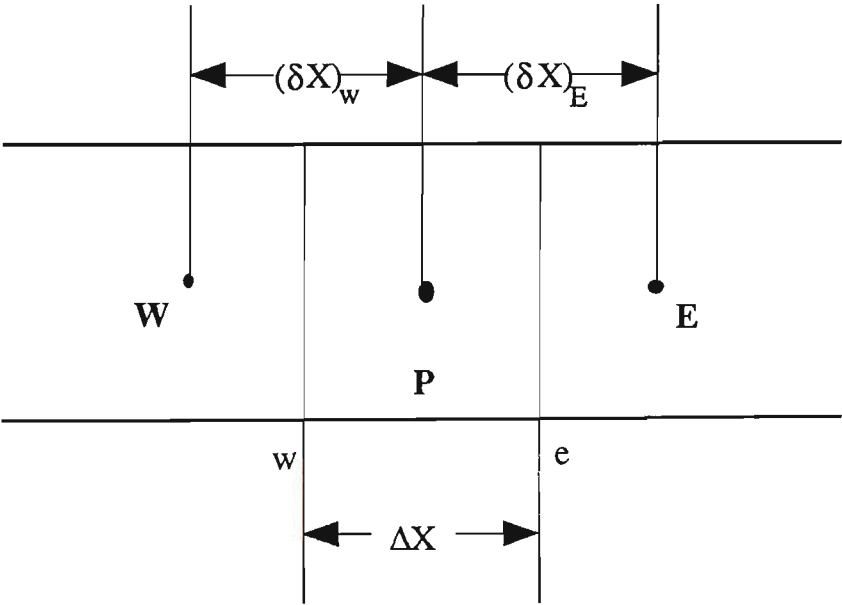


Fig. 5-2 Position of P and its adjacent points

$$\begin{aligned}
 \left[ \rho C_p \frac{\Delta X}{\Delta t} + \frac{K_E}{(\delta X)_E} + \frac{K_W}{(\delta X)_W} \right] T_p &= \rho C_p \frac{\Delta X}{\Delta t} T_p^0 + \frac{K_E}{(\delta X)_E} T_E + \frac{K_W}{(\delta X)_W} T_W + D T_\infty^4 \Delta X \\
 &+ A \Delta X + F \Delta X T_\infty + [ - ( D T_p^3 \Delta X + F \Delta X ) ] T_p \dots\dots\dots(5-9)
 \end{aligned}$$

After moving terms:

$$\begin{aligned}
 \left( \rho C_p \frac{\Delta X}{\Delta t} + \frac{K_E}{(\delta X)_E} + \frac{K_W}{(\delta X)_W} - S_p \right) T_p &= \frac{K_E}{(\delta X)_E} T_E + \frac{K_W}{(\delta X)_W} T_W \\
 &+ \rho C_p \frac{\Delta X}{\Delta t} T_p^0 + S_c \dots\dots\dots(5-10)
 \end{aligned}$$

which can be written as:

$$a_p T_p = a_E T_E + a_W T_W + b \dots\dots\dots(5-11)$$

where  $a_E = \frac{K_E}{(\delta X)_E}$

$$a_W = \frac{K_W}{(\delta X)_W}$$

$$S_p = -(D T_p^3 + F) \Delta X$$

$$a_p = a_E + a_W - S_p + \rho C_p \frac{\Delta X}{\Delta t}$$

$$b = S_c + \rho C_p \frac{\Delta X}{\Delta t} T_p^0$$

$$A = I^2 \frac{\Omega}{S^2 W^2}$$

$$D = \frac{2\epsilon\sigma(S+W)}{S*W}$$

$$F = \frac{2(S+W)h}{S*W}$$

Equation (5-11) is the temperature equation at point P expressed by the implicit method.

5.4 BOUNDARY CONDITIONS

5.4.1 At center and edges

At the center :  $\frac{\partial T}{\partial X} = 0$ , i.e.  $T(I,J) = T(I,J-1)$

At the edges :  $T = T_0$  ( room temperature )

Normally we put in a relaxation coefficient to control the iteration, i.e.

$$T_p = T_p^* + \alpha \left( \frac{(\sum a_n b^* T_n b + b)}{a_p} - T_p^* \right) \dots\dots\dots(5-12)$$

where  $\alpha$  --- relaxation coefficient.  $T_p^*$  can be obtained from equation (5-11).

5.4.2 Curved parts of a specimen

For the curved parts of a specimen, we may change the width of the specimen with iteration (shown in Figure 5-3 ).

For the flag :  $W = \text{WID2} \text{ ( } J < \text{NUMX2) }$

For the gauge :  $W = \text{WID1} \text{ ( } J > (\text{NUMX2} + \text{NUMX3}))$

For the curved parts :  $W = \text{WID1} + 2\text{RAD} - 2\Delta W(J - \text{NUMX2})$

Where  $\Delta W = \frac{\text{RAD}}{\text{NUMX3}}$      $\text{NUMX3} = \text{RAD} * \frac{\text{NUMX1}}{L1}$

Therefore

$$W = W( D1 + 2\text{RAD} - 2\text{RAD} * \frac{\text{NUMX1}}{L1} * (J - \text{NUMX2}) \dots\dots\dots(5-13)$$

$$( \text{NUMX2} < J < ( \text{NUMX2} + \text{NUMX3} ) )$$

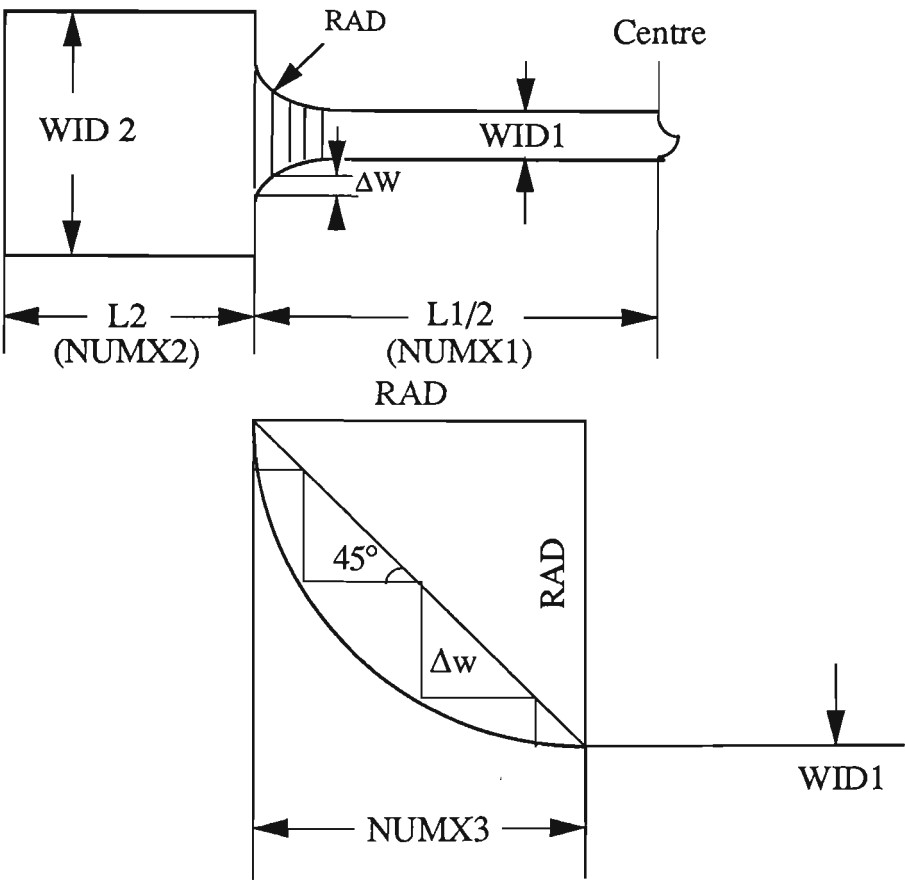


Fig. 5-3 The curved part of a specimen

5.5 VARIATION OF THE PHYSICAL PROPERTIES WITH TEMPERATURE

The equation used for iron was obtained either directly from the literature or by regression analysis of data obtained from the literature.

The equations used are:

(1) Thermal conductivity :

$$K = 91.745 - 0.065T \text{ ( } 273^{\circ} \text{ K} < T < 673^{\circ} \text{ K)} \quad \dots\dots\dots(5-14)$$

$$K = 79.968 - 0.0475T \text{ ( } 673^{\circ} \text{ K} < T < 1100^{\circ} \text{ K)} \quad \dots\dots\dots(5-15)$$

units : W/m\*K

(2) Heat capacity :

$$C_p = 665.164 + 1.105 \times 10^{-1}T - 4226.965 \times T^{-0.5} \text{ (} 273^{\circ}\text{K} < T < 1100^{\circ}\text{K)} \quad \dots\dots\dots(5-16)$$

units : J/K\*kg

(3) Resistivity :

$$\Omega = (9.918 - 2.024 \times 10^{-2}T + 1.034 \times 10^{-4}T^2) \times 10^{-8} \text{ (} 273^{\circ}\text{K} < T < 1100^{\circ}\text{K)} \quad \dots\dots\dots(5-17)$$

units : ohms\*m

(4) Emissivity :

The emissivity of iron was taken as a constant at 0.2.

(5) Density :

The density of iron was taken as 7865 kg/m<sup>3</sup>

(6) Heat convection coefficient :



The heat convection coefficient is very complicated. There are different values for different ranges, as shown in Table 5-1.

Table 5-1 Constants for isothermal vertical surface

Geometry	$G_{rf} * P_{rf}$	C	m
Vertical planes and cylinders	$10^{-1}$ - $10^4$	1.5849	4 / 25
	$10^4$ - $10^9$	0.59	1 / 4
	$10^9$ - $10^{13}$	0.10	1 / 3

where

$$N_{uf} = \frac{hx}{K}$$

$$h = \frac{N_{uf} K}{x}$$

.....(5-18)

and

$$N_{uf} = C ( G_{rf} * P_{rf} )^m$$

.....(5-19)

C and m can be obtained from Table 5-1.

$$G_{rf} = \frac{gb(T_W - T_{\infty})x^3}{u^2}$$

.....(5-20)

$$P_{rf} = \frac{\nu}{\alpha} = \frac{C_p \mu}{K}$$

.....(5-21)

$$\beta = \frac{1}{T_f}$$

$$T_f = \frac{T_W + T_{\infty}}{2}$$

.....(5-22)

5.6 COMPARISON WITH THE EQUATIONS OF THE EXPLICIT METHOD

As mentioned earlier, the usefulness of the heat transfer analysis in resistance heating lies in the production of a temperature profile for a system at any point for any moment, which is based on the finite elements  $\Delta X$  and  $\Delta t$ . At each stage in the calculation, no matter how small  $\Delta X$  and  $\Delta t$  are, some roundoff errors exist. However, stability and convergence must be taken into account in addition to the roundoff errors for the explicit method when heat transfer is applied to the resistance heating problem.

5.6.1 Stability

The equation used to describe the temperature profile of a test piece in a finite-difference by the explicit method is of the form [7]:

$$T(X,t+\Delta t)=\frac{\alpha\Delta t}{(\Delta X)^2}(T(X+\Delta X,t) + T(X-\Delta X,t)) + \left(1 - \frac{2\alpha\Delta t}{(\Delta X)^2}\right)T(X,t) \quad \dots\dots\dots(5-23)$$

where  $\alpha = \frac{k}{\rho C_p}$

The important term to note in equation (5-23) is  $\frac{\alpha\Delta t}{(\Delta X)^2}$ , i.e.,  $\frac{1}{M}$  ( $M = \frac{(\Delta X)^2}{\alpha\Delta t}$ ). Equation (5-23) is stable only when  $M \geq 2$ , i.e.,  $\frac{1}{M} \leq 0.5$ . If  $\frac{1}{M}$  is larger than 0.5, equation (5-23) describes heat transferring from a colder region to a hotter one, which is impossible. This relationship becomes the stability criteria for one dimensional solution of the finite difference.

Besides, the temperatures predicted by the explicit method show a tendency to increase as the heating time increases ( see Fig. 5-4) under the circumstance of stability, while the values predicted by the implicit method ( Fig. 5-5) in the present investigation are quite stable no matter how long the heating time is. For comparison, the data predicted by both the explicit and the implicit method with the time interval of 0.1, 0.05 and 0.02 seconds are listed in Tables 5-2 and 5-3.

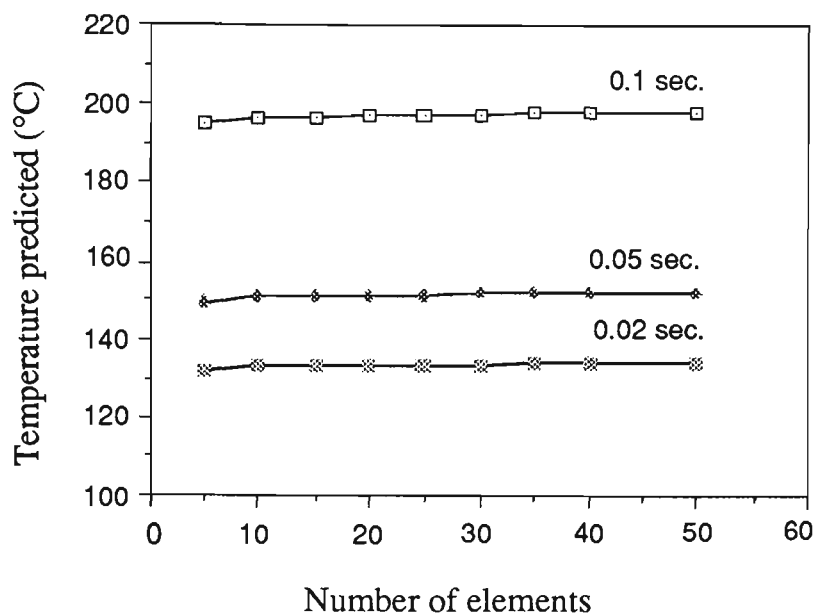


Fig. 5-4 The temperatures predicted by the explicit method under conditions of  $t_1 = 0.2$  sec.,  $t_2 = 0.3$  sec. and  $V_1 = 130$  V, showing that the values are not stable as the time interval changes.

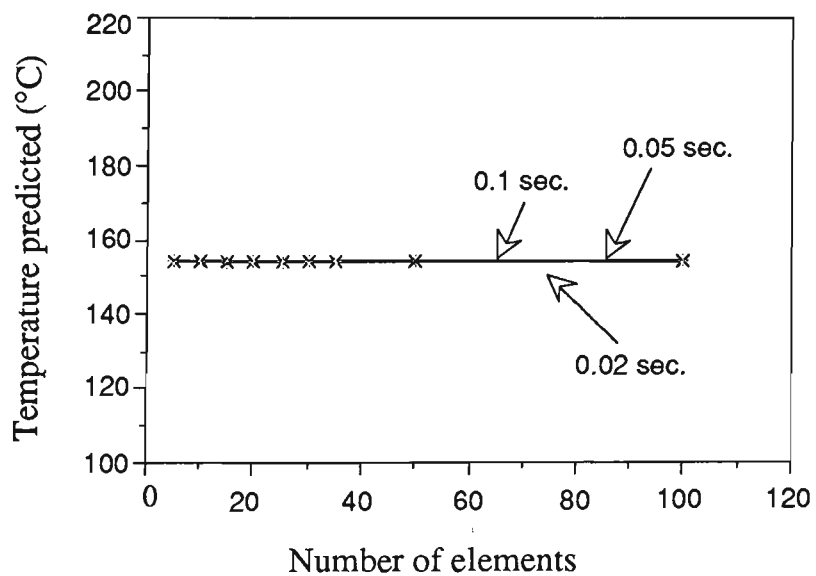


Fig. 5-5 The temperatures predicted by the implicit method under conditions of  $t_1 = 0.2$  sec.,  $t_2 = 0.3$  sec. and  $V_1 = 130$  v, showing that the values are very stable no matter what the time interval is.

Table 5-2 Temperatures predicted by the **explicit** method

No. of elements	Temperature(°C) $t_i = 0.1 \text{ sec.}$	Temperature(°C) $t_i = 0.05 \text{ sec.}$	Temperature(°C) $t_i = 0.02 \text{ sec.}$
5	194.6075	149.67614	132.53579
10	196.1390	150.62492	133.35139
15	196.5405	150.88803	133.57326
20	197.0405	151.19576	133.91762
25	197.2110	151.29433	133.91762
30	197.5328	151.49946	134.08796
35	197.7050	151.59875	134.22675
40	197.7063	151.59469	134.15559
50	197.9260	151.71313	134.23960

Table 5-3 Temperatures predicted by the **implicit** method

No. of elements	Temperature(°C) $t_i = 0.1 \text{ sec.}$	Temperature(°C) $t_i = 0.05 \text{ sec.}$	Temperature(°C) $t_i = 0.02 \text{ sec.}$
5	153.89611	153.89612	153.89614
10	153.89609	153.89610	153.89612

Table 5-3 Temperatures predicted by the **implicit** method (continued)

15	153.89596	153.89597	153.89599
20	153.89567	153.89568	133.91762
25	153.89713	153.89714	153.89516
30	153.89672	153.89673	153.89675
35	153.89738	153.89739	153.89741
50	153.89739	153.89740	153.89741
100	153.89739	153.89740	153.89741

5.6.2 Convergence

The temperature change with time interval under various numbers of elements is shown in Figs. 5-6 and 5-7.

The temperatures predicted by the explicit method (Fig. 5-6) show a big gap at different time intervals. The condition  $\Delta t < \frac{\rho C_p (\Delta X)^2}{2k}$  must be checked to ensure the convergence.

The temperatures predicted by the implicit method (Fig.5-7) approach a stable value when enough time intervals are selected, no matter what  $\Delta t$  is. Therefore, the implicit method has better convergence.

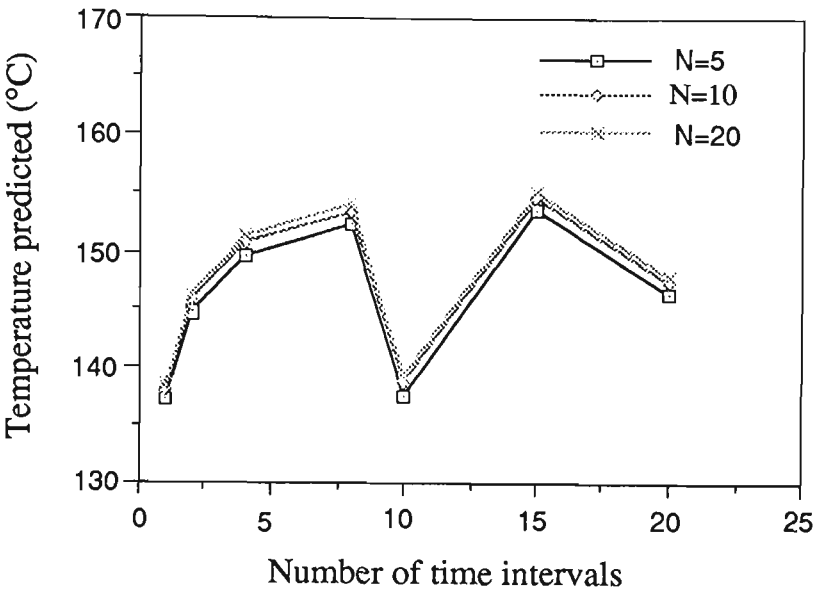


Fig. 5-6 The temperatures predicted by the explicit method under the conditions of  $t_1=0.2$  sec.,  $t_2=0.3$  sec. and  $V_1=150$  V, showing that the values do not convergence to a stable one.

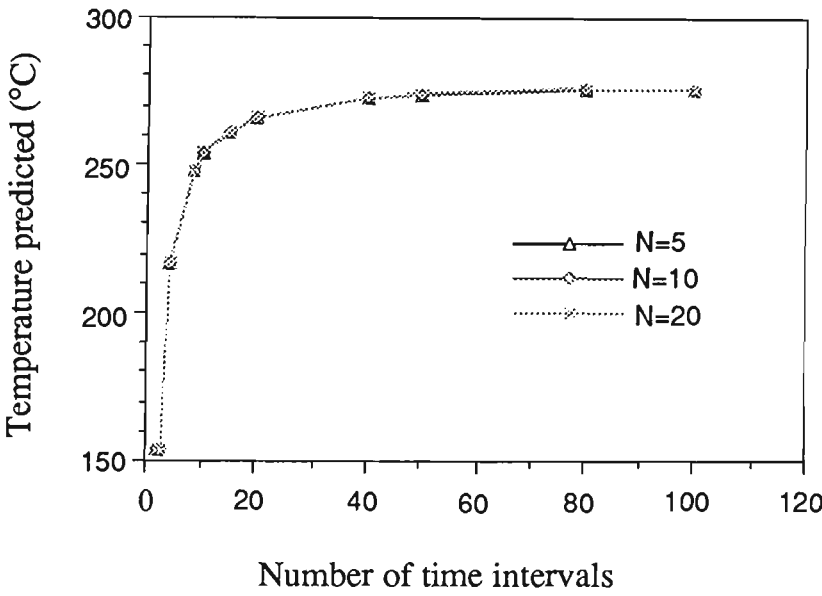


Fig. 5-7 The temperatures predicted by the implicit method under the conditions of  $t_1=0.2$  sec.,  $t_2=0.3$  sec. and  $V_1=150$ v, showing that the values do converge to a stable one no matter what the number of elements.

## 5.7 RESULTS AND DISCUSSION

Measurements of the actual temperature profiles of the specimen at varying heating rates were obtained by using the three wire thermocouple network. This network gives correct and reproducible emf values which are converted to the corresponding temperature values. The results of the temperature measurement show that as the rate of heating becomes higher the temperature profile of the specimen flattens out as predicted by the computer model (shown in Fig. 5-8 ). This is due to the fact that conduction at higher temperatures becomes less efficient since there is not as steep a temperatures gradient along the specimen as when the heating rate is low. Also at high temperature , heat loss due to radiation and convection becomes more important, while conduction heat transfer becomes negligible.

The present computer model gives an overall underestimate of the temperature distribution along the length of the specimen, as shown in Fig. 5-9. As the number of elements considered by the programme increases, the temperature profile predicted by the model converges to give a reasonable temperature profile. This is because that as the length of the element decreases, and for a small time increment, the model approaches steady state heating conditions which is the basic assumption of the model. Also, the algorithm is a form of a finite difference method and the model becomes more accurate with smaller element size.

By comparing the temperatures experimentally measured and calculated by computer (see Fig. 5-10), it is found that the value calculated by computer is very close and the error is less than 1%. This has not been achieved before.

In summary, the computer model established on conduction, radiation and convection heat transfer gives a very satisfactory temperature profile which exerts significant contributions to the study of ultra-rapid annealing.

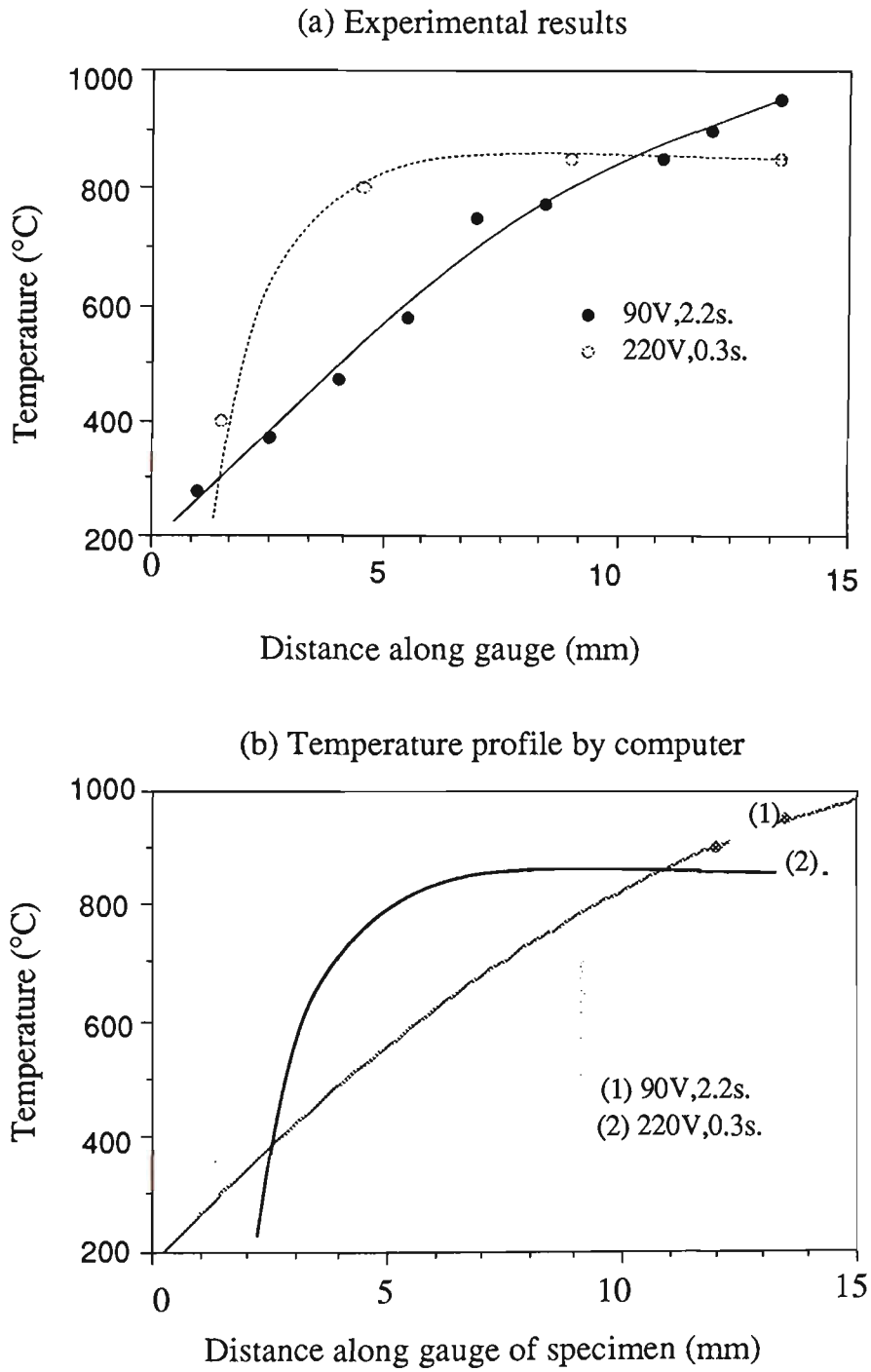


Fig. 5-8 Comparison of the temperatures (a) experimentally measured and (b) predicted by the computer modelling using the implicit method.



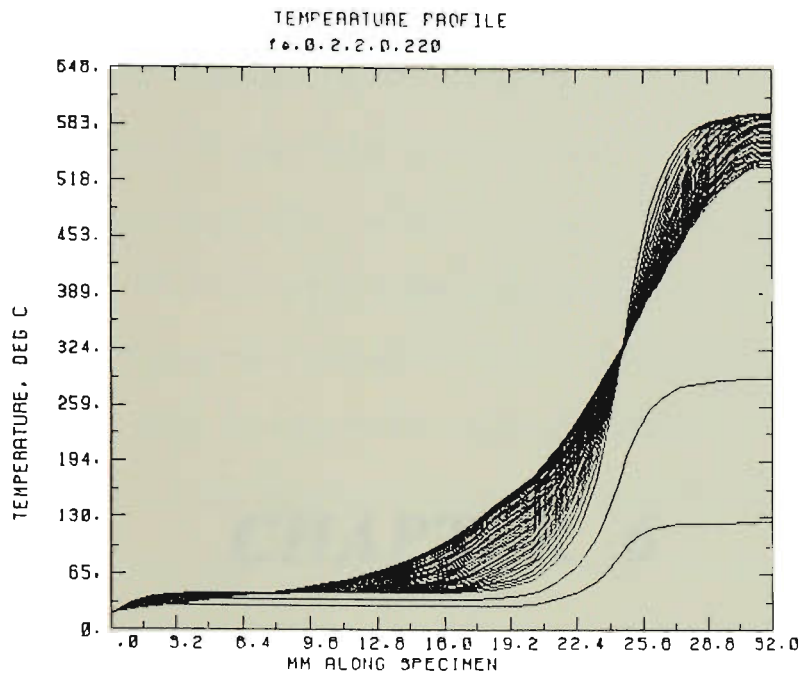


Fig. 5-9 The temperature profiles predicted by computer modelling using the implicit method during ultra-rapid annealing at  $t_1 = 0.2$ ,  $t_2 = 1.8$  sec. and  $V_1 = 220$  V. (the time interval for plotting the curve is 0.05 sec.)

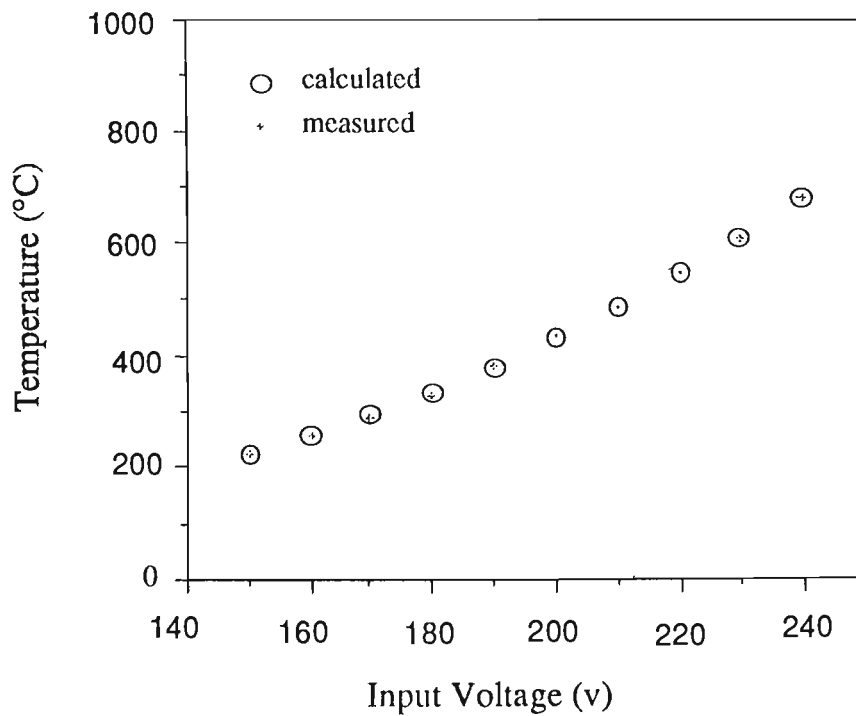


Fig. 5-10 Comparison of the temperatures experimentally measured and predicted by the computer modelling using the implicit method at various input voltages.

# ***CHAPTER 6***

## **RESULTS**

## 6.1 INTRODUCTION

The experimental procedures and techniques are described in the fourth chapter of the thesis. The results of the investigation are presented in the following five sections. In the first part, the primary task of calibration of the resistance heating apparatus is described, i.e. investigating the variables of the first heating voltage  $V_1$ , the heating rate, the second heating voltage  $V_2$ , the maximum (constant) temperature  $T_c$ , the soak time and the specimen size. The effect of these variables on softening is ascertained using experiments 1 through 6 in Table 4-3. In the second section, results relating to the influence of different heat treatments (ultra-rapid annealing and batch annealing), prior recovery processes and cold reductions on softening behaviour of the material are presented. Hardness distributions in the samples after various heat treatments are given in the next section, followed by tensile property measurements. Finally, optical and electron microstructures representing various heat treatment conditions are presented and the results of measurements and analysis of the grain size distributions are given.

## 6.2 CALIBRATIONS OF THE RESISTANCE HEATING APPARATUS

Material with 70% cold reduction was used in the following experiments which were designed to calibrate the resistance heating apparatus.

### 6.2.1 The Heating Rate and the Maximum Temperature during the First Heating (Experiment 1, Table 4-3)

The temperature variation with time during the first heating is dependent on the first heating input voltage. Figure 6-1 shows typical experimental results in which each curve represents the temperature variation at the specified first heating voltage for a common first heating time of 0.2 seconds. The maximum temperature can be obtained from the curve and the first heating rate can then be calculated by dividing the maximum temperature by the first heating time  $t_1$ . The relationship between the first heating voltage and the maximum temperature obtained at the end of the first heating for  $t_1 = 0.2, 0.3$  and 0.5 seconds is given in Fig. 6-2. The results indicate that for the present material the maximum temperature for a certain heating time depends on the first heating voltage, i.e., the higher the first heating voltage, the higher the maximum temperature. Also, the maximum temperature was higher for a longer heating time at a constant heating voltage.

The maximum temperature contours at various heating voltages and heating times are shown in Fig. 6-3. It can be deduced that the same maximum temperature can be achieved by using either a lower first heating voltage and a longer heating time or a higher heating voltage and a shorter heating time. However, since it is only possible to obtain about 500°C for a first heating time of  $t_1 = 0.1$  seconds at the maximum heating voltage  $V_1 = 240$  volts, there is a limitation on the possible combinations of the first heating voltage and the first heating time.

The relationship between the first heating rate and the first heating voltage can be obtained from Fig. 6-2 and this is shown in Fig. 6-4. The results indicate that the heating rate of ultra-rapid annealing strongly depends on the first heating voltage. The heating

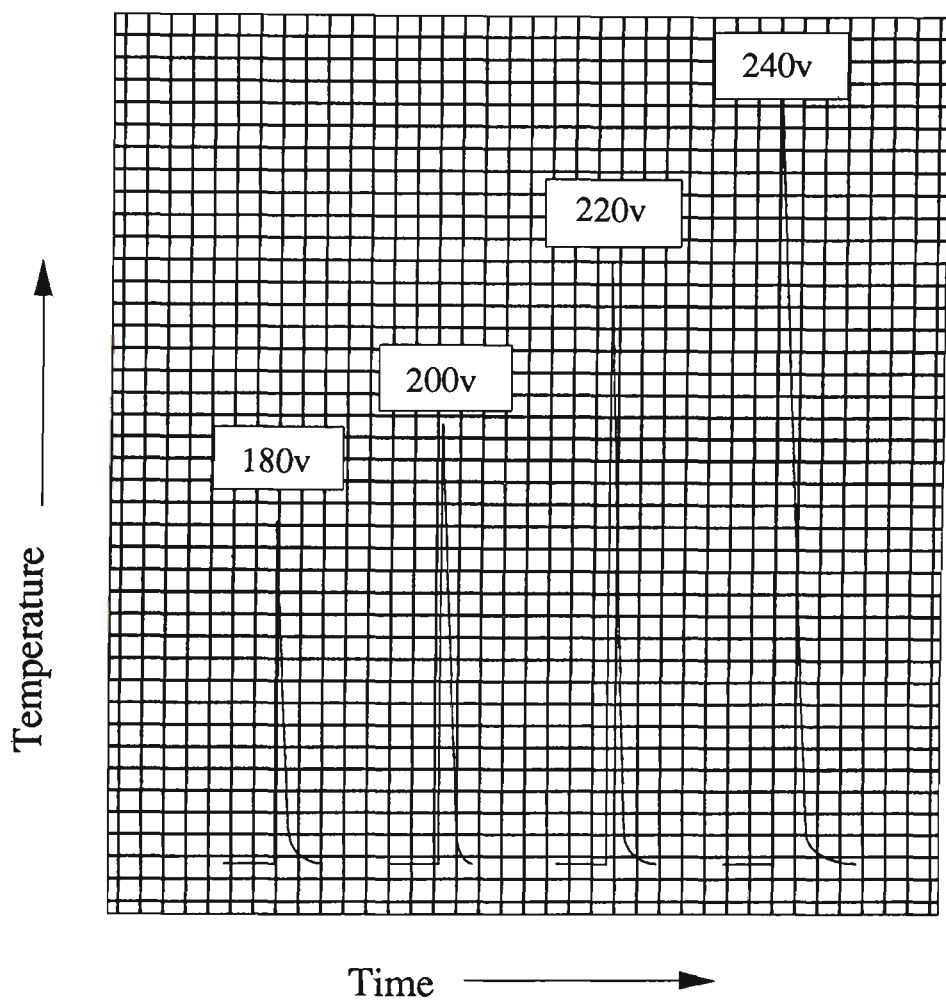


Fig. 6-1 Experimental curves showing the temperature variation with time for several first heating voltages in a sample with 70% cold reduction. ( $t_1 = 0.2$  sec.,  $t_2 = 0.1$  sec.)

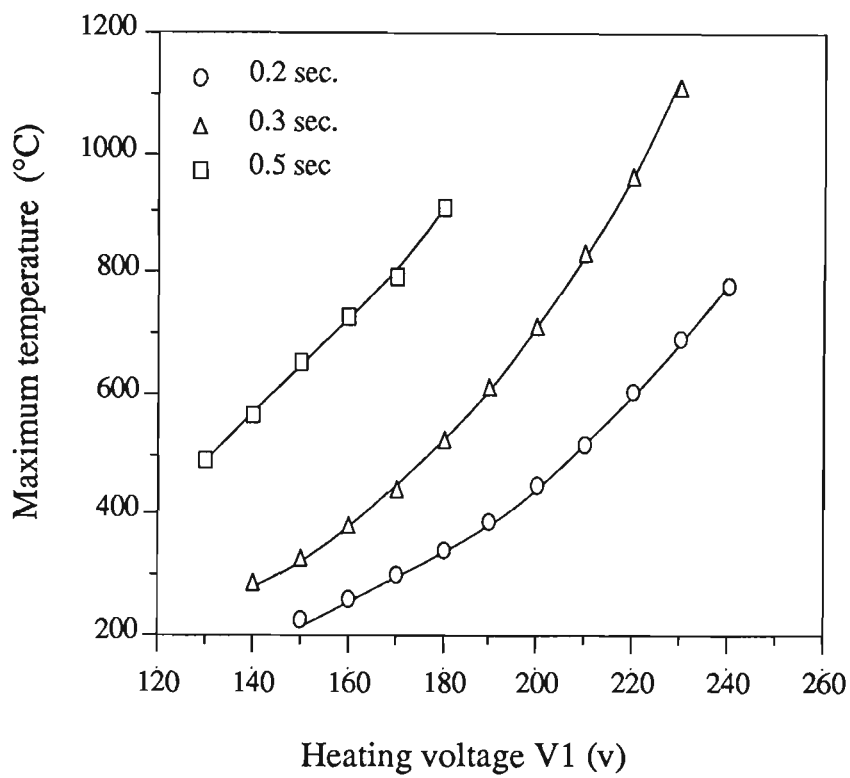


Fig. 6-2 The relationship between the maximum temperature at the end of the first heating voltage for  $t_1 = 0.2, 0.3$  and  $0.5$  seconds. ( $t_2 = 0.1$  second )

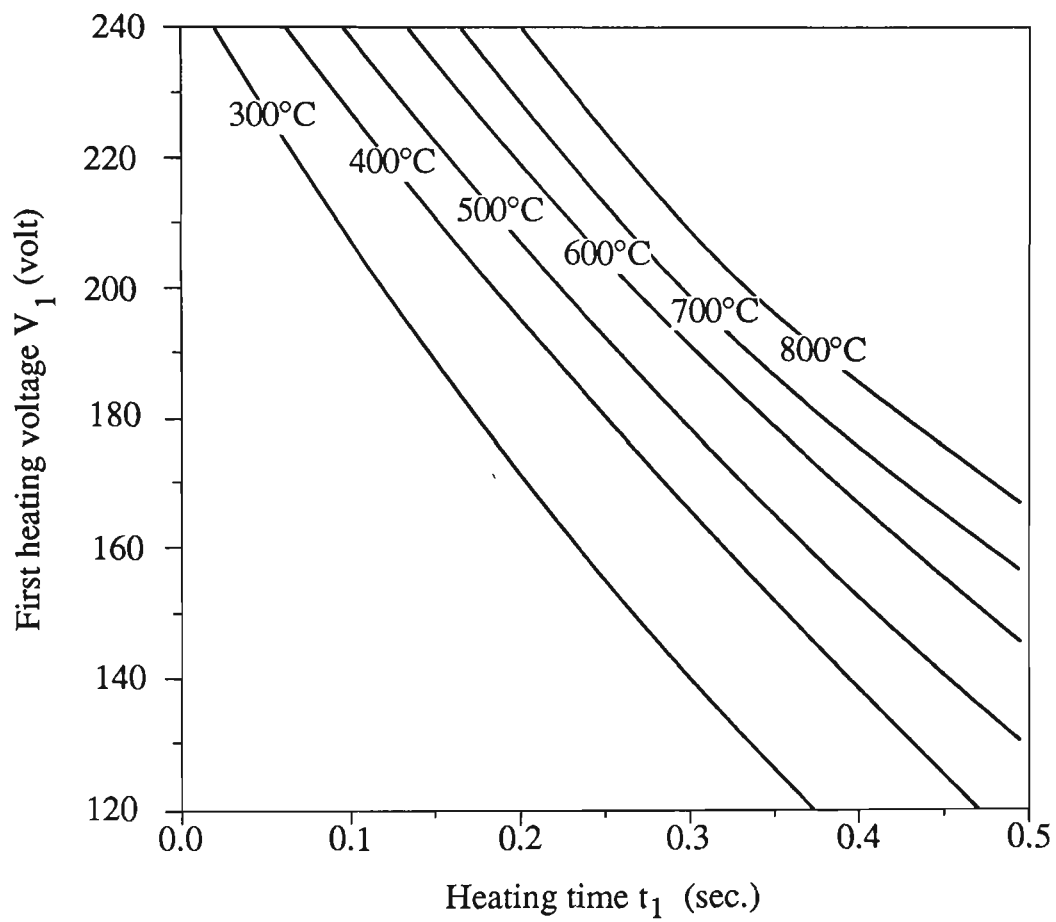


Fig. 6-3 Maximum temperature contours for various first heating voltages and heating times. ( $t_2 = 0.1$  sec.)

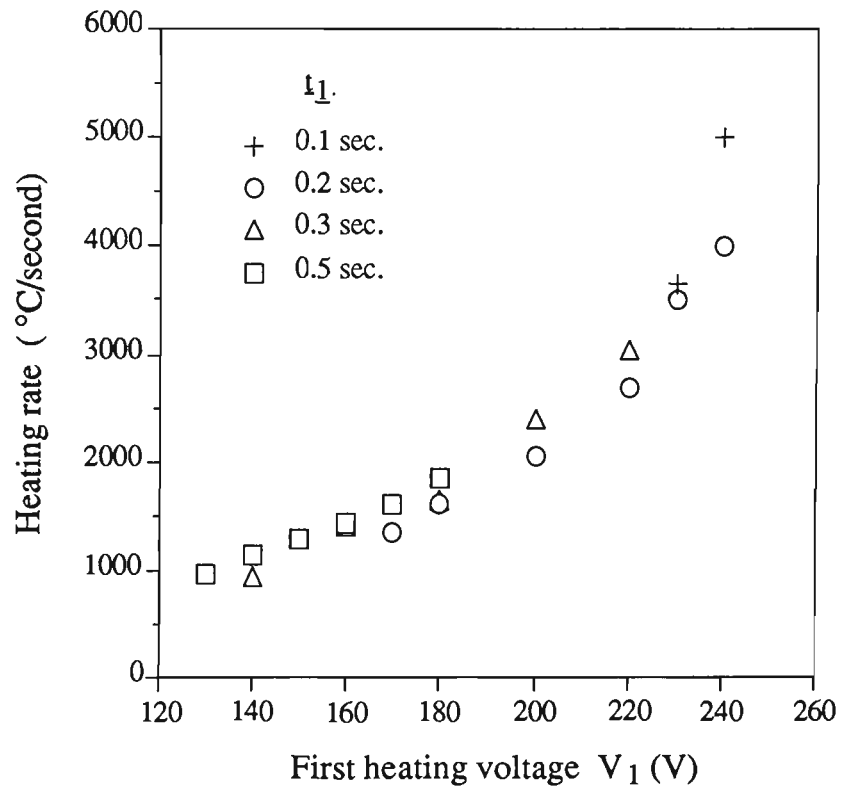


Fig. 6-4 The relationship between the average heating rate and the first heating voltage with  $t_1 = 0.2, 0.3$  and  $0.5$  sec. ( $t_2 = 0.1$  sec.)



rate can exceed  $4000^{\circ}\text{C}/\text{sec}$ . when  $V_1 = 240$  volts, while it is approximately  $3600^{\circ}\text{C}/\text{second}$  when  $V_1 = 230$  volts. In practice the apparatus is capable of rates up to  $5000^{\circ}\text{C}/\text{second}$  using  $t_1 = 0.1$  seconds. For  $t_1 = 0.1$  seconds and a hold time  $t_2 = 0.1$  seconds, the maximum possible specimen temperature is  $\sim 500^{\circ}\text{C}$  and for these conditions substantial, but, incomplete, softening occurred in 70% cold rolled samples. Full softening could be obtained, however, by increasing the hold time  $t_2$  to 0.3 seconds.

### 6.2.2 Effect of Second Voltage $V_2$ on Thermal Profile (Experiment 2, Table 4-3)

The temperature variation during the second heating is determined by the second heating voltage, and some of the experimental curves obtained are shown in Fig. 6-5. The results reveal that the temperature after the first heating can rise, fall or remain constant depending on the second heating voltage. In other words, "heating" may refer to holding the temperature constant or even cooling down the specimen in the second heating period. The second heating voltage at which the temperature of the sample after the first heating can be kept constant for at least several seconds is termed  $V_{2c}$  and the constant temperature is called  $T_c$  which is equal to the maximum temperature at the end of the first heating.

For  $V_1 = 160$  V and  $t_1 = 0.2$  seconds,  $V_{2c}$  was found to be 85 V as shown in Fig. 6-6 ( $V_2 = 70$  and  $100$  V gave cooling and heating, respectively). However, the experimental results for  $V_1 = 240$  V showed that all of the second heating voltages used resulted in a cooling effect (Fig. 6-6). Therefore,  $V_{2c}$  is related to the first heating voltage. Figure 6-7 shows the relationship between the first heating voltage and the second voltage  $V_{2c}$  for various constant temperatures obtained after ultra-rapid annealing for  $t_1 = 0.2$  seconds and  $t_2 = 6.0$  seconds. The results indicate that as the first heating voltage rises,  $V_{2c}$  also increases to maintain a constant temperature.

Similar experiments were conducted for a first heating time of 0.3 seconds. The results are plotted together with those for  $t_1 = 0.2$  seconds in Fig. 6-8. A similar relationship

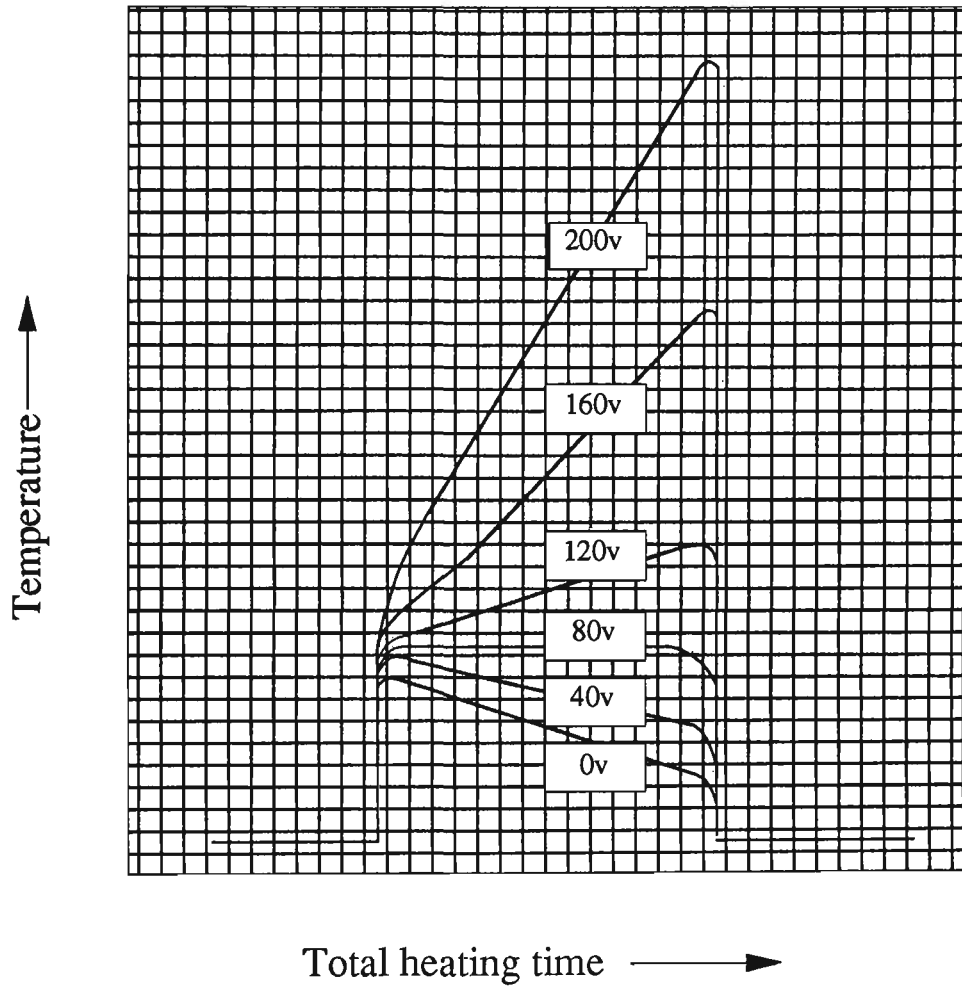


Fig. 6-5 Some of the experimental heating cycles obtained as a function of second voltage  $V_2$  for a sample with 70% cold reduction and  $V_1 = 150$  V,  $t_1 = 0.2$  and  $t_2 = 6.0$  seconds.

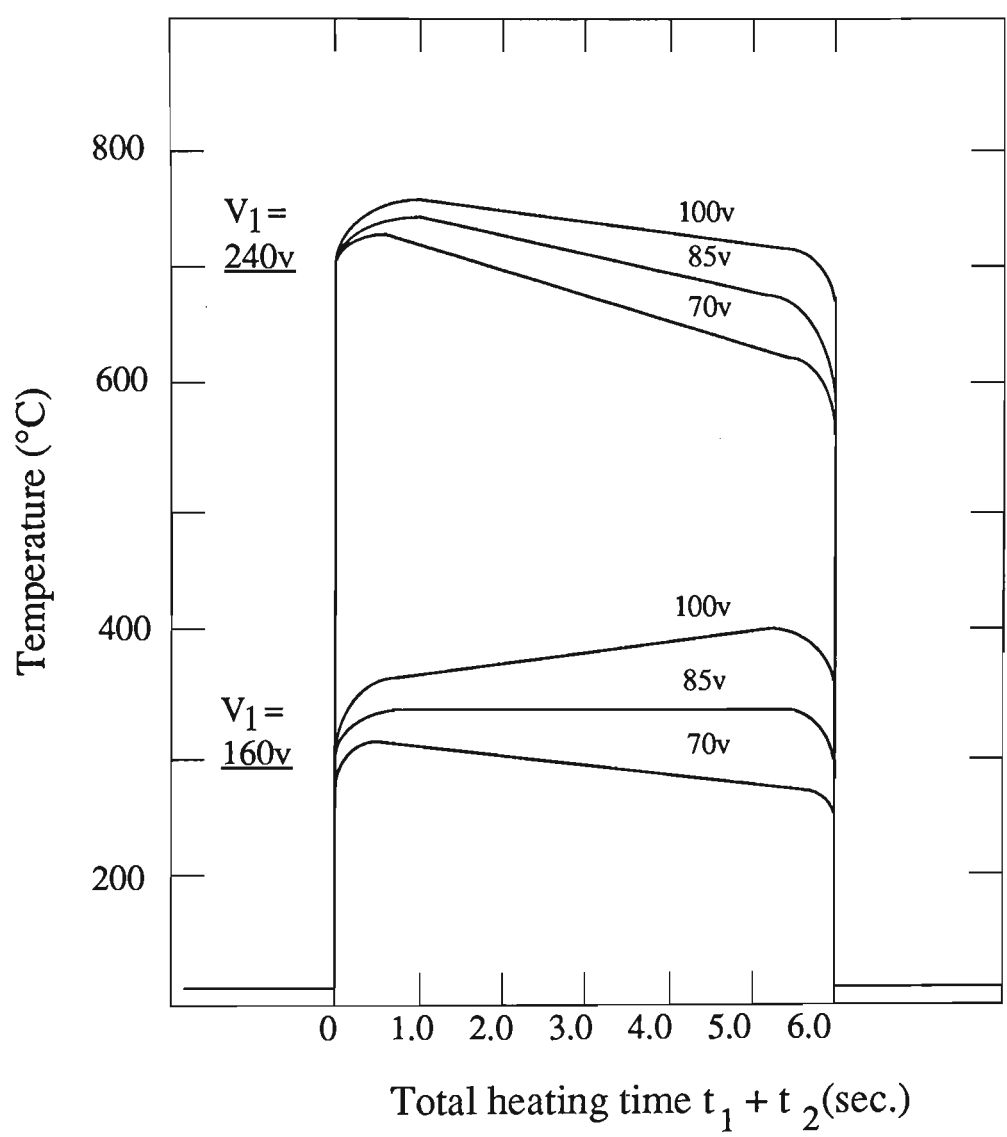


Fig. 6-6 Temperature variations for different second heating voltages for  $V_1=160$  V and  $V_1=240$  V, respectively. ( $t_1 = 0.2$  seconds)

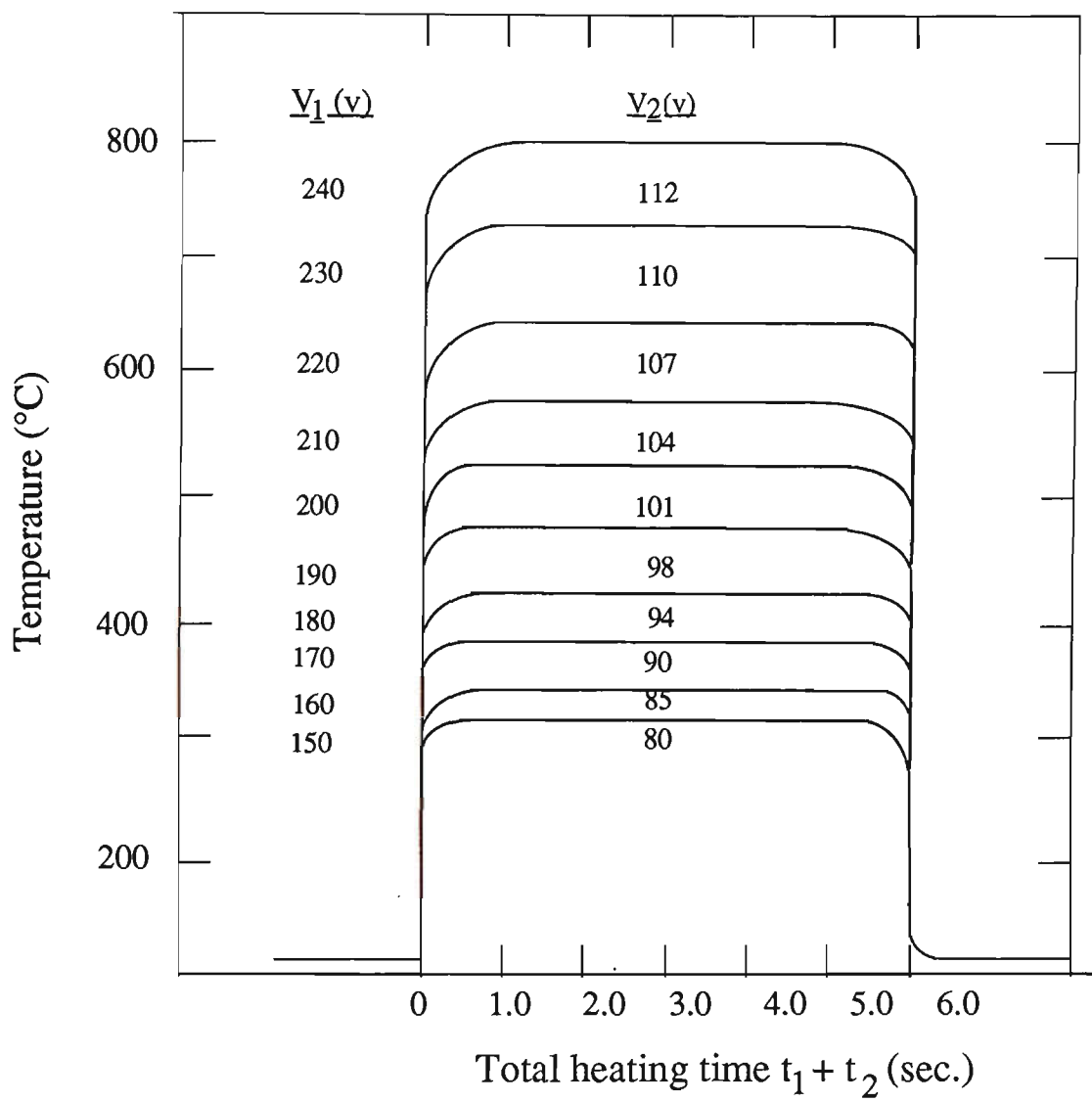


Fig. 6-7 Temperature profiles for different combinations of  $V_1$  and  $V_2$  which bring about a constant sample temperature. ( $t_1=0.2$  and  $t_2=6.0$  sec.)

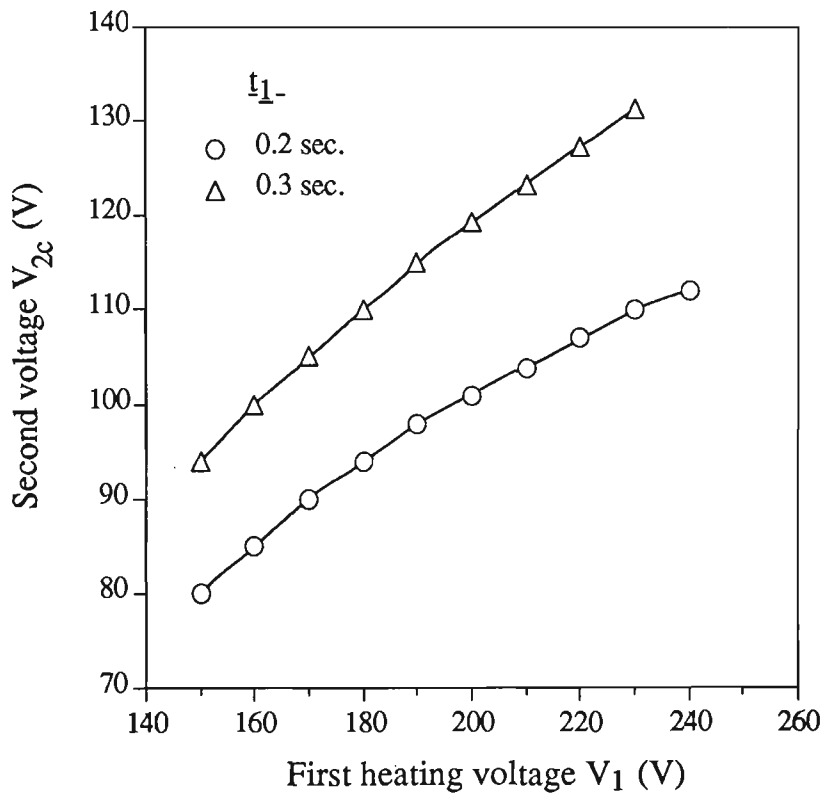


Fig. 6-8 The relationship between the first heating voltage and the second heating voltage  $V_{2c}$  for  $t_1 = 0.2$  and 0.3 sec.

between  $V_1$  and  $V_{2c}$  existed although a longer first heating time required a higher second heating voltage to keep the temperature constant for the same first heating voltage.

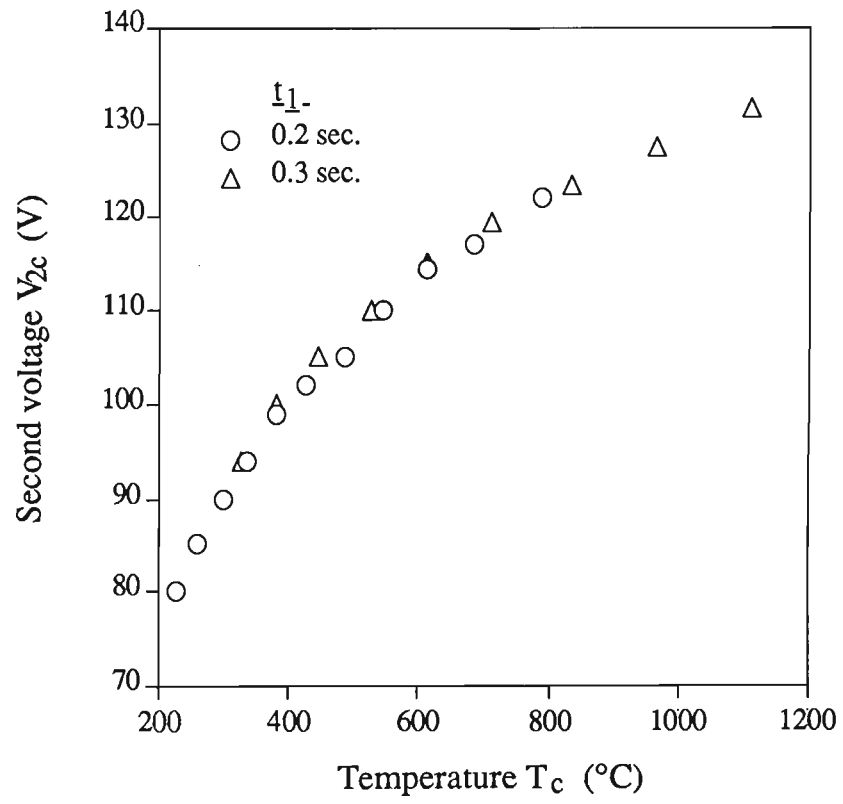
Figures 6-7 and 6-8 are combined in Fig. 6-9 in which  $V_{2c}$  is plotted as a function of the constant temperature,  $T_c$ . It can be concluded that the essential factor that determines  $V_{2c}$  is the plateau temperature: a higher constant temperature requires a higher second heating voltage.

### 6.2.3 The Soak Time (Experiment 3, Table 4-3)

The time during which the constant temperature is maintained is defined as the soak time,  $t_2$ . The influence of the soak time on hardness is shown in Fig. 6-10. The results show that the hardness decreased only slightly. Similar results were also obtained at the same  $T_c$  for a first heating time of 0.5 seconds. Therefore, most of the softening appeared to have taken place during the first heating period ( $t_1 \leq 0.2$  seconds). Since the smallest possible value for  $t_2$  was 0.1 sec., the hardness values after  $t_1 + 0.1$  sec. were taken as those at the end of the first heating.

### 6.2.4 The Heating Rate (Experiment 4, Table 4-4)

In the present investigation various heating rates were obtained by changing the first heating voltage as described in Section 6.2.1. The second voltage was chosen as that required to maintain the temperature obtained after the first heating. Therefore for these conditions,  $T_c$  equals the peak or maximum temperature of the thermal cycle. Figure 6-11 illustrates the influence of the heating rate on softening for a certain maximum (constant) temperature. The hardness underwent a pronounced drop when the heating rate increased from 2286 to 3430°C/s corresponding to a shortened first heating time. Therefore, the heating rate makes a significant contribution to softening. The actual heating rates used were selected in the range of 1000 - 5000 °C/second to study the softening behaviour.



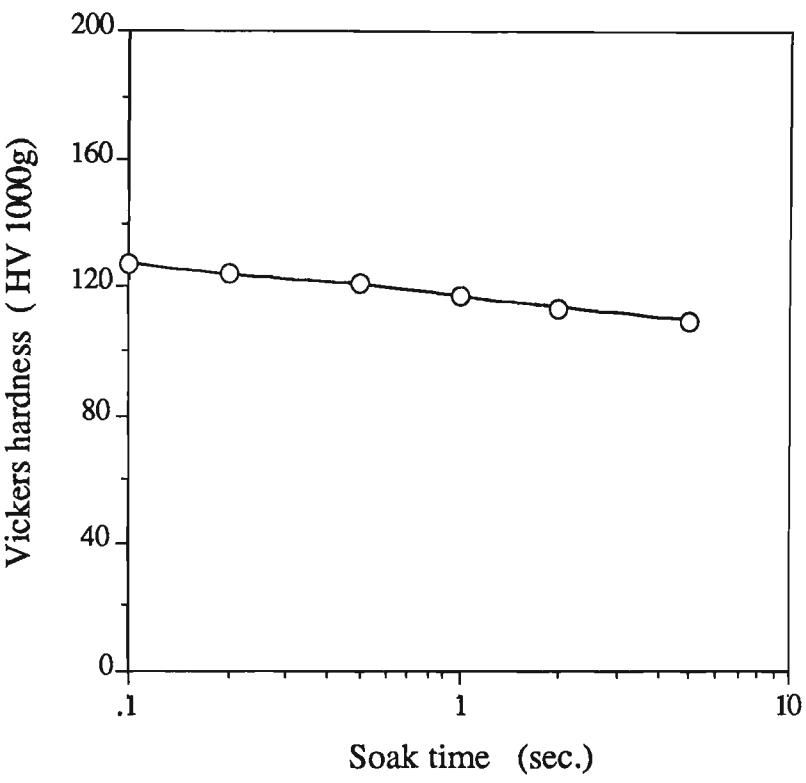


Fig. 6-10 The influence of the soak time on hardness.  
( $T_c = 685^{\circ}\text{C}$  and  $t_1 = 0.2$  seconds)



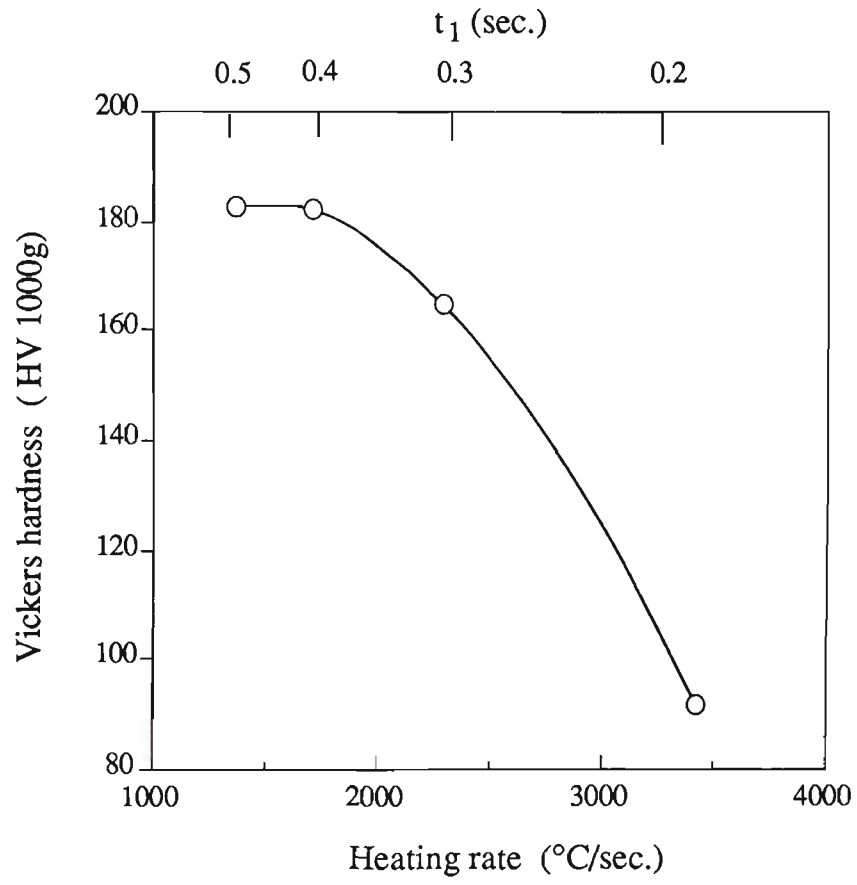


Fig. 6-11 The influence of the heating rate on softening at  $T_c = 686^\circ\text{C}$ . ( $t_2 = 0.1$  second)

### 6.2.5 The Maximum Temperature (Experiment 5, Table 4-3)

Samples were ultra-rapid annealed to the maximum temperatures of 320, 480, 640, 800 and 960°C at the same heating rate of 1600°C/second. Hardness tests were conducted after each treatment. The influence of the maximum temperature on hardness is shown in Fig. 6-12. Significant softening did not occur until ~600°C.

### 6.2.6 The Cross-sectional Area of the Specimen (Experiment 6, Table 4-3)

Samples with widths of 3.8, 3.97, 4.21, 4.5 and 4.8 mm (the length and thickness were constant) were ultra-rapid annealed with  $V_1 = 240$  V,  $t_1 = 0.2$  seconds and  $V_2 = 112$  V to study the effect of specimen size on softening ( Fig. 6-13). It is seen that the softening occurred in the gauge section, but the "flag" part of the sample maintained the original hardness. The hardness distributions were very similar, but the hardness value in the gauge section decreased with reducing width of the specimen. The reason for this effect is that with a smaller cross-sectional area the gauge section experienced a greater resistive heating for identical heating voltages and times. Therefore, it was necessary to machine the samples into an identical cross-sectional area to make them comparable with each other during the investigation. The standard tensile test piece was determined by computer modelling ( described in 4.3.2.3 ) and was used throughout the experiments.

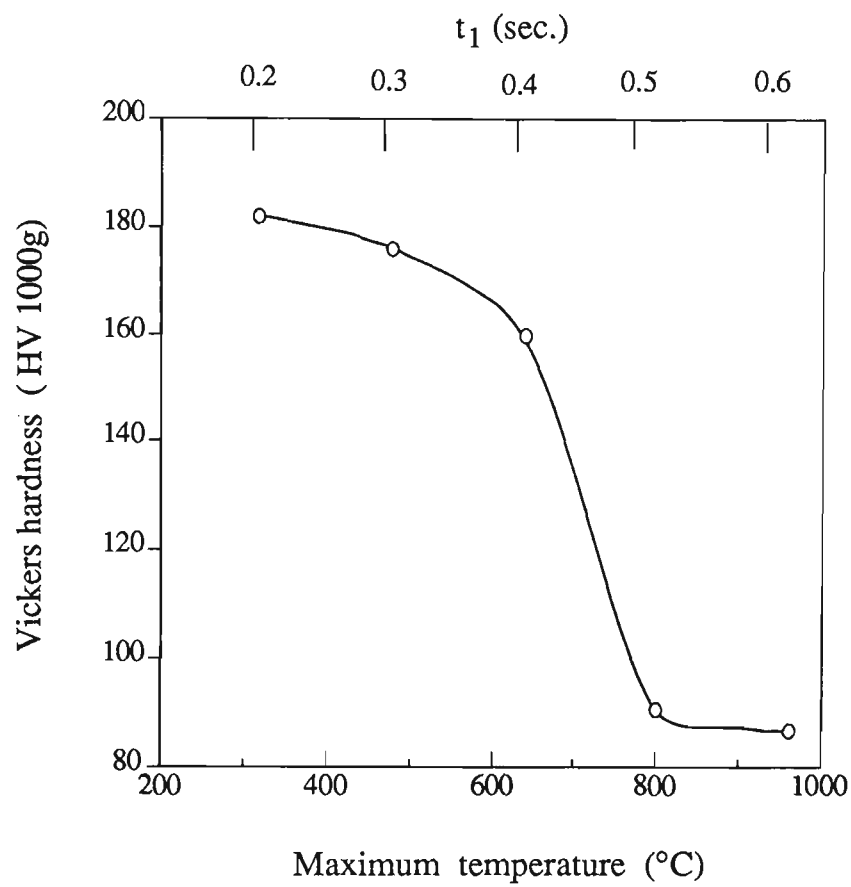


Fig. 6-12 Effect of the maximum temperature on softening of 70% cold reduced samples for a heating rate of  $\sim 1600^\circ\text{C}/\text{sec.}$  and  $t_2 = 0.1$  sec.

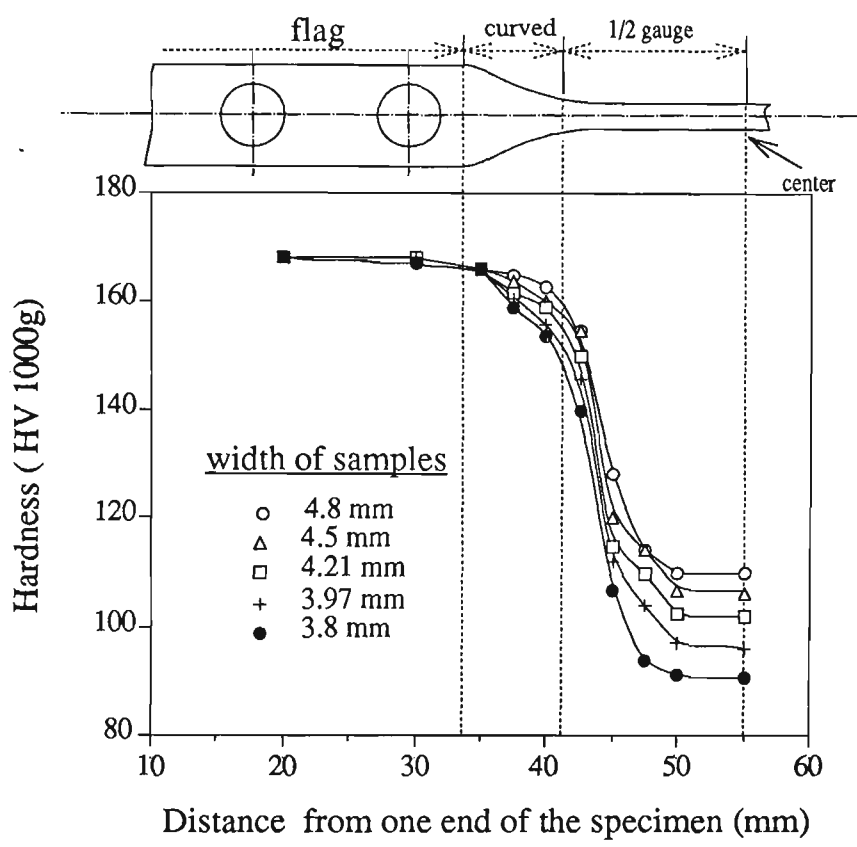


Fig. 6-13 The effect of the sample width ( at constant length and thickness) on softening. ( $V_1 = 240$  V,  $t_1 = 0.2$  sec.,  $V_2 = 112$  V and  $t_2 = 0.1$  sec.)

### 6.3 EXAMINATION OF SOFTENING BEHAVIOUR

Softening responses of the decarburised steel to various annealing processes were studied. The results are presented in terms of the two types of annealing processes: ultra-rapid annealing and batch annealing. In each case, annealed 70% cold reduced samples are considered as well as the effect of changing the cold reduction.

#### 6.3.1 Ultra-rapid Annealing

##### 6.3.1.1 Annealed 70% cold reduced samples

70% cold reduction samples were ultra-rapid annealed for  $t_1 = 0.2, 0.3$  and  $0.5$  seconds, and the corresponding hardness values were shown in Fig. 6-14. It was found that the temperature at which the hardness dropped shifted significantly from  $\sim 560$  to  $700^\circ\text{C}$  when  $t_1$  was increased from  $0.2$  to  $0.5$  seconds. The maximum softening occurred with  $t_1 = 0.2$  seconds for a given temperature, i.e., the highest heating rate gave rise to the greatest softening.

##### 6.3.1.2 Influence of cold reduction (Experiment 7, Table 4-3)

Similar experiments were carried out on samples with 40%, 60%, 70% and 80% cold reduction for a first heating time of  $0.2$  seconds to observe the influence of deformation on hardness. Figure 6-15 shows the hardness results for four different cold reductions but the same heating practice. The point at the middle of the hardness decrement (the linear part of the hardness curve) is taken as the softening point and the temperature at this point is called the softening temperature. Table 6-1 lists the softening temperatures and the hardness decrement.

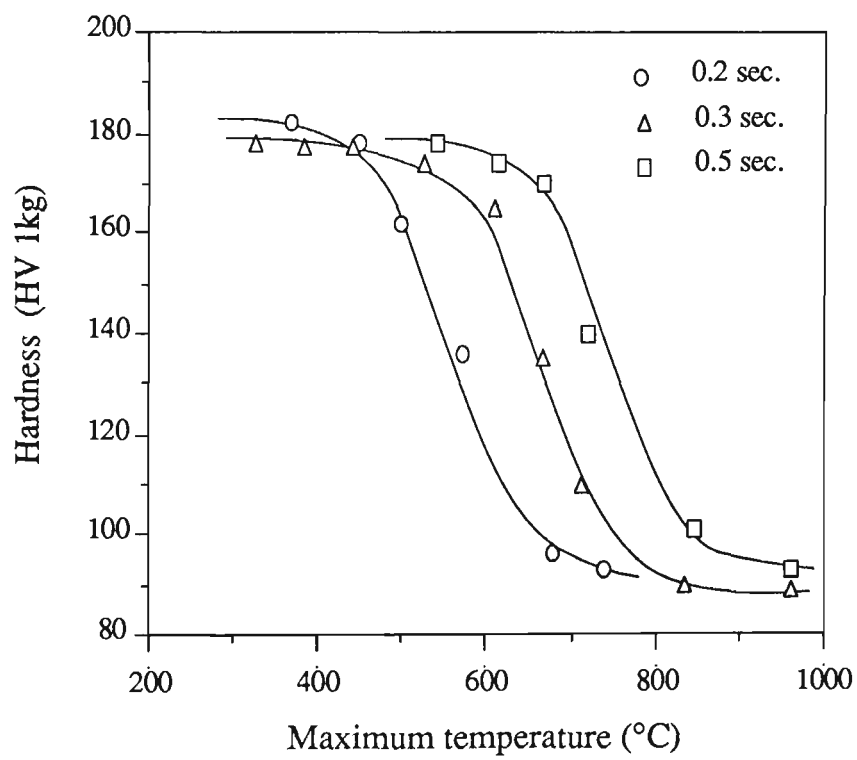


Fig. 6-14 The softening behaviour of a sample with 70% cold reduction after ultra-rapid annealing. ( $t_2 = 0.1$  sec.)

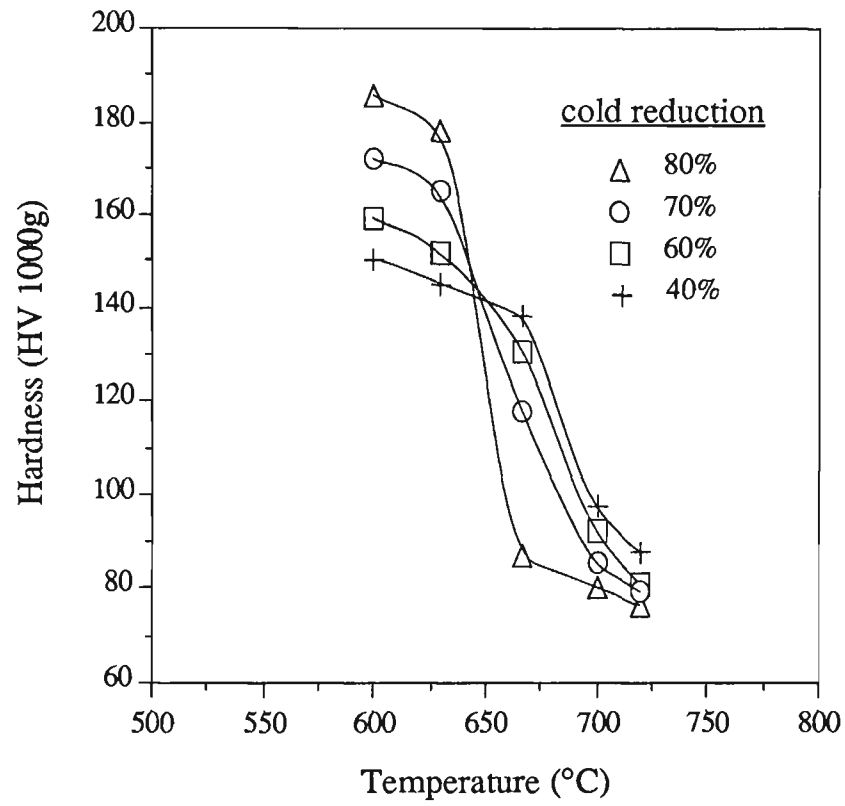


Fig. 6-15 Softening behaviour after ultra-rapid annealing in samples with different cold reductions. ( $t_1 = 0.3$  and  $t_2 = 0.1$  sec.)

Table 6-1 Comparison of the softening temperatures and hardness decrements after ultra-rapid annealing of samples with different cold reductions

Cold reduction	40%	60%	70%	80%
Softening temp. (°C)	681	675	655	647
Hardness decrement*	64	81	97	110

\* Hardness decrement is the difference between the upper and lower shelves in the curves of Fig.6-15.

By comparing the results in Table 6-1, it is obvious that the softening temperature is lowered with increasing cold reduction, while the hardness decrements increase as the reduction increases.

6.3.2. Batch Annealing

6.3.2.1 Annealed 70% cold reduced samples

To draw comparisons with the effect of ultra-rapid annealing, specimens with 70% cold reduction were also batch annealed at different temperatures and the hardness values were determined after the treatment. Annealing was carried out in a laboratory furnace at 400, 450, 550, 650 and 700°C for 30 minutes. The plot of hardness against temperature is shown in Fig. 6-16, which indicates that the hardness decrease with increasing temperature was not as sharp as that in ultra-rapid annealing (Fig. 6-14). On the other hand, the softening temperature was ~500°C for batch annealing which is lower than that for any ultra-rapid annealing conditions.

6.3.2.2 Influence of cold reduction (Experiment 8, Table 4-3)

Similar treatments were carried out on samples with 40%, 60%, 70% and 80% cold reduction to study the influence of cold reduction on softening. The results are presented in Fig. 6-17. It was found that the softening temperature decreased with increasing deformation (Table 6-2), and this is similar to the trend in ultra-rapid annealing. It is also seen from Table 6-2 that the sample with 80% cold reduction exhibited the largest



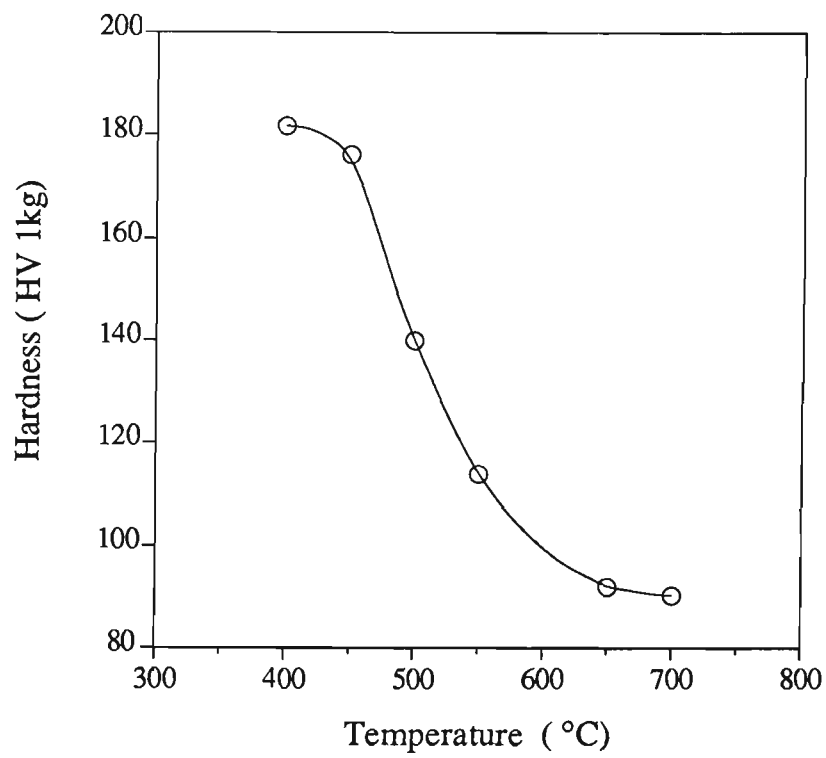


Fig. 6-16 The softening behaviour in a sample with 70% cold reduction after batch annealing at different temperatures for 30 min.

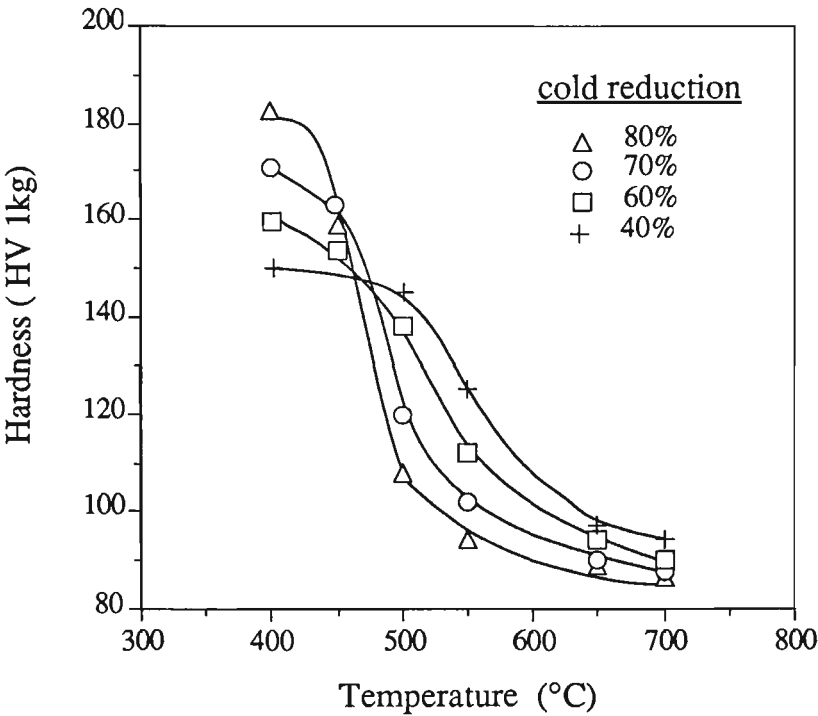


Fig. 6-17 Influence of cold reduction on the softening behaviour after batch annealing at various temperatures for 30 minutes.

hardness decrement that with 40% deformation showed the smallest. Samples with 60% and 70% cold reduction had very similar hardness decrements.

Table 6-2 Comparison of the softening temperatures and hardness decrements after batch annealing of samples with different cold reductions

Cold reduction	40%	60%	70%	80%
Softening temp. (°C)	550	510	490	473
Hardness decrement	87	89	90	92

### 6.3.3 Ultra-rapid Annealed Samples with Prior Recovery (Experiment 9, Table 4-3)

#### 6.3.3.1 Annealed 70% cold reduced samples

In conventional annealing, recrystallization is characterized by a sharp decrease in hardness which is associated with an appreciable increase in the rate of energy release. Recovery, however, involves a lower rate of energy release and is characterized by a slower decrease in hardness. Prior recovery treatments are known to reduce the extent of recovery on subsequent annealing as well as retarding recrystallization. In order to examine the effect of recovery prior to ultra-rapid annealing, samples with 70% cold reduction were recovered at 100°C for 1.5, 3, 5 and 10 hours before ultra-rapid annealing. Hardness measurements are presented in Fig. 6-18. The hardness values at the end of the first heating stage for samples with no prior recovery were assumed to be the same as those measured after 0.1 second of the second heating stage. This assumption is justified in Section 6.2.3.

Comparing the softening behaviour of prior recovered samples with those which did not undergo prior recovery annealing ( designated as "no recovery" in the legend of Fig. 6-18), it was found that the prior recovery process increased the second heating time required to soften the sample. The longer the prior recovery treatment time, the larger

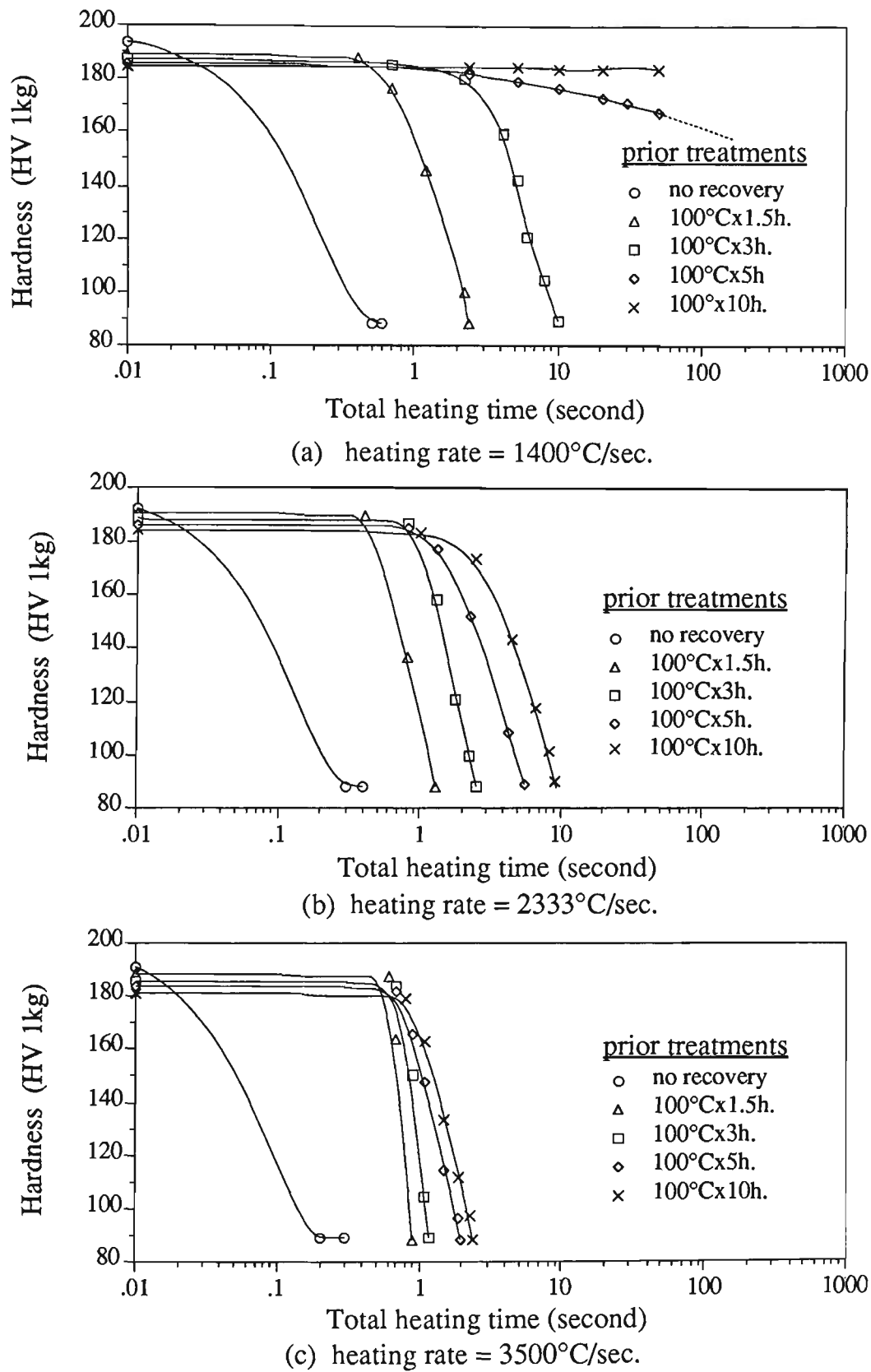


Fig. 6-18 Effect of prior recovery on softening behaviour in samples with 70% cold reduction ultra-rapid annealed at heating rates of 1400, 2333 and 3500°C/sec. ( $t_1 = 0.3$  sec.,  $T_c = 700^\circ\text{C}$ )

was the time necessary for softening. Also, with the same annealing temperature (  $T_c = 700^\circ\text{C}$  ), a higher heating rate resulted in faster softening (Fig. 6-18). Samples subjected to 5 hours or longer of prior recovery annealing at  $100^\circ\text{C}$  could not be softened by the following ultra-rapid annealing at heating rates of  $1400^\circ\text{C}/\text{sec.}$  for hold times up to  $\sim 50$  seconds (see Fig. 6-18(a)).

#### 6.3.3.2 Influence of cold reduction

The same prior recovery treatments were conducted on a sample with 40% cold reduction, which was then ultra-rapid annealed at  $T_c = 700^\circ\text{C}$  with  $t_1 = 0.3$  seconds. Figure 6-19 shows the hardness plotted against the total heating time for samples subjected to prior recovery annealing at  $100^\circ\text{C}$  for 1.5, 3, 5 and 10 hours, respectively. Sample with 40% cold reduction softened slightly more slowly than those with 70% deformation, although they generally responded in a similar way to different prior recovery treatments.

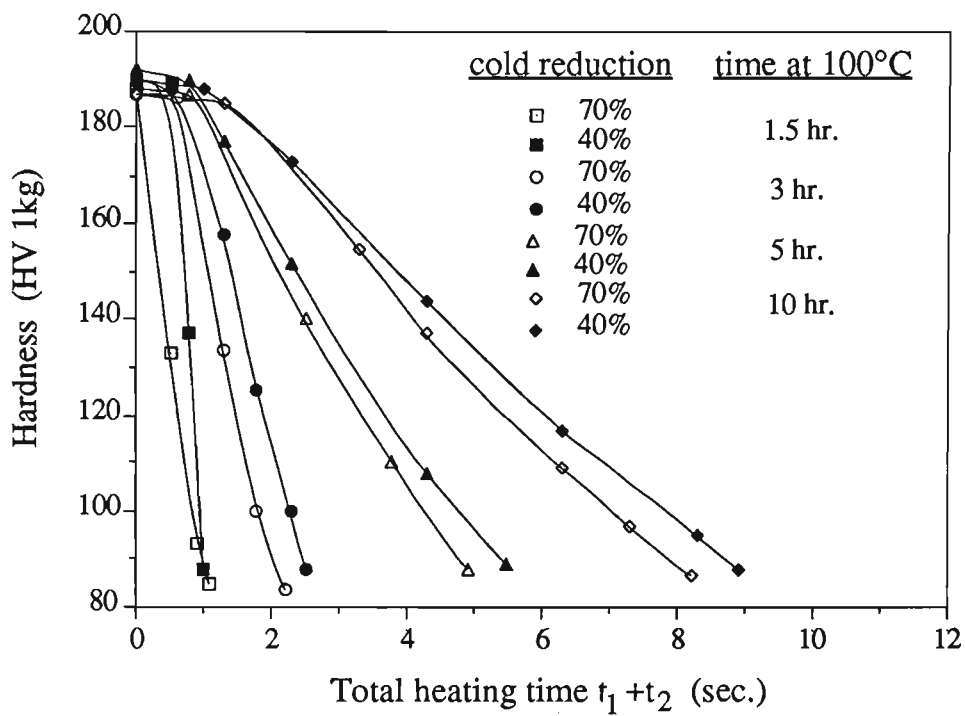


Fig. 6-19 Hardness versus the total heating time for samples with 40% and 70% cold reduction subjected to prior recovery annealing at 100°C for 1.5, 3, 5 and 10 hours followed by ultra-rapid annealing ( $t_1 = 0.3$  sec.,  $T_c = 700^\circ\text{C}$ ).

## 6.4 HARDNESS DISTRIBUTIONS

### 6.4.1 Ultra-rapid Annealed Samples

#### 6.4.1.1 Annealed 70% cold reduced samples

Hardness frequency measurements were conducted in the central gauge region after ultra-rapid annealing at 520°C, 600°C, 667°C and 820°C for  $t_1 = 0.3$  and  $t_2 = 0.1$  seconds on samples with 70% cold reduction. The total number of measurements for each sample was ~100. The distributions of indentation diagonals are shown in Fig. 6-20. At 520°C the diagonal lengths of the indentation were about 100  $\mu\text{m}$  which corresponds to a hardness value of 182 (HV 1000g). However, two separate peaks centered about ~115 and ~140  $\mu\text{m}$  were observed when  $T_c = 667^\circ\text{C}$ . When the temperature increased to 820°C, the hardness values were again centered around one peak which was at ~150  $\mu\text{m}$ . It is seen from Fig. 6-14 that for a heating time of 0.3 seconds, 520 and 820°C correspond to the softening start and the softening finish temperatures, respectively.

#### 6.4.1.2 Influence of cold reduction

Similar measurements were carried out on samples with 40%, 60%, 70% and 80% cold reduction, heated to 650°C ( $t_1 = 0.3$  and  $t_2 = 0.1$  sec.). The results are shown in Fig. 6-21. There were two peaks in each case. However, the second peak was less obvious with decreasing deformation. From Fig. 6-15, it is seen that the diminution of the second peak is related to the fact that 650°C corresponds to the middle of the softening range for 80% cold reduction and approximately to the start point of the softening range for 70% and 60% cold reduction. The hardness frequency measurements can be used to identify the softening zone in ultra-rapid annealing.

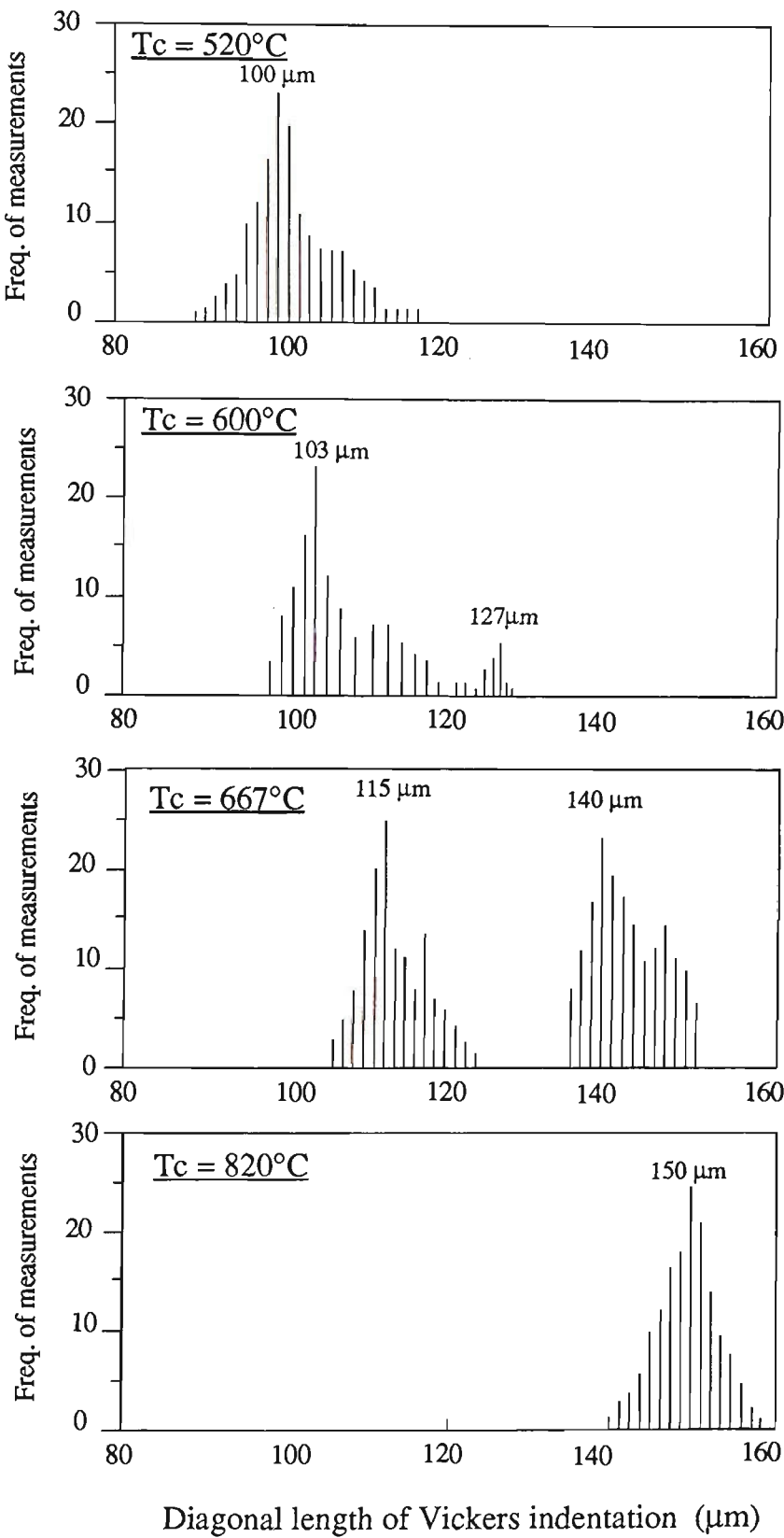


Fig. 6-20 The distributions of hardness measurements in samples with 70% cold reduction after ultra-rapid annealing at  $T_c = 520^\circ\text{C}$ ,  $600^\circ\text{C}$ ,  $667^\circ\text{C}$  and  $820^\circ\text{C}$ , corresponding to 0%, 13%, 50% and 100% softening. ( $t_1 = 0.3$  and  $t_2 = 0.1$  seconds)



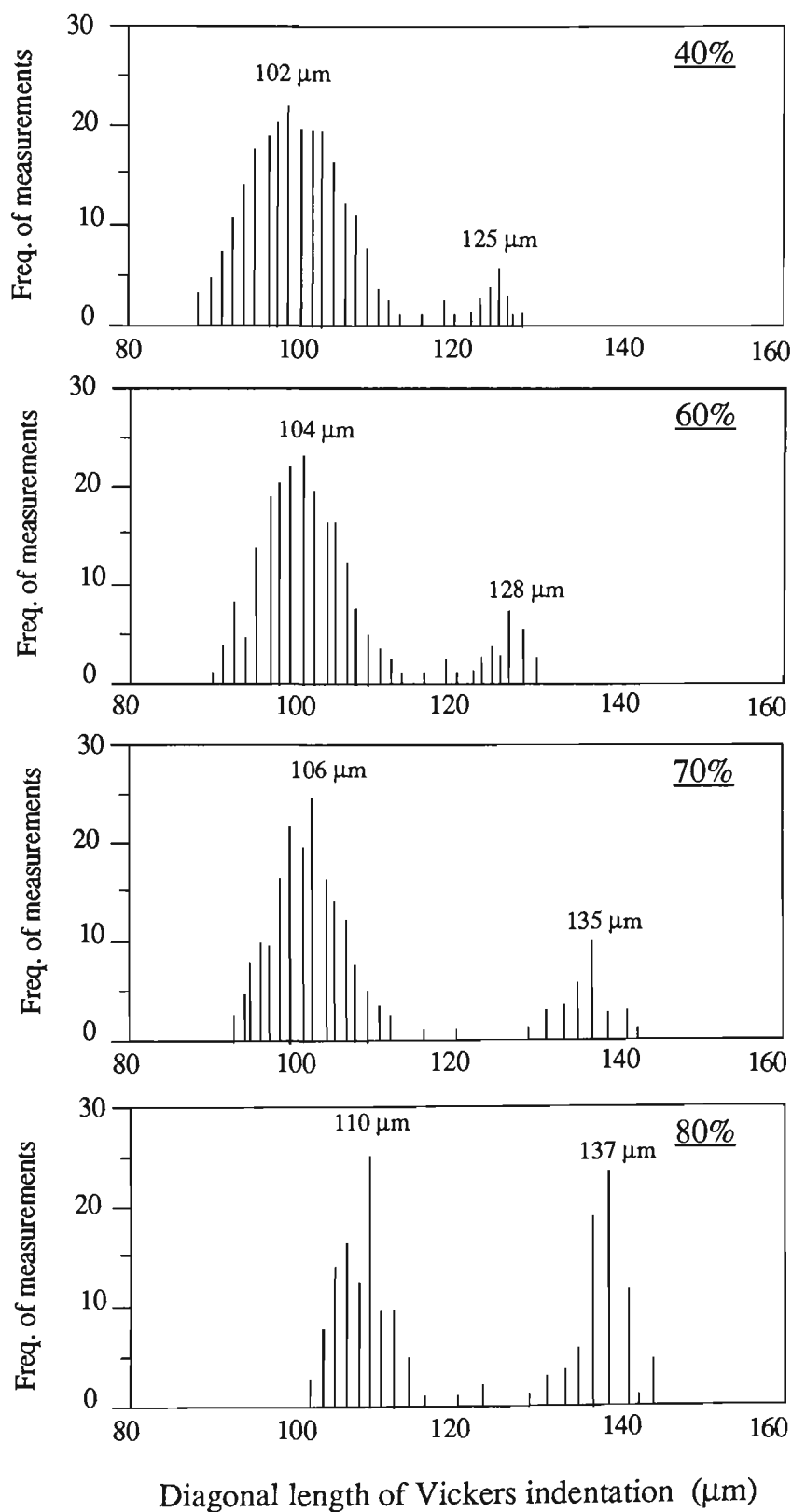


Fig. 6-21 The distributions of hardness measurements in samples with different deformations after ultra-rapid annealing at  $T_c = 650^\circ\text{C}$ ,  $t_1 = 0.3$  and  $t_2 = 0.1$  seconds. (see Fig. 6-15)

## 6.4.2 Batch Annealed Samples

### 6.4.2.1 Annealed 70% cold reduced samples

Similar experimental methods were applied to the samples with 70% cold reduction after batch annealing at 450, 500 and 650°C for 30 minutes. The results are illustrated in Fig. 6-22. Only one peak appeared in the hardness distribution diagrams and peak splitting as seen in the case of the ultra-rapid annealing (shown in Fig. 6-20) was not observed. The peak was simply shifted as the temperature increased.

### 6.4.2.2 Influence of cold reduction

The influence of cold reduction after batch annealing at 500°C for 30 minutes on hardness distribution is shown in Fig. 6-23. The results show that the sample with 80% cold reduction had the largest indentation size, which indicated the lowest hardness value and the sample with 40% cold reduction displayed the highest hardness value.

## 6.4.3 Ultra-rapid Annealing with Prior Recovery

One 70% cold reduced sample was examined after prior recovery at 100°C for 10 hours and ultra-rapid annealing at 667°C for  $t_1 = 0.3$  sec. The results are illustrated in Fig. 6-24. The plot show that the hardness distribution did not exhibit the split peaks despite the temperature being approximately the softening temperature under conditions of no prior recovery. The indentation size extended from ~90 to 140  $\mu\text{m}$  with the peak at ~115  $\mu\text{m}$ .

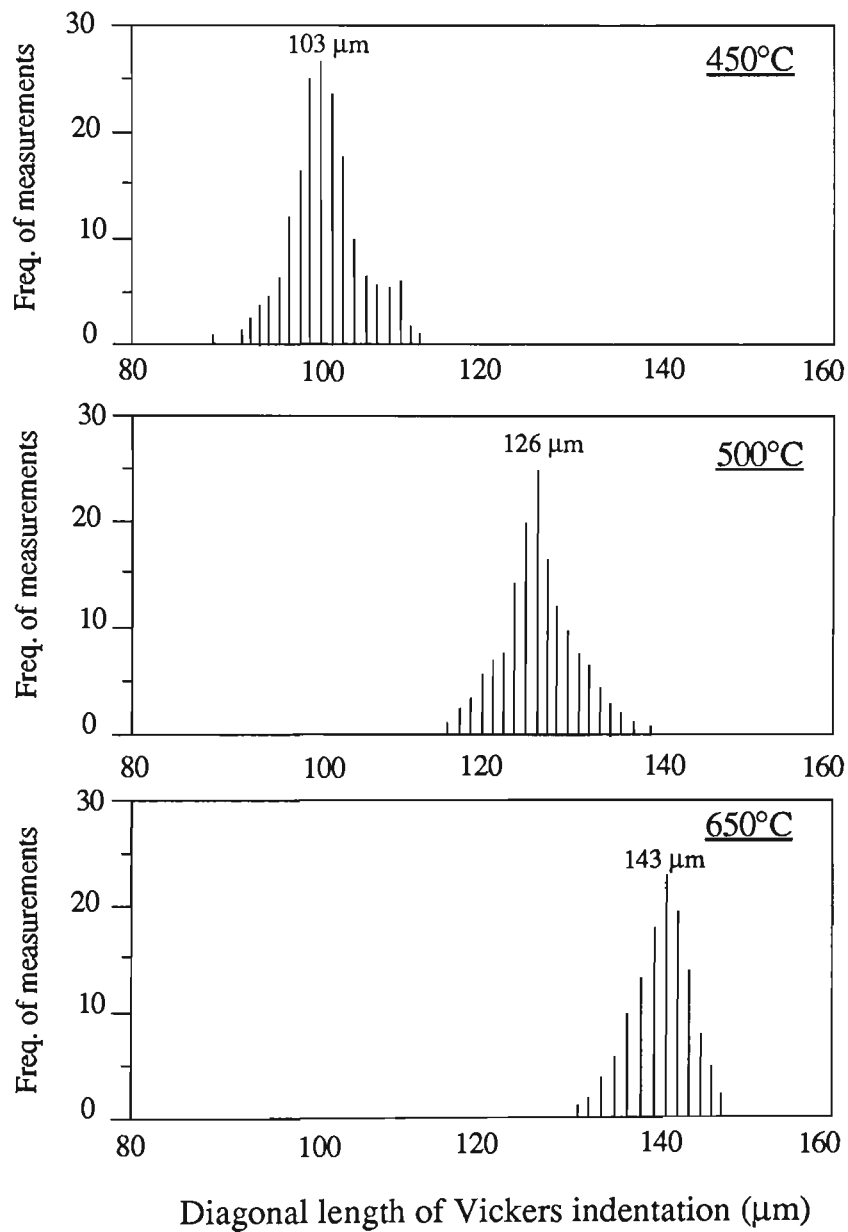


Fig. 6-22 The distributions of hardness measurements in samples with 70% cold reduction after batch annealing at temperature of 450°C, 500°C and 650°C, corresponding to 0%, 50% and 100% softening for 30 minutes. (see Fig. 6-16)

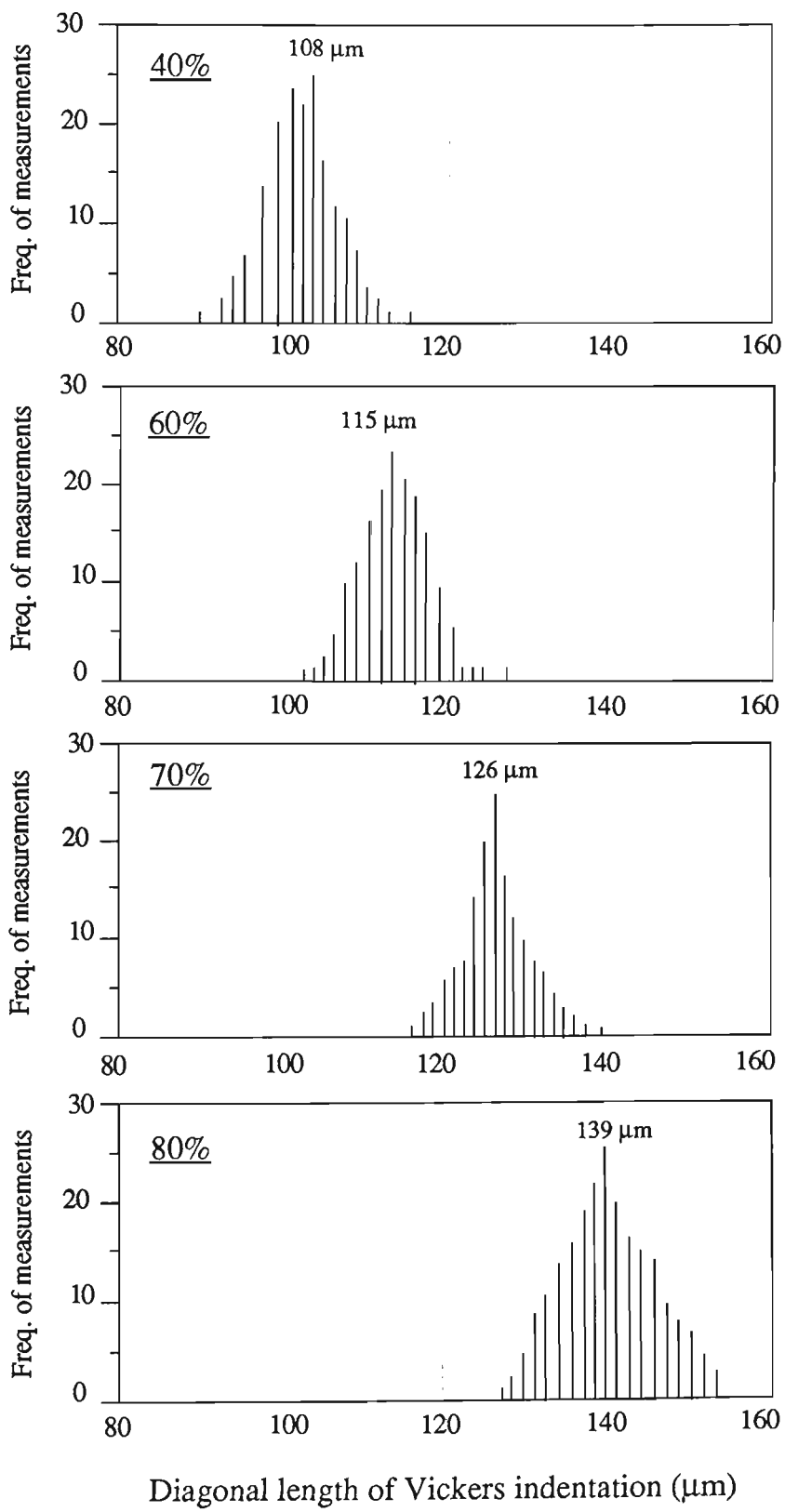


Fig. 6-23 The distributions of hardness measurements in samples with different deformations after batch annealing at 500°C for 30 minutes. (see Fig. 6-17).

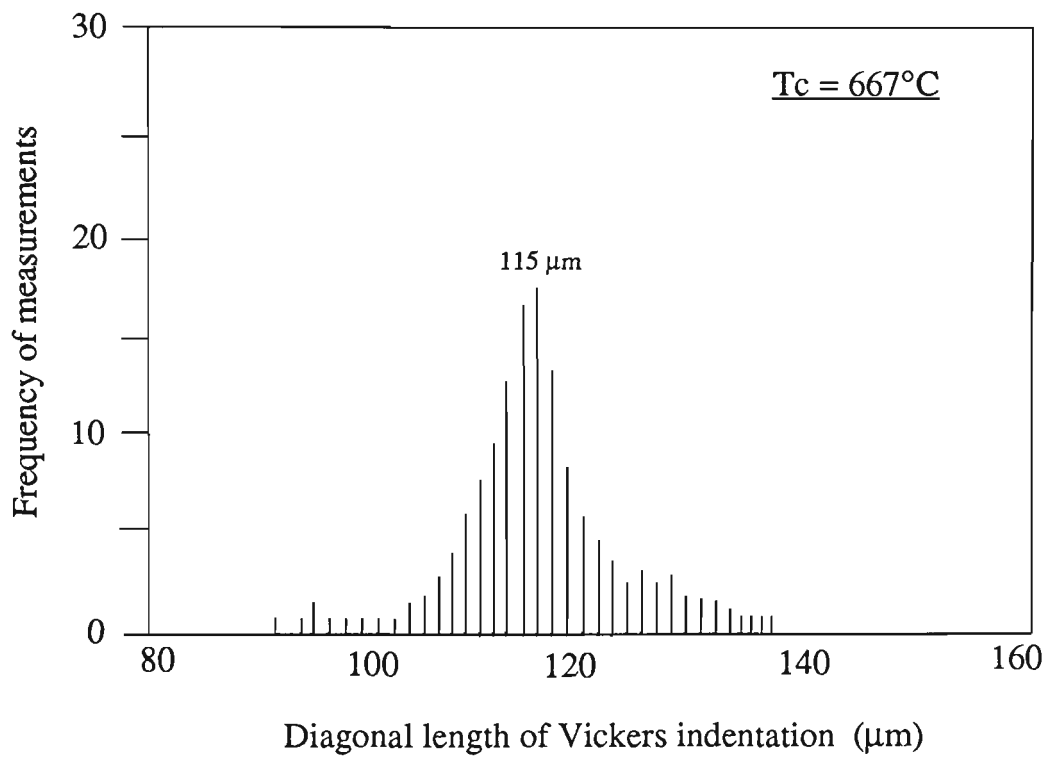


Fig. 6-24 The distributions of hardness in sample with 70% cold reduction after prior recovery at 100°C for 10 hours and ultra-rapid annealing at 667°C for  $t_1 = 0.3$  and  $t_2 = 0.1$  seconds.

6.5 TENSILE PROPERTIES

6.5.1 Ultra-rapid Annealed Samples

6.5.1.1 Annealed 70% cold reduced samples

Samples with 70% cold reduction were ultra-rapid annealed at 630, 667, 700 and 720°C with  $t_1 = 0.3$  and  $t_2 = 0.1$  seconds ( around the softening temperature range) and tested for their tensile properties. The plots of stress against strain are shown in Fig. 6-25. The ultimate tensile stress (UTS) decreased as the temperature increased and correspondingly, the total elongation increased from 9% to 29%.

6.5.1.2 Influence of cold reduction

Samples with 40%, 60%, 70% and 80% cold reduction were also tested after ultra-rapid annealing at 720°C with  $t_1 = 0.3$  and  $t_2 = 0.1$  seconds. The plots of stress against strain are shown in Fig. 6-26. Table 6-3 lists the tensile properties of ultra-rapid annealed samples with different cold reductions. The sample with 80% cold reduction showed the highest ductility, while the sample with 40% cold reduction had the lowest ultimate tensile stress.

Table 6-3 Comparison of the tensile properties after ultra-rapid annealing at 720°C with  $t_1 = 0.3$  and  $t_2 = 0.1$  seconds in samples with different cold reductions

Cold reduction	40%	60%	70%	80%
UTS (MPa)	409.77	456.7	505.83	506.35
Strain (%)	18.1	24.8	29.2	29.8

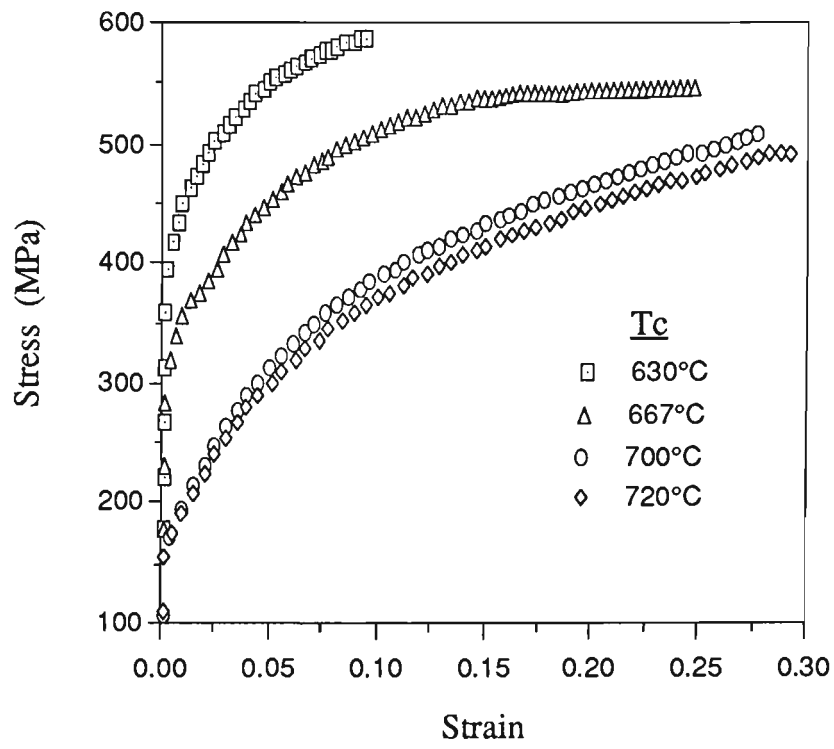


Fig. 6-25 Tensile testing results of 70% cold reduced samples after ultra-rapid annealing at  $T_c = 630, 667, 700$  and  $720^\circ\text{C}$ . ( $t_1 = 0.3$  and  $t_2 = 0.1$  sec.)

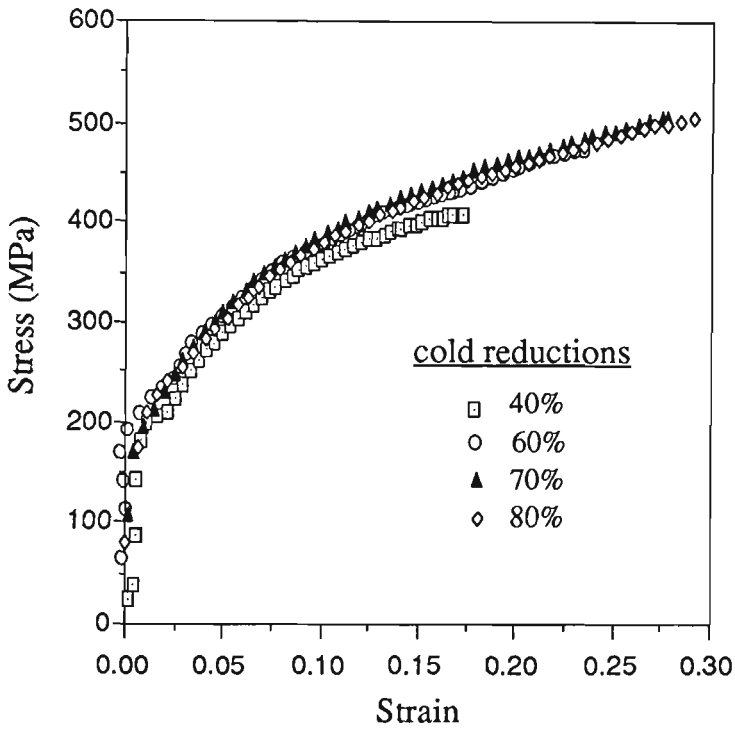


Fig. 6-26 Comparison of the tensile testing results of samples with different cold reduction after ultra-rapid annealing at  $T_c = 720^{\circ}\text{C}$ . ( $t_1 = 0.3$  and  $t_2 = 0.1$  sec.)



6.5.2 Batch Annealing

6.5.2.1 Annealed 70% cold reduced samples

Samples with 70% cold reduction were tensile tested after batch annealing at 680°C for 30 minutes to draw comparisons with samples subjected to ultra-rapid annealing. Stress is plotted against strain in Fig. 6-27. By comparing Fig. 6-27 with Fig. 6-25, it is seen that after ultra-rapid annealing at ~680°C the UTS is higher ( 550 MPa vs 350 MPa) and the elongation is greater( 25% vs 21% ) than that for samples batch annealed at 680°C.

6.5.2.2 Influence of cold reduction

Similar experiments were conducted on samples with 40%, 60% , 70% and 80% cold reduction after batch annealing at 680°C for 30 minutes. The plots were shown in Fig. 6-28. It is to be noted that none of these samples exhibited obvious yielding. The UTS and the strain to necking for each sample is presented in Table 6-4.

Table 6-4 Comparison of the tensile properties after batch annealing at 680°C for 30 minutes in samples with different cold reductions

Cold reduction	40%	60%	70%	80%
UTS (MPa)	286.8	344.7	350.1	355.6
Strain (%)	18.1	24.8	21.8	24.3

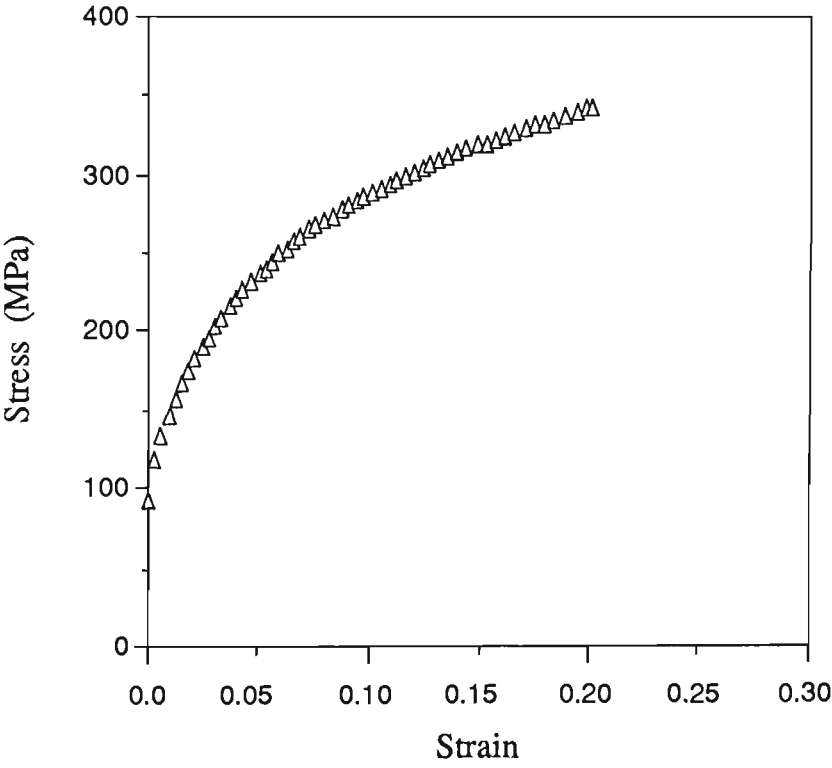


Fig. 6-27 Tensile testing result in a 70% cold reduction sample after batch annealing at 680°C for 30 minutes.

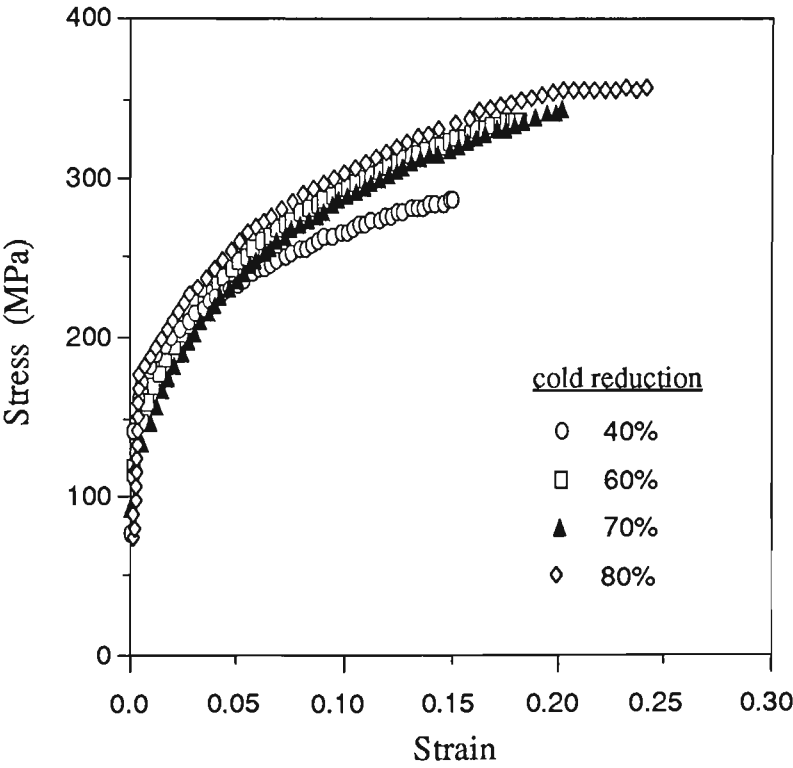


Fig. 6-28 Comparison of the tensile testing results of 40, 60, 70 and 80% cold reduced samples after batch annealing at 680°C for 30 minutes.

## 6.6 MICROSTRUCTURAL EXAMINATION

### 6.6.1 Optical Microscopy

Optical microscopy was carried out on metallographically prepared cross-sections through the gauge length of samples subjected to ultra-rapid annealing. Similar analysis was conducted on batch annealed samples.

#### 6.6.1.1 Ultra-rapid Annealing

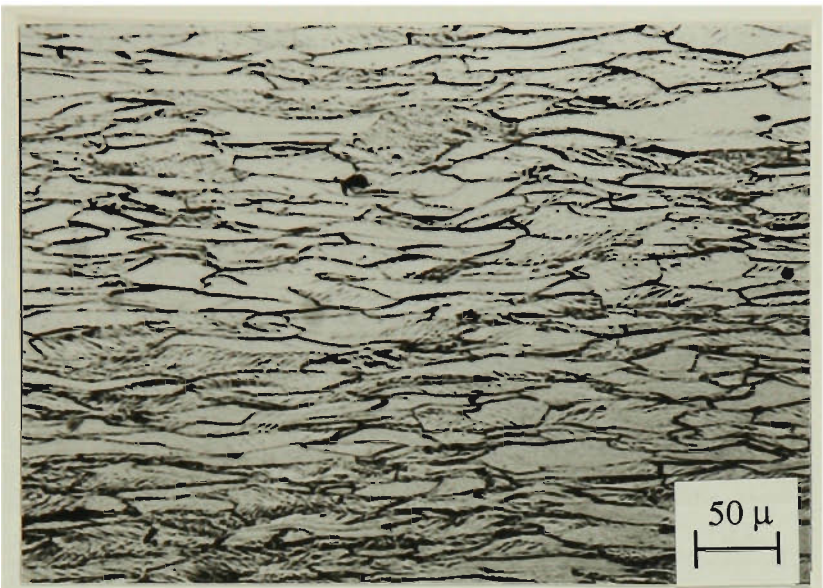
(a)  $t_1 = 0.2$  sec.

Observations of microstructures were conducted primarily on samples with 70% cold reduction, annealed with  $V_1 = 200, 208, 210, 215, 220, 230$  and  $233$  V with  $t_1 = 0.2$  and  $t_2 = 0.1$  sec. These conditions corresponded to temperatures  $T_c$  of  $450, 510, 530, 550, 650, 700$  and  $720^\circ\text{C}$ . Figure 6-29 shows micrographs representing the above treatments. The first equiaxed grains appeared at  $\sim 510^\circ\text{C}$  (Fig. 6-29b). Below  $510^\circ\text{C}$ , the structure consisted of cold rolled grains, while at  $510^\circ\text{C}$ , the recrystallized grains were approximately  $0.2\text{-}1.4\text{ }\mu\text{m}$  in diameter (Fig. 6-28(b)). Recrystallization started in the boundaries of the cold rolled grains, where the recrystallized grains were easily nucleated because of the high driving force. The recrystallized grains were not uniformly distributed and had a range of grain sizes. More new grains formed in the cold rolled structures as the temperature increased. Recrystallization was virtually complete at a temperature of  $720^\circ\text{C}$  (Figs. 6-29(g) and 6-29(h)), but the grains were not uniform in size, ranging from  $5\text{-}30\text{ }\mu\text{m}$ .

The relationship between microstructure and hardness is schematically shown in Fig. 6-30.

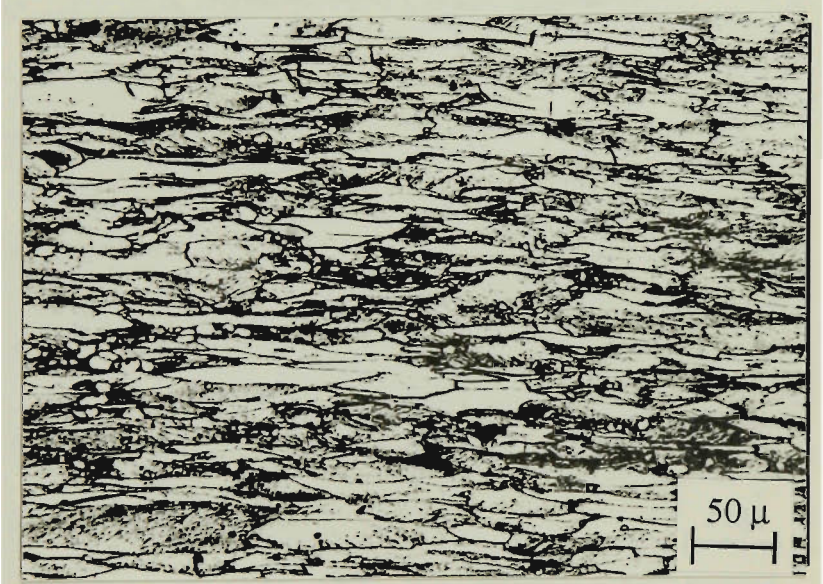
(a)

$T_c=450^{\circ}\text{C}$



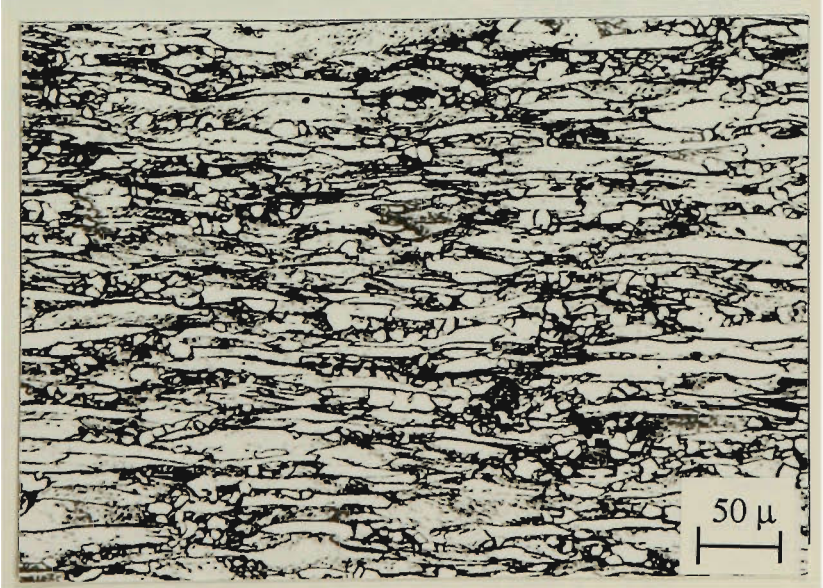
(b)

$T_c=510^{\circ}\text{C}$



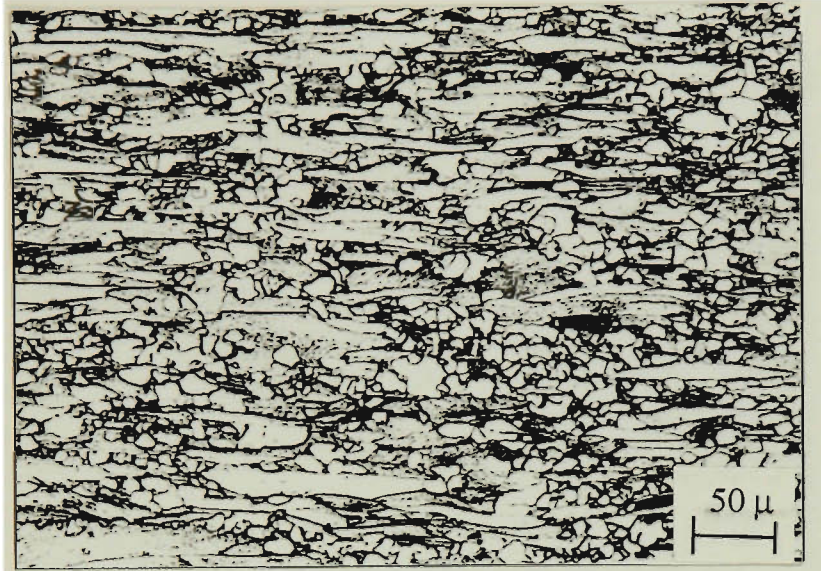
(c)

$T_c=530^{\circ}\text{C}$

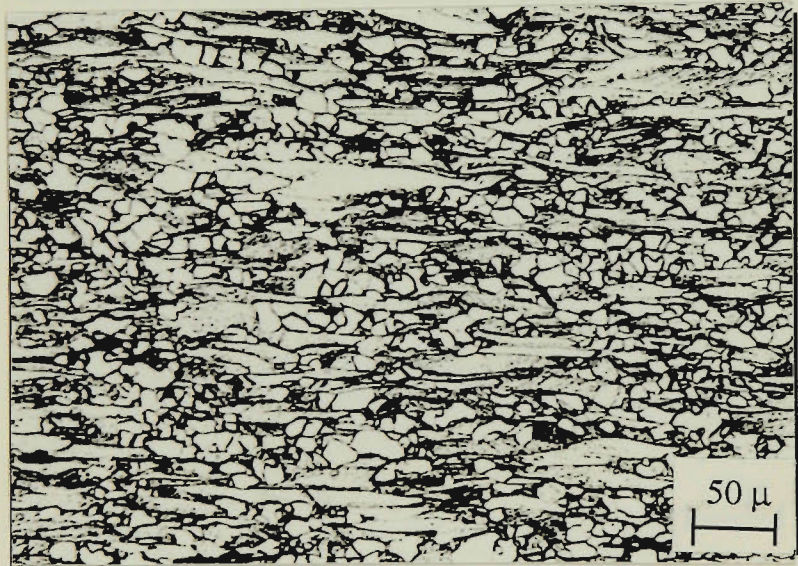




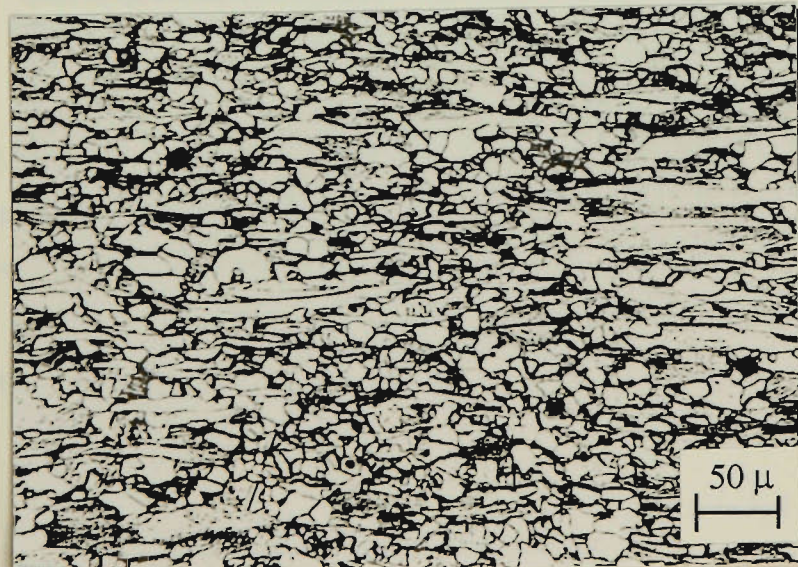
(d)  
T<sub>c</sub>=550°C



(e)  
T<sub>c</sub>=650°C

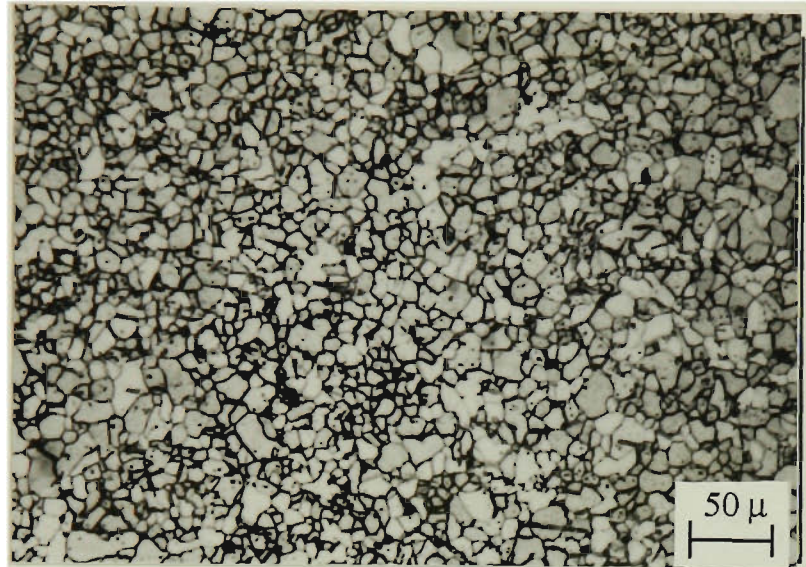


(f)  
T<sub>c</sub>=700°C





(g)  
 $T_c = 720^\circ\text{C}$



(h)  
 $T_c = 720^\circ\text{C}$

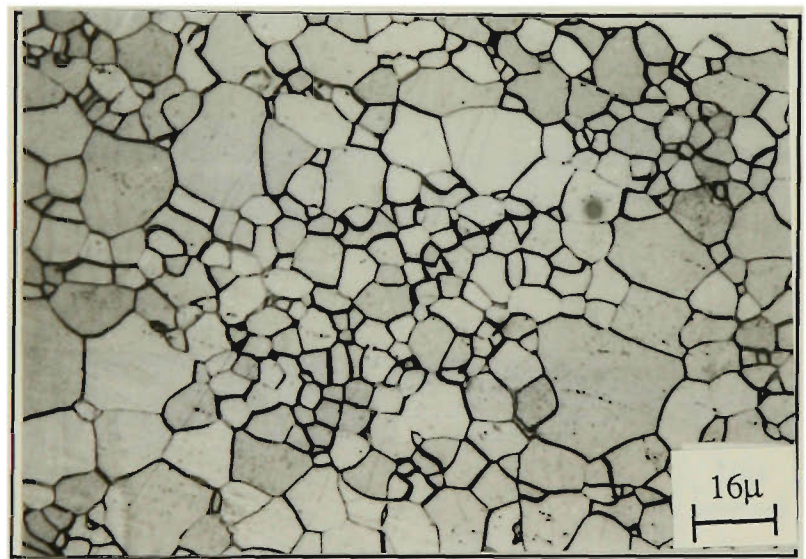


Fig. 6-29 Microstructures of samples with 70% cold reduction after ultra-rapid annealing with  $t_1 = 0.2$ ,  $t_2 = 0.1$  seconds with  $T_c =$  (a)  $450^\circ\text{C}$ ; (b)  $510^\circ\text{C}$ ; (c)  $530^\circ\text{C}$ ; (d)  $550^\circ\text{C}$ ; (e)  $650^\circ\text{C}$ ; (f)  $700^\circ\text{C}$  and (g)  $720^\circ\text{C}$ . (h) is a higher magnification of (g). (see Fig. 6-14)

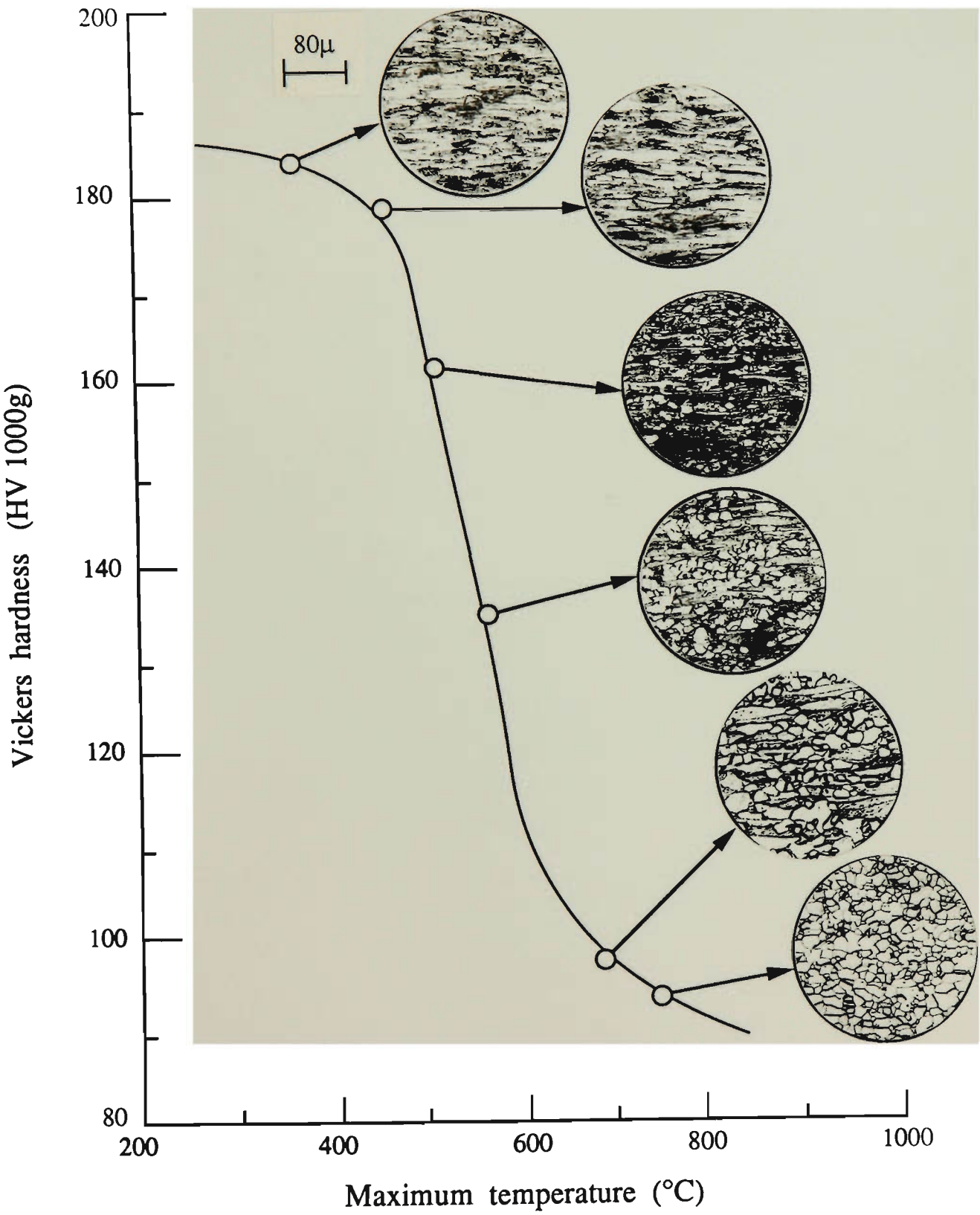


Fig. 6-30 Microstructure changes with maximum temperature and the corresponding hardness for a sample with 70% cold reduction after ultra-rapid annealing with  $t_1=0.2$  and  $t_2=0.1$  sec.



(b)  $t_1 = 0.5$  sec.

Microstructural studies were also carried out on samples with 70% cold reduction, ultra-rapid annealed with  $t_1 = 0.5$  and  $t_2 = 0.1$  seconds. Micrographs are shown in Fig. 6-31 (a)-(j) which correspond to temperatures of 510, 600, 650, 700, 720, 750, 820, 857 and 912°C.

The difference between 0.5 seconds and 0.2 seconds heating was that the first equiaxed grains appeared at  $\sim 650^\circ\text{C}$  instead of  $\sim 510^\circ\text{C}$ , i.e., the temperature for the start of recrystallization in the case of  $t_1 = 0.5$  seconds was higher than for  $t_1 = 0.2$  sec. Recrystallization finished at  $\sim 912^\circ\text{C}$  which was also higher than that for  $t_1 = 0.2$  sec. ( $720^\circ\text{C}$ ). Thus, the recrystallization process covered a higher temperature range in the  $t_1 = 0.5$  sec. samples. Again the nucleation of recrystallized grains occurred at the boundaries of the cold rolled grains and were not uniformly distributed throughout the material. The grain sizes ranged from 10 - 38  $\mu\text{m}$  ( Fig. 6-31(j)).

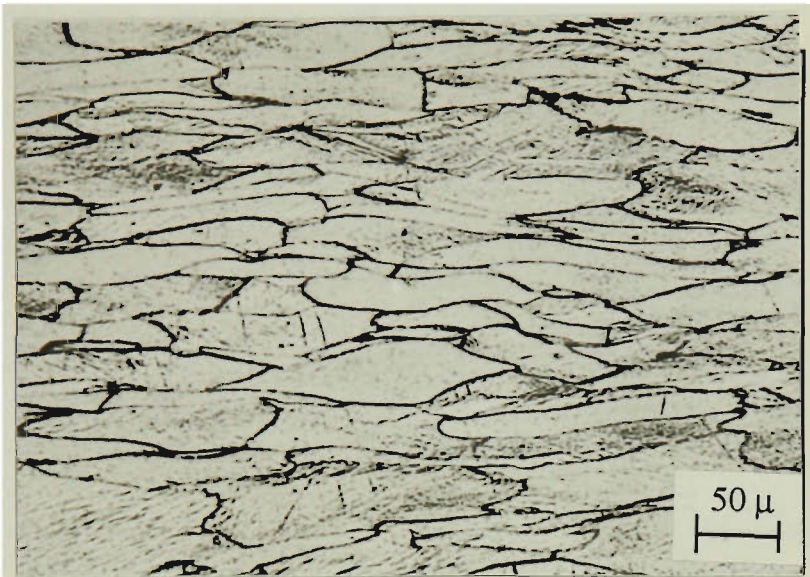
The microstructures and the corresponding hardness values are shown in Fig. 6-32.

(c) Influence of cold reduction on structures

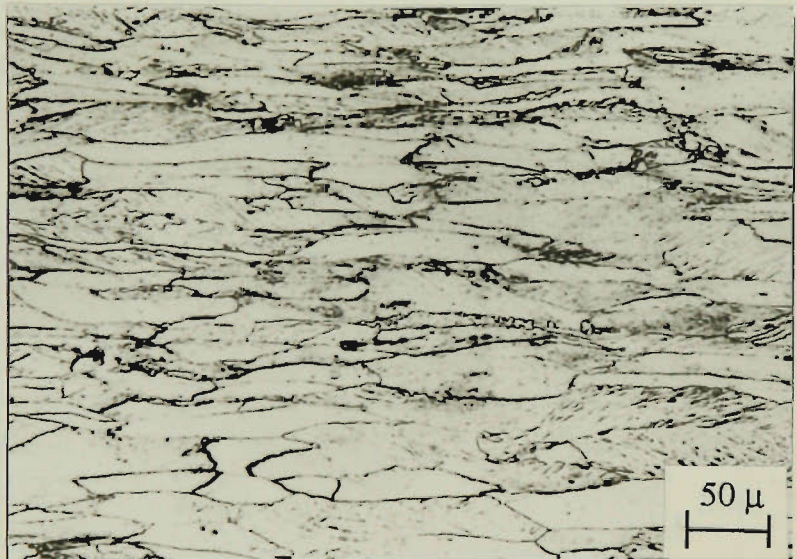
Samples with 40%, 60%, 70% and 80% cold reduction were examined after ultra-rapid annealing at 600, 630, 667, 700 and  $720^\circ\text{C}$  with  $t_1 = 0.3$  and  $t_2 = 0.1$  sec. Photomicrographs typical of these conditions are shown in Fig. 6-33. The horizontal rows represent the microstructure changes with temperature at the same cold reduction, and the vertical columns show the microstructural changes with deformation after heating to the same temperature.

Samples with 80% cold reduction recrystallized at the lowest temperature - the first nucleated grains appeared below  $600^\circ\text{C}$  and recrystallization was complete at  $\sim 700^\circ\text{C}$ .

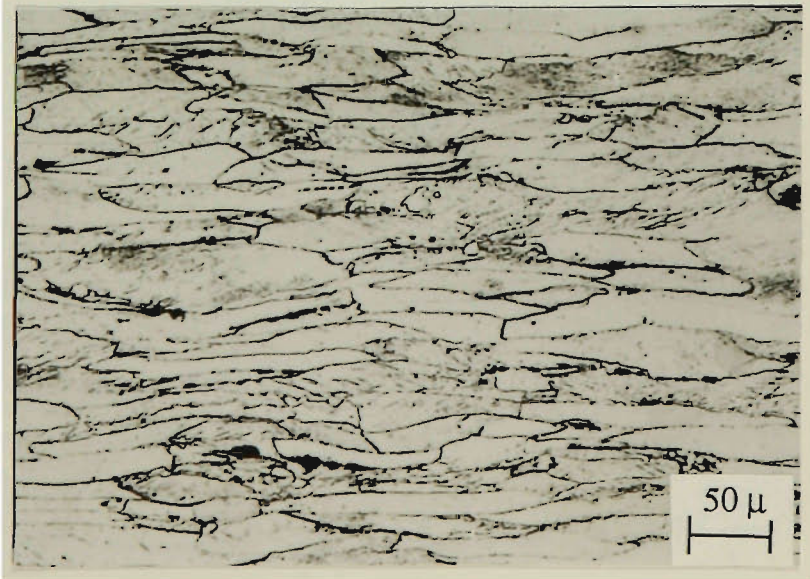
(a)  
 $T_c=510^{\circ}\text{C}$



(b)  
 $T_c=600^{\circ}\text{C}$

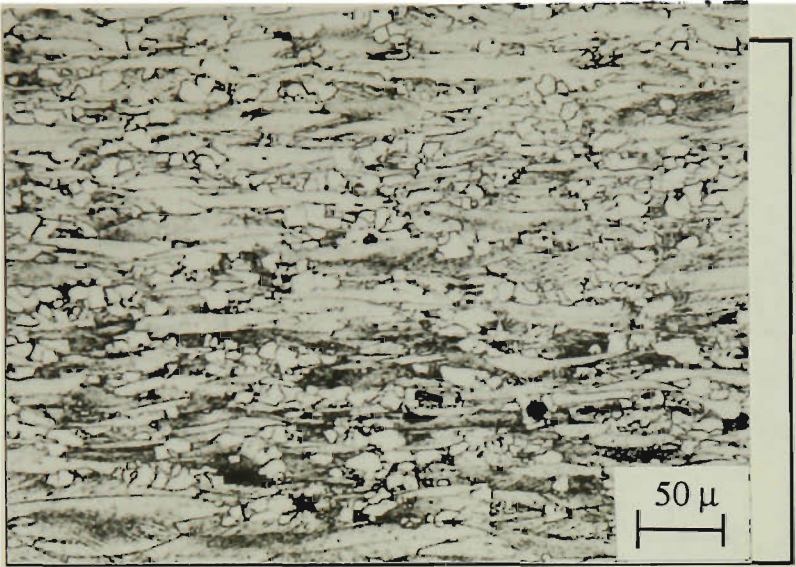


(c)  
 $T_c=650^{\circ}\text{C}$

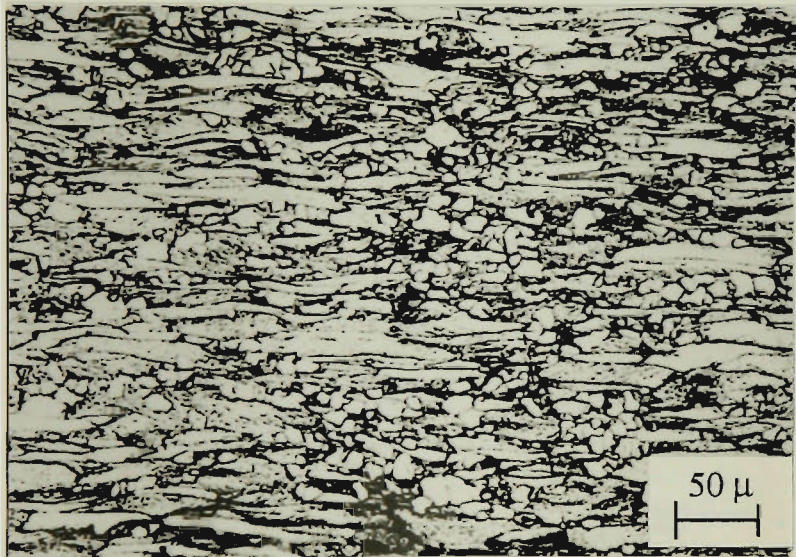




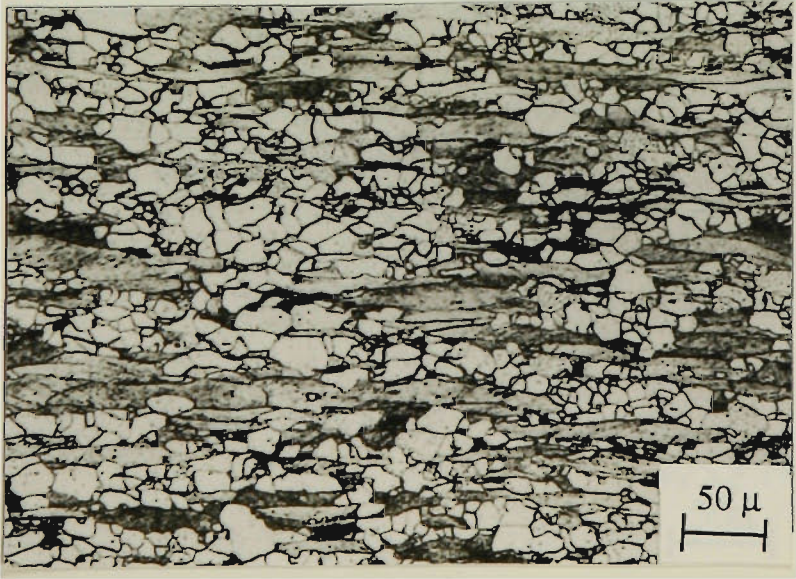
(d)  
 $T_c=700^{\circ}\text{C}$



(e)  
 $T_c=720^{\circ}\text{C}$



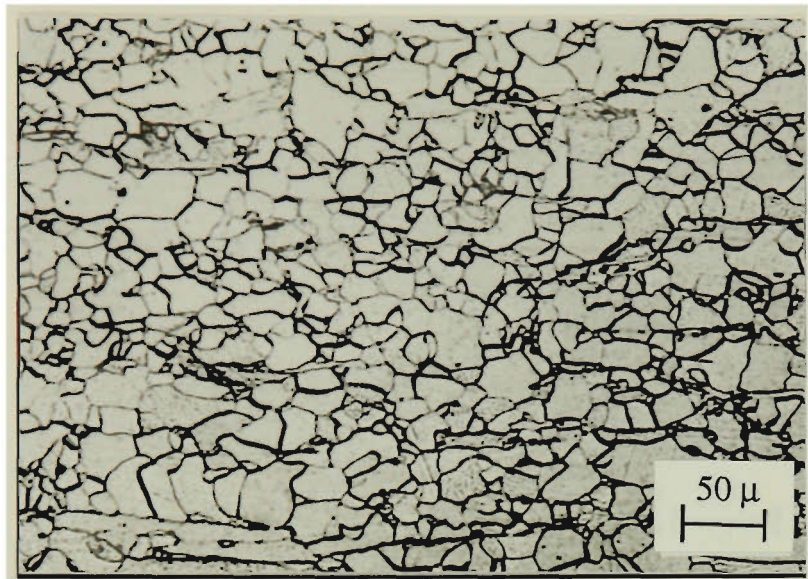
(f)  
 $T_c=750^{\circ}\text{C}$





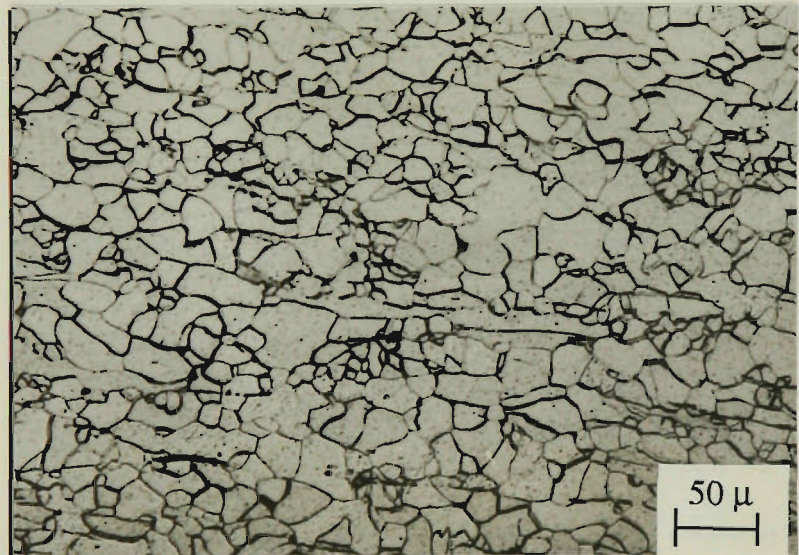
(g)

$T_c=820^{\circ}\text{C}$



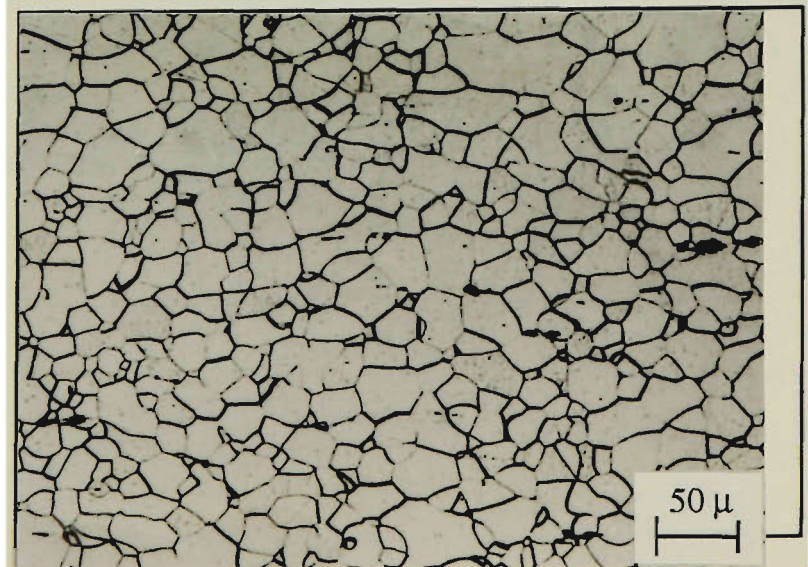
(h)

$T_c=857^{\circ}\text{C}$



(i)

$T_c=912^{\circ}\text{C}$



(j)  
Tc=912°C

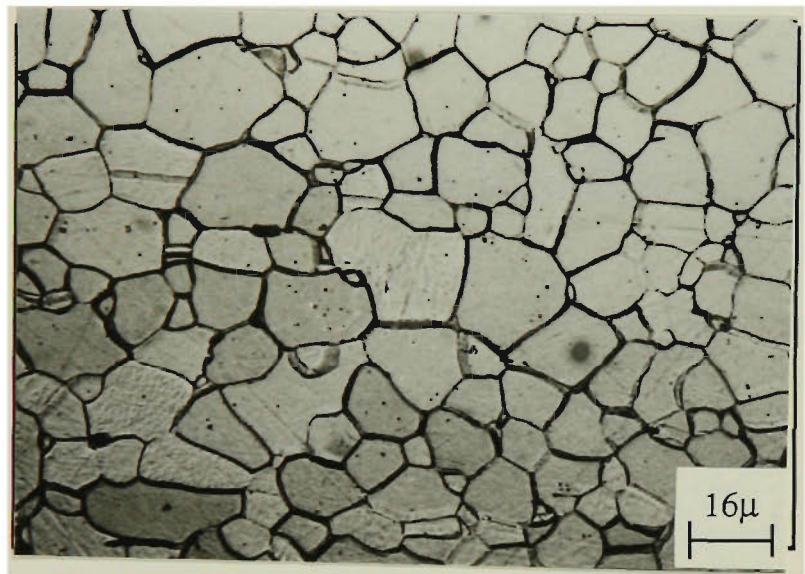


Fig. 6-31 Microstructures of a sample with 70% cold reduction after ultra-rapid annealing with  $t_1 = 0.5$ ,  $t_2 = 0.1$  seconds and at  $T_c =$  (a) 510°C; (b) 600°C; (c) 650°C; (d) 700°C; (e) 720°C; (f) 750°C; (g) 820°C; (h) 857°C; (i) 912°C. (j) is a higher magnification of (i). (see Fig. 6-14)

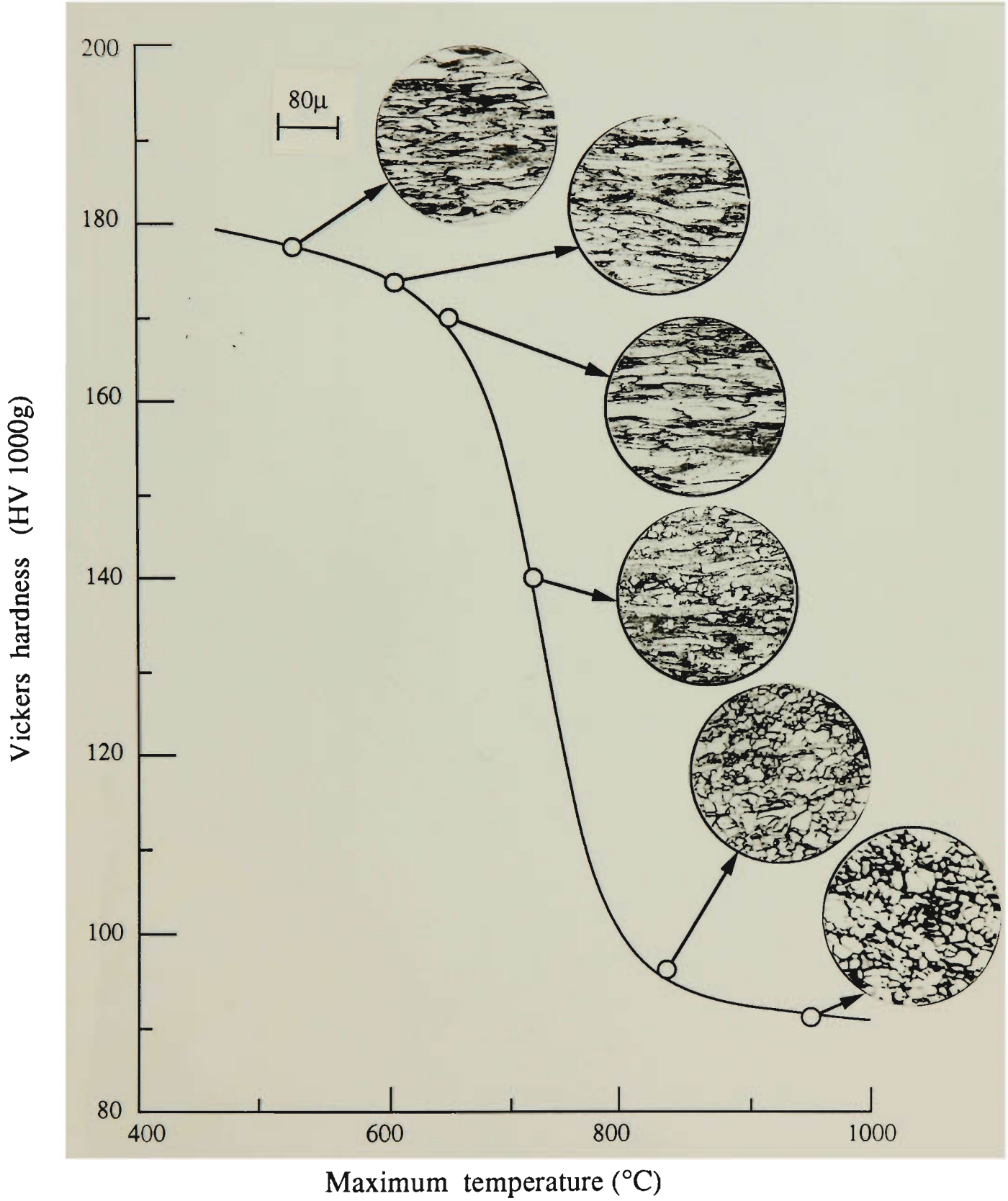


Fig. 6-32 Microstructure changes with maximum temperature and the corresponding hardness for a sample with 70% cold reduction after ultra-rapid annealing for  $t_1=0.5$  and  $t_2=0.1$  sec.



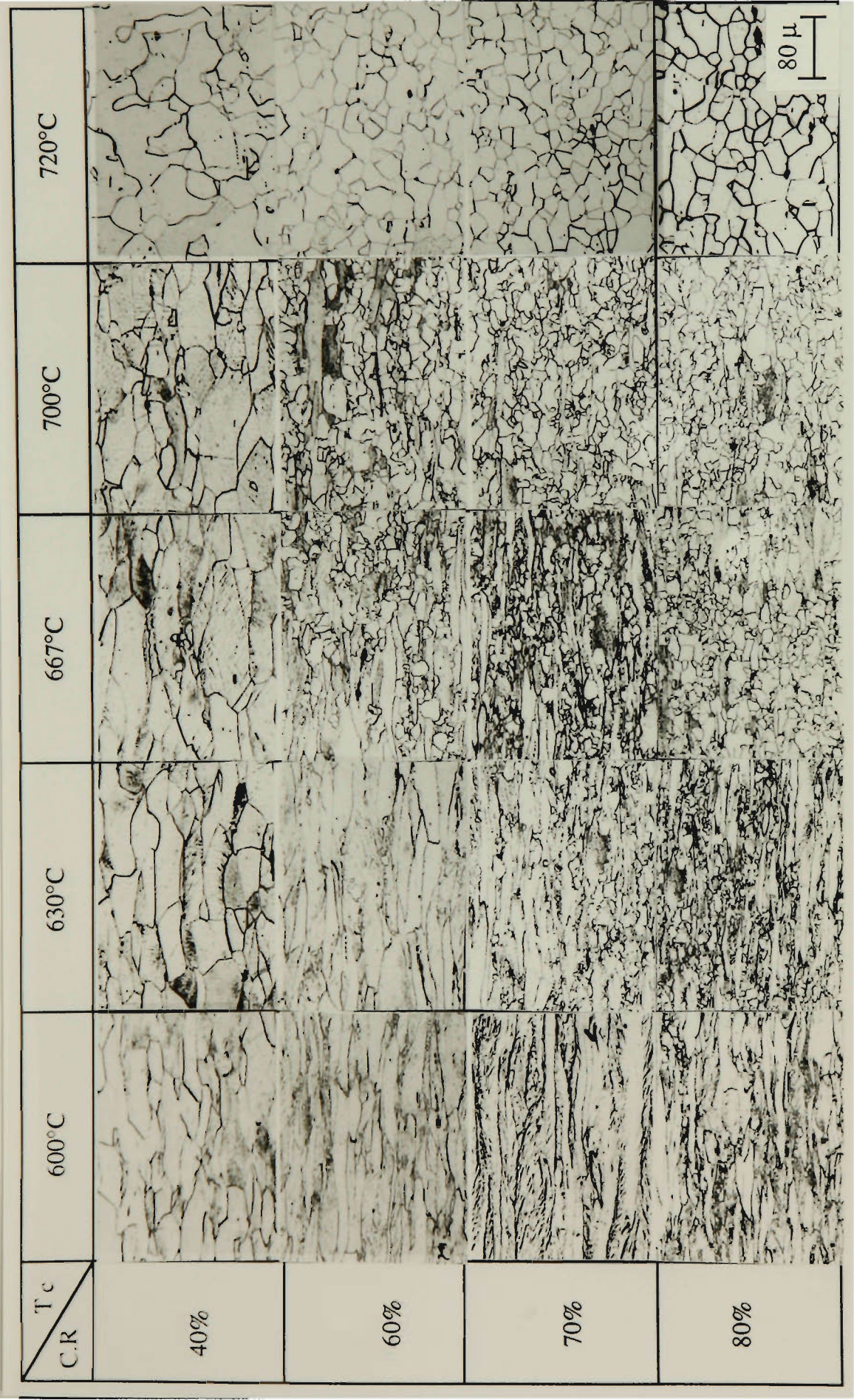


Fig. 6-33 Microstructures of samples with different cold reductions after ultra-rapid annealing for  $t_1=0.3$  and  $t_2=0.1$  sec. at  $T_c = 600, 630, 667, 700$  and  $720^\circ\text{C}$ .

The sample with 70% cold reduction seemed to start recrystallization at  $\sim 630^{\circ}\text{C}$  and the process finished at  $\sim 720^{\circ}\text{C}$ . For 40% cold reduction recrystallization did not commence until  $700^{\circ}\text{C}$  and the behaviour of samples with 60% cold reduction was intermediate between those with 70% and 40% reduction.

#### 6.6.1.2 Batch Annealing

Metallographic observations were made on samples with 40%, 60%, 70% and 80% cold reduction after batch annealing at  $680^{\circ}\text{C}$  for 30 minutes. The results are illustrated in Fig. 6-34 which shows the fully recrystallized structures. All the samples had larger grain sizes than samples subjected to ultra-rapid annealing.

#### 6.6.2 Measurements of Grain Size Distributions

In order to gauge the uniformity of the recrystallized grain size after ultra-rapid and batch annealing, the grain size distribution was measured using a graphics tablet connected to an Apple IIE computer.

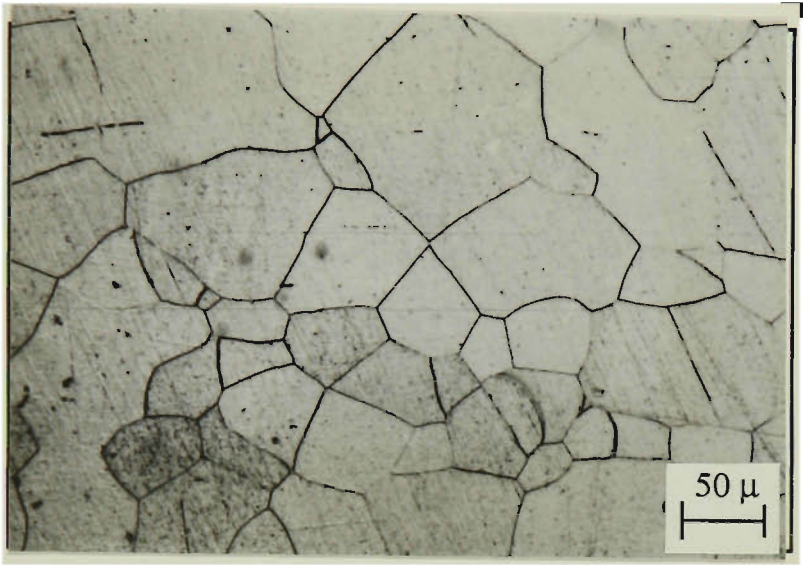
##### 6.6.2.1 Grain Size Distributions in Ultra-rapid Annealed Samples

###### (a) Annealed 70% cold reduced sample

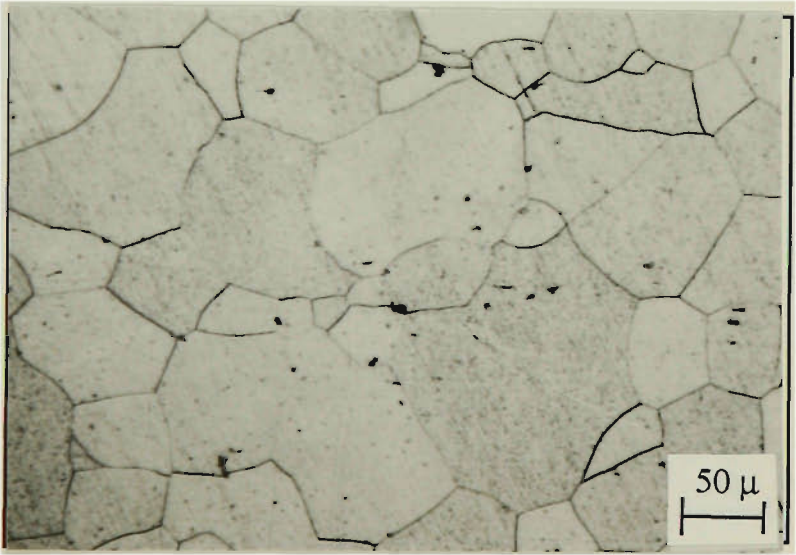
Analysis of grain size distributions was carried out initially for a sample with 70% cold reduction after ultra-rapid annealing at 510, 530, 550, 650, 700 and  $720^{\circ}\text{C}$  with  $t_1 = 0.2$  and  $t_2 = 0.1$  seconds. The results are presented in Table 6-5.



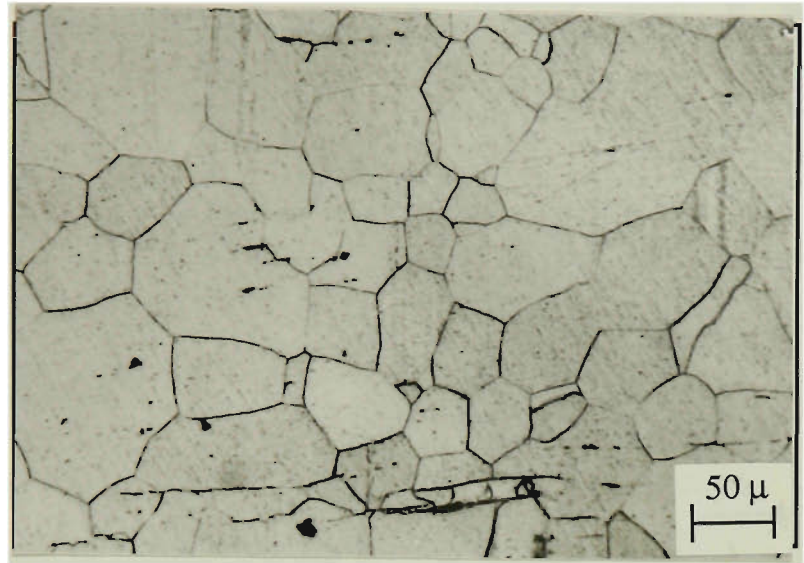
(a)  
40%



(b)  
60%



(c)  
70%



(d)  
80%

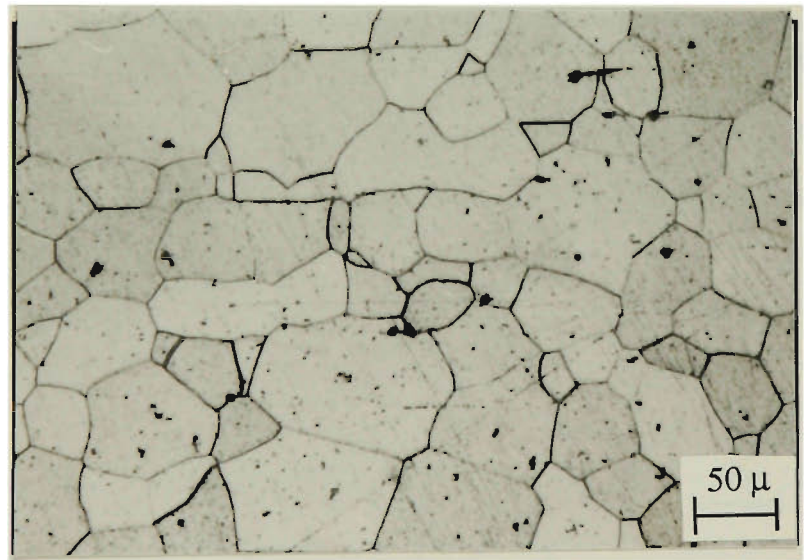


Fig. 6-34 Microstructures of samples with different cold reductions after batch annealing at 680°C for 30 minutes.

Table 6-5 Analysis of size distributions of the recrystallized grains in an ultra-rapid annealed sample with 70% cold reduction (ref. Fig. 6-29)

Temp. (°C)	510	530	550	650	700	720
%Recrystallization	3.5	22.4	50	70	85	100
$\bar{D}$ (μm)	0.8	6.0	9.8	13.5	15.2	16.8
$\sigma$	0.44	4.15	4.42	6.09	8.57	8.87
Range (μm)	0.2-1.4	1-12	4-17	4-21	5-29	5-30
$\gamma$	139	243	285	308	394	120

The grain sizes in ultra-rapid annealed materials were not normally distributed (Figs. 6-29(h) and 6-31(j)) but were, to varying degrees, skewed to higher grain sizes than the mean. At 720°C, recrystallization was complete, the grains had an average diameter of 16.8 μm and the distribution was characterised by a comparatively low index of skewness ( $\gamma = 120$ ) because of elimination of small grains by growth. However, recrystallization started as fine grains ( $\bar{D} = 0.8 \mu\text{m}$ ) at ~510°C and a pronounced increase in the average size occurred as the temperature increased and the percentage of recrystallization increased.

(b) Influence of cold reduction

A similar analysis was carried out for samples with 40%, 60%, 70% and 80% cold reductions after ultra-rapid annealing at 720°C with  $t_1 = 0.3$  and  $t_2 = 0.1$  seconds. The characteristic quantities of the grain size distributions are listed in Table 6-6.

At 720°C, the material with higher cold reduction exhibited finer grain sizes, lower deviation  $\sigma$  and lower skewness ( $\gamma$ ).

Table 6-6 Analysis of size distributions of the recrystallized grains  
in ultra-rapid annealed samples with  
different cold reduction ( $T_c=720^{\circ}\text{C}$ )

Cold reduction	40%	60%	70%	80%
% Recrystallized	60	73	95	100
$\bar{D}$ ( $\mu\text{m}$ )	37	17.2	17.8	18.7
$\sigma$	24.14	13.13	9.78	15.15
Range ( $\mu\text{m}$ )	12-80	2-38	3-30	5-45
$\gamma$	267	246	120	98

6.6.2.2 Grain Size Distributions of Batch Annealed Samples

Samples with 40%, 60%, 70% and 80% cold reduction were batch annealed at  $680^{\circ}\text{C}$  for 30 minutes .

Compared with the grain size distributions in the materials after ultra-rapid annealing, the grain sizes in batch annealed materials were coarser by a factor of about 2. The results of the analysis are given in Table 6-7.

Table 6-7 Analysis of grain size distributions for samples  
with different cold reductions after batch  
annealing at  $680^{\circ}\text{C}$  for 30 minutes

Cold reduction	40%	60%	70%	80%
$\bar{D}$ ( $\mu\text{m}$ )	69	68	43	42
$\sigma$	38.56	41.39	32.36	29.80
Range ( $\mu\text{m}$ )	13-120	11-130	10-100	10-94
$\gamma$	201	186	178	164

### 6.6.3 Transmission Electron Microscopy

#### 6.6.3.1 Cold Rolled Structures

The foils examined were rolling plane foils and therefore, the observations are not as definitive as they are normally for longitudinal sections. Roughly equiaxed cell structure was common, but in some cases elongated cells were observed (Fig. 6-35) which are consistent with the microbands reported in cold rolled low carbon steels and other metals with high stacking fault energy [374]. Figure 6-36 shows a grid of dislocation lines in a 40% cold reduced sample. Selected area diffraction identified the orientation of the foil as  $\langle 110 \rangle_{\text{bcc}}$ . The dislocation network is a grid of dislocations derived from dislocations on different slip planes and can be regarded as an initial stage in the development of a cell structure (Fig. 6-37).

#### 6.6.3.2 Ultra-rapid Annealed Samples

##### (a) Annealed 70% cold reduced samples

Figure 6-38 shows a small well-deformed subgrain in a sample with 70% cold reduction after ultra-rapid annealing at 630°C for  $t_1 = 0.3$  seconds. The size of the subgrain was only  $\sim 1.5 \mu\text{m}$  and it is a likely precursor to the formation of a recrystallized grain. Electron diffraction indicated that the subgrain had relatively low angle boundaries with neighbouring cells. Increasing temperature resulted in the growth in both size and number of the subgrains. Figure 6-39 shows a sample with 70% cold reduction after ultra-rapid annealing at 650°C. Figure 6-40 is a higher magnification of grain A in Fig. 6-39. It is seen that the subgrain originated from a region with high density of dislocations and some arrays of dislocations still existed inside the subgrains (Fig. 6-41). Dislocation structures observed in a sample with 70% cold reduction after ultra-rapid annealing at 667°C are shown in Figs. 6-42 and 6-43.

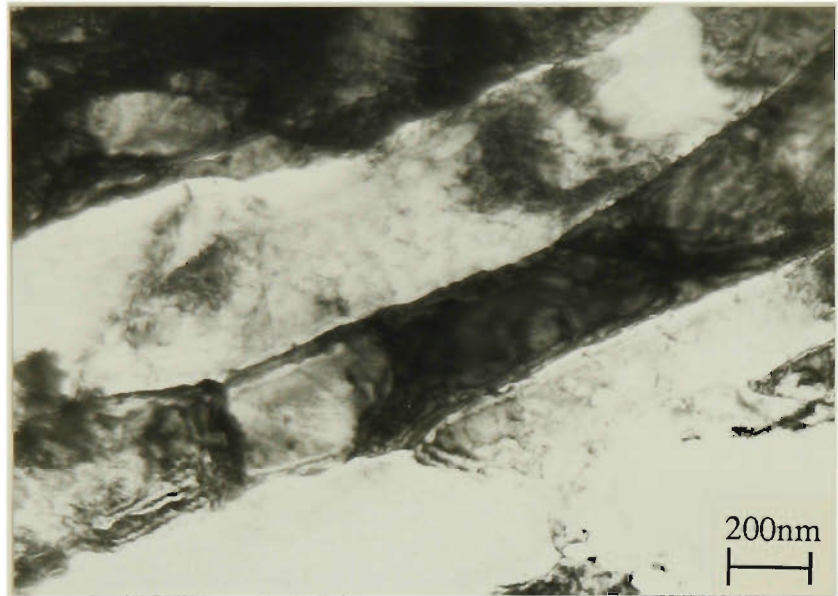
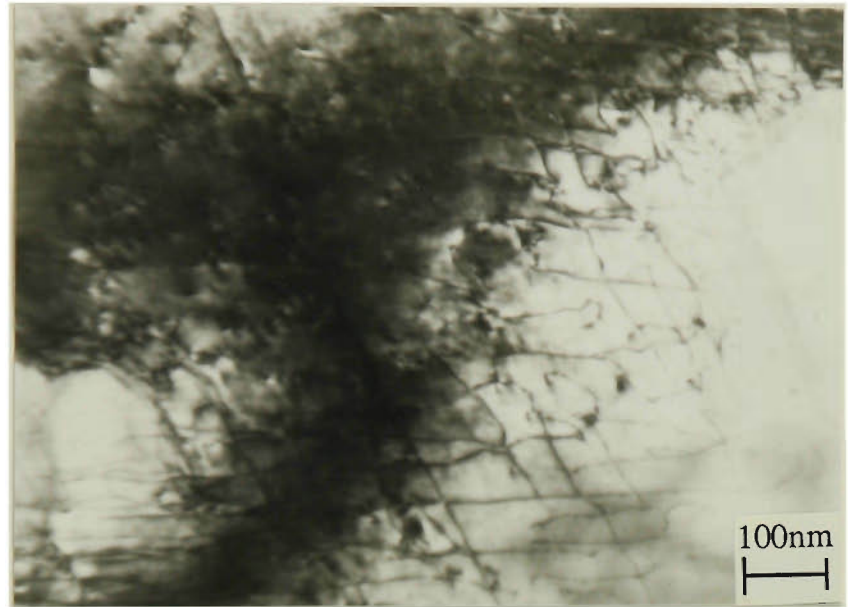


Fig. 6-35 Cold rolled structure found in a sample with 40% cold reduction showing elongated cells or microbands.

(a)



(b)

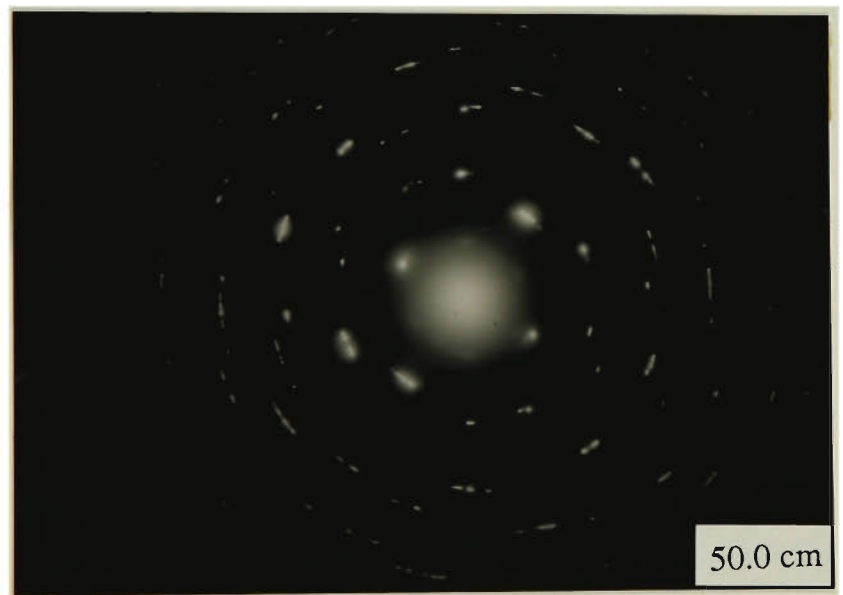


Fig. 6-36 Intersecting dislocation grid in a sample with 40% cold reduction showing (a) intersecting dislocations; (b) the corresponding diffraction pattern close to an  $\langle 110 \rangle_{\text{bcc}}$  axis.



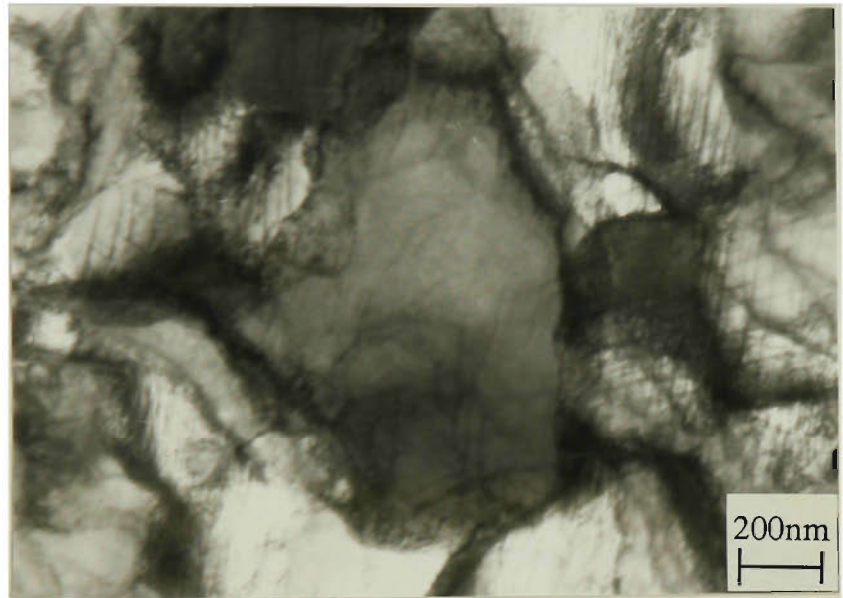


Fig. 6-37 Dislocation networks and cell boundaries observed in a sample with 40% cold reduction.





Fig. 6-38 Subgrains (arrowed) observed in a sample with 70% cold reduction after ultra-rapid annealing at 630°C for  $t_1 = 0.3$  and  $t_2 = 0.1$  sec.

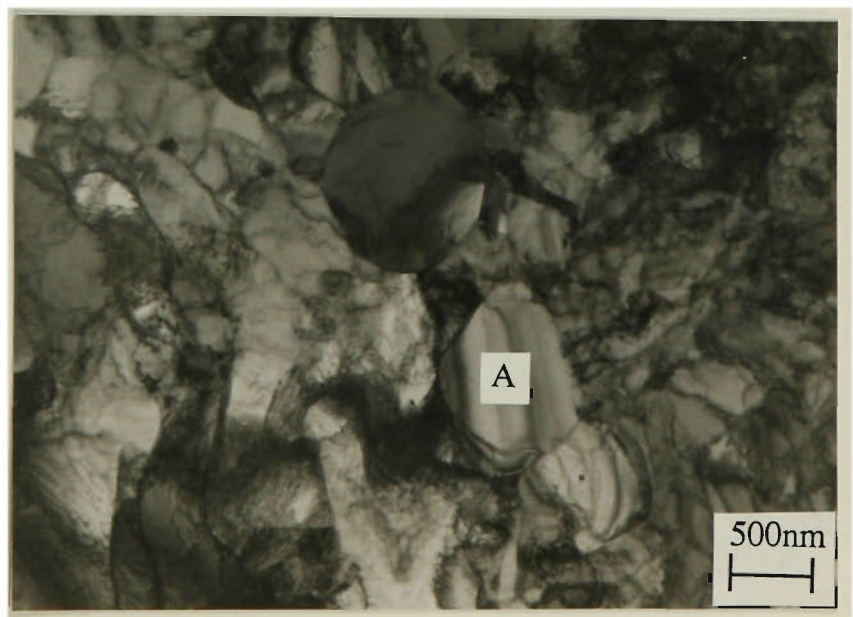


Fig. 6-39 Typical microstructure of a sample with 70% cold reduction after ultra-rapid annealing at 650°C for  $t_1 = 0.3$ ,  $t_2 = 0.1$  sec. showing large subgrains.

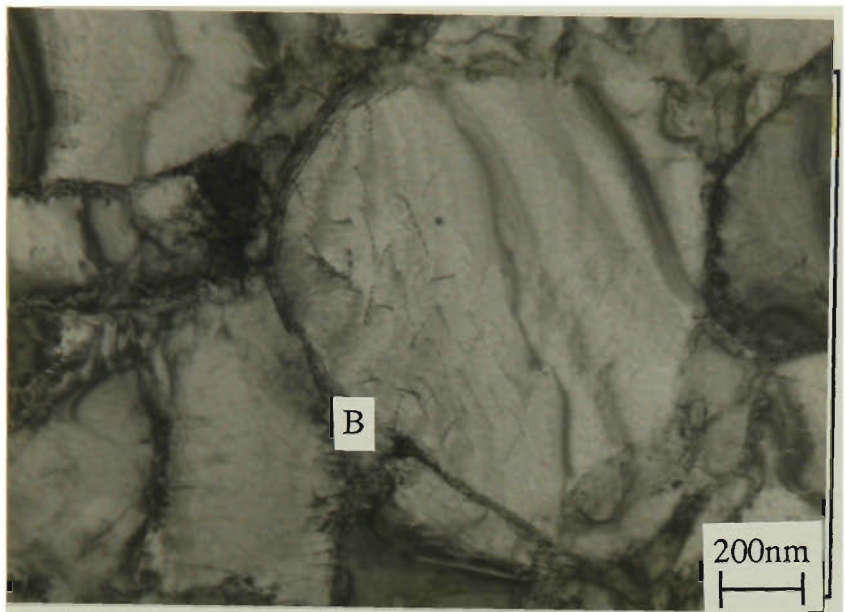


Fig. 6-40 Close up of grain "A" in Fig. 6-39.



Fig. 6-41 High magnification around the point B in Fig. 6-40.

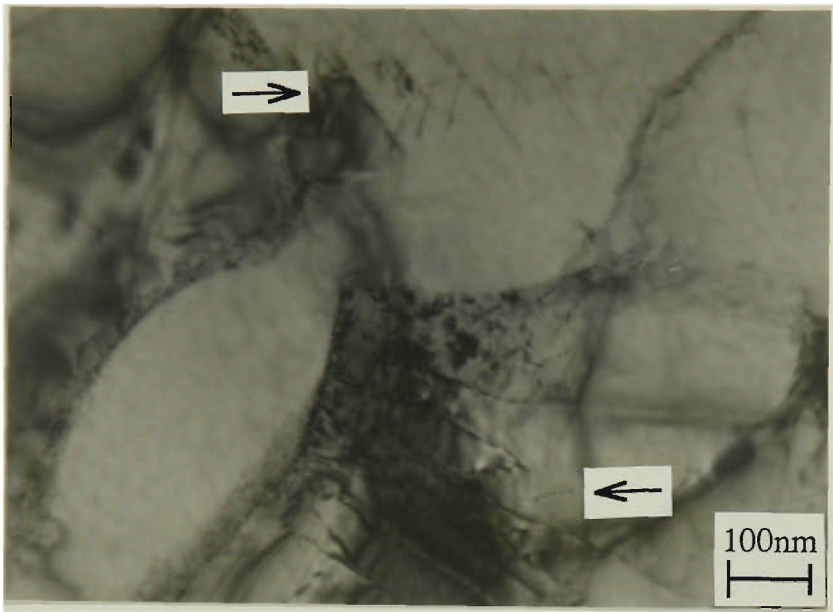


Fig. 6-42 Dislocation structures observed in a sample with 70% cold reduction after ultra-rapid annealing at 667°C for  $t_1 = 0.3$  and  $t_2 = 0.1$  seconds.

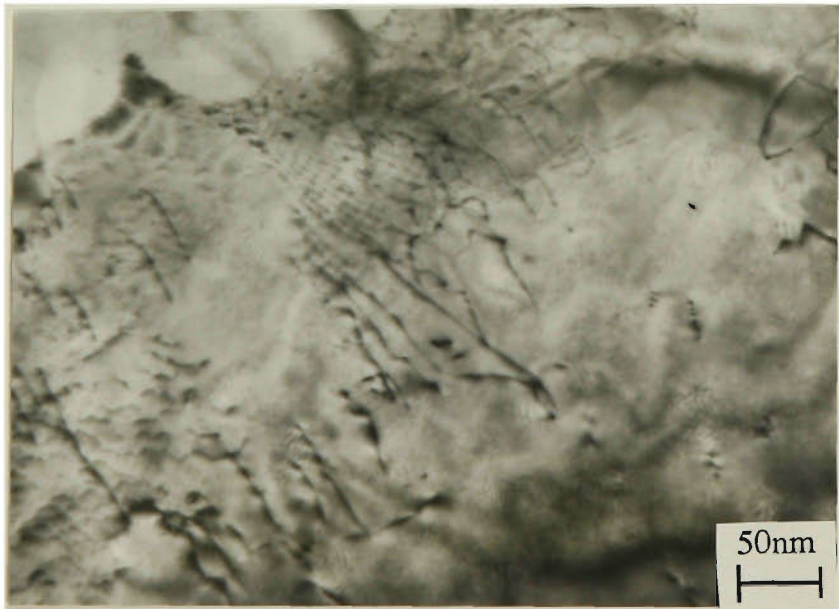


Fig. 6-43 Dislocation networks found in a sample with 70% cold reduction after ultra-rapid annealing at 667°C for  $t_1 = 0.3$  and  $t_2 = 0.1$  seconds.

It is worth noting that large angle boundaries were also observed after annealing at 700°C as shown in Figs. 6-44 and 6-45. The angles between grain boundaries were  $\sim 120^\circ$  corresponding to the most stable state.

Recrystallization was completed at 720°C for a sample with 70% cold reduction after ultra-rapid annealing for  $t_1 = 0.3$  sec. The microstructures consisted of recrystallized grains in place of the cold rolled cells as shown in Fig. 6-46. Note that there was a relatively high dislocation density within the recrystallized grains.

#### (b) Influence of cold reduction

Observations were also made on the samples with 40%, 60% and 80% cold reduction. The "microbulging" of grain boundaries, which has been described by Bailey [88], Bailey and Hirsch [89], Chopra and Niessen [375] and Naka et al. [376], was found in a sample with 40% cold reduction and ultra-rapid annealed at 600°C (Fig. 6-47). This temperature is below the softening temperature. A composite micrograph of a grain boundary in a sample with 60% cold reduction and ultra-rapid annealed at 600°C is shown in Fig. 6-48.

#### 6.6.3.3 Batch Annealed Structures

Compared with the structures after ultra-rapid annealing, batch annealing gave rise to larger grain sizes at the same annealing temperature. Figure 6-49 shows the grain structure in a sample with 70% cold reduction after annealing at 680°C for 30 minutes. Note the low dislocation density within the recrystallized grains. Subgrain structures were found in a material batch annealed at 450°C for 60 minutes (Fig. 6-50). Figure 6-51 is a close up of point A in Fig. 6-50.



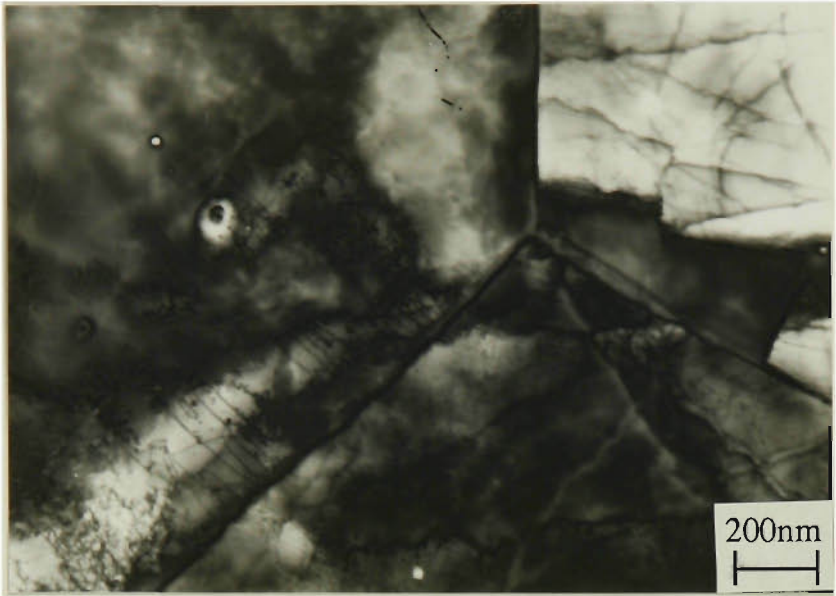


Fig. 6-44 Large angle boundaries observed in a sample with 70% cold reduction after ultra-rapid annealing at 700°C for  $t_1 = 0.3$  and  $t_2 = 0.1$  sec.



Fig. 6-45 Dark field image showing a large angle grain boundary in Fig. 6-44.

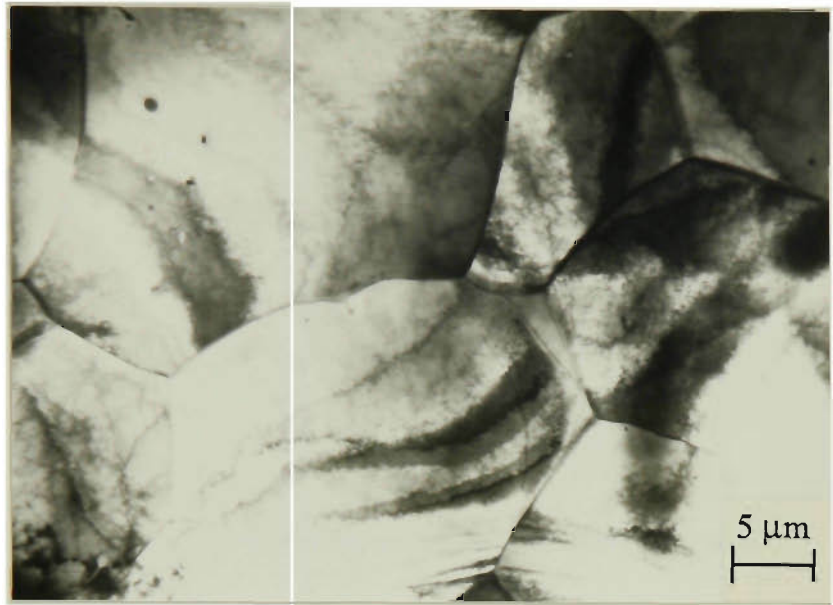


Fig. 6-46 Completely recrystallized structures observed in a sample with 70% cold reduction after ultra-rapid annealed for  $t_1 = 0.3$ ,  $t_2 = 0.1$  seconds, and  $T_c = 720^\circ\text{C}$ .

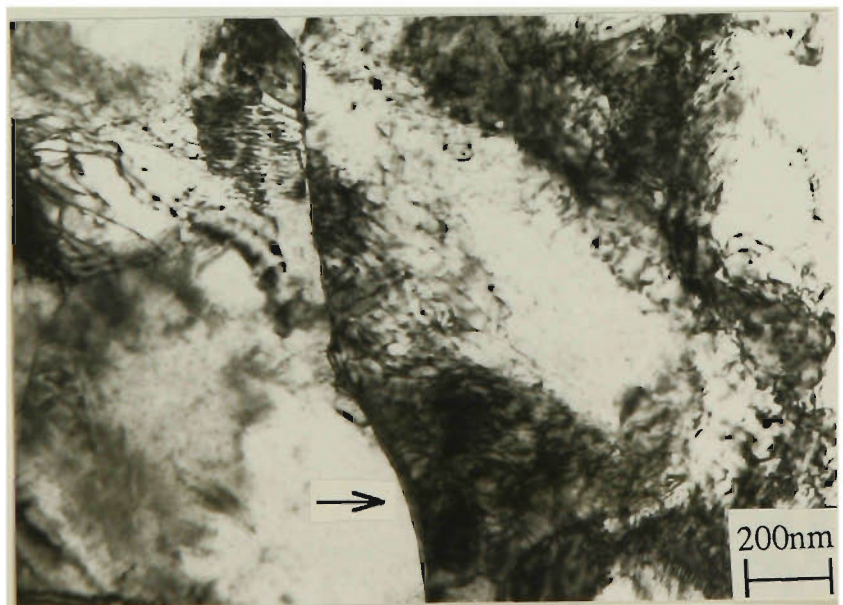


Fig. 6-47 The "microbulging" of grain boundaries found in a sample with 40% cold reduction and ultra-rapid annealed at  $600^\circ\text{C}$  for  $t_1 = 0.3$  and  $t_2 = 0.1$  seconds.

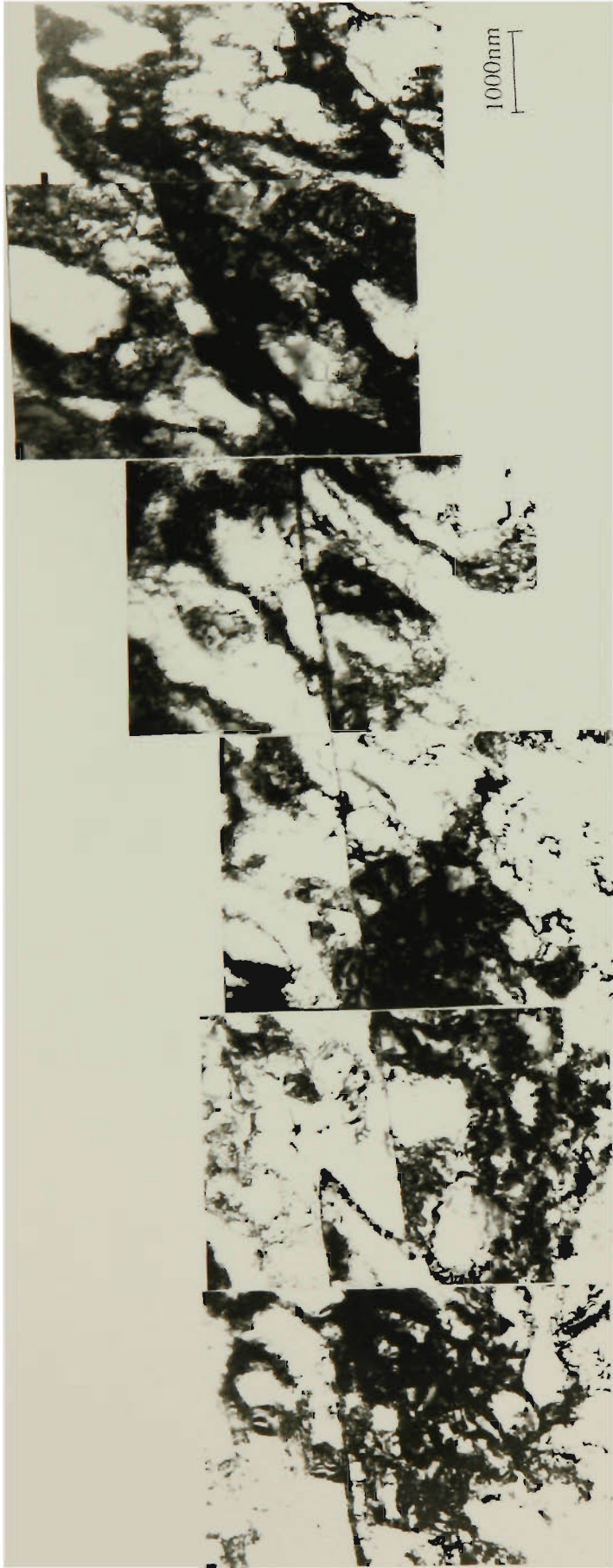


Fig. 6-48 Grain boundary with different cell structures across the boundary . 60% cold reduction and ultra-rapid annealed at 600°C with  $t_1 = 0.3$  and  $t_2 = 0.1$  sec.



Fig. 6-49 Grains observed in a sample with 70% cold reduction after batch annealing at 680°C for 30 minutes.



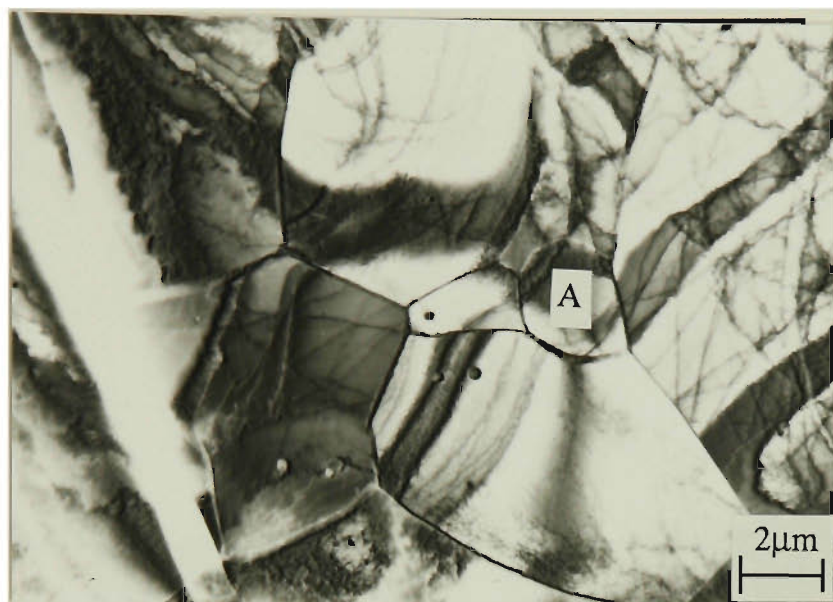


Fig. 6-50 Subgrain structures observed in a sample with 70% cold reduction and batch annealed at 450°C for 60 min.

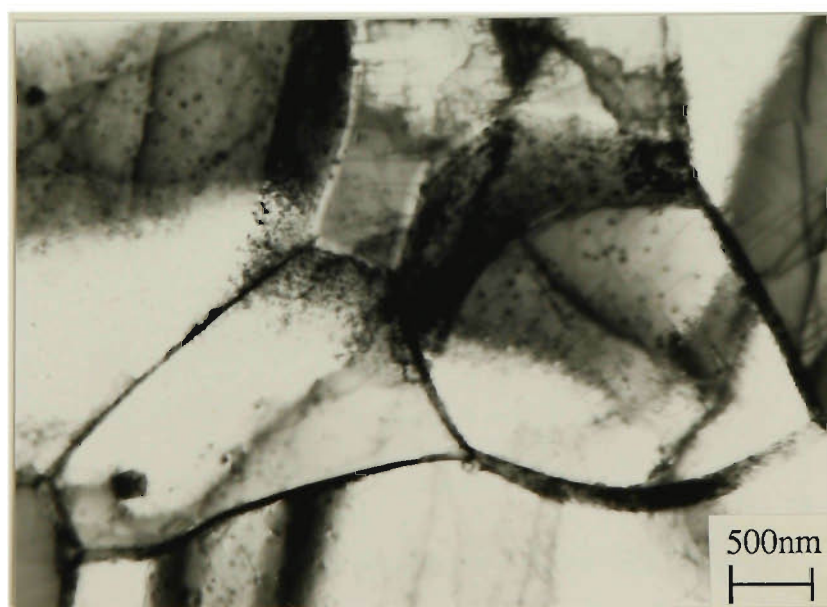


Fig. 6-51 Close up of point "A" in Fig. 6-50.

***CHAPTER 7***

**DISCUSSION**

## 7.1 INTRODUCTION

Basic information on ultra-rapid annealing of cold rolled decarburized steel has been obtained by resistance heating. Variations of softening temperature ranges with ultra-rapid heating rates were observed and are compared with observations of other investigators in Section 7.2. The recrystallization kinetics and nucleation mechanisms at high heating rates are discussed in Sections 7.3 and 7.4, respectively.

In studying the effect of heating rates on recrystallization in iron and low carbon steels, determination of the softening point is very important. Section 7.5 compares the two techniques --- micro-hardness measurements and metallography --- used in the present investigation.

Deformation is necessary to initiate recrystallization. Section 7.6 covers the effect of the different degrees of cold reduction on softening behaviour during ultra-rapid annealing.

The mechanism of softening during ultra-rapid annealing is considered in Section 7.7.

Finally, the tensile properties of a material undergoing ultra-rapid annealing and batch annealing are discussed in terms of yield stress ( $S_0$ ), tensile strength ( $S_u$ ), ductility ( $e_f$  and  $q$ ), toughness ( $U_T$ ) and plastic strain ratio ( $R$ ) in Section 7.8.

## 7.2 INFLUENCE OF HEATING RATE ON SOFTENING TEMPERATURE RANGES

The experimental results shown in Fig. 7-1 and 7-2 (derived from Fig. 6-14) indicate a definite influence of heating rate on the temperature ranges over which softening occurs under ultra-rapid annealing conditions. Figure 7-3 gives the softening temperature range at various heating rates. As the heating rates were increased to over  $1250^{\circ}\text{C}/\text{sec.}$ , both the start and finish temperatures for softening were lowered (Fig. 7-3). Such an effect of high heating rates on softening temperature range by resistance heating has not been reported previously. For comparison, results obtained by previous researchers covering the range of heating rates from 10 to  $1250^{\circ}\text{C}/\text{sec.}$  are presented, in Figs. 7-4 and 7-5, which show softening temperatures versus heating time and the heating rate, respectively. Each band in these figures represents the softening range, i.e., the bottom line denotes the start temperature and the top boundary, the finish temperature of softening. In Fig. 7-4, the data from Andrews and Atkinson [6] were obtained by induction heating ( zone A ) and salt bath heating ( zone B ), and correspond to zone 1 and zone 2 in Fig. 7-5. Also shown in Fig. 7-4 are the predictions by Andrews of the possible softening ranges with pre-recovery ( zone D ) and without pre-recovery ( zone C ). The results of Staüb [40], L'vov [38] and Mohri [39] are illustrated in areas 3, 4, 5, respectively, in Fig. 7-5. The present results from resistance heating are plotted as zone E in Fig. 7-4 and zone 6 in Fig. 7-5.

It is clearly seen that the present investigation extends the heating rate beyond those of previous studies. Also, the results show that the softening temperature range decreases as the heating rate increases in the range  $1500 - 3500^{\circ}\text{C}/\text{sec.}$  It should be noted that the data given in Figs. 7-4 and 7-5 were obtained from different kinds of low-carbon steels or iron which were subjected to different cold rolling treatments and therefore, close agreement in terms of temperature ranges is not to be expected.

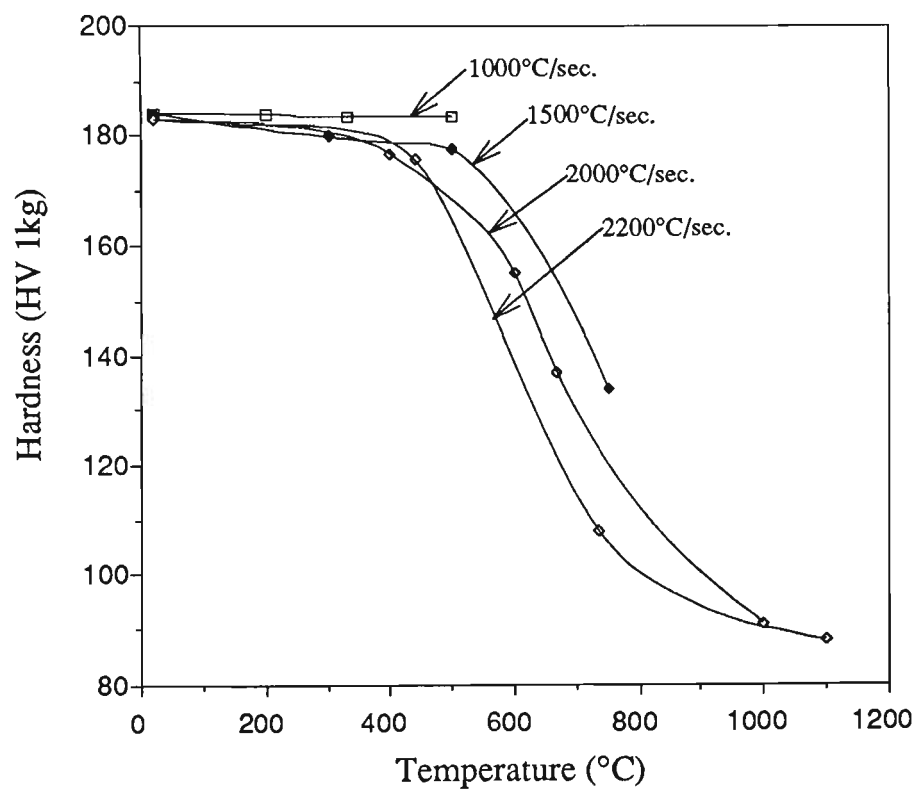


Fig. 7-1 The softening behaviour of 70% cold rolled samples after ultra-rapid annealing at various heating rates.

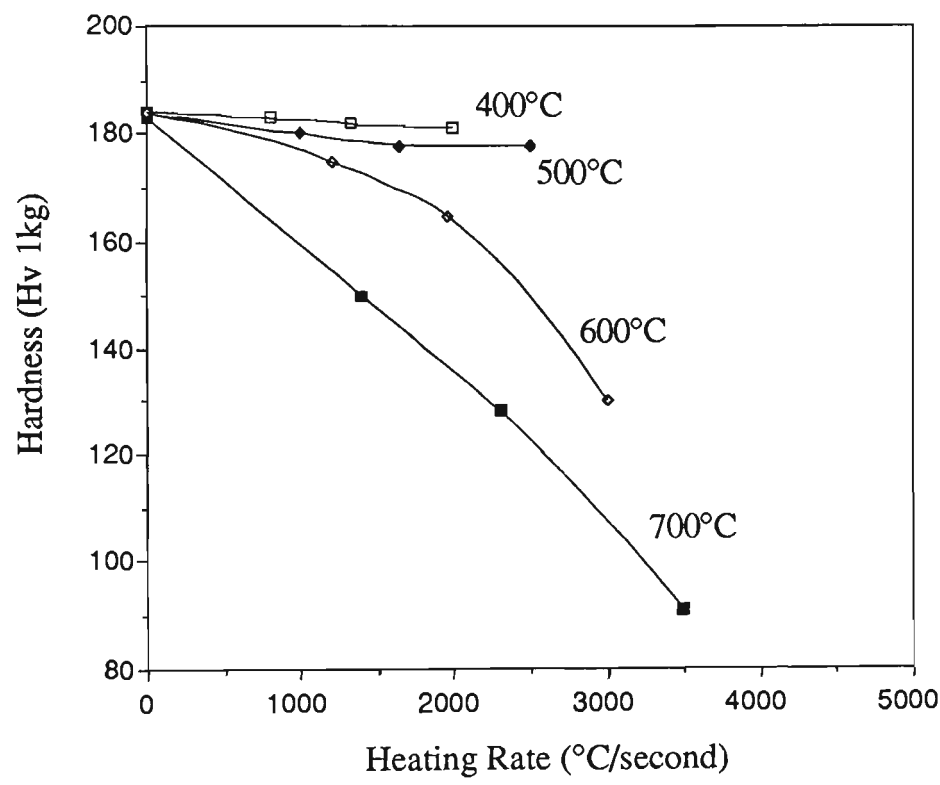


Fig. 7-2 The effect of heating rates to the indicated temperature on the hardness of 70% cold rolled samples.

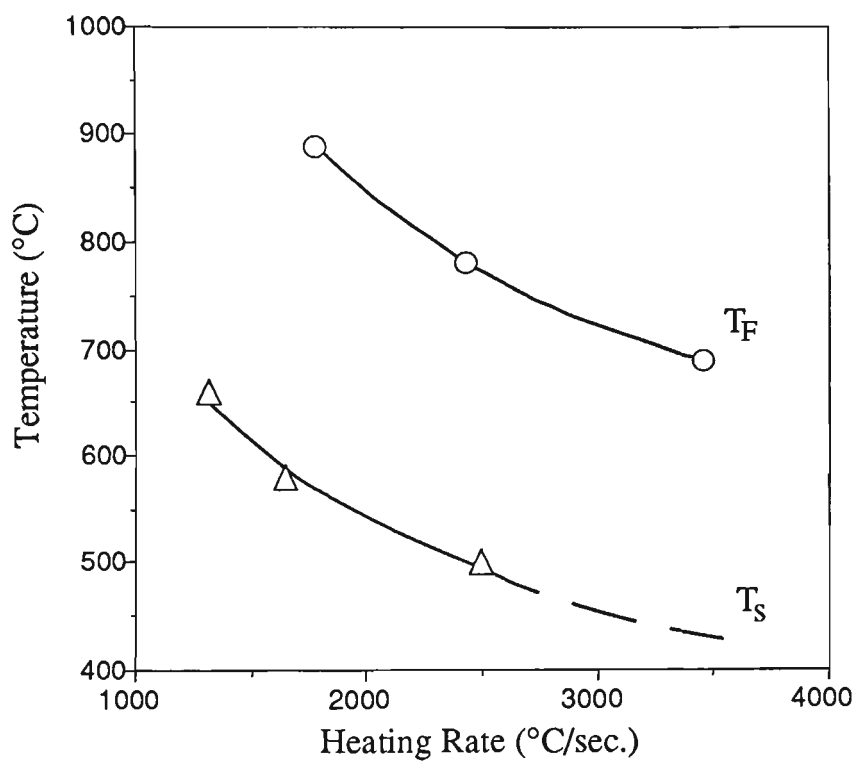


Fig. 7-3 The effect of heating rate on the start ( $T_S$ ) and finish ( $T_F$ ) temperatures for softening.

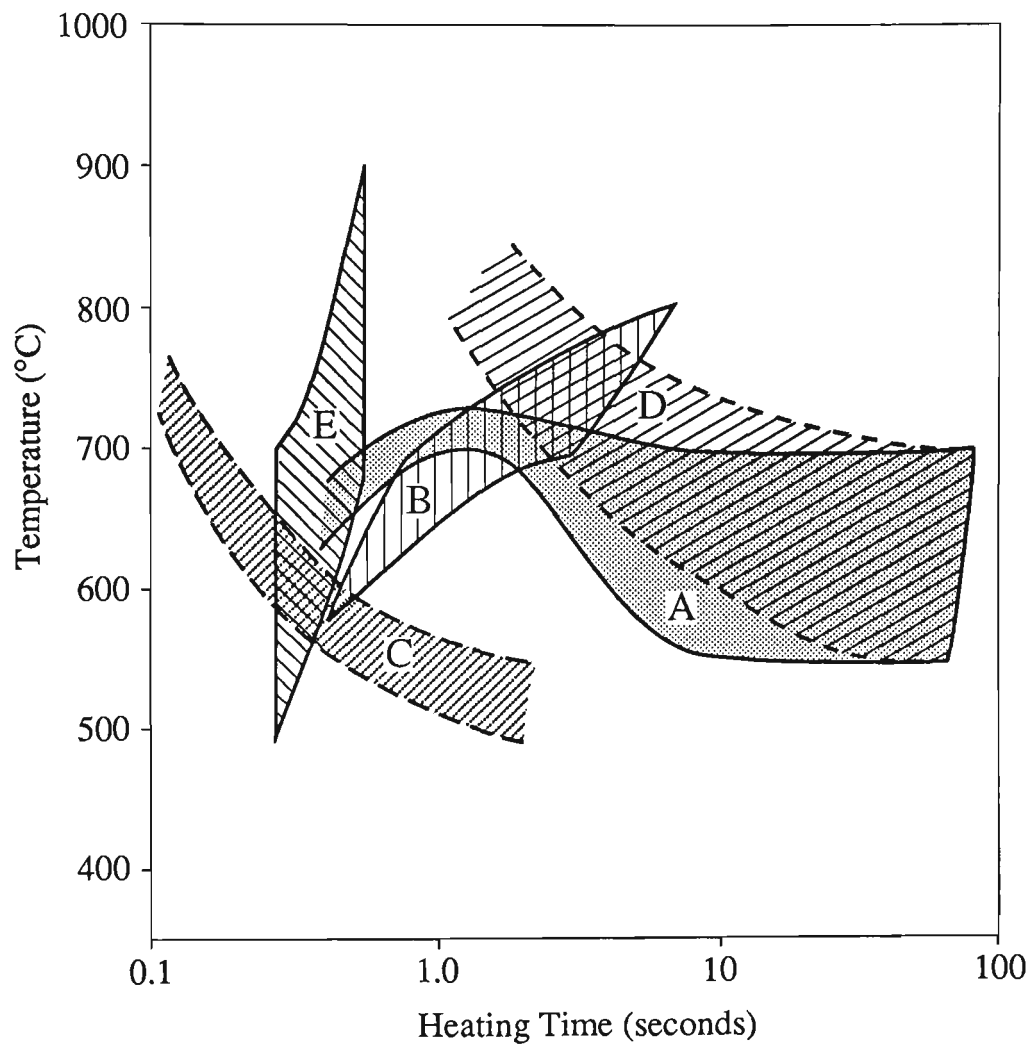


Fig. 7-4 Recrystallization temperature ranges at different heating rates. Zones A and B were reported by Andrews [6] using induction and salt bath heating, respectively. Zones D and C are the predictions by Andrews, of the effect of annealing with and without recovery, respectively. Zone E shows the result of the present investigation for resistance heating of decarburised steel.



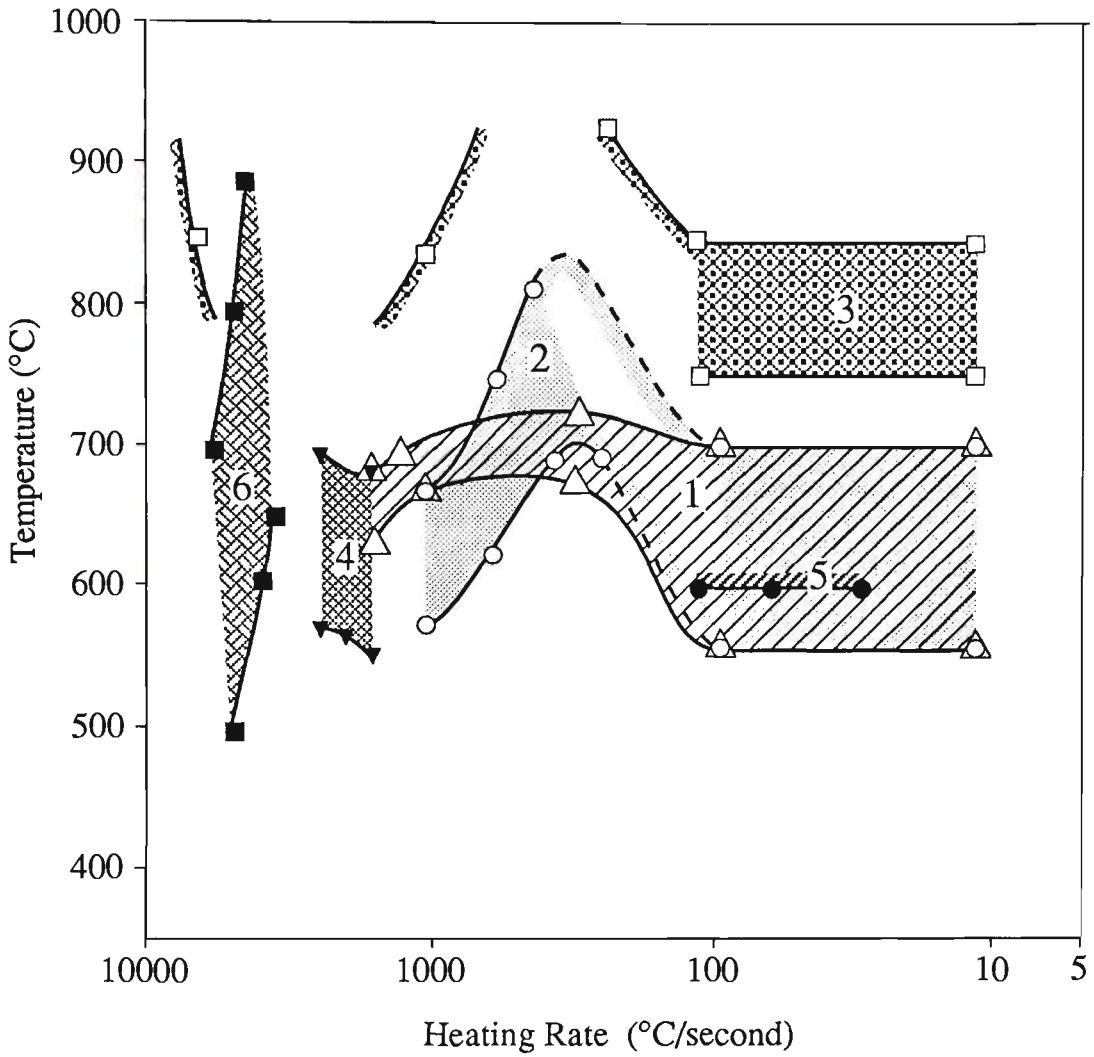


Fig. 7-5 Effect of heating rates on recrystallization temperatures ranges obtained by various researchers. Zones 1 and 2 were reported by Andrews [6] and correspond to Zones A and B in Fig. 7-4. Zones 3 is the result by Staüb [40]; Zone 4 by L'vov [38] and Zone 5 by Mohri [39]. Zone 6, corresponding to Zone E in Fig. 7-4, was obtained in the present investigation.

Discrepancies amongst the results could arise therefore from (1) the different materials used and the different degree of deformation prior to recrystallization; (2) different ways of heating (e.g. induction and salt bath heating used by Andrews as opposed to resistance heating used in the present study); (3) different thermal histories and/or starting grain size; and (4) different definitions of softening or recrystallization temperature. Despite the differences, the trend of decreasing softening range with increasing rate found in the present work using resistance heating is supported by the results of Andrews who used salt bath and induction heating of rimmed steels [6].

In the present investigation, it was found that the softening process is enhanced or accelerated as heating rate increases. Both the softening start and finish temperatures were lowered as the heating rate increased (see zone 6 in Fig. 7-5). Accelerated softening has previously been attributed mainly to rapid recrystallization produced by recovery suppression [6]. During an isothermal anneal, an increase in heating rate to the soak temperature results in a decrease in the amount of recovery before recrystallization owing to the decreasing time available for recovery to occur. By extrapolation, the softening at ultra-rapid heating rates could be due to accelerated recrystallization, associated with suppressed recovery by virtue of the negligible heating time. It seems logical that the suppression of recovery processes prior to recrystallization leaves more stored energy available as the driving force for the nucleation of recrystallization, thereby accelerating the recrystallization process. The validity of this hypothesis appears to be confirmed by the experiments involving ultra-rapid annealing with and without prior-recovery treatments. A definite retardation of softening in the prior-recovery treated specimens is observed, as in Figs. 6-18 and 6-19. With the occurrence of recovery, softening during ultra-rapid annealing is retarded and the longer the prior-recovery anneal the longer the time for full to softening to occur.

Despite the apparent support for the suppressed recovery hypothesis, other evidence is presented in Section 7.5.1 which suggests that this model is not tenable.

Another possible contribution to accelerated recrystallization, comes from the fact that the structure of the material used in the present study was ferrite containing a small amount of carbide due to the presence of 0.005 wt% carbon. When a sample is heated to above the recrystallization temperature by high heating rates like those in zone 6 of Fig. 7-5, most carbon still exists in the ferrite matrix as carbides since there is insufficient time for dissolution. These undissolved carbides may act as the sites for nucleation of recrystallization thus accelerating the recrystallization process.

7.3 KINETICS

The micrographs shown in Figs. 6-29, 6-31 and 6-34 indicate that a sample subjected to ultra-rapid annealing (URA) has a much finer grain size than one treated by batch annealing (BA). This observation suggests that the nucleation rate was so high during ultra-rapid annealing that grain impingement occurred at a small grain size. Therefore, the nucleation of recrystallization might be the controlling process during ultra-rapid heating. Conversely, the slower heating practice ( typical of the batch annealing) may allow significant prior recovery with a subsequent reduction in the nucleation rate, leaving more opportunity for grain growth. Therefore, the difference in heating rates results in different kinetics between the ultra-rapid annealing and batch annealing.

An analysis of the kinetics of ultra-rapid annealing reveals that recrystallization progresses in a sigmoidal manner with respect to time (see Fig. 7-6). The process starts by the nucleation of new grains at certain sites within the deformed material. The rate of change during this period is initially slow and then accelerates. Nucleation and growth continue until the grains impinge on each other and the rate of change becomes low again. Grain growth occurs during and after recrystallization.

The data presented in Fig. 7-6 were obtained using the experimental procedure shown schematically as Experiment 3 in Table 4-3. Although samples were isothermally treated for up to 1 sec. at the selected peak temperatures  $T_c$ , the heating time  $t_1$  was constant at 0.3 sec. and thus the heating rate varied depending on the value of  $T_c$ . Despite the different heating rates, the data were analysed as for conventional isothermal recrystallization experiments.

The Avrami equation (Section 2.3.1.2) gives a relationship between the recrystallization fraction,  $X$ , and the annealing time,  $t$ , of the form:

$$X = 1 - \exp ( -Bt^n ) \qquad \dots\dots\dots(7.1)$$

where  $B$  and  $n$  are constants.

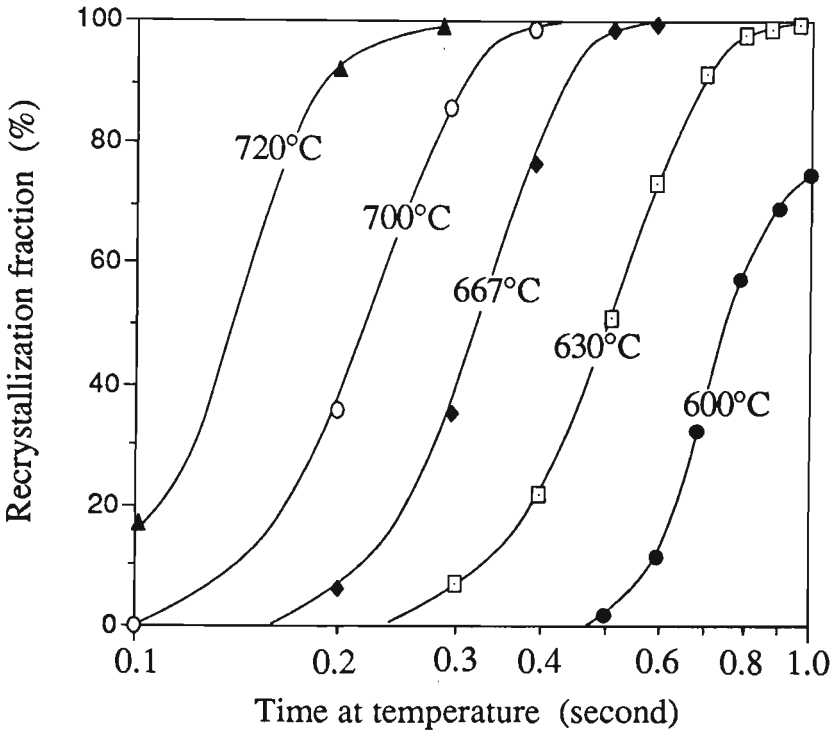


Fig. 7-6 Recrystallization kinetics for a material with 70% cold reduction and ultra-rapid annealed at 630, 667, 700 and 720°C, showing that recrystallization progresses in a sigmoidal manner with respect to time.

The Johnson-Mehl equation for three-dimensional recrystallization is:

$$1 - X = \exp \left( - \frac{f G^3 \dot{N} t^4}{3} \right) \dots\dots\dots(7.2)$$

where *f* is a shape factor, *G* is the growth rate and  $\dot{N}$  is the nucleation rate. Comparing equation 7.1 and 7.2, it is found the  $B = \frac{f G^3 \dot{N}}{3}$  and *n* = 4.

For a certain shape of nucleus, *f* is constant. Thus,

$$B = C (G^3 \dot{N}) \dots\dots\dots(7.3)$$

where *C* is a constant.

Equation 7.3 indicates that the constant *B* during isothermal annealing is proportional to the product of *G*<sup>3</sup> and  $\dot{N}$ . Therefore, *B* is an important parameter in describing the kinetics of recrystallization.

Equation 7.1 can be expressed in a logarithmic form:

$$\log \left[ \ln \frac{1}{1-X} \right] = \log B + n \log t \dots\dots\dots(7.4)$$

by plotting  $\log \left[ \ln \frac{1}{1-X} \right]$  against  $\log t$  at a certain temperature as in Fig. 7-7, *B* and *n* can be determined. Table 7-1 gives the results for the present work under various conditions.

Table 7-1 Parameters for  $X = 1 - \exp (-Bt^n)$

Conditions	B	n
URA 630°C	1.27	2.91
URA 667°C	7.59	2.96
URA 700°C	45.65	2.97
URA 720°C	171.36	2.96
BA 550°C	2.16x10 <sup>-13</sup>	3.81

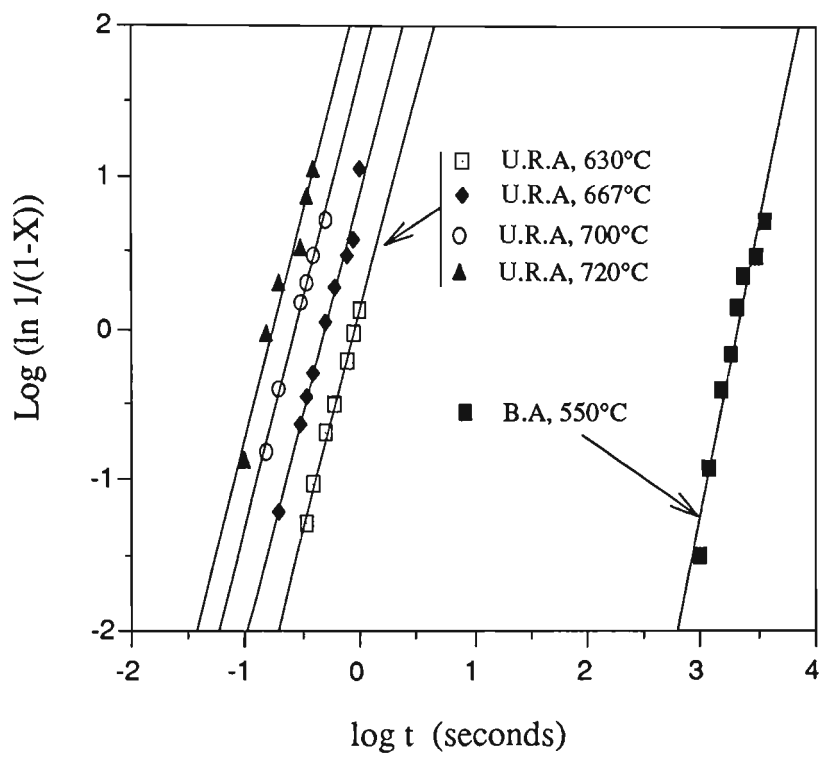


Fig. 7-7 Comparison of recrystallization kinetics for a material with 70% cold reduction subjected to various heating rates.

It is seen that for the ultra-rapid heating , the value of B changes from 1.27 at 630°C to 171.36 at 720°C, resulting from enhanced nucleation and growth rates with increasing temperature. The value of n ( average = 2.95) is at the lower limit of the range 3 - 4 for three-dimensional recrystallization [377].

The large difference in B between ultra-rapid annealing and batch annealing is very significant. The value of B at 720°C for URA is larger than the B value for BA at 550°C by 14 orders of magnitude. As mentioned before, the value of B is proportional to the product of  $G^3$  and  $\dot{N}$  at constant temperature. This huge difference between URA and BA cannot be attributed to the temperature influence only. Figure 7-8 shows a plot of B versus URA temperature. Extrapolation to 550°C indicates a B value of ~0.25 compared with  $2.16 \times 10^{-13}$  for BA at 550°C.

The recrystallized grains in the ultra-rapid annealed samples are much finer than those in the batch annealed samples. Since the grain size can be expressed as [377],

$$d \propto \left( \frac{G}{\dot{N}} \right)^{1/4} \dots\dots\dots(7.5)$$

the ratio  $\frac{G}{\dot{N}}$  must decrease with ultra-rapid annealing. For about 2x reduction in grain size compared with batch annealed samples (Tables 6-6 and 6-7), the ratio is reduced 16x. As the rate of recrystallization is significantly increased, the decrease in the ratio is far less likely to be associated with a decrease in G than an increase in  $\dot{N}$ .

Therefore, it is concluded that the kinetics of the recrystallization process in URA is predominantly controlled by the nucleation of new grains in the deformed matrix.



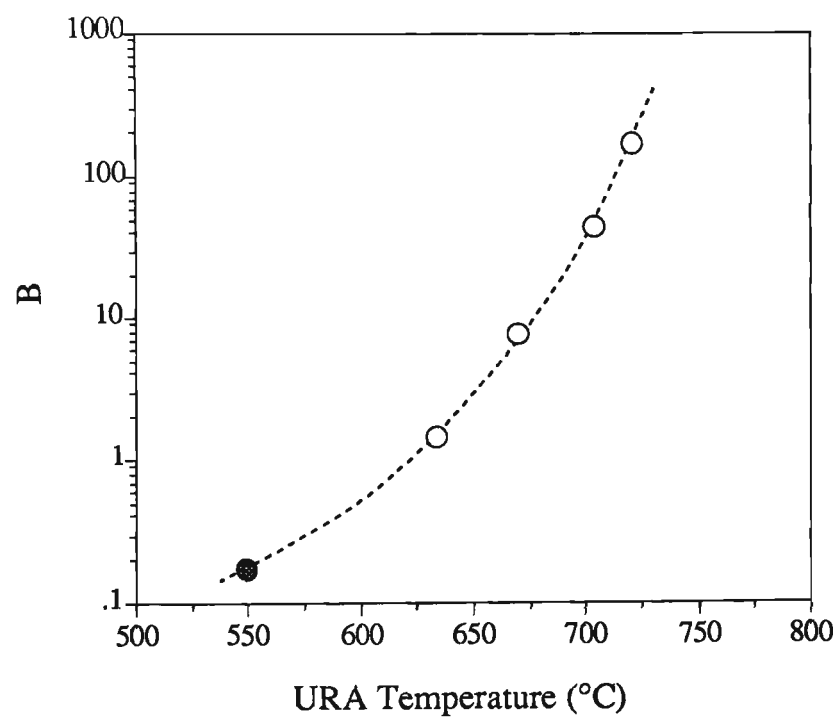


Fig. 7-8 Plot of value B from Avrami equation versus ultra-rapid annealing temperature.

## 7.4 NUCLEATION MECHANISMS FOR RECRYSTALLIZATION DURING ULTRA-RAPID ANNEALING

The analysis of the kinetics of ultra-rapid annealing indicates that recrystallization is controlled primarily by nucleation, whereas recrystallization during batch annealing is controlled by both nucleation and growth. Despite the remarkable increase in softening rate by ultra-rapid annealing, the recrystallization process appeared to be similar to that occurring under normal batch annealing or continuous (rapid) annealing conditions. Nucleation occurred predominantly at grain boundary surfaces and corners of the deformed ferrite grains (see Fig. 6-29(b)).

If no new sites for recrystallization are generated by ultra-rapid annealing, then the established nucleation mechanisms (Section 2.2.6) would be expected to operate: (1) nucleation at grain boundaries by strain-induced-boundary-migration (SIBM); (2) nucleation by subgrain growth or coalescence; (3) nucleation by coarse particles; and (4) nucleation at deformation and transition bands within the grains.

### 7.4.1 Electron Microscopical Observations

Electron microscopy of rolling plane foils showed evidence by both nucleation by grain boundary bulging (Fig. 6-47) and by subgrain growth (Figs. 6-38 and 6-39).

Compared with samples recrystallized by batch annealing, no well defined subgrain structure was observed during ultra-rapid annealing (compare Figs. 7-9 and 6-50), and the fully recrystallized structure showed a higher than expected dislocation density (compare Figs. 6-46 and 6-49). This latter effect could be due to thermal stresses arising from the rapid heating and quenching.

The cold rolled structure is shown in Figs. 7-10 and consisted of a dislocation cell structure with a cell diameter of about 1  $\mu\text{m}$ . Sharpening of the cell wall structure occurred on URA (Figs. 7-9 and 7-11) without the development of a well defined subgrain structure. Isolated subgrains or groups of subgrains developed locally into

recrystallized grains (Fig. 7-12) and structural heterogeneity, in terms of the distribution of dislocations and stored energy, appeared to be a feature of the pre-recrystallization structure of samples subjected to URA.

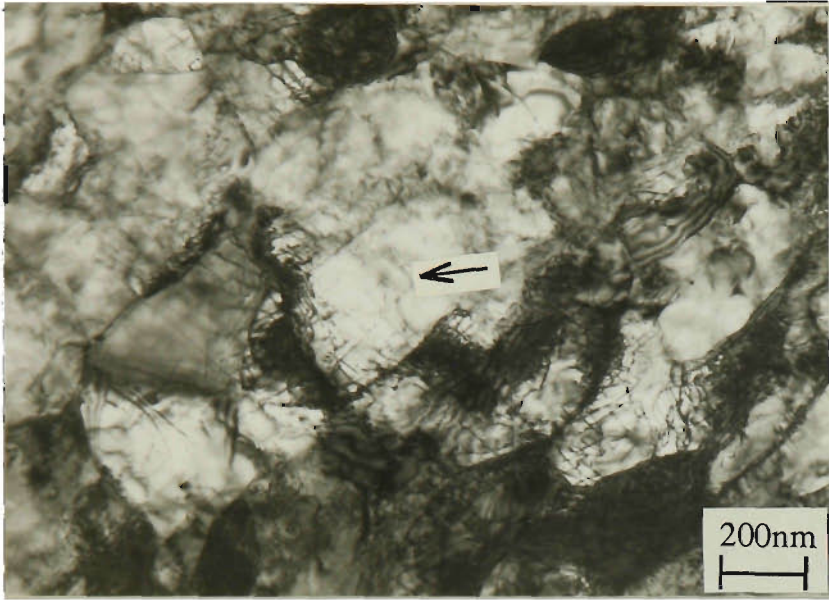


Fig. 7-9 Partially recovered cell structure observed in a sample with 70% cold reduction ultra-rapid annealed at 510°C.



Fig. 7-10 Transmission electron micrograph showing the deformed structure observed in a sample of 80% cold reduction prior to ultra-rapid annealing.

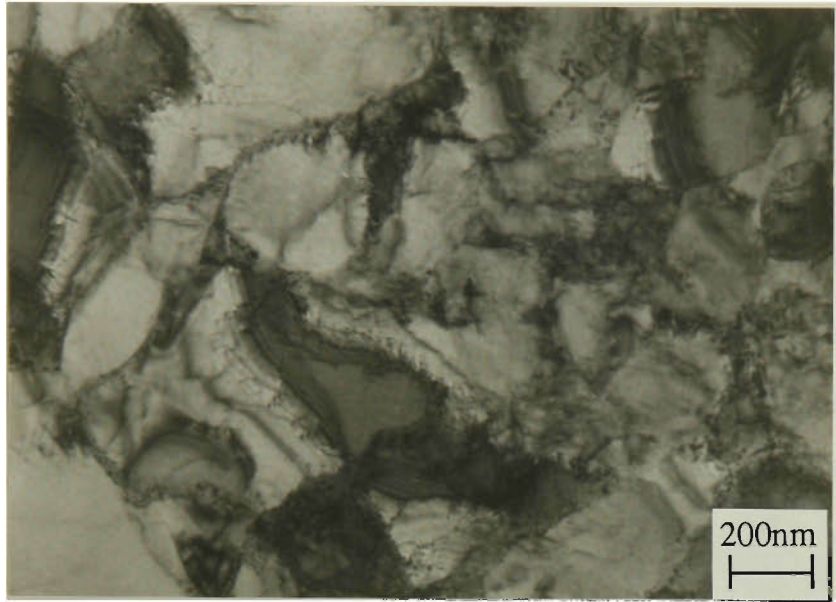


Fig. 7-11 Transmission electron micrograph showing partially recovered cell structure in a sample with 70% cold reduction ultra-rapid annealed at 550°C.

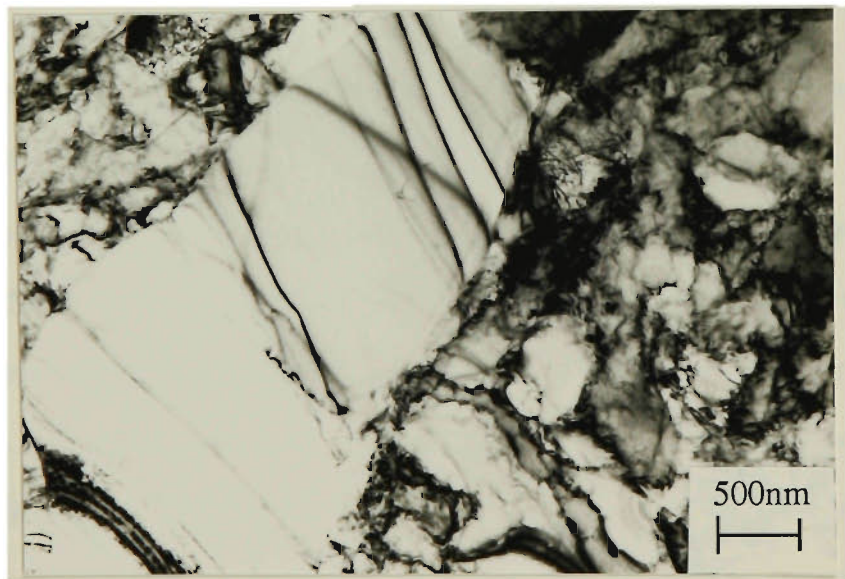


Fig. 7-12 Transmission electron micrograph showing the partially recrystallized structure observed in a sample with 70% cold reduction after ultra-rapid annealing at 667°C for  $t_1 = 0.3$  sec. and  $t_2 = 0.1$  sec.

## 7.5 MICRO-HARDNESS AND METALLOGRAPHIC STUDIES OF SOFTENING BY ULTRA-RAPID HEATING

On commencing this study of the effect of heating rates on the recrystallization process in low carbon steel, it was found necessary to make an accurate assessment of the relative merits of the various techniques which are available for the determination of the recrystallization temperature and also for following the structural changes which occur during the process of recrystallization. The requirements for such a technique are (a) sensitivity, (b) accuracy and (c) reproducibility of results, together with a reasonable degree of speed and ease of application. The conventional techniques of micro- or macro-hardness measurement and metallography are attractive. However, these two techniques often give different values for the temperature or time at which 50% recrystallization appears to occur. Discrepancies can be based on experimental error: (a) inaccuracy of hardness values or (b) difficulty in measuring percentage of recrystallization; but they can also be real because 50% softening does not necessarily correspond to 50% recrystallization [67].

An example of experimental error is the use of macro-hardness measurements to detect the start of recrystallization. The recrystallization process may be considerably advanced before the proportion of new recrystallized grains is sufficient to significantly reduce the overall average hardness value. Consequently, the results of a macro-hardness technique often suggest a later start to the recrystallization process than do the results of metallography [67]. An example of a real difference between the time or temperature of 50% softening and 50% recrystallization is the case of high stacking fault metals in which significant pre-recrystallization softening by recovery can occur prior to and during recrystallization, so that 50% softening precedes the occurrence of 50% recrystallization [67].

In the present case the hardness load was limited because of the limited thickness of the samples ( 0.31 mm for 80% cold rolled samples). Therefore, the use of micro-hardness

measurements combined with metallography, was considered to be appropriate to elucidate the recrystallization behaviour of ultra-rapid annealed samples.

#### 7.5.1 Variations in Hardness and Microstructure with Annealing Conditions

Hardness measurements were used to establish average values in the uniformly heated gauge region after annealing and hardness distribution data were also obtained. (see Section 7.5.2).

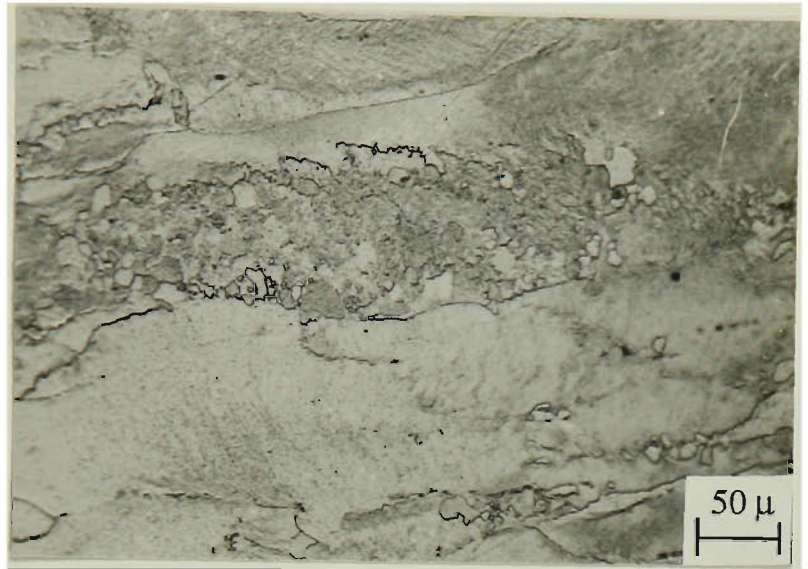
Figure 6-14 shows average micro-hardness values (HV 1000 g) for 70% cold rolled samples heated to the indicated peak temperature in time  $t_1$  (0.2, 0.3 and 0.5 sec.) for a constant dwell or hold time  $t_2$  of 0.1 sec. Corresponding microstructures for selected peak temperatures and  $t_1 = 0.2$  sec. are given in Fig. 6-29. At a temperature of 550°C, corresponding to 50% softening, the microstructure (Fig. 6-29(d)) indicated that less than 50% recrystallization had occurred. Even at 700°C, which corresponded to a hardness close to the minimum, the sample was incompletely recrystallized (Fig. 6-29(f)). Figure 6-29(b) reveals that the first few percent of recrystallization had occurred at  $T_c = 510^\circ\text{C}$ , yet the hardness values indicated that substantial softening had taken place. This trend is also confirmed by Fig. 6-31 which shows the microstructural evolution in 70% cold rolled samples, ultra-rapid annealed for  $t_1 = 0.5$  sec.

These observations indicate that much of the softening response is due to recovery type processes rather than recrystallization.

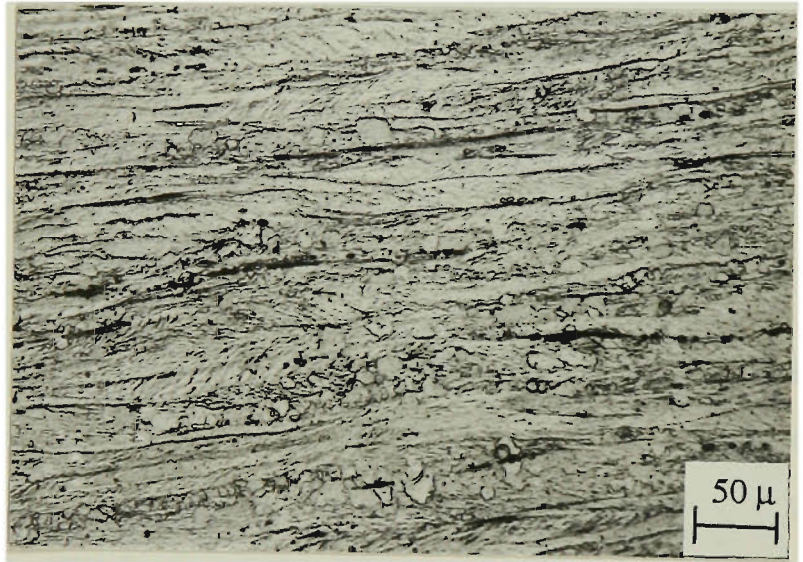
The hardness data discussed above were measured in the rolling plane, whereas the microstructural information was sampled from transverse sections parallel to the axis of the test piece. In order to test the uniformity of both the structure and hardness in the "uniformly heated" gauge region, hardness measurements were conducted on the transverse section and microstructural analysis was carried out on rolling plane sections. The results of this survey are illustrated in Fig. 7-13 for a sample with 70% cold reduction, ultra-rapid annealed under the conditions  $T_c = 667^\circ\text{C}$ ,  $t_1 = 0.3$  sec.,  $t_2 =$



(a)



(b)



(c)

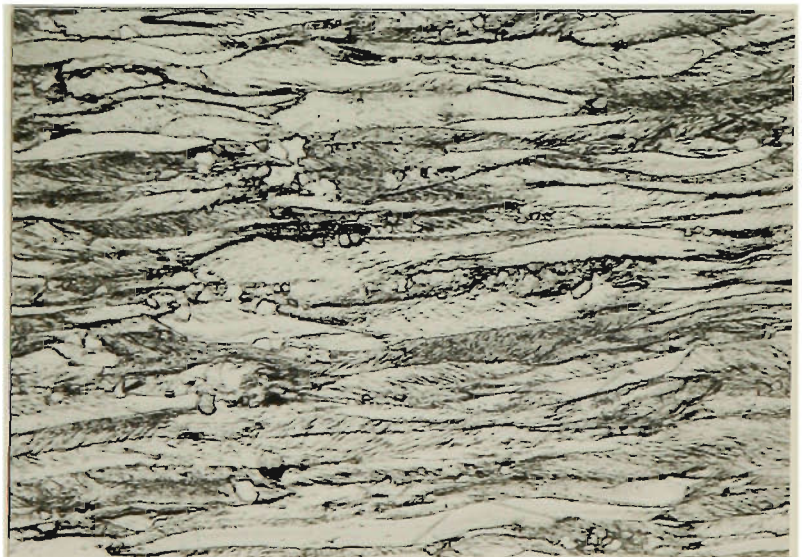


Fig. 7-13 Microstructures showing the (a) rolling plane section, (b) transverse section close to the free edge of the test piece, and (c) in the centre of the test piece after ultra-rapid annealed at  $667^{\circ}\text{C}$  for  $t_1 = 0.3$  and  $t_2 = 0.1$  sec.



0.1 sec. (middle curve, Fig. 6-14). The microstructure in the sheet plane, Fig. 7-13 (a), consisted of slab-shaped deformed ferrite grains with a small volume fraction of fine recrystallized grains. Transverse sections close to the free edge of the test piece, Fig. 7-13 (b), and in the centre of the test piece, Fig. 7-13 (C), showed the expected change in shape of the ferrite grains, but had a volume fraction of recrystallized grains similar to that evident in the rolling plane section. These results confirm the structural uniformity and thus the uniformity of temperature in the central gauge region of the test piece.

Average hardness values from the sheet plane, edge transverse and centre transverse positions were 128, 126 and 130 (HV 1kg) respectively, in close agreement with each other and the value of about 130 (HV 1kg) given by the middle curve in Fig. 6-14 for 667°C. Thus the structure and hardness of the central gauge zone were uniform after ultra-rapid annealing.

The important conclusion of this analysis is that for ultra-rapid annealing conditions which resulted in ~50% softening, the structure was far less than 50% recrystallized. A comparison of the percentage of softening (determined by hardness measurements) and the percentage of recrystallization (determined by metallography) is given in Table 7-2 for both ultra-rapid annealing ( $t_1 = 0.3$  sec.,  $t_2 = 0.1$  sec.) and batch annealing. In the case of batch annealing the 50% softening point (Fig. 6-16) corresponds to slightly less than 50% recrystallization; however, for ultra-rapid annealing, the percentage of recrystallization is 23% at the 50% softening point. The implication is that significant softening occurs by recovery and that the recovery suppression hypothesis is not valid. In fact, both recovery and recrystallization are accelerated by ultra-rapid heating, with recovery softening being accelerated relative to recrystallization.

Table 7-2 The percentage softening compared with  
the percentage of recrystallization

	Ultra-rapid annealing			Batch annealing		
	600°C	667°C	720°C	450°C	500°C	650°C
% softening	13	50	100	4	50	100
% recrystallization	0.0	23	100	0.0	47	100

An adequate explanation of the marked acceleration of recovery and recrystallization must also take into account that for rapid heating rates (100 - 500°C/sec.), previous studies have shown that the softening range is actually raised as heating rate increases [6] (Fig. 7-5). It seems reasonable to view this trend as suppression of the time and temperature dependent restoration processes, resulting in elevation of the softening temperatures. The observed reversal of this trend at ultra-rapid rates (500 - 5000°C/sec.) seems to suggest that a new mechanism comes into play which allow restoration to be accelerated. This problem is discussed further in Section 7.7.

7.5.2 Micro-hardness Distributions

As well as average hardness determinations, distributions were measured in an attempt to gain an insight into the softening process. Results for such measurements depend strongly on the hardness load and thus indentation size relative to the sizes of the structural units. A relatively large load (1 kg) was used, but the purpose was to make a comparison between the ultra-rapid annealing and the batch annealing conditions.

The results in Figs. 6-20 and 6-22 were obtained for similar degrees of softening during ultra-rapid heating and slow heating (batch), respectively. It is seen that for very high heating rates the hardness distribution splits into two peaks during the progress of softening, e.g. the histogram for  $T_c = 667^\circ\text{C}$  in Fig. 6-20. It is tempting to conclude that these two peaks represent the hardness values of the recovering matrix and the new grains

formed by recrystallization. If this is the case, then the relative intensities of the two peaks indicate the extent of recrystallization. However, the recrystallized grain size was small relative to the indentation size and it is therefore likely that the "soft" regions are composites of recrystallized and recovered grains. However, it is also possible that the "soft" regions are well recovered grains in a matrix in which recovery has been relatively retarded. The hardness measurements were carried out on the rolling plane and a typical diagonal of the indentation of about 120  $\mu\text{m}$  should be compared with an average width of the deformed of  $\sim 50 \mu\text{m}$  and a typical diameter of the recrystallized grains of about 10  $\mu\text{m}$  (see Fig. 7-14).

The main feature of the hardness distribution data is the apparently heterogeneous nature of the structure of the ultra-rapid annealed samples relative to batch annealed samples during the course of restoration. It is implied that locally soft regions develop because of enhanced recovery and recrystallization and that these are distinguishable from more heavily dislocated "hard" regions. Batch annealing conditions on the other hand seem to promote a more uniform distribution of hard and soft regions, such that the hardness values are unimodal.

In both batch annealed and ultra-rapid annealed samples a unimodal distribution of hardness was obtained after complete recrystallization.

### 7.5.3 Recrystallized Grain Size and Grain Size Distributions

As reported in Section 6.6.2.1 (b) and discussed in Section 7.3, ultra-rapid annealing resulted in a much finer recrystallized grain size than batch annealing. It is inferred that ultra-rapid heating results in a marked acceleration of the nucleation rate for recrystallization. A limited amount of data was obtained on trends in grain size with increasing heating rate in the ultra-rapid heating range. Section 6.6.2.1 (b) gives results for 70% cold reduced material heated to 720°C with  $t_1 = 0.2$  sec. (Table 6-5) and to the same temperature with  $t_1 = 0.3$  sec. (Table 6-6). The two average rates are 3600°C/sec. and 2400°C/sec., respectively. Although the mean grain size was slightly higher

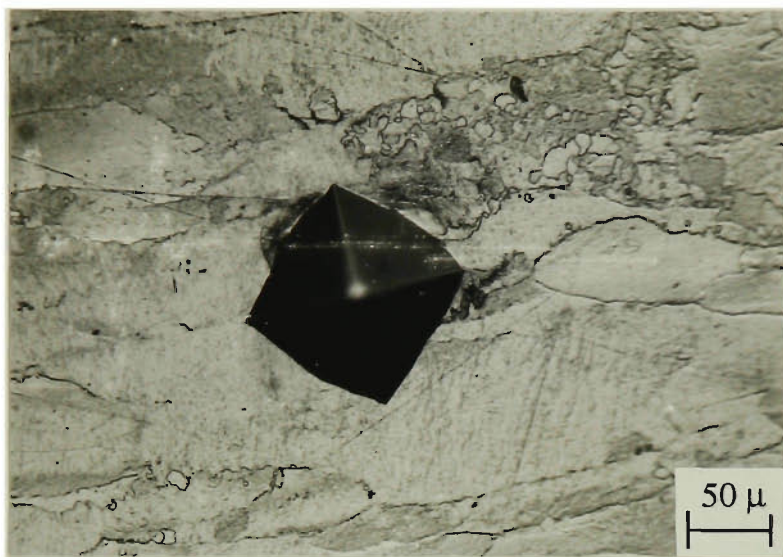


Fig. 7-14 Micrograph showing the microstructure and hardness indentation size of a sample ultra-rapid annealed at  $667^{\circ}\text{C}$  for  $t_1 = 0.3$  and  $t_2 = 0.1$  sec.

(17.8  $\mu\text{m}$  vs 16.8  $\mu\text{m}$ ) for the lower rate the change in grain size is so small that it cannot be claimed that a significant change occurs.

However, the effect of cold reduction is clearer: increasing cold reduction results in decreasing recrystallized grain size for constant heating conditions ( $T_c = 720^\circ\text{C}$ ,  $t_1 = 0.3$  sec.,  $t_2 = 0.1$  sec., Table 6-6). Although there appears to be little difference in mean grain size in the range 60 - 80% reduction (Table 6-6), it should be noted that for reductions of 60 and 70%, recrystallization was incomplete and that the fully recrystallized grain size is likely to be higher in these two cases because of further opportunity for grain growth.

Thus the results indicate that recrystallized grain size does not change significantly with changing rate of ultra-rapid annealing at constant reduction, but that grain size decreases substantially as percentage of reduction is increased at constant heating rate.

The distribution of grain sizes was skewed for both the case of ultra-rapid annealing and that of batch annealing (see Section 6.6.2.1). The skewness fell markedly following the completion of recrystallization in ultra-rapid annealed samples due to the elimination of small grains by rapid grain growth.

## 7.6 INFLUENCE OF COLD REDUCTION

A basic requirement for recrystallization is the presence of a significant stored energy (i.e., a high dislocation density). To satisfy this requirement, cold deformation before annealing is necessary. The following sections will discuss how deformation affects the softening behaviour and micro-hardness histograms with high heating rates and slow heating rates.

### 7.6.1 The softening behaviour

As the amount of deformation increases, there is an increasing tendency to produce grains which are both heavily and unevenly deformed, i.e., the formation of transition bands and other types of local misorientations is increased within the grains. Consequently, potential nucleation sites for recrystallization become increasingly prevalent within the deformed grains. Electron microscopic evidence suggests that grain-boundary-located nucleation (even at high deformation) is usually of the strain-induced-boundary-migration type [182]. Higher nucleation rates are therefore to be expected with increasing deformation and the experimental results in Fig. 7-15 give support to this proposition.

Samples undergoing higher cold reductions showed a more rapid initial drop in hardness, but the overall time required for the elimination of the cold worked structure was similar in all cases, with the more heavily deformed samples taking slightly less time under the ultra-rapid annealing conditions (Fig. 7-15). However, when softening was effected at 667°C, the 40% cold worked samples softened over a significantly longer total time than those with 80% cold reduction (Fig. 7-16). This result clearly shows that an increase in deformation accelerates the softening process.

This conclusion is true irrespective of the heating rate. The results presented in Fig. 7-17 for batch annealing at 550°C for 30 minutes show that higher cold reduction results in more rapid softening even through the heating rate to the hold temperature is much slower. The cold-worked state contains local misorientations over a finite region of the

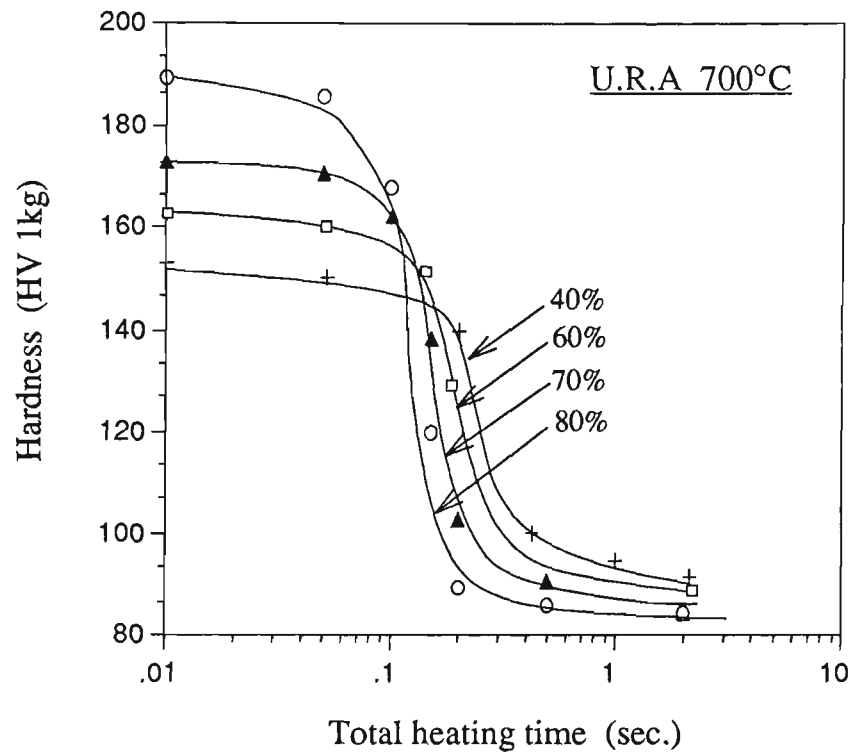


Fig. 7-15 The effect of cold reduction on softening behaviour after ultra-rapid annealing at 700°C.

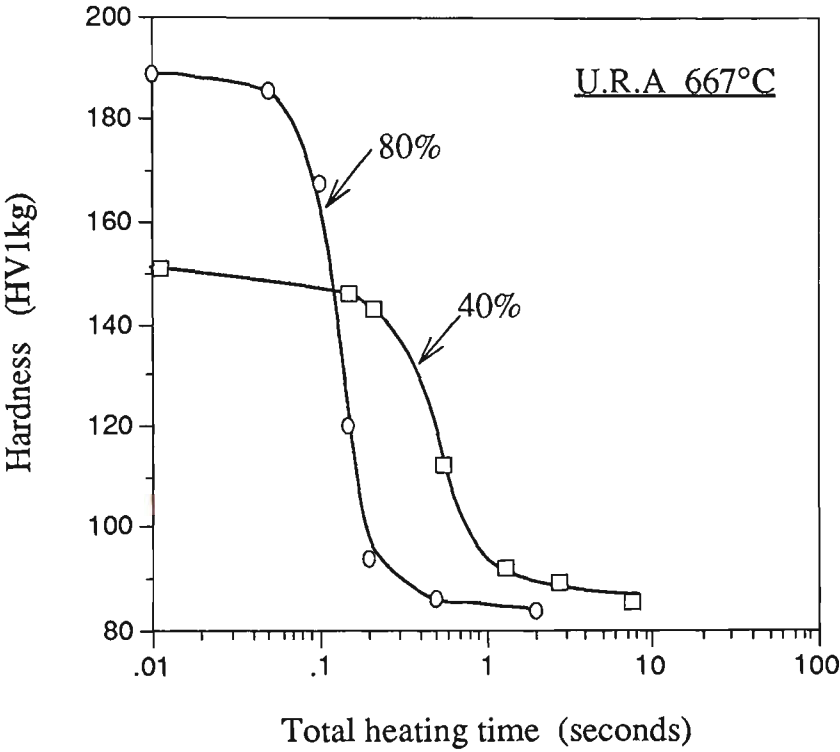


Fig. 7-16 Effect of cold reduction on softening behaviour of sample subjected to ultra-rapid annealing at 667°C.



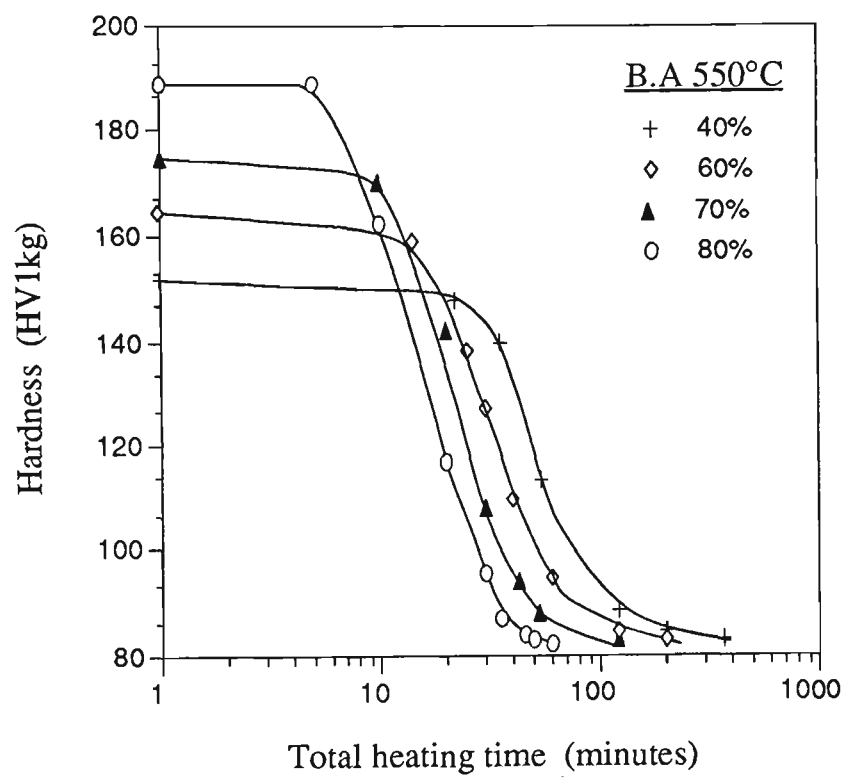


Fig. 7-17 The effects of cold reduction on softening behaviour after batch annealing at 550°C, indicating that higher deformation results in shorter softening time.

deformed grains. The nucleation process therefore involves preferential development of some selected subgrains to acquire the appropriate misorientation as viable nuclei. The accelerated recrystallization by enhanced nucleation during ultra-rapid annealing is likely to be due, as discussed in Section 7.7, to the development of a more heterogeneous environment in terms of dislocation density and the associated stored strain energy.

#### 7.6.2 Micro-hardness distributions

Different cold reductions before ultra-rapid annealing resulted in similar histograms for the micro-hardness distributions, indicating that similar softening mechanisms occur for the range of cold reductions investigated (Fig. 6-21) .

## 7.7 THE MECHANISM OF SOFTENING DURING ULTRA-RAPID ANNEALING

The present work demonstrates that softening of cold rolled low carbon steel can be effected in times less than 1 second at temperatures below about 700°C for sufficiently high heating rates and cold reductions. The results show that the softening range decreases with increasing heating rate (Fig. 7-3) and a significant part of the initial softening is due to recovery effects (Section 7.5.1). The inescapable conclusion is that ultra-rapid annealing accelerates both recovery and recrystallization, with more marked acceleration of recovery. Any proposed mechanism for this effect must also be capable of explaining the observations that:

- (i) for identical heating conditions, samples with higher cold reduction softened more rapidly ( Fig. 6-15 );
- (ii) for a fixed reduction, softening was more pronounced the higher the heating rate to a given peak temperature (Fig. 7-2);
- (iii) the recrystallized grain size was finer the higher the reduction for the same ultra-rapid heating conditions (Table 6-7);
- (iv) prior recovery treatment considerably retarded the softening process during ultra-rapid heating ( Fig. 6-18 ).

In Section 7.4.1 it was concluded that there were no outstanding differences in the fine scale microstructures of samples which had been ultra-rapid and batch annealed. However, differences were noted in terms of the reduced tendency for development of a well defined subgrain structure and in the presence of greater structural heterogeneity after ultra-rapid annealing.

For heating at rates  $\geq 1000^{\circ}\text{C}/\text{sec.}$  for a fraction of a second, restoration takes place in a rapidly changing temperature field and the heirarchy of recovery processes identified as a

function of time or temperature under normal heating conditions are condensed into overlapping and competing processes.

Although it is beyond the scope of this work to elucidate the detailed mechanism of recovery under ultra-rapid annealing conditions, it seems likely that rapid heating facilitates defect rearrangements and annihilations which locally reduce stored strain energy and establish energy gradients which enhance the subsequent nucleation of recrystallized grains.

The relative contributions of recovery and recrystallization to softening are changed by ultra-rapid heating, with recovery being enhanced more than recrystallization. Acceleration of recovery is likely to result from the stimulation of dislocation climb in the presence of a high vacancy concentration due to cold work and multiplication. The elimination of jogs and dipoles by climb results in untangling of dislocations in cell walls and allows glide and climb to produce self-elimination or re-organization into stable arrays.

None of the evidence obtained in this work points to any novel mechanisms for either recovery or recrystallization. The relative contributions to softening are changed by ultra-rapid heating, but the basic mechanisms of the competing restoration processes appear to remain unchanged. Supporting evidence is that the trends in softening rate on ultra-rapid annealing with changing percentage of reduction are consistent with those of normal restoration processes (Section 7.6.1).

The decrease in softening temperature with increasing rate (Fig. 7-3) under ultra-rapid heating conditions is in marked contrast with the reported increase for increasing rates in the rapid range [6]. This latter effect was discussed in Section 7.5.1 and it was concluded that this trend is due to suppression of the time and temperature dependent restoration processes with increasing heating rate. The reversal of this trend on even faster rates, if not due to a new mechanism, must be due to removal of a barrier which restricts restoration under "normal" batch or rapid heating conditions.

It has been proposed [378] that the source of this barrier is carbon and nitrogen which go into solution during conventional heat treatments and retard the motions of dislocations which are necessary to produce recovery and recrystallization. Above a certain heating rate, it is considered that solution of interstitials is restricted before substantial restoration occurs. The extent of solution becomes more restricted the faster the rate, thereby facilitating recovery and recrystallization.

In term of the observations (i) to (iv), (i) is consistent with an increased driving force for recovery and recrystallization with increasing cold reduction, which leads to more rapid softening. Observation (ii) can be accounted for in terms of the suppressed solution model: decreasing dissolution of interstitials with increasing heating rate facilitates softening. Grain refinement with increasing reduction, (iii), is compatible with an increase in the density of nucleating sites, as in conventional recrystallization treatments.

Finally, the compatibility of the solution model with observation (iv), related to the prior recovery results (Section 6.3.3), will be discussed. The prior recovery treatments at 100°C provide a means of reducing the level of stored strain energy and thus the driving force for recrystallization. In addition, the concentration of interstitials in solution would be raised by partial dissolution of carbide and nitride particles. In effect, cold rolled samples were subjected to enhanced strain ageing, which would be expected to lock dislocations and inhibit restoration. The combined effect of these changes resulted in retarded softening during ultra-rapid annealing (Fig. 6-18). However, increasing the rate of heating significantly enhanced the softening process. These observations are consistent with restriction of further solution of carbon and nitrogen on heating to temperatures above 100°C, with the effectiveness of this suppression increasing with heating rate.

### 7.7.1 Effect of Type of Heating Method

The trend of decreasing softening range with increasing URA rate by resistance heating, confirms earlier reports for salt bath and induction heating [6] and indicates that the effect is a general one which is independent of heating method. Notwithstanding this conclusion, there have been recent reports of accelerated restoration of copper and its alloys by application of short duration, high current electrical pulses to samples undergoing isothermal annealing [379]. These findings have been interpreted in terms of electron fluxes facilitating defect motion and consequent restoration processes. On this basis, the contribution of an electro-pulse effect cannot be discounted in the present case in which heating was effected by an alternating current (50 HZ) of high magnitude.

7.8 TENSILE PROPERTIES OF ULTRA-RAPID ANNEALING

The strength of materials is one of the most important aspects in engineering applications, which constitutes the body of knowledge dealing with the relationship between internal stresses, deformation strain and external loads. The basic data on the mechanical properties of a ductile metal are obtained from a tension test because it is widely used as an acceptance test for the specification of materials. Therefore, it was decided to compare samples subjected to ultra-rapid and low heating rates in terms of yield stress, tensile strength, ductility, toughness and plastic strain ratio ( R ) derived from the tensile stress-strain curves.

7.8.1 Yield Stress and Tensile Strength

The yield stress ( $S_O$ ) was taken as the 0.2% proof stress. The tensile strength, or the ultimate tensile strength ( $S_U$ ), is the maximum load ( $P_{max}$ ) divided by the original cross-sectional area ( $A_O$ ) of the specimen [380], that is:

$$S_U = \frac{P_{max}}{A_O} \dots\dots\dots(7.6)$$

The tensile strength is the value most often quoted from the results of a tension test. For ductile metals, the tensile strength should be regarded as a measure of the maximum load which a metal can withstand under the very restrictive conditions of uniaxial loading. The values of  $S_O$  and  $S_U$  as well as the ratio  $S_U/S_O$  are given in Table 7-3.

Figure 6-25 shows the stress-strain curves of samples with 70% cold reduction tested after ultra-rapid annealing at 630°C, 667°C, 700°C and 720°C. Both the  $S_U$  and  $S_O$  were found to decrease as the peak temperature of ultra-rapid annealing increased. It should be noted that the temperature of 630°C represents the starting point of softening and the the temperature of 720°C the finishing temperature for softening ( see Fig. 6-33). Therefore, the process of restoration results in a reduction in tensile strength under ultra-rapid heating practice.

Table 7-3 Yield stress and tensile strength of 70% cold reduced samples subjected to URA\* and BA\*\*

Conditions	S <sub>O</sub> (MPa)	S <sub>U</sub> (MPa)	S <sub>U</sub> /S <sub>O</sub>
URA630°C	357.6	587.6	1.64
URA667°C	282.3	537.8	1.91
URA720°C	154.9	495.1	3.20
BA 680°C	110.5	343.3	3.11

\* t<sub>1</sub> = 0.3 sec., t<sub>2</sub> = 0.1 sec. (Fig. 6-14)  
\*\* 30 mintes at 680°C.

Comparison of the stress-strain curves obtained for full recrystallization for both ultra-rapid heating (to 720°C) and slow heating (batch annealing at 680°C) reveals that the samples subjected to ultra-rapid annealing had a tensile strength of ~495 MPa, whereas it was only ~343 MPa for furnace annealing. This difference is likely to be due to the finer grain size obtained after ultra-rapid annealing. The ratio Su/So indicates the capacity for work hardening. High capacity corresponds to high value of Su/So. The ratio was similar for both URA 720°C and BA 680°C.

7.8.2 Ductility

Ductility is a more qualitative property of a material. The conventional measures of ductility from a tension test are the engineering strain at fracture e<sub>f</sub> (usually called the total elongation) and the reduction of area at fracture q [380]. Both of these properties are obtained after fracture by putting the specimen back together and taking measurements of L<sub>f</sub> (length at fracture) and A<sub>f</sub> (area at fracture). By definition:

$$e_f = \frac{L_f - L_0}{L_0}$$

.....(7.7)



and 
$$q = \frac{A_0 - A_f}{A_0} \dots\dots\dots(7.8)$$

$e_f$  can also be regarded as the maximum strain value corresponding to the tensile strength in the stress-strain curve. The ductility of sample with 70% cold reduction subjected to various annealing conditions is given in Table 7-4.

Table 7-4 Ductility of samples with 70% cold reduction  
subjected to URA\* and BA\*\*

Conditions	$e_f$ (%)	$q$ (%)
URA 630°C	9.0	16.19
URA 667°C	25.1	17.14
URA 700°C	27.4	19.51
URA 720°C	29.2	20.87
BA 680°C	22.4	24.65

\*  $t_1 = 0.3$  sec.,  $t_2 = 0.1$  sec. (Fig. 6-14)  
\*\* 30 mintes at 680°C.

It was found that both  $e_f$  and  $q$  increased as the annealing temperature increased during ultra-rapid annealing. The increase in ductility can be attributed to the higher degree of recrystallization with higher temperature.

Differences in heating rates also resulted in different ductilities. For full recrystallization, the samples ultra-rapid annealed at 720°C had a higher elongation and lower reduction in area than those which were batch annealed. This result suggests that an increase in heating rate can improve the total elongation and reduce the extent of necking.

7.8.3 Toughness

Toughness is a commonly used concept involving both strength and ductility. One definition is that it is the total area under the stress-strain curve [380]. This area is an indication of the amount of work per unit volume which can be done on the material

without causing it to rupture. For ductile materials, the area ( $U_T$ ) under the curve can be approximately expressed by the form:

$$U_T \approx S_u \cdot e_f$$

.....(7.9)

The toughness values of a sample with 70% cold reduction subjected to various annealing conditions are given in Table 7-5.

Table 7-5 Toughness of samples with 70% cold reduction  
subjected to URA\* and BA\*\*

No.	Conditions	$U_T$ (MPa)
1	URA 630°C	52.83
2	URA 667°C	134.54
3	URA 700°C	138.60
4	URA 720°C	147.43
5	BA 680°C	77.056

\*  $t_1 = 0.3$  sec.,  $t_2 = 0.1$  sec. (Fig. 6-14)  
\*\* 30 mintes at 680°C.

Therefore, the toughness increases as the annealing temperature increases during URA because the increase in ductility is the dominant factor. By comparing the high heating rate ( No.4) with the slow heating rate (No.5), it is found that the material is tougher after ultra-rapid annealing compared with batch annealing. This result implies that an increase in the heating rate enhances the ability of the material to withstand stresses above the yield stress without fracture.

7.8.4 Plastic strain ratio - R

The factor which is usually considered to govern the deep drawability of sheet metal is the tendency of the material in the flange of a pressing to increase in thickness and decrease in the dimension perpendicular to the drawing direction. This tendency depends on metallographic texture of the sheet. However, it is usually measured as a mechanical

property of the sheet itself [380]. This factor is called plastic strain ratio (R), which is defined as:

$$R = \frac{\epsilon_w}{\epsilon_t} = \frac{\ln (w_1/w_o)}{\ln (t_1/t_o)} \dots\dots\dots(7.10)$$

where  $\epsilon_w$  and  $\epsilon_t$  are the strain in width  $w_1$  (the original width is  $w_o$ ) and thickness  $t_1$  ( the original thickness is  $t_o$ ), respectively. Since thickness measurements are difficult to make with precision on thin sheets, equation (7.10) can be rewritten using the constancy-of-volume criterion as [381]:

$$R = - \frac{\epsilon_w}{(\epsilon_l + \epsilon_w)} \dots\dots\dots(7.11)$$

$\epsilon_l$  is the strain in the length direction, or the total elongation,  $\epsilon_f$ . The R values of a samples with 70% cold reduction subjected to various annealing conditions are presented in Table 7-6.

Table 7-6 Plastic strain ratio of samples with 70% cold reduction  
subjected to URA\* and BA\*\*

No.	Conditions	R
1	URA 630°C	0.71
2	URA 667°C	0.97
3	URA 700°C	1.52
4	URA 720°C	1.67
5	BA 680°C	1.55

\*  $t_1 = 0.3$  sec.,  $t_2 = 0.1$  sec. (Fig. 6-14)  
\*\* 30 mintes at 680°C.

The gauge section of the test piece was 30 mm long (Table 4-2) and a gauge length of 14 mm was set for measurement of the length and width strain necessary to calculate R (equation 7.11). This small gauge length was necessary because of the limited uniformly heated zone (between 22 and 26 mm depending on  $T_c$ ). Although the R values were

determined from regions of uniform structure, the small size of the test piece casts some doubt on the accuracy of the values obtained [382]. Despite this reservation the trend in R value with heating conditions is expected to be valid.

The value of R depends solely on the initial texture of the material and the test direction and is therefore determined by the composition and processing history of the material. The variation in R after ultra-rapid annealing at 630°C, 667°C, 700°C and 720°C is attributed to the progress of recrystallization which will give rise to different grain orientations from those in the deformed matrix, thus resulting in different strains in width and thickness directions.

A larger value of R denotes high resistance to thinning in the thickness direction [380]. The slightly higher R value shown after ultra-rapid annealing (No.4) indicates higher resistance to thinning, compared with batch annealed samples (No.5). This result is consistent with the lower reduction in area after ultra-rapid annealing compared with batch annealing ( Table 7-4 ). On the other hand, the substantial deviation of R from 1 after ultra-rapid annealing suggests that the higher heating rate brings about larger anisotropy ( $R = 1$  for an isotropic sheet).

In summary, in the ultra-high heating range, annealed samples exhibited a decrease in tensile strength and an increase in ductility , toughness and plastic strain ratio as the temperature increased. In particular, the large difference in heating rate between URA and BA gives rise to an increase in ductility and toughness in the ultra-rapid annealed samples although similar values of tensile strength were observed in the two cases.

## ***CHAPTER 8***

# **CONCLUSIONS**

The present investigation involved the study of the softening behaviour of decarburized steel, ultra-rapid annealed by resistance heating, with reference to the batch annealed condition. The following conclusions were drawn on the basis of the investigation:

1. Ultra-rapid heating of  $1000 - 5000^{\circ}\text{C}/\text{second}$  can be achieved by resistance heating. A cold rolled, decarburized low carbon steel was softened in a fraction of a second by using heating rates in this range.
2. A three wire thermocouple arrangement was found to give accurate and reproducible temperature readings, even for heating rates of up to  $5000^{\circ}\text{C}/\text{sec}$ .
3. A computer model was established using an implicit method to predict the temperature profile of a resistance heated sample and to allow the optimum specimen shape to be determined. The predicted temperatures agreed with the measured temperatures with less than 1% error. In addition, the present model has advantages in stability and convergence over previous models using an explicit method.
4. Softening of cold rolled, decarburised steel was shown to be greatly enhanced or accelerated as the heating rate was increased within the ultra-rapid heating range. The accelerated softening is attributed to rapid restoration by both recovery and recrystallization, with recovery being promoted more than recrystallization.
5. The observation that increased heating rate reduces the softening range confirms, for resistance heating and faster heating rates, the effect that has been reported previously for salt bath and induction heating.
6. Metallographic results showed that recovery is enhanced rather than suppressed by ultra-rapid heating and that the recovery suppression model, proposed to account for accelerated softening, is not tenable.
7. There was no evidence of any novel mechanisms for recovery and recrystallization in ultra-rapid annealed, as apposed to batch annealed, samples. However, differences were

detected in terms of a reduced tendency to develop a well defined subgrain structure and greater structural heterogeneity in ultra-rapid annealed samples.

8. Very high heating rates resulted in a bimodal micro-hardness distribution during the progress of recrystallization, while batch annealing gave a unimodal distribution. This difference supports the observation of greater structural heterogeneity in the ultra-rapid annealed samples.

9. Softening during ultra-rapid annealing resulted in an increase in ductility and toughness. With progressive softening as the annealing temperature increased, tensile strength decreased while ductility, toughness and plastic strain ratio (R) increased.

10. An increase in percentage of cold deformation before annealing accelerated the softening process for both ultra-rapid and batch annealed samples.

11. Prior recovery at 100°C significantly slowed the softening rate but increasing the ultra-rapid heating rate reduced the effect of this retardation.

12. The experimental observations of trends with increasing ultra-rapid heating rate are consistent with a suppressed solution model in which carbon and nitrogen solution is restricted by rapid heating, thus facilitating restoration by both recovery and recrystallization.

# APPENDIX

- A. Computer programme written by Hua SHI using the implicit method.
- B. Relevant publications.



# A. Computer programme written by Hua SHI using the implicit method.

```

1:*****
2:* THIS PROGRAM ASSIGNS THE VALUES TO THE COEFFICIENTS *
3:* TO THE EQUATIONS WHICH DESCRIBE THE TEMPERATURE      *
4:* PROPERTIES OF MATERIALS. THESE VALUES ARE THEN USED *
5:* TO CALCULATE THE TEMPERATURE PROFILE OF A SPECIMEN  *
6:* HEATED USING THE RESISTANCE HEATER AT THE U.O.W.    *
7:* DEPARTMENT OF METALLURGY AND MATERIALS ENGINEERING. *
8:* OUTPUT IS IN BOTH TABULAR AND GRAPHICAL FORMS.      *
9:* WRITTEN BY HUA SHI                                   *
10:*****
11:    REAL KA1,KB1,KC1,KA2,KB2,KC2,TRANST,DENSE,EA,EB,EC,CPA
12:    REAL RA,RB,RC,RD,CPB,CPC,CPD
13:    CHARACTER*26 MNAME
14:    INTEGER MORE
15:    COMMON KA1,KB1,KC1,KA2,KB2,KC2,TRANST,DENSE,EA,EB,EC,CPA,CPB,CPC,
16:    &RA,RB,RC,RD,MNAME,CPD
17:    OPEN(15,FILE='DATA22.')
18:    OPEN(12,FILE='CDATA12.')
19: 11  WRITE(6,*)'WHICH MATERIAL ARE YOU USING'
20:    WRITE(6,*)' '
21:    WRITE(6,*)'SELECT ONE OF THE FOLLOWING MATERIALS BY NUMBER'
22:    WRITE(6,*)'IF YOU SELECT (4) YOU WILL HAVE TO SUPPLY '
23:    WRITE(6,*)'          1. THERMAL CONDUCTIVITY'
24:    WRITE(6,*)'          2. DENSITY'
25:    WRITE(6,*)'          3. HEAT CAPACITY'
26:    WRITE(6,*)'          4. RESISTIVITY'
27:    WRITE(6,*)'          5. EMISSIVITY'
28:    WRITE(6,*)' '
29:    WRITE(6,*)' FOR THE OTHERS THESE VALUES ARE SUPPLIED'
30:    WRITE(6,*)' '
31: 19  WRITE(6,*)' CHOOSE ONE OF THE FOLLOWING BY NUMBER'
32:    WRITE(6,*)' '
33:    WRITE(6,*)'          (1) IRON'
34:    WRITE(6,*)'          (2) ALUMINUM'
35:    WRITE(6,*)'          (3) LOW CARBON STEEL'
36:    WRITE(6,*)'          (4) OTHER METAL'
37:
38:    READ(5,*) MATL
39:    IF ((MATL.LT.1).OR.(MATL.GT.4)) THEN
40:      WRITE(6,*)'INVALID CHOICE PLEASE ENTER AGAIN'
41:      GOTO 19
42:    ELSE IF (MATL.EQ.1) THEN
43:      MNAME='IRON'
44:*
45:* THERMAL CONDUCTIVITY
46:*
47:*
48:* FIRST TEMPERATURE RANGE
49:*
50:* THE FORMAT OF THESE EQUATIONS IS :
51:*  $K=KA+KBT+KCT**2$ 
52:* UNITS ARE WATTS/(METER.KELVIN)
53:    KA1=91.745

```

```

54:          KB1=-0.065
55:          KC1=0.0
56:*
57:* TRANSITION TEMPERATURE
58:*
59:          TRANST=946
60:*
61:* FOR SECOND TEMPERATURE RANGE
62:*
63:          KA2=78.285
64:          KB2=-0.0475
65:          KC2=0
66:*
67:* DENSITY  KG/(METER**3)
68:*
69:          DENSE = 7.885E3
70:*
71:* HEAT CAPACITY
72:* THE STANDARD FORM OF HEAT CAPACITY EQUATION IS
73:*  $CP=A+BT+CT**2+DT**(-0.5)$ 
74:* UNITS ARE JOULE/(KELVIN.KG)
75:*
76:          CPA=665.164
77:          CPB=1.105E-1
78:          CPC=0
79:          CPD=-4226.965
80:*
81:* RESISTIVITY
82:* USING POLYNOMIAL REGRESSION EQUATIONS FOR THE
83:* VARIATION OF RESISTIVITY WITH TEMPERATURE
84:* HAVE BEEN FOUND. THE FORM OF THESE EQUATIONS IS
85:*  $R = (RA+RBT+RCT**2+RDT**3)*1E-8$ 
86:* UNITS ARE OHMS.METER
87:*
88:          RA=9.918
89:          RB=-2.024E-2
90:          RC=1.03E-4
91:*
92:*
93:* EMISSIVITY
94:* AGAIN THIS IS A POLYNOMIAL REGRESSION EQUATION
95:*  $E=EA+EBT+ECT**2$ 
96:*
97:          EA=0.8
98:          EB=0
99:          EC=0
100:*
101:* FOR ALUMINIUM
102:*
103:          ELSE IF (MATL.EQ.2) THEN
104:*
105:* SAME AS FOR 1 WITH DIFFERENT CONSTANTS
106:          MNAME='ALUMINUM'
107:*

```

```

108:* THERMAL CONDUCTIVITY
109:*
110:*
111:* FIRST TEMPERATURE RANGE
112:*
113:* THE FORMAT OF THESE EQUATIONS IS
114:*  $K=KA+KBT+KCT**2$ 
115:* UNITS ARE WATTS/(METER.KELVIN)
116:      KA1=0.18182565453E2
117:      KB1=0.12328397
118:      KC1=-0.17917E-3
119:*
120:* TRANSITION TEMPERATURE
121:*
122:      TRANST=932
123:*
124:* FOR SECOND TEMPERATURE RANGE
125:*
126:      KA2=1
127:      KB2=1
128:      KC2=0
129:*
130:* DENSITY KG/(METER**3)
131:*
132:      DENSE=2.710E3
133:*
134:* THE STANDARD FORM OF HEAT CAPACITY EQUATION IS
135:*  $CP=A+BT+CT**2+DT**3-0.5$ 
136:* UNITS ARE JOULE/(KELVIN.KG)
137:*
138:      CPA=765.9
139:      CPB=4.589E-1
140:      CPC=0
141:      CPD=0.0
142:*
143:* RESISTIVITY
144:* USING POLYNOMIAL REGRESSION EQUATIONS FOR THE
145:* VARIATION OF RESISTIVITY WITH TEMPERATURE
146:* HAVE BEEN FOUND. THE FORM OF THESE EQUATIONS IS
147:*  $R=(RA+RBT+RCT**2+RDT**3)*1E-8$ 
148:* UNITS ARE OHMS.METER
149:*
150:      RA=-0.81024114
151:      RB=0.01228012
152:      RC=-1.9204841E-6
153:      RD=2.25199E-9
154:*
155:* EMISSIVITY
156:* AGAIN THIS IS A POLYNOMIAL REGRESSION EQUATION
157:*  $E=EA+EBT+ECT**2$ 
158:*

```

```

159:      EA=0.1537E-1
160:      EB=0.2E-3
161:      EC=0
162:      EC=0
163:*
164:* FOR LOW CARBON STEEL
165:*
166:      ELSE IF (MATL.EQ.3) THEN
167:*
168:* SAME AS FOR 1 WITH DIFFERENT CONSTANTS
169:      MNAME='LOW CARBON STEEL'
170:*
171:* THERMAL CONDUCTIVITY
172:*
173:*
174:* FIRST TEMPERATURE RANGE
175:*
176:      KA1=68.9668
177:      KB1=-0.0299
178:      KC1=-7.41342E-6
179:*
180:* TRANSITION TEMPERATURE
181:*
182:      TRANST=1073
183:*
184:* FOR SECOND TEMPERATURE RANGE
185:*
186:      KA2=1
187:      KB2=1
188:      KC2=0
189:*
190:* DENSITY KG/(METER**3)
191:*
192:      DENSE =7.865E3
193:*
194:* HEAT CAPACITY
195:* THE STANDARD FORM OF HEAT CAPACITY EQUATION IS
196:*  $CP=A+BT+CT**2+DT**3-0.5$ 
197:* UNITS ARE JOULE/(KELVIN.KG)
198:*
199:      CPA=772.3644
200:      CPB=-0.67567
201:      CPC= 0.00153
202:      CPD=0.0
203:*
204:* RESISTIVITY
205:* USING POLYNOMIAL REGRESSION EQUATIONS FOR THE
206:* VARIATION OF RESISTIVITY WITH TEMPERATURE
207:* HAVE BEEN FOUND. THE FORM OF THESE EQUATIONS IS
208:*  $R=(RA+RBT+RCT**2+RDT**3)*1E-8$ 
209:* UNITS ARE OHMS.METER
210:*
211:      RA = 35.284307
212:      RB = -0.167548
213:      RC = 3.6987651E-4

```

```

214:          RD = -1.44327E-7
215:*
216:* EMISSIVITY
217:* AGAIN THIS IS A POLYNOMIAL REGRESSION EQUATION
218:*  $E = EA + EBT + ECT**2$ 
219:*
220:          EA = 0.8
221:          EB = 0
222:          EC = 0
223:*
224:*
225:*
226:* IF MATERIAL IS NOT LISTED BUT ANALYSIS OF MATERIAL
227:* IS WANTED.
228:*
229:      ELSE
230:          WRITE(6,*) ' FOR THE MATERIAL YOU ARE USING'
231:          WRITE(6,*) ' THE FOLLOWING INFORMATION CONCERNING THE '
232:          WRITE(6,*) ' VARIATION OF PROPERTIES WITH TEMPERATURE '
233:          WRITE(6,*) ' MUST BE INPUT INTO THE PROGRAM '
234:          WRITE(6,*) ' INPUT THE MATERIAL NAME : '
235:          READ(5,*) MNAME
236:          WRITE(6,*) ' THERMAL CONDUCTIVITY '
237:          WRITE(6,*) ' '
238:          WRITE(6,*) ' THE GENERAL EQUATION FOR THERMAL CONDUCTIVITY IS '
239:          WRITE(6,*) '       $K = A + BT + CT**2$  '
240:          WRITE(6,*) ' THE UNITS ARE WATTS/(METER.KELVIN) '
241:          WRITE(6,*) ' THIS EQUATION MAY ONLY BE VALID OVER A LIMITED '
242:          WRITE(6,*) ' TEMPERATURE RANGE. THIS PROGRAM ALLOWS ENTRY '
243:          WRITE(6,*) ' OF TWO EQUATIONS WITH A TRANSITION TEMPERATURE '
244:          WRITE(6,*) ' BETWEEN THEM. IF YOU ONLY WANT ONE EQUATION '
245:          WRITE(6,*) ' THEN ENTER THE MELTING POINT AS THE TRANSITION'
247:          WRITE(6,*) ' SECOND EQUATION. '
248:          WRITE(6,*) ' INPUT CO-EFFICIENTS A, B, C (ENTER) '
249:          READ(5,*) KA1,KB1,KC1
250:          WRITE(6,*) ' INPUT TRANSITION TEMPERATURE IN DEG KELVIN '
251:          READ(5,*) TRANST
252:          WRITE(6,*) ' INPUT CO-EFFICIENTS A, B AND C FOR THE SECOND '
253:          WRITE(6,*) ' EQUATION IN THE FORMAT A, B, C (ENTER) '
254:          READ(5,*) KA2,KB2,KC2
255:          WRITE(6,*) ' DENSITY OF THE MATERIAL '
256:          WRITE(6,*) ' UNITS ARE KG/(METER**3) '
257:          READ(5,*) DENSE
258:          WRITE(6,*) ' HEAT CAPACITY '
259:          WRITE(6,*) ' '
260:          WRITE(6,*) ' THE STANDARD FORM OF THE HEAT CAPACITY '
261:          WRITE(6,*) ' EQUATION IS  $CP = A + BT + C(T**2) + D(T**-0.5)$  '
262:          WRITE(6,*) ' UNITS ARE JOULE/(KELVIN.KG) '
263:          WRITE(6,*) ' INPUT THE CO-EFFICIENTS A, B, C AND D IN THE FORMAT'
264:          WRITE(6,*) ' A, B, C, D (ENTER) '
265:          READ(5,*) CPA,CPB,CPC,CPD
266:          WRITE(6,*) ' RESISTIVITY '

```

```

267:      WRITE(6,*) ' '
268:      WRITE(6,*) ' USING POLYNOMIAL REGRESSION TECHNIQUES '
269:      WRITE(6,*) ' EQUATIONS FOR RESISTIVITY VARIATION '
270:      WRITE(6,*) ' WITH TEMPERATURE SHOULD BE ESTABLISHED. '
271:      WRITE(6,*) ' THE FORM OF THESE SHOULD BE '
272:      WRITE(6,*) '  $R = (A+BT+CT**2+D**3)*1E-8$  '
273:      WRITE(6,*) ' UNITS ARE OHMS.METER '
274:      WRITE(6,*) ' INPUT THE CO-EFFICIENTS A, B, C AND D IN THE FORMAT'
276:      READ(5,*) RA,RB,RC,RD
277:      WRITE(6,*) ' EMISSIVITY '
278:      WRITE(6,*) ' '
279:      WRITE(6,*) ' AGAIN POLYNOMIAL REGRESSION TECHNIQUES GIVE '
280:      WRITE(6,*) ' EQUATION OF THE FORM  $E = A+BT+CT**2$  '
281:      WRITE(6,*) ' INPUT CO-EFFICIENTS A,B AND C IN FORMAT: '
282:      WRITE(6,*) ' A,B,C (ENTER) '
283:      READ(5,*) EA,EB,EC
284:      END IF
285:* CALL SUBROUTINE FOR HEAT TRANSFER MODEL
286:*
287: 21  CALL MODEL
288:
289:*
290:* PROGRAM FLOW CONTROL
291:*
292:      WRITE(6,*) ' CHOOSE ONE OF THE FOLLOWING '
293:      WRITE(6,*) ' '
294:      WRITE(6,*) ' 1. DO ANOTHER ANALYSIS WITH THE SAME MATERIAL '
295:      WRITE(6,*) ' 2. DO ANOTHER ANALYSIS WITH A DIFFERENT MATERIAL'
296:      WRITE(6,*) ' 3. END PROGRAM'
297:      READ(5,*)MORE
298:      IF (MORE.EQ.1) THEN
299:          GOTO 11
300:      ELSE IF (MORE.EQ.2) THEN
301:          GOTO 21
302:      END IF
303:      CLOSE (15)
304:      CLOSE(12)
305:      END

```

```

1:      SUBROUTINE MODEL
2:      DIMENSION DX(100),SDX(100),T(100,100),DTEM(100)
3:      DIMENSION T1(100),TEMPH(100),TEMPO(100)
4:      REAL KA1,KB1,KC1,KA2,KB2,KC2,L1,L2,NUMX1,NUMX2,KW,KE
5:      REAL MID(100),INTRES,MI
6:      COMMON KA1,KB1,KC1,KA2,KB2,KC2,TRANST,DENSE,EA,EB,EC,CPA,CPB,CPC,

7:      &RA,RB,RC,RD,MNAME,CPD
8:      INTEGER CENTER
9:*
10:* SPECIMEN ID FOR PLOT
11:*
12: 34  WRITE(6,*) ' INPUT SPECIMEN IDENTIFICATION'
13:     READ(5,'( A)') ID
14:*
15:* INPUT SPECIMEN DIMENSIONS
16:
17:     WRITE(6,*) ' INPUT ALL DIMENSIONS IN MM'
18:     WRITE(6,*) ' '
19:     WRITE(6,*) ' FLAG WIDTH = '
20:     READ(5,*) WID2
21:     WRITE(6,*) ' FLAG LENGTH = '
22:     READ(5,*) L2
23:     WRITE(6,*) ' GAUGE WIDTH = '
24:     READ(5,*) WID1
25:     WRITE(6,*) ' GAUGE LENGTH = '
26:     READ(5,*) L1
27:     WRITE(6,*) ' SPECIMEN THICKNESS = '
28:     READ(5,*) S
29:* SET START SPECIMEN THICKNESS
30:     S=S*0.001
31:*
32:* CONVERT DIMENSIONS AND TEMPERATURE TO PROGRAM UNITS
33:*
34:     WID2 = 0.001*WID2
35:     L2 = 0.001*L2
36:     WID1 = 0.001*WID1
37:     L1 = 0.001*L1
38:*
39:* INPUT PROCESS VARIABLES
40:*
41: 44  WRITE(6,*) ' ALL TEMPERATURES IN DEG. CENTIGRADE'
42:     WRITE(6,*) ' '
43:     WRITE(6,*) ' PRIMARY VOLTAGE = '
44:     READ(5,*) PVOLT
45:     WRITE(6,*) ' SECONDARY VOLTAGE = '
46:     READ(5,*) TVOLT
47:     WRITE(6,*) ' HEATING TIME = '
48:     READ(5,*) HTIME
49:     WRITE(6,*) ' DWELL TIME = '
50:     READ(5,*) DTIME
51:*
52:* INPUT ITERATION VARIABLES
53:*

```

```

54:      WRITE(6,*) ' NUMBER OF DIVISIONS ALONG GUAGE LENGTH '
55:      READ(5,*) NUMX1
56:      WRITE(6,*) ' NUMBER OF DIVISIONS ALONG FLAG LENGTH '
57:      READ(5,*) NUMX2
58:      WRITE(6,*) ' TIME INTERVAL BETWEEN ITERATIONS (SEC.) '
59:      READ(5,*) DT
60:*
61:* CALCULATE NUMBER OF DIVISIONS ALONG HALF OF THE SPECIMEN
62:*      I.E.  FLAG + GUAGE LENGTH
63:*
64:      CENTER = INT(NUMX1+NUMX2)
65:*
66:* SET CONSTANTS AND INITIALISE VARIABLES '
67:*
68:      INTRES = 0.092600833875
69:      BOLTZ = 5.67E-8
70:      ALFA=1.0
71:      RAD=5.175E-3
72:      AV=TVOLT/PVOLT
73:      VOT= PVOLT/3.0
74:      VOLT=TVOLT/3.0/3.0
75:      NX=2*RAD*NUMX1/L1
76:      M=INT(DTIME/DT)
77:      KI=INT(HTIME/DT)
78:      WRITE(15,*) M
79:      WRITE(15,*) CENTER
80:*
81:* FOR EACH SEGMENT OF THE SPECIMEN
82:      DX1=L1/(NUMX1-0.5)/2.0
83:      DX2=L2/(NUMX2-0.5)
84:      DO 10 J=1,CENTER
85:          IF (J.NE.1) GOTO 15
86:          DX(J)=0.5*DX2
87:          GOTO 10
88: 15      IF (J.GT.NUMX2) GOTO 14
89:          DX(J)=DX2
90:          GOTO 10
91: 14      IF (J.NE.CENTER) GOTO 16
92:          DX(J)=0.5*DX1
93:          GOTO 10
94: 16      DX(J)=DX1
95: 10      CONTINUE
96:      N=CENTER-1
97:      DO 20 J=1,N
98:          IF (J.EQ.1) GOTO 21
99:          IF (J.EQ.N) GOTO 22
100:      SDX(J)=0.5*(DX(J)+DX(J+1))
101:      GOTO 20
102: 21      SDX(J)=DX(J)+0.5*DX(J+1)
103:      GOTO 20
104: 22      SDX(J)=0.5*DX(J)+DX(J+1)
105: 20      CONTINUE
106:      MID(1)=0.0
107:      DO 25 J=2,CENTER
108: 25      MID(J)=MID(J-1)+SDX(J-1)

```



```

109:      DO 60 J=1,CENTER
110:      T(1,J)=293.0
111:      T(2,J)=T(1,J)
112: 60    T1(J)=T(1,J)
113:      DO 30 I=2,M
114:      TIME=I*DT
115:      WRITE(15,*) TIME
116:      RT=0.0
117:      DO 290 J=1,CENTER
118:      IF (J.LE.NUMX2) THEN
119:      WID=WID2
120:      GOTO 285
121:      ENDIF
122:      IF ((J.GT.NUMX2).AND.(J.LT.(NUMX2+NX))) THEN
123:      WID=WID1+2*RAD-L1*(J-NUMX2)/NUMX1
124:      GOTO 285
125:      ENDIF
126:      IF (J.GT.(NUMX2+NX)) WID=WID1
127: 285    RESIS=(RA+RB*T(I,J)+RC*T(I,J)**2+RD*T(I,J)**3)*1E-8
128:      R=2.0*RESIS*DX(J)/S/WID
129:      RT=RT+R
130: 290    CONTINUE
131:      IF (I.GT.KI) VOT=VOLT
132:      RT=RT+INTRES
133:      CUR=VOT/RT
134:      WRITE(12,*) TIME,RT,CUR
135: 185    K=1
136:      DO 190 J=1,CENTER
137:      IF (J.EQ.1) GOTO 160
138:      IF (J.EQ.CENTER) GOTO 170
139:      IF (T(I,J).GT.TRANST) GOTO 130
140:      KW=(KA1+KB1*(T(I,J-1)+T(I,J))/2.0+KC1*(T(I,J-1)**2+T(I,J)**2)
141:      &/2.0)
142:      KE=(KA1+KB1*(T(I,J)+T(I,J+1))/2.0+KC1*(T(I,J)**2+T(I,J+1)**2)
143:      &/2.0)
144:      GOTO 140
145: 130    KW=(KA2+KB2*(T(I,J-1)+T(I,J))/2.0+KC2*(T(I,J-1)**2+T(I,J)**2)
146:      &/2.0)
147:      KE=(KA2+KB2*(T(I,J)+T(I,J+1))/2.0+KC2*(T(I,J)**2+T(I,J+1)**2)
148:      &/2.0)
149: 140    CP=CPA+CPB*T(I,J)+CPC*T(I,J)**2+CPD*T(I,J)**(-0.5)
150:      E=EA+EB*T(I,J)+EC*T(I,J)**2
151:      IF (J.LE.NUMX2) THEN
152:      WID=WID2
153:      GO TO 85
154:      ENDIF
155:      IF (J.GT.(NUMX2).AND.(J.LT.(NUMX2+NX))) THEN
156:      WID=WID1+2*RAD-L1*(J-NUMX2)/NUMX1
157:      GO TO 85
158:      ENDIF
159:      IF (J.GE.(NUMX2+NX)) WID=WID1
160: 85    A=CUR**2*RESIS/S**2/WID**2
161:      D=2.0*E*BOLTZ*(S+WID)/S/WID
162:      AW=KW/SDX(J)

```

```

163:      AE=KE/SDX(J+1)
164:      AP=AE+AW+DENSE*CP*DX(J)/DT+D*T(I,J)**3*DX(J)
165:      B=DENSE*CP*DX(J)/DT*T(I-1,J)+D*(293.0**4)*DX(J)+A*DX(J)
166:      T(I,J)=T(I,J)+ALFA*((AE*T(I,J+1)+AW*T(I,J-1)+B)/AP-T(I,J))
167:      PRINT *,I,J,T(I,J)
168:      GOTO 175
169:160    T(I,J)=293.0
170:      GOTO 175
171: 170    T(I,J)=T(I,J-1)
172: 175    DTEM(J)=T(I,J)-T1(J)
173:      T1(J)=T(I,J)
174:      IF (DTEM(J).LT.0.1) GOTO 190
175:      K=0
176: 190    CONTINUE
177:      IF (K.EQ.0) GOTO 185
178:      DO 195 J=1,CENTER
179:      TEMPH(J)=T(I,J)-273.0
180:      TEMPD(J)=T(I,J)-273.0
181:      T(I+1,J)=T(I,J)
182:      MI=MID(J)*1000.0
183:      WRITE(15,*) J,MI,TEMPH(J),TEMPD(J)
184: 195    CONTINUE
185:30     CONTINUE
186:*
187:* OUTPUT ROUTINES
188:*
189:      WRITE(6,200)' TEMPERATURE PROFILE FROM RAPID ANNEALER'
190:*
191:      WRITE(6,*)' '
192:      WRITE(15,'(A,A)')MNAME,' ',ID
193:      WRITE(6,*)' SPECIMEN DIMENSIONS'
194:      WRITE(6,*)' '
195:      WRITE(6,*) 'FLAGWIDTH = ', WID2*1000,'MM'
196:      WRITE(6,*) 'FLAG LENGTH = ', L2*1000,'MM'
197:      WRITE(6,*) 'GUAGE LENGTH = ', L1*1000,'MM'
198:      WRITE(6,*) 'GUAGE WIDTH = ', WID1*1000,'MM'
199:      WRITE(6,*) 'INITIAL THICKNESS = ', S,'MM'
200:      WRITE(6,*) 'FINAL THICKNESS = ', S*1000,'MM'
201:      WRITE(6,*) ' '
202:      WRITE(6,*) 'PROCESS VARIABLES'
203:      WRITE(6,*) ' '
204:      WRITE(6,*) ' PRIMARY VOLTAGE', PVOLT,'VOLT'
205:      WRITE(6,*) ' SECONDARY VOLTAGE', TVOLT,'VOLT'
206:      WRITE(6,*) ' HEATING TIME',HTIME,'SECS'
207:      WRITE(6,*) ' DWELL TIME',DTIME,'SECS'
208:      WRITE(6,*) ' '
209:      WRITE(6,*) ' ITERATION VARIABLES'
210:      WRITE(6,*) ' '
211:      WRITE(6,*) ' NUMBER OF DIVISIONS ALONG GUAGE LENGTH',NUMX1
212:      WRITE(6,*) ' NUMBER OF DIVISIONS ALONG FLAG LENGTH',NUMX2
213:      WRITE(6,*) ' TIME INTERVAL BETWEEN ITERATIONS',DT,'SECS'
214:      WRITE(6,*) ' '
215:      WRITE(6,*) ' TEMPERATURES'
216:      WRITE(6,*) ' '
217:      WRITE(6,*) ' ELEMENT DISTANCE MIDPOINT TEMPERATURE TEMPERATURE'

```

```

218:      WRITE(6,*) ' NUMBER ALONG SPECIMEN AFTER HEAT AFTER DWELL '
219:      DO 61 J=1,CENTER
220:      MID(J)=MID(J)*1000.0
221:      WRITE(6,*) J,MID(J),TEMPH(J),TEMPD(J)
222: 61    CONTINUE
223:      WRITE(6,*) ' '
224:      WRITE(6,*) ' CHOOSE ONE OF THE FOLLOWING BY NUMBER '
225:      WRITE(6,*) '      1. END THE PROGRAM '
226:      WRITE(6,*) '      2. RETURN THE PROGRAM WITH SAME SPECIMEN SIZE '
227:      WRITE(6,*) '      3. RETURN THE PROGRAM WITH A DIFFERENT SPECIMEN '

228:      READ(5,*) MORE
229:      IF (MORE.EQ.2) THEN
230:      GOTO 44
231:      ELSE IF (MORE.EQ.3) THEN
232:      GOTO 34
233:      ENDIF
234: 200  FORMAT(1 A)
235:      RETURN
236:      END
EOF:236 SCAN:22

```

## B. Relevant Publications

- a. H. SHI, M. ATKINSON and D. P. DUNNE, RAPID ANNEALING OF COLD ROLLED IRON BY RESISTANCE HEATING, Recrystallization'90 International Conference on Recrystallization in Metallic Materials, January 22 - 26, 1990, The University of Wollongong, Australia.
- b. H. SHI, M. ATKINSON and D. P. DUNNE, EFFECT OF MODE OF RECRYSTALLIZATION ON MECHANICAL PROPERTIES OF ANNEALED LOW-CARBON STEELS, A Symposium on Microstructure Control to Achieve Properties in Modern Steels, Jan. 30 - Feb. 1, 1990, Melbourne, Australia.
- c. M. ATKINSON and H. SHI, FRICTION EFFECT IN LOW-LOAD HARDNESS TESTING OF IRON, *Materials Science and Technology*, The Institute of Metals, London, UK, Vol. 5, June, 1989, pp 613-614.
- d. H. SHI and M. ATKINSON, A FRICTION EFFECT IN LOW-LOAD HARDNESS TESTING OF COPPER AND ALUMINIUM, *Journal of Material Science*, UK., Vol.25, Nov. 6, April, 1990.
- e. H. SHI and M. ATKINSON, ULTRA-RAPID ANNEALING TECHNOLOGY, The First Chinese Youth Metallurgist Conference, Beijing, P. R. China, Sept., 1987. (in Chinese).

f. H. SHI and M. ATKINSON, INVESTIGATIONS INTO THE ULTRA-RAPID ANNEALING OF IRON INCORPORATING COMPUTER MODELLING, *Numerical Methods in Engineering* ( to be published).

g. H. SHI and M. ATKINSON, ULTRA-RAPID ANNEALING OF IRON AND LOW-CARBON STEELS, *Journal of Northeast University of Technology*, Shenyang, P. R. China (to be published in Chinese).

h. H. SHI and M. ATKINSON, APPLICATIONS OF COMPUTER MODELLING IN ULTRA-RAPID ANNEALING, *Journal of Northeast University of Technology* , Shenyang, P.R.China (to be published in Chinese).

## ULTRA-RAPID ANNEALING OF COLD ROLLED IRON BY RESISTANCE HEATING

H. Shi , M. Atkinson and D. Dunne

Department of Materials Engineering,  
The University of Wollongong,  
P.O.Box 1144, Wollongong,  
N.S.W, Australia 2500

### Abstract

The trend in continuous annealing lines for cold reduced low carbon sheet steels is towards increasing line speeds and more compact furnaces, with the aim of reducing processing costs. However, a complicating factor has been a movement to lower carbon, fully killed, continuously cast steels and "interstitial-free" steel with improved resistance to quench and strain aging. Compared with rimmed steels these types of steels have relatively low levels of iron carbide and relatively high levels of fine alloy nitrides or carbides, with both structural features having the potential to retard softening under continuous annealing conditions.

Rapid heating experiments ( $< 2000^{\circ}\text{C}/\text{sec.}$  ) have been reported previously which involved induction and salt bath heating and which indicated that softening of cold rolled rimmed steels was possible in heat treatment times of less than 1 second.

The present paper describes an investigation of the softening behaviour of cold rolled iron (decarburised steel), as an example of a steel type which is more resistant to softening than rimmed steel. A resistance heating method was used with heating rates up to  $3500^{\circ}\text{C}/\text{sec.}$  The results confirm that very rapid softening ("ultra-rapid annealing") can be obtained in heat treatment times of less than 1 second.

### Introduction

Industrial emphasis on energy saving and high productivity provides a catalyst for the development of continuous annealing lines with higher line speeds and more compact annealing furnaces. Detailed work on rapid annealing of drawing grade rimmed steels was carried out at the Steel Company of Wales in the early 1960's [1] . This work showed that recrystallization of cold reduced sheet steels could be completed in less than a second by using sufficiently high heating rates. These investigations involved the use of salt baths and induction heating which resulted in a maximum heating rate of  $1600^{\circ}\text{C}/\text{sec.}$

The present paper describes a resistance heating method which enables sheet samples to be heated at rates of 1000 to 5000°C/sec. to produce softening by recrystallization. In order to indicate heating rates higher than those normally described as "rapid", the current method is referred to as "ultra-rapid heating" and the softening process in cold rolled steel samples is referred to as "ultra-rapid annealing".

Experimental Methods and Materials

Material

The material used in the present investigation was decarburised steel sheet, 1.56 mm thick. The sheet was unidirectionally cold rolled using a Hille 25 (40 kN) rolling mill with two-high, 115 mm dia. rolls to a total reduction of 70%. In order to limit recovery occurring during cold rolling, care was taken to ensure that the cold rolled strip remained cool, by using small rolling reductions (less than 5% per pass) and rapid water quenching after each pass. Details of chemical composition are given in Table I.

Table I Chemical composition of material tested

Element	C	P	Mn	Si	S	Ni	Cr	Mo
Wt %	.005	.015	.40	<.005	.010	.023	.016	.003
Element	Ca	Sn	Ti	V	N <sub>2</sub>	O <sub>2</sub>	sol. Al	
Wt %	.021	.003	<.002	<.002	.0006	.0375	.010	

The cold reduced sheets were machined into test pieces after rolling and then heat treated by resistance heating to peak temperatures in the range 500-1100°C .

Resistance Heating Method

Resistance heating was achieved by an apparatus designed originally by A. Pearce and developed over a number of years in the Department of Materials Engineering at the University of Wollongong. The heating unit consists basically of a controller, an electrical system, a specimen and a water quenching device, linked as shown schematically in Figure 1.

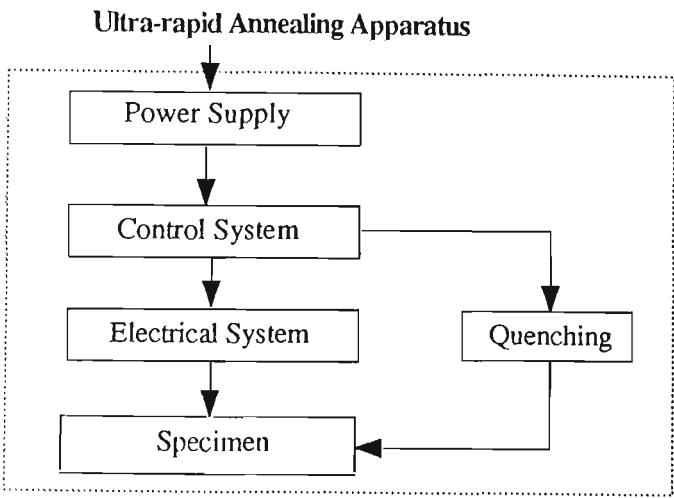
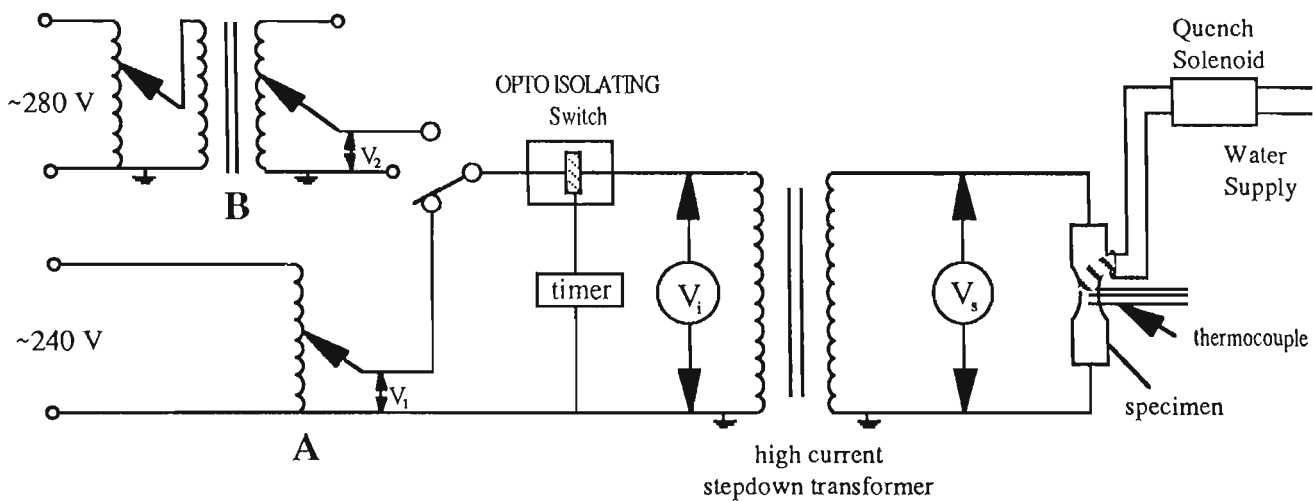


Figure 1 Schematic diagram of ultra-rapid annealing apparatus.

**Test Piece Design and Preparation** The test piece was machined in the form of a tensile test profile for fixing onto hangers and the clamping of electrical leads at either end. The reduced ("gauge") section of the test piece had dimensions of 30mm x 4.65mm x 0.64mm and was carefully milled to prevent recovery due to heat generation. The uniform temperature zone was mapped both experimentally [2,3] and by computer modelling [4] and depended on the voltage applied to the test piece. The uniform zone extended for more than 5 mm on either side of the centre, increasing with increasing voltage up to  $\pm 13$ mm.

**Electrical System** A schematic diagram of the resistance heating circuit is given in Figure 2. Heating was effected in two stages - initial heating to peak temperature and an isothermal hold at this temperature. The first heating stage was accomplished by a variac autotransformer (A in Figure 2) which supplied an input voltage  $V_i$  between 0 and 240 volts to the step-down transformer and determined the specimen heating rate. A second transformer (B in Figure 2) supplied a voltage that produced the isothermal hold. Voltage  $V_2$  from transformer B varied from 0 to ~93 volts and was obtained by 3:1 reduction of the input voltage of 0 to 280 volts. The durations of the first and second stages of heating were determined by setting the timer in the control system.



$V_i$  = input voltage (either  $V_1$  or  $V_2$ );  $V_s$  = voltage applied to specimen.

Figure 2 Diagram showing the electrical system of the ultra-rapid annealing apparatus.

**Control System** The control system consisted of a logic unit, a timer and a zero crossing switch. The logic unit controlled the start of the first and second heating stages as well as the start of quenching. The timer was used to set the duration of the first heating stage  $t_1$ , the total heating time ( $t_1 + t_2$ ) and the quenching time. The zero crossing detector monitored the voltage waveform from the combination of the logic unit and the timer, and switched on or off the appropriate electrical circuit. The duration of heating was measured by counting the number of half cycles of alternating current.

**Quenching System** Quenching was accomplished by spraying the test piece with water. A nozzle connected to a water supply was installed above the test piece and was activated after a pre-set time by the control unit.

### Temperature Measurements

Accurate temperature measurements are essential in quantifying both the heating rate and peak temperatures obtained in the thermal cycle. A three wire Chromel/Alumel thermocouple arrangement was used to construct a Wheatstone electrical bridge to measure specimen temperature. The three thermocouple wires were spot welded to the centre part



of the specimen at spacings of approximately 2.5 mm, with the Alumel wire in the middle flanked by two Chromel wires. The thermocouple output from one of the Chromel/Alumel pair was monitored on a Houston instrument chart recorder.

A three wire thermocouple arrangement has the advantage of being able to be balanced so that the emf generated by the current flowing in the test piece can be cancelled [5]. Balancing was achieved by the Wheatstone bridge circuit which, when balanced, allowed the recorder to receive an emf which was determined solely by the temperature of the specimen.

Temperature measurements obtained during a rapid annealing cycle are shown in Figure 3 for three specimens subjected to the same heating conditions. The peak temperatures varied by only 1°C, establishing that the measurements of peak temperature are reproducible.

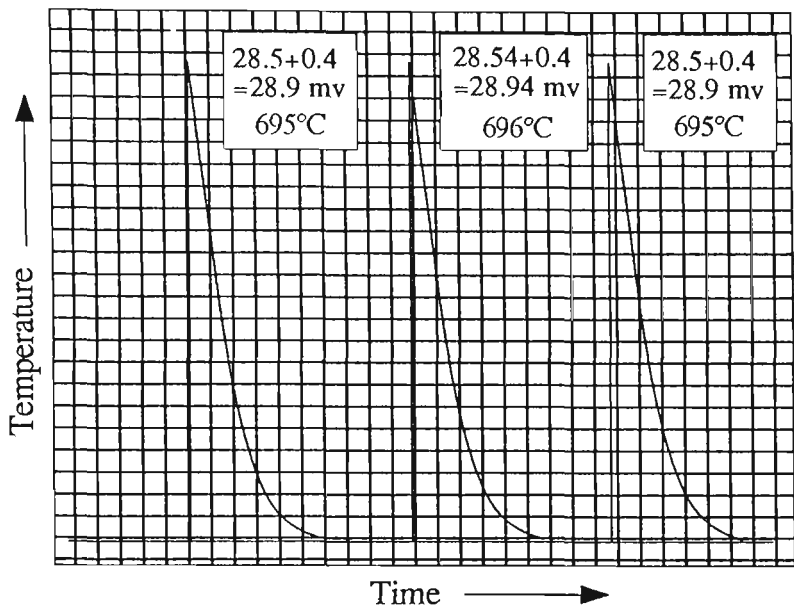


Figure 3 Temperature recorder traces showing reproducibility of temperature profile.  
 $t_1 = 0.2 \text{ sec.}$ ,  $t_2 = 0.1 \text{ sec.}$ ,  $V_1 = 240 \text{ V}$  and  $V_2 = 112 \text{ V}$ .

Hardness Measurements

Vickers hardness measurements were made in the uniform temperature zone near the centre of the test piece. A low load (1 kg) was used to minimise problems associated with the limited thickness of the sheet ( 0.64 mm ) and a calibration factor was applied to ensure a close correlation with hardness values for higher loads [6].

Results

Specimens of the 70% cold reduced steel were heat treated for total times (  $t_1+t_2$  ) in the range 0.3 to 0.6 sec. by adjusting the heating voltage  $V_1$  from about 120 to 240 V. Figure 4 shows specimen hardness as a function of peak temperature reached for each of the heating times indicated and a hold time of 0.1 sec. The evolution of microstructure corresponding to the progress of softening in the curve for  $t_1 = 0.2 \text{ sec.}$  is illustrated in Figure 5.

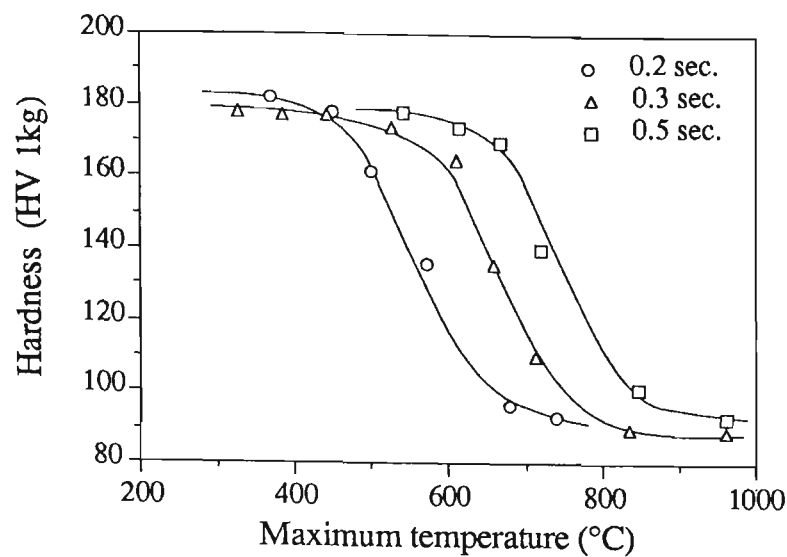


Figure 4 The softening behaviour of 70 % cold reduced samples for  $t_1 = 0.2, 0.3$  and  $0.5$  sec. and  $t_2 = 0.1$  sec.

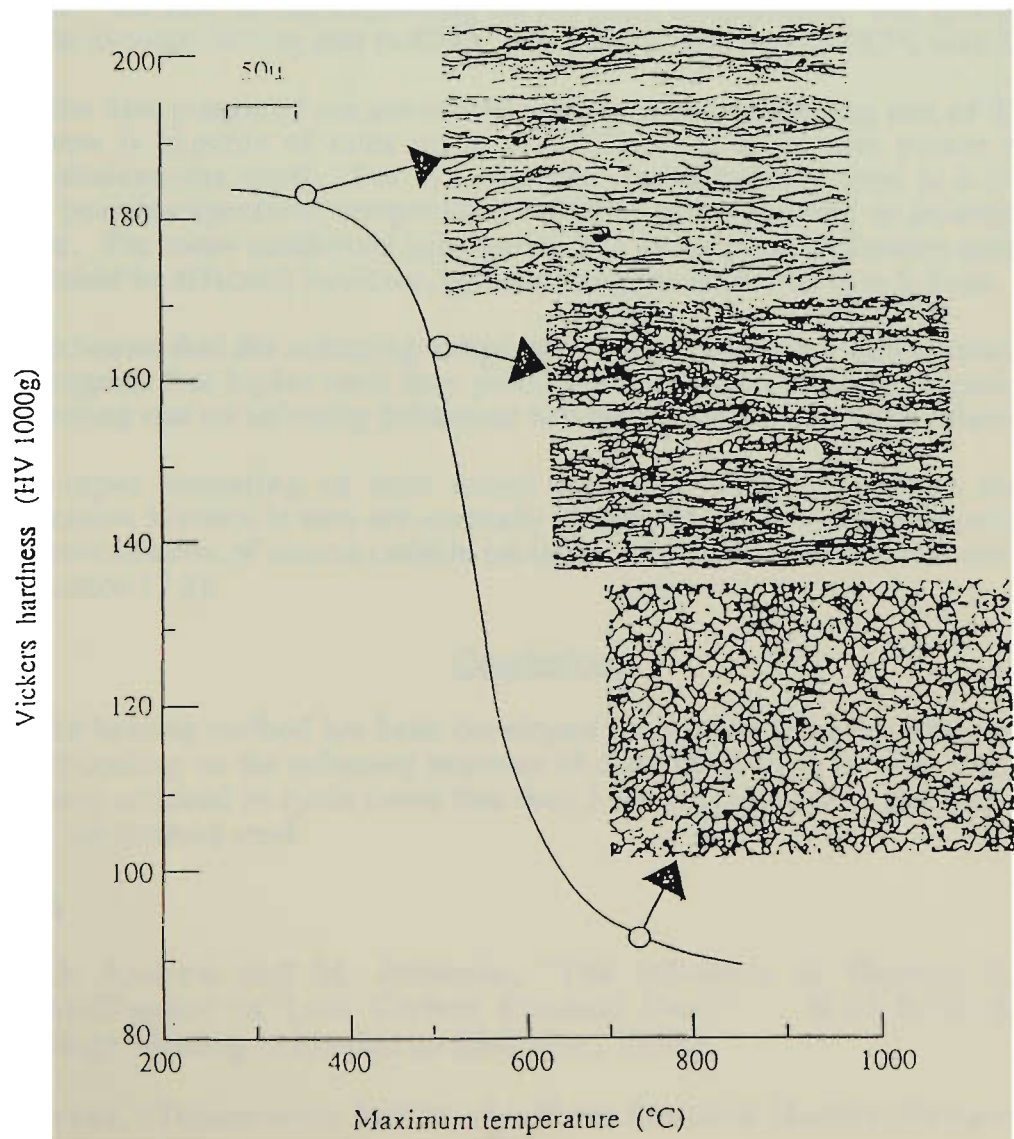


Figure 5 The evolution of microstructure corresponding to the progress of softening for a heating time of 0.2 sec. and a hold time of 0.1 sec.

### Discussion

Problems associated with accurate recording of the thermal cycle during ultra-rapid heating were overcome by using careful experimentation, the use of a three wire thermocouple and repeated tests to establish the reproducibility of the results.

Hardness results are plotted in Figure 4 for sets of test pieces heated for fixed times ( $t_1$ ) to different peak temperatures. A trial sample with thermocouple attached was used to establish the voltage-temperature relationship prior to thermal cycling of the test sample under identical conditions but with no thermocouple. This procedure was followed to avoid any hardness variations which could arise from spot welding of leads to the test piece. Previous work [2] indicated that localised recovery due to spot welding can interfere with restoration behaviour during ultra-rapid annealing, leading to non-uniformity of hardness.

The sharp decrease in hardness with increasing peak temperature was associated with recrystallization of the deformed ferrite grains ( Figure 5 ). For  $t_1 = 0.2$  sec., recrystallization was complete on reaching a temperature of about 700°C and holding for 0.1 sec. It should be noted that the curves in Figure 4 do not correspond to a constant heating rate - the rate varied depending on the peak temperature. For  $t_1 = 0.2$  sec., for example, the average heating rate to 400°C was 2000°C/sec. and to 700°C was 3500°C/sec.

Although the data presented are associated with a maximum heating rate of 3500°C/sec., the apparatus is capable of rates up to 5000°C/sec. at maximum power and for the specimen dimensions used. For  $t_1 = 0.1$  sec. and a holding time  $t_2 = 0.1$  sec., the maximum possible specimen temperature is 500°C corresponding to an average rate of 5000°C/sec. For these conditions substantial, but incomplete, softening occurred. Full softening could be effected, however, by increasing the hold time  $t_2$  to 0.3 sec.

Figure 4 indicates that the softening temperature range decreased with increasing heating rate and suggests that higher rates may produce even lower softening temperatures. The effect of heating rate on softening behaviour will be the subject of a more detailed paper.

The ultra-rapid annealing of cold rolled iron was obtained despite the fact that recrystallization kinetics in iron are normally slower than in low carbon steels because of the low concentration of coarse carbide particles, which can provide nucleating sites for recrystallization [7,8].

### Conclusions

A resistance heating method has been developed for investigating the effect of very rapid heating and cooling on the softening response of cold rolled sheet metals. Cold rolled iron samples were softened in cycle times less than 1 second, consistent with results reported previously for rimmed steel.

### References

- [1] T. O. Andrew and M. Atkinson, "The Influence of Heating Rate on the Recrystallization of Low Carbon Rimmed Steel", ( B.I.S.R.A/I.S.I Physical Metallurgy Meeting in London on 23rd Nov., 1966.).
- [2] P. Howes, "Temperature Profile of a Short Resistive Heating Element", (B. Met. Thesis, University of Wollongong, 1982.)
- [3] E. Spunar, "Ultra-rapid Annealing of Iron and Low Carbon Steel", (B. Met. Thesis, University of Wollongong, 1983.)

- [4] H. Shi, " Investigations into Softening Behaviour of Ultra-rapid Annealing of Cold Rolled Low-carbon Steel by Resistance Heating", (PhD Dissertation, The University of Wollongong, 1990.)
- [5] W. L. Haworth and J. Gordon Parr, "The Effect of Rapid Heating on the Alpha-Gamma Transformation in Iron", Trans. of ASM, 58 ( 1965 ), 477 - 487
- [6] M. Atkinson and H. Shi, "A Friction Effect in Low-Load Hardness Testing of Iron", Materials Science and Technology, 5 ( 1989 ), 613 - 614
- [7] J. D. Baird and J. M. Arrowsmith, JISI, 240, (1966), 191.
- [8] P. Cotterill and P. R. Mould, Recrystallization and Grain Growth in Metals, (Surry University Press, 1976), 190-193.

### Acknowledgements

The contributions of A. Pearce, P. Howes, R. Yip, E. Spunar, J. Vourliotis, P. Kelly and J. Conran are gratefully acknowledged in the development over a period of years of the equipment and techniques for ultra-rapid annealing.

# EFFECT OF MODE OF RECRYSTALLIZATION ON MECHANICAL PROPERTIES OF ANNEALED LOW-CARBON STEELS

H. Shi, M. Atkinson and D. Dunne

Department of Materials Engineering, The University of Wollongong, Wollongong, N. S. W., Australia 2500

## ABSTRACT

The effects of "batch" annealing and ultra-rapid annealing on mechanical properties of 70% cold rolled, decarburised low carbon steel have been investigated. Properties reported are tensile strength, ductility, toughness and plastic strain ratio (R) determined from tensile stress-strain curves.

It was found that samples subjected to ultra-rapid heating exhibited a decrease in yield and tensile strengths and an increase in ductility, toughness and plastic strain ratio as the percentage recrystallization increased. It was also observed that complete recrystallization by ultra-rapid heating resulted in increases in ductility, toughness and plastic strain ratio compared with those of samples which were softened by simulated batch annealing.

## INTRODUCTION

Ultra-rapid annealing by resistance heating [1] provides a potentially economical way to soften cold rolled metals compared with conventional continuous and batch annealing methods. However, the resultant mechanical properties are of over-riding importance and it is necessary to establish that ultra-rapid annealing can produce properties which are comparable to those achieved by batch annealing.

Basic data on the mechanical properties of a ductile metal are usually obtained from a tensile test because it can provide design information on yield stress, tensile strength, ductility, toughness and plastic strain ratio (R). Tensile tests were used in this work to compare the properties of samples subjected to high heating rates and a short hold time (ultra-rapid annealing, URA) and to comparatively low heating rates with a long isothermal hold (furnace annealing, FA). The latter process was used as an approximation of commercial batch annealing.

## EXPERIMENTAL

### Material and heat treatments

The material used in the present study was decarburised steel sheet, 1.56 mm thick. The chemical composition and cold rolling processes are the same as those described in reference [1]. The total cold rolling reduction was 70%.

The cold reduced sheet was machined into test pieces with axis parallel to the rolling direction. Samples were heated at heating rates up to 2400°C/sec. in a time  $t_1=0.3$  sec to the following peak temperatures:

- (1) 720°C (fully recrystallized);
- (2) 667°C (partially recrystallized);
- (3) 630°C (partially recrystallized).

A hold time at peak temperature,  $t_2 = 0.1$  sec. was employed before water quenching.

For comparison, identical samples were annealed at 680°C in a muffle furnace for 30 minutes to obtain a fully recrystallized structure.

Tensile tests

Tests were carried out with a screw-driven "hard" tensile testing machine in conjunction with a data-logging device. An electromechanical extensometer was used and, before testing, force and extension were calibrated. The start parameters were selected as follows: the original opening of the extensometer ( $E_0$ ) was ~14 mm (full opening = 21 mm); the original force ( $F_0$ ) was about 5 N (full scale = 200 N); the data collecting interval was 9/100 second; and the testing speed was 4 mm/min.

**RESULTS AND DISCUSSION**

Specimens of the 70% cold reduced steel were ultra-rapid heated for total times of 0.4 sec. ( $t_1=0.3$ ,  $t_2=0.1$  sec.) by adjusting the heating voltage. Peak temperatures obtained were 630, 667 and 720°C, corresponding to average heating rates of ~2100, 2220 and 2400°C/sec., respectively. Figure 1 shows the relationship between stress and strain for samples subjected to the above annealing conditions. The stress-strain curve for an identical specimen batch annealed at 680°C for 30 minutes, is also given in Figure 1. The tensile tests were characterised by little no discontinuous yielding and showed relatively uniform elongation with minor necking at the point of fracture.

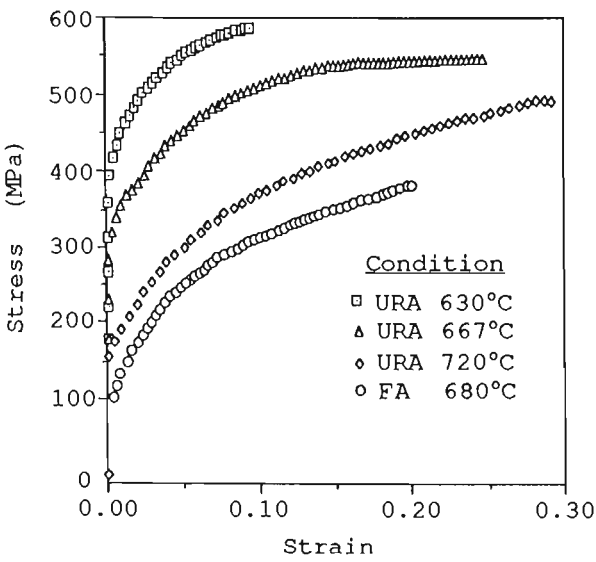


Figure 1 Tensile test results for 70% cold reduced samples after ultra-rapid annealing at 630, 667 and 720°C ( $t_1=0.3$  and  $t_2=0.1$  sec.), and furnace annealing at 680°C for 30 minutes.

Yield stress and tensile strength

The yield stress ( $S_0$ ) was taken as the 0.2% proof stress. The tensile strength ( $S_u$ ) was calculated from the maximum load divided by average cross-sectional area  $A_0$ . The values of  $S_0$  and  $S_u$  as well as the ratio  $S_u/S_0$  are given in Table 1.

Table 1 Yield stress and tensile strength of 70% cold reduced samples subjected to URA and FA

Conditions	$S_0$ (MPa)	$S_u$ (MPa)	$S_u/S_0$
URA 630°C	357.6	587.6	1.64
URA 667°C	282.3	537.8	1.91
URA 720°C	154.9	495.1	3.20
FA 680°C	110.5	343.3	3.11

Both the  $S_u$  and  $S_0$  were found to decrease as the peak temperature of ultra-rapid annealing increased. Metallographic analysis indicated that 630°C was the

start temperature for recrystallization and 720°C, the finishing temperature for recrystallization. Therefore, the observed reduction in tensile strength with increasing peak temperature was due to the increased amount of recrystallization.

Comparison of the stress-strain curves obtained for full recrystallization for both ultra-rapid heating (to 720°C) and slow heating (furnace annealing at 680°C) reveals that the samples subjected to ultra-rapid annealing had a tensile strength of ~495 MPa, whereas it was only ~343 MPa for furnace annealing. This difference is likely to be due to the finer grain size obtained after ultra-rapid annealing. The ratio  $S_u/S_o$  indicates the capacity for work hardening. High capacity corresponds to high value of  $S_u/S_o$ . The ratio was similar for both URA 720°C and FA 680°C.

### Ductility

The conventional measures of ductility from a tension test are the engineering strain at fracture  $e_f$  (usually called the total elongation) and the reduction of area at fracture  $q$  [2]. By definition:

$$e_f = \frac{L_f - L_o}{L_o} \quad (1)$$

and

$$q = \frac{A_o - A_f}{A_o} \quad (2)$$

Where  $l_o$  and  $l_f$  are the original and final gauge lengths and  $A_o$  and  $A_f$ , the original and final cross-sectional areas at the point of fracture. Because of minimal necking,  $e_f$  can be regarded as the strain corresponding to the ultimate tensile strength in the stress-strain curve. The ductilities of samples after various annealing conditions are given in Table 2.

Table 2 Ductility of 70% cold reduced samples subjected to URA and FA

Condition	$e_f$ (%)	$q$ (%)
URA 630°C	9.0	16.19
URA 667°C	25.1	17.14
URA 720°C	29.2	20.87
FA 680°C	22.4	24.65

It was found that both  $e_f$  and  $q$  increased as the annealing temperature increased during ultra-rapid annealing. The increase in ductility can be attributed to the increasing degree of recrystallization with increased peak temperature.

### Toughness

Toughness is a commonly used concept involving both strength and ductility. One definition is that it is the total area under the stress-strain curve [2]. This area is an indication of the amount of work per unit volume which can be done on the material without causing it to rupture. For ductile materials, the area ( $U_T$ ) under the curve can be approximately expressed by the form:

$$U_T \approx S_u * e_f \quad (3)$$

The toughness values of 70% cold reduced samples after various annealing conditions are given in Table 3.

Despite the decrease in  $S_u$ , the toughness of the material increased as the annealing temperature increased during URA, because the increase in ductility is the dominant factor.

Table 3 Toughness of 70% cold reduced samples subjected to URA and FA

No.	Conditions	U <sub>T</sub> (MPa)
1	URA 630°C	52.83
2	URA 667°C	134.54
3	URA 720°C	147.43
4	FA 680°C	77.056

Plastic strain ratio - R

The factor which is usually considered to govern the deep drawability of sheet metal is its resistance to through thickness thinning [2]. This ability depends basically on the metallographic texture of the sheet, but it can be quantified in terms of a mechanical property of the sheet: the plastic strain ratio (R), which is defined as:

$$R = \frac{\epsilon_w}{\epsilon_t} = \frac{\ln (w_f/w_o)}{\ln (t_f/t_o)} \quad (4)$$

where  $\epsilon_w$  and  $\epsilon_t$  are the true strains in a tensile test piece in the width ( $w_f$ ,  $w_o$ ) and thickness ( $t_f$ ,  $t_o$ ) directions, respectively. The subscripts f and o refer to final and original values. Since thickness measurements are difficult to make with precision on thin sheets, equation (4) can be rewritten using the constancy-of-volume criterion as [3]:

$$R = - \frac{\epsilon_w}{(\epsilon_l + \epsilon_w)} \quad (5)$$

$\epsilon_l$  is the strain in the length direction, or the total elongation,  $\epsilon_f$ . The R values of 70% cold reduced samples following various annealing conditions are presented in Table 4. The R values were measured at

a strain of 0.2 except for the sample URA 630°C for which the fracture strain of 0.09 was used.

Table 4 Plastic strain ratio of 70% cold reduced samples subjected to URA and FA

No.	Conditions	R
1	URA 630°C	0.71
2	URA 667°C	0.97
3	URA 720°C	1.67
4	FA 680°C	1.55

The value of R is insensitive to strain in the uniform elongation range [3] and depends solely on the initial texture of the material and therefore, the test direction. The texture value is determined by the composition and processing history of the material.

The variation in R after ultra-rapid annealing at 630, 667 and 720°C is attributed to the variation in the extent of recrystallization and thus the overall texture.

A larger value of R denotes high resistance to thinning in the thickness direction [2]. The higher R value after ultra-rapid annealing (No.3) compared with the furnace annealed sample (No.4) indicates slightly better drawability. However, it should be noted that R was measured only from test pieces cut parallel to the rolling direction and that no conclusions can be drawn about average values for the sheet and the value of the planar anisotropy,  $\Delta R$ .

## CONCLUSIONS

Fully recrystallized samples of 70% cold rolled low carbon steel showed a higher ultimate tensile strength, higher tensile ductility, lower reduction in



area, higher toughness and higher R value following ultra-rapid annealing compared with furnace annealing. These differences are due to differences in grain size and texture. Although the grain size was finer after URA, the grain texture resulted in a higher value of plastic strain ratio in samples cut from the rolling direction of the sheet.

#### REFERENCES

- [1] H. Shi, M. Atkinson and D. Dunne, Ultra-rapid annealing of Cold Rolled Iron by Resistance Heating, Recrystallization of Metallic Materials '90 Conference, Wollongong, NSW, Australia, Jan., 22-26, 1990.
- [2] G. E. Dieter, (editor) *Mechanical Metallurgy*, second edition, McGRAW-HILL International Book Co., Sydney, 1976.
- [3] J. S. H. Lake, D. J. Willis and H. G. Fleming, in *Met. Trans.*, June, 1987.

---

*Short  
Communication*

**Friction effect in  
low load  
hardness testing  
of iron**

*Vickers hardness tests were carried out on specimens of iron in a cold rolled or annealed condition to investigate apparent variation of hardness in the load range 15 g-20 kg. This hardness variation was markedly reduced by lubrication. Therefore, it is suggested that the indentation size effect in these conditions is controlled by friction. Strain hardening seemed to be an important secondary factor.*

MST/1023

M. Atkinson  
H. Shi

© 1989 The Institute of Metals. Manuscript received 29 November 1988. The authors are in the Department of Metallurgy and Materials Engineering, The University of Wollongong, NSW, Australia.

---

Please refer to print copy of thesis for this article.

## **A Friction Effect in Low-Load Hardness Testing of Copper and Aluminium**

**H. Shi and M. Atkinson**

Department of Metallurgy and Materials Engineering

The University of Wollongong

PO Box 1144, Wollongong

NSW, Australia 2500

### **Synopsis**

Vickers hardness tests were conducted on samples of copper and aluminium in a cold rolled or annealed condition to determine the apparent hardness variation in the load range 15g to 20kg. The variation was greatest for the soft specimens. Lubrication with an extreme-pressure lubricant was effective in reducing the hardness values to a virtually constant level for each metal. It is therefore reaffirmed that the hardness variation is attributable to friction and that strain hardening propensity is important in governing the magnitude of the variation. Comparison of these findings with data previously reported for similar tests on iron suggests that the phenomenon is probably an indentation size effect.

### **Keywords**

Vickers hardness, low-load hardness, microhardness, microindentation, indentation size effect, friction, lubrication, strain hardening.

### **1. Introduction**

Microindentation hardness testing is a convenient means of investigating the mechanical properties of a small volume of material [1,2], but variation of the hardness value with load is widely reported. Buckle [3] has identified three ranges of Vickers hardness testing conditions: 'microhardness' (<200g), 'low-load hardness' and normal hardness (>2kg load). At that time only the 'low-load' conditions were definitely associated with increasing hardness for lower load. However, recent reviewers [4-6] have recognised that the effect extends to much lower load, and have also preferred to describe the phenomenon as an indentation size effect.

The cause of the hardness variation remains uncertain. Perhaps the most popular explanation is based on error in measurement of the indentation size arising from limited optical resolution [4]. This does not seem to be an adequate explanation for hardness variation in the 'low-load' range when the indentations may be fairly large.

Recent tests on iron [7] have established that lubrication may have a marked effect in reducing the hardness variation, from which it was deduced that friction is the main factor causing the variation. Strain hardening was also thought to contribute to the magnitude of the variation. There appears to be no independent support for these findings. This paper reports further tests on different metals which show similar effects.

## 2. Experiment

Commercially pure aluminium and copper were chosen as the test materials. The former was cut from a warm-rolled plate about 6mm thick, the latter from a bar with approximately the same thickness. One specimen of each was annealed to restore the strain hardening propensity. All specimens were polished to metallographic standard.

Two hardness testing machines, a standard Vickers machine and a Leitz low-load hardness tester, each with a Vickers indenter, were used. These are the same machines used for the tests on iron reported previously [7]. As noted then, the hardness values obtained with 1kg load on either machine could not be separated and the variation of indentation size through the combined load range of 15g to 20kg appeared to be continuous.

Indentation tests with several loads revealed the expected load dependence of hardness values for both copper and aluminium. The effect was greater for the soft specimens, which showed significant hardness variation well into the normal Vickers load range. These results are shown graphically in Fig.1-4, where averaged results of five repeat tests are plotted. It is of practical interest to note that hardness values for the hard and soft copper specimens were very similar when tested at 15g load.

A similar series of tests was conducted with the specimens lubricated. The same polybutene based drawing lubricant chosen previously [7] as being likely to function effectively in the high pressure conditions of indentation was used in these tests. This was applied as a thin film by smearing it on the surface of the testpiece and then wiping to remove excess. The hardness variation obtained with lubricated specimens was much smaller than for dry tests: in fact the hardness values are virtually constant. Averaged data from these tests are superimposed in Figs. 1 to 4.

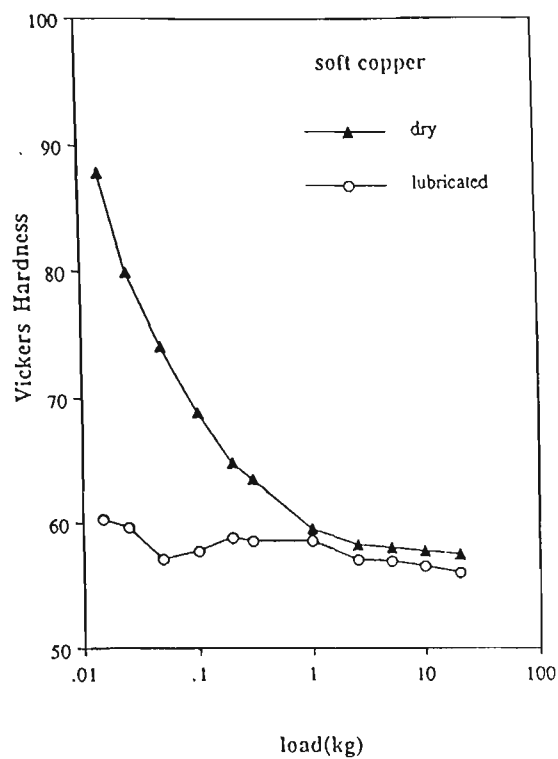


Fig.1 Effect of lubrication in suppressing the variation of hardness with test load for annealed copper

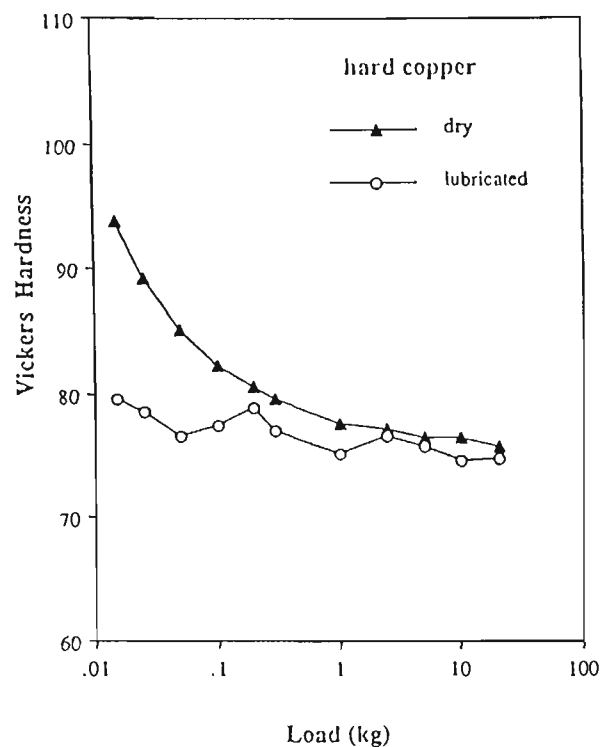


Fig.2 Effect of lubrication in suppressing the variation of hardness with test load for cold-rolled copper

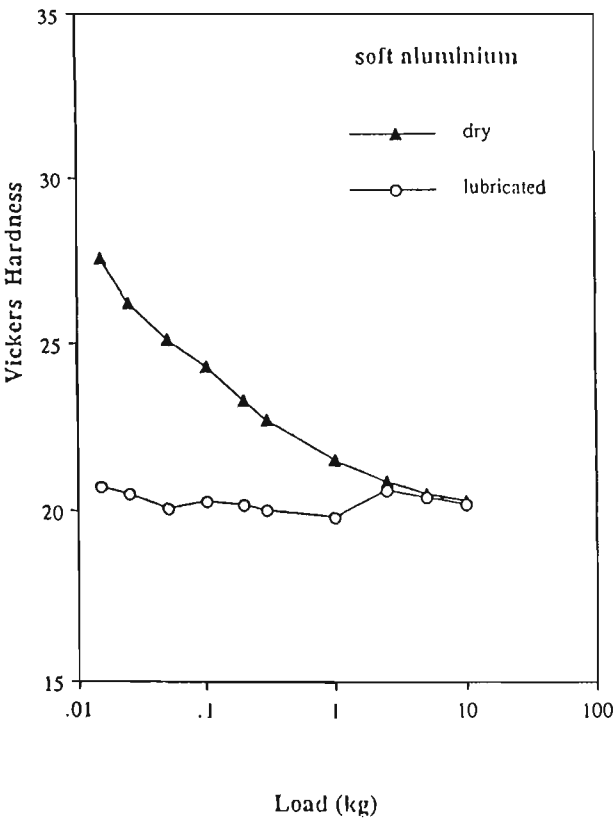


Fig.3 Effect of lubrication in suppressing the variation of hardness with test load for annealed aluminium

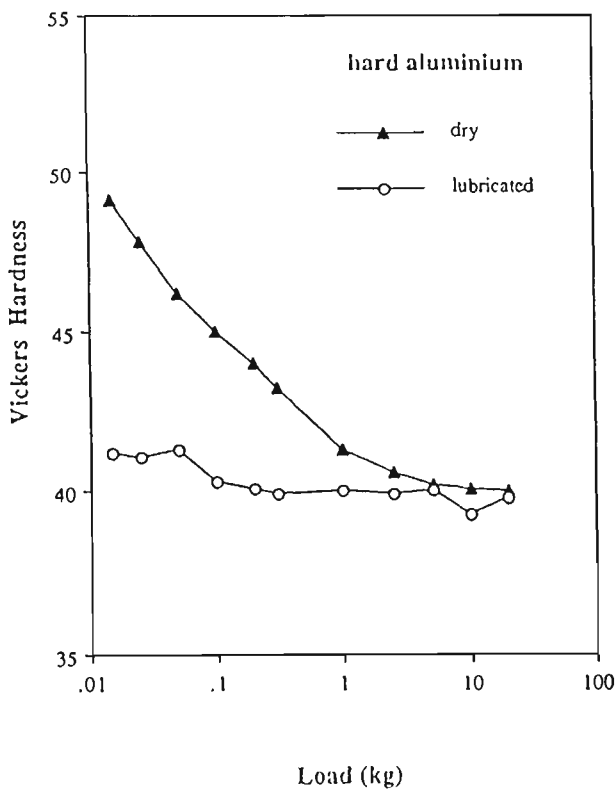


Fig.4 Effect of lubrication in suppressing the variation of hardness with test load for cold-rolled aluminium

### 3. Discussion

The observed load dependence, or indentation size dependence, of hardness for tests on copper and aluminium is similar to that observed in the earlier tests on iron [7]: i.e. the hardness value increases most rapidly at the lowest loads. Although indentation of cold-rolled iron using 15g load produced a small impression with diagonal length of only 10 $\mu$ m, the smallest indentation in the soft aluminium was much larger with a diagonal length of 30 $\mu$ m. It is difficult to believe that limited optical resolution could account for the apparent hardness variation in these tests on aluminium.

The effects of lubrication and of prior deformation in reducing the hardness variation are also very similar. Hardness values for the lubricated specimens are virtually constant and coincident with the hardness values determined for dry specimens using 20kg test load. These observations clearly support the proposition [7] that friction is the main factor governing the phenomenon. The greater hardness variation for the annealed specimens affirms the suggestion that strain hardening propensity is an important secondary factor controlling the magnitude of the hardness variation.

A generalised view of the hardness variation can be obtained by comparing the data now available for three metals. In each case the hardness values tend asymptotically to a low level for large test load. It seems reasonable to estimate the minimum, which may be described as  $H_0$ , as equal to the value at 20kg load. The variation of hardness from the minimum,  $\Delta H$ , may then be normalised by reference to  $H_0$ , giving the dimensionless parameter  $\Delta H/H_0$  as a basis for comparison.

The normalised hardness variations are found to fall into two distinct groups. For the soft specimens, which presumably have rather similar strain hardening propensities, the variation is large and the relationship with test load is distinct for each metal. This is illustrated in Fig.5. For the hard specimens, the variation is much less and the relationships with test load are rather similar. See Fig.6. This is curious because the processing histories of the metals are presumed to be sufficiently different to deny a common condition.

When the hardness variations are compared on the basis of indentation size a different picture emerges: now the soft specimens are seen to be similar and the hard specimens appear to respond differently. These relationships are shown in Figs.7 and 8. This comparison is probably more informative because there are stronger grounds for believing that it is the soft specimens which are in a similar condition and likely to behave similarly. It would follow that the phenomenon is better described as an indentation size effect, but it also seems that a rigorous proof might be difficult. Nevertheless, it seems

clear that strain hardening is an important factor governing the magnitude of the hardness variation in low-load testing.

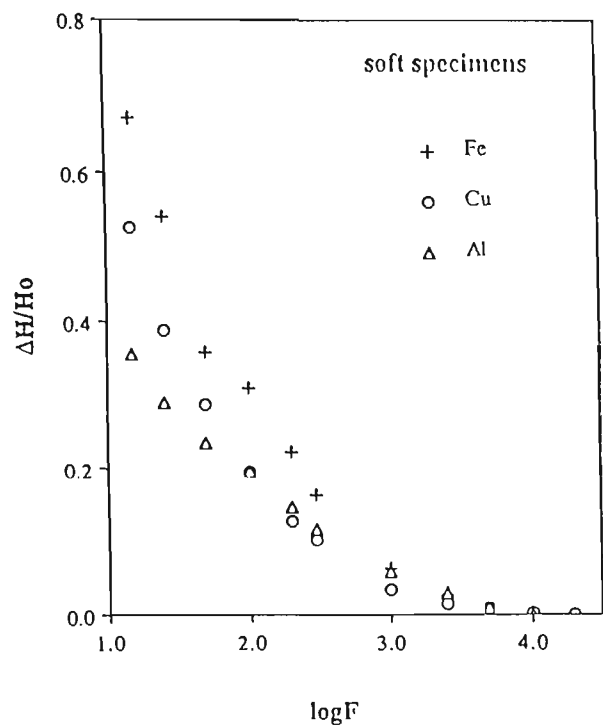


Fig. 5 Relationships between normalised hardness variation and test load, for soft specimens

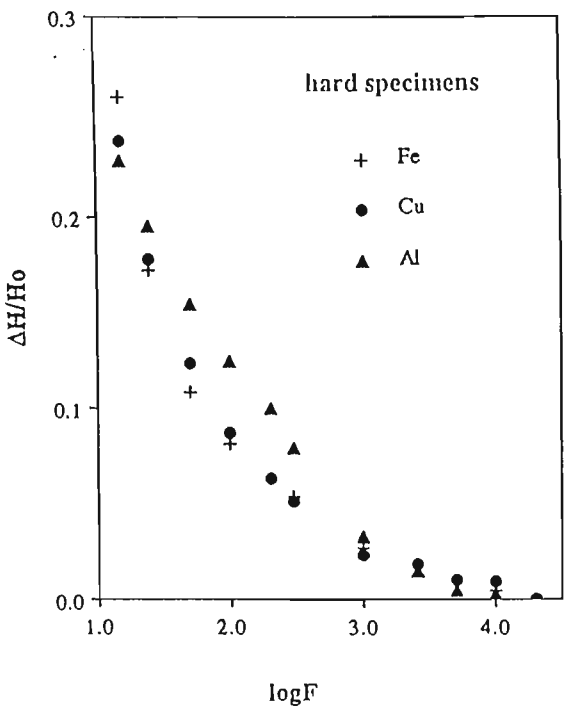


Fig. 6 Relationships between normalised hardness variation and test load, for hard specimens

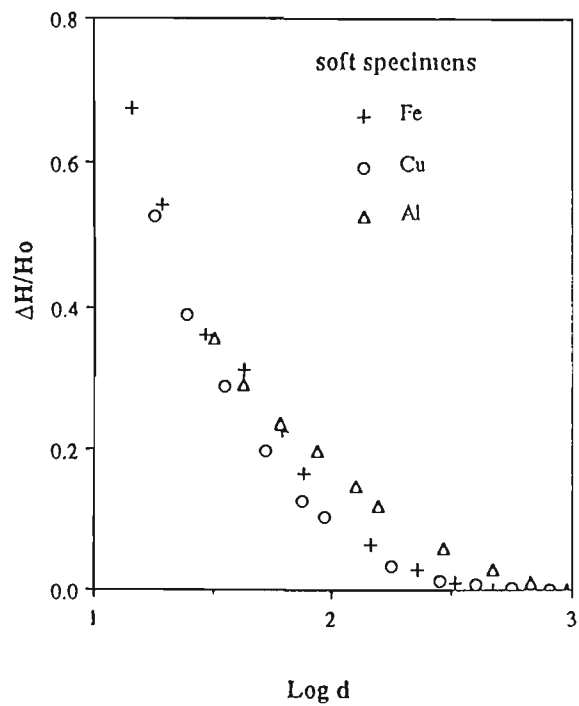


Fig. 7 Relationships between normalised hardness variation and indentation size, for soft specimens

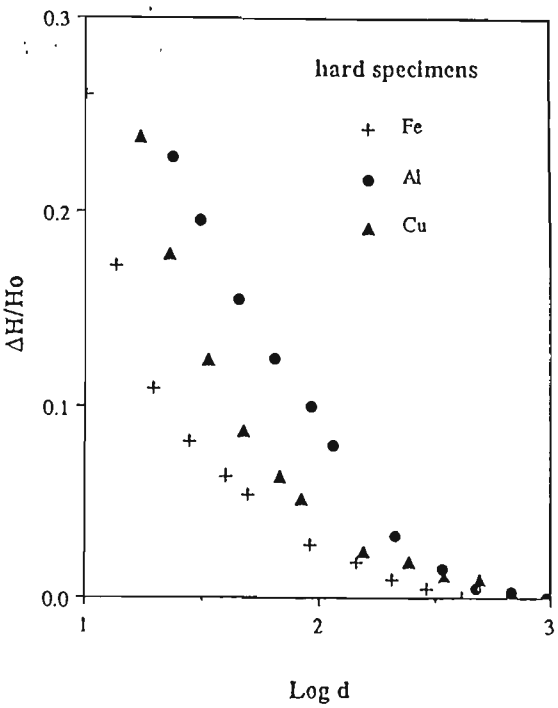


Fig. 8 Relationships between normalised hardness variation and indentation size, for hard specimens

## 4. Conclusions

Vickers indentation tests on copper and aluminium in a cold rolled or an annealed condition, using loads in the range 15g to 20kg, indicate higher hardness at low load. A continuous trend in hardness values was observed throughout this load range.

Similar tests conducted in the presence of a polybutene based drawing lubricant markedly reduced the variation of hardness with load.

These observations are similar to those reported previously for tests on iron and support the view that friction is the principal factor causing load-dependence of hardness values in low-load testing.

The greater hardness variation for annealed specimens appears to confirm the importance of strain hardening propensity.

It seems likely that the phenomenon is an indentation size rather than a load effect.

## 5. Acknowledgement

Thanks are due to Mr. W. Crouch of MM Metals, Port Kembla, for recommendation and provision of the lubricant.

## 6. References

1. "Microindentation Hardness Testing" by B.W. Mott, (Butterworths, London, 1956).
2. "Microindentation Techniques in Materials Science and Engineering" edited by J.H. Westbrook and H. Conrad (A.S.T.M., Philadelphia, 1985).
3. H. Buckle, *Met. Reviews*, **4**, (1959) 49.
4. L.E. Samuels, in "Microindentation Techniques in Materials Science and Engineering" (A.S.T.M., Philadelphia, 1985) STP889, 5.
5. P.M. Sargent, *ibid*, p.160.
6. J.D.J. Ross in "Indentation Hardness of Crystalline Solids at Low Loads", (PhD thesis, Exeter University, 1985).
7. M. Atkinson & H. Shi, "A Friction Effect in Low-Load Hardness Testing of Iron" *Materials Science and Technology*, The Institute of Metals, London, UK. Vol. 5, June, 1989, 613-614..



## Figure Captions

Figure 1. Effect of lubrication in suppressing the variation of hardness with test load, for soft copper.

Figure 2. Effect of lubrication in suppressing the variation of hardness with test load, for hard copper.

Figure 3. Effect of lubrication in suppressing the variation of hardness with test load, for soft aluminium.

Figure 4. Effect of lubrication in suppressing the variation of hardness with testload, for hard aluminium.

Figure 5. Relationships between normalised hardness variation and test load, for soft specimens.

Figure 6. Relationships between normalised hardness variation and test load, for hard specimens.

Figure 7. Relationships between normalised hardness variation and indentation size, for soft specimens.

Figure 8. Relationships between normalised hardness variation and indentation size, for hard specimens.

## REFERENCES

- [1] P. Cotterill and P. R. Mould, (editors) *Recrystallization and Grain Growth in Metals*, Surrey University Press, London, 1976, 1.
- [2] K. Matsudo, K. Osawa and K. Kurihara, in *Technology of Continuously Annealed Cold-Rolled Sheet Steel*, ed. by R. Pradhan, The Metallurgical Society of AIME, 1984, 3.
- [3] J. D. Keller, *Iron and Steel Engineer*, Nov., 1959, 125-133.
- [4] C. E. Peck, *Iron and Steel Engineer*, Feb., 1957, 74-79.
- [5] W. M. Gibbon, in *Recent Developments in Annealing*, Special Report 79, Iron and Steel Institute, London, 1963, 101-111.
- [6] T. O. Andrews, *The Influence of Heating Rate on the Recrystallization of A B26 Grade Rimmed Steel*, S. C. W report No. MR/E/5b/4, Oct., 1968.
- [7] R.K.Yip, "*Heating and Softening effects in Resistance Heated Specimens for Rapid Annealing*" B.Met thesis, the University of Wollongong, 1983.
- [8] T. O. Andrews and M. Atkinson, *A Summary of a made to the joint BISRA/ISI Physical Metallurgy Committee Meeting* in London on the 23rd Nov., 1966.
- [9] E. Spuna, "*Ultra-rapid Annealing of Iron and Low-carbon Steel*", B.Met thesis, University of Wollongong, 1983.
- [10] R.Kalisher, *Ber. Deut. Chem. Gas*, **14**, 1881, 2747.
- [11] R. Becker, *Z. Tech. Phys.*, **7**, 1926, 547.
- [12] J.Czochralski, *Z. Metallk.*, **19**, 1927, 316.

- [13] W. G. Burgers, *Handbuch der Metallphysik*, **3**, pt.2, 1941.
- [14] R. F. Mehl, *Metals Handbook*, American Society for Metals, Cleveland, Ohio, 1948, 259.
- [15] J. E. Burke, *Grain Control in Industrial Metallurgy*, American Society for metals, Cleveland, Ohio, 1949, 1.
- [16] J. E. Burke and D. Turnbull, *Progr. Metal Phys.*, **3**, 1952, 220.
- [17] P. A. Beck, *Advan. Phys.*, **3**, 1954, 245.
- [18] J. J. Gilman, *Acta Metallurgica*, **3**, 1955, 277.
- [19] E. R. Bradley and D. H. Polonis, *Acta Metallurgica*, **36**, No.2, 1988, 393.
- [20] J. D. Embury in *Strengthening Methods in Crystals*, ed. by A. Kally, 1971, 331.
- [21] S. K. Varma and B. L. Willits, *Metallurgical Trans.*, **15A**, 1984, 1502.
- [22] G. Glover and C. M. Sellars, *Met. Trans.*, **4**, 1973, 765.
- [23] K. Okazaki and H. Conrad, *Met. Trans.*, **3**, 1972, 2411.
- [24] E. Ruibal, J. J. Urcola and M. Fuentes, *Materials Science and Technology*, **1**, Sept., 1985, 732.
- [25] H. Hu, in *Metallurgical Treatises*, ed. by J. K. Tien and J. F. Elliott, the Metallurgical Society of AIME, 1981, 385.
- [26] S. Weissmann, T. Imura and N. Hosokawa, in *Recovery and Recrystallization in Metals*, ed. by L. Himmel, Interscience Publishers Co., 1963, 241.
- [27] J. C. M. Li, *J. Appl. Phys.*, **33**, No.10, 1962, 2958.

- [28] A. R. Jones, in *Grain Boundary Structure and Properties*, ed. by G. A. Chadwick, London (etc) Academic Press, 1976, 379.
- [29] R. W. Cahn, *Canadian Metallurgical Quarterly*, **13**, 1974, 253.
- [30] B. Ralph, in *Grain Boundary Structure and Properties*, ed. by G. A. Chadwick, London (etc) Academic Press, 1976, 181.
- [31] J. E. Hillard, in *Recrystallization, Grain Growth and Textures*, ed. by American Society for Metals, Metals Park, Ohio, 1965, 267.
- [32] R. Gronsky, in *Grain Boundary Structure and Properties*, ed. by G. A. Chadwick, London (etc) Academic Press, 1976, 45.
- [33] J. J. Jonas, in *High Strength Low Alloy Steels*, ed. by D. Dunne and T. Chandra, University of Wollongong, Australia, 1985, 80.
- [34] K. Rajan, *Metallurgical Transactions*, **15A**, July, 1984, 1335.
- [35] I. Weiss and J. J. Jonas, *Met. Trans.*, **10A**, July, 1979, 831.
- [36] T. Chandra, I. Weiss and J. J. Jonas, *Metal Science*, **16**, Feb., 1982, 97.
- [37] R. W. Cahn, ( editor) *Physical Metallurgy*, North Holland Publ. Co., Amsterdam, 1965 1st ed., 1970 2nd ed..
- [38] G. K. L'vov in *Physics of Metals and Metallography*, **7**, 1959, 155.
- [39] A. F. Mohri , *Iron and Steel Engineer*, **33**, 1956, July, 148.
- [40] F. Staüb and I. Cieslak, *Accelerated Recrystallization of Cold-rolled Low Carbon Steel Sheets*, BISITS Trans., No. 3660.
- [41] J.Vourliotis, "*Ultra-rapid Annealing of Iron* ", B.Met thesis, University of Wollongong, 1984.

- [42] R. H. Goodenow, *Trans. of the ASM*, **59**, 1966, 804.
- [43] H. Kimura, H. Matsui and S. Takaki, in *Mechanical Properties of BCC Metals*, ed. by M. Meshii, The Metallurgical Society of AIME, U.S.A., 1981, 125.
- [44] S. R. Goodman and A. R. Chauhry, in *Metallurgy of Continuous-Annealed Sheet Steel*, ed. by B. L. Bramfitt and P. L. Mangonon, Jr., The Metallurgical Society of AIME, 1982, 229.
- [45] T. Chandra, S. Misra and D. P. Dunne, in *High Strength Low Alloy Steels*, eds. by D. P. Dunne and T. Chandra, University of Wollongong, N. S. W., Australia, 1985, 101.
- [46] O. V. Abramov, in *High Strength Low Alloy Steels*, ed. by D. Dunne and T. Chandra, University of Wollongong, Australia, 1985, 260.
- [47] P. Messien, J. C. Herman and T. Grday, in *Metallurgy of Continuous-Annealed Sheet Steel*, ed. by B. L. Bramfitt and P. L. Mangonon, Jr., The Metallurgical Society of AIME, 1982, 271.
- [48] R. A. Vandermeer and P. Gordon, in *Recovery and Recrystallization in Metals*, ed. by L. Himmel, Interscience Publishers Co., New York, 1963, 211.
- [49] L. M. Clarebrough, M. E. Hargreaves and M. H. Lorretto, in *Recovery and Recrystallization in Metals*, ed. by L. Himmel, Interscience Publishers Co., New York, 1963, 63.
- [50] P. Gordon, *Rev. Sci. Instrum.*, **25**, 1954, 1173.
- [51] P. Gordon, *Trans. Met. Soc. AIME*, **203**, 1955, 1043.
- [52] S. Sato, *Sci. Repts*, Tôhoku Imp. Univ., **20**, 1931, 140.
- [53] J. E. Bailey and P. B. Hirsh, *Phil. Mag.*, **5**, 1960, 485.

- [54] H. Hu, in *Recovery and Recrystallization in Metals*, ed. by L. Himmel, Interscience Publishers Co., New York, 1963, 311.
- [55] W. C. Leslie, J. T. Michalak and F. W. Aul, in *Metallurgy of Continuous-Annealed Sheet Steel*, ed. by B. L. Bramfitt and P. L. Mangonon, Jr., The Metallurgical Society of AIME, 1982, 119.
- [56] H. Hort, *Z. ver. deut. Ing.*, **50**, 1906, 1831.
- [57] M. B. Bever, P. L. Holt and A. L. Titchener, *Proge. in Materials Sci.*, **17**, Pergamon Press, Oxford, 1973.
- [58] G. I. Taylor and H. Quinney, *Proc. Roy. Soc. (London)*, **A143**, 1934, 307.
- [59] D. P. Dunne, *The microstructure of Annealed Metals*, a paper prepared for a seminar on "annealing" organised by the Port Kembla Branch of AIM on August 27, 1975.
- [60] D. McLean, *Mechanical Properties of Metals*, Wiley and Son. New York, U. S. A., 1962.
- [61] P. R. Mould and P. Cotterill, *J. Mater. Sci.*, **2**, 1967, 241.
- [62] W. A. Anderson and R. F. Mehl, *Trans. Met. Soc. AIME*, **161**, 1945, 140.
- [63] E. C. W. Perryman, *Acta. Met.*, **2**, 1954, 26.
- [64] E. E. Underwood, (editor) *Quantitative Stereology*, Addison-wesley Publ. Co., London etc. 1970.
- [65] E. C. W. Perryman, *J. Metals*, 1955, 1053.
- [66] H. J. Wallbaum and R. Mischner, *Z. Metallik*, **40**, 1949, 179.
- [67] P. R. Mould and P. Cotterill, *Metallurgia*, **71**, 1965, 149.

- [68] P. Gordon, *Trans. Met. Soc. AIME*, **203**, 1955, 1043.
- [69] P. H. Thornton and R. W. Cahn, *J. Inst. Metals.*, **89**, 1960-1961, 455.
- [70] L. M. Clarebrough and M. E. Hargreaves, *Progr. Metal Phys.*, **8**, 1959, 1.
- [71] L. M. Clarebrough, M. E. Hargreaves and M. H. Lorretto, in *Recovery and Recrystallization in Metals*, ed. by L. Himmel, Interscience Publishers Co., New York, 1963, 63.
- [72] P. M. Robinson and P. N. Richards, *Phil. Mag.*, **11**, 1965, 407.
- [73] T. S. Kê, *Trans. Met. Soc. AIME*, **188**, 1950, 581.
- [74] L. M. Clarebrough, M. E. Hargreaves and M. H. Lorretto, in *Recovery and Recrystallization in Metals*, ed. by L. Himmel, Interscience Publishers Co., New York, 1963, 63.
- [75] G. H. Kinchin and M. W. Thompson, *J. Nuclear Energy*, **6**, pts.4, 1958, 275.
- [76] D. G. Martin, *Acta Met.*, **5**, 1957, 371.
- [77] H. R. Peiffer, *Trans. AIME*, **212**, 1958, 647.
- [78] D. Wruck and C. Wert, *Acta Met.*, **3**, 1955, 115.
- [79] T. H. Blewitt, R. R. Coltman, D. K. Holmes and T. S. Noggle, *Creep and Recovery*, Am. Soc. Metals, Cleveland, Ohio, 1957, 84.
- [80] G. Masing and J. Raffelsieper, *Z. Metallk*, **41**, 1950, 65.
- [81] C. H. Li, J. Washburn and E. R. Parker, *Trans. Met. Soc. AIME*, **197**, 1953, 1223.

- [82] R. W. Cahn, ( editor) *Physical Metallurgy*, North Holland Publ. Co., Amsterdam, 1965 1st ed., 1970 2nd ed..
- [83] T. J. Koppenall and M. E. Fine, *Trans. Met. Soc. AIME*, **221**, 1961, 178.
- [84] T. J. Koppenall and M. E. Fine, *J. Appl. Phys.*, **32**, 1961, 1781.
- [85] G. Sachs and K. R. Van Horn, *Practical Metallurgy*, Amercian Society for Metals, Ohio, 1940, 123.
- [86] W. Koester, *Z. Metallk*, **20**, 1928, 189.
- [87] I. Kvernes, *Z Metallk*, **54**, 1963, 449.
- [88] J. E. Bailey, *Phil. Mag.*, **5**, 1960, 833.
- [89] J. E. Bailey and P. B. Hirsh, *Proc. Roy. Soc.*, **267A**, 1962, 11.
- [90] J. E. Bailey, *Electron Microscopy and Strength of Crystals*, ed. by G. Thomas and J. Washburn, Interscience, New York, 1963, 535.
- [91] W. T. Lankford, S. C. Snyder and J. A. Banscher, *Trans. ASM*, **42**, 1950, 1197.
- [92] W. F. Hosford and N. A. Backhofen,(editors), *Fundamentals of deformation processing* , 1964, New York, Syracuse Press, 259.
- [93] D. V. Wilson, *J. Inst. Met.*, **94**, 1966, 84.
- [94] R. L. Whiteley, *Trans. ASM*, **52**, 1960, 154.
- [95] I. L. Dillamore, R. E. Smallman, and D. V. Wilson, paper 10, *Ninth Commonwealth Mining and Metallurgical Congress*, 1969.
- [96] D. V. Wilson, *Met. Rev.*, **14**, 1969, 175.



- [97] R. H. Heyer, D. E. McCabe, and J. A. Elias, in *Flat Rolled Products III*, ed. by E. W. Earhart, Interscience, 1962, 29.
- [98] R. L. Whiteley and D. E. Wise, *ibid*, 47.
- [99] R. S. Burns and R. H. Heyer, *Sheet Met. Ind.*, **35**, 1958, 261.
- [100] R. L. Whiteley, D. E. Wise and D. J. Blickwede, *Sheet Met. Ind.*, **38**, 1961, 349.
- [101] F. A. Hultgren, *Blast Furnace and Steel Plant*, **56**, 1968, 149.
- [102] J. A. Elias, R. H. Heyer and J. H. Smith, *Trans. Met. Soc. AIME*, **224**, 1962, 679.
- [103] W. F. Hosford, *Trans. Trans. Met. Soc. AIME*, **227**, 1963, 272.
- [104] S. Nagashima, S. Sekino and H. Kato, *Trans. J. I. M.*, **5**, 1962, 244.
- [105] J. F. Held, in *Mechanical Working and Steel Processing IV*, ed. by D. A. Edgecombe, 1965, 3.
- [106] S. Nagashima, H. Takechi and H. Kato, in *Textures in Research and Practice*, eds. by J. Grewen and G. Wassermann, 1969, 444.
- [107] P. N. Richards, in John Lysaght ( Australia) Research Report No. 371, 1967.
- [108] I. L. Dillamore, C. J. E. Smith and T. W. Watson, *Met. Soc. J.*, **1**, 1967, 49.
- [109] C. A. Stickels and C. M Yen, *Trans. Met. Soc. AIME*, **242**, 1968, 833.
- [110] H. Takechi, H. Kato and S. Nagashima, *Trans. Met. Soc. AIME*, **242**, 1968, 56.
- [111] H. Akamatsu and T. Sakamoto, *Trans. J. I. M.*, **7**, 1966, 82.

- [112] S. R. Goodman and H. Hu, *Met. Trans.*, **1**, 1970, 1629.
- [113] I. L. Dillamore, C. J. E. Smith and T. W. Watson, *Met. Sci. J.* **1**, 1967, 49.
- [114] T. R. Thomson and J. M. Baker, *J. Aust. Inst. Met.*, **14**, 1969, 84.
- [115] G. Pomey, T. Sakamoto, M. Grumbach and P. H. Carpentier, in *Textures in Research and Practice*, eds. by J. Grewen and G. Wassermann, Clausthal-Zellerfeld, 1969, 348.
- [116] C. J. E. Smith, *report from the Dept. of Physical Metallurgy and Science of Materials*, Univ. of Birmingham.
- [117] C. Dasarathy and R. C. Hudd, *paper presented at the Deutsche Gesellschaft fur Metallkunds Hauptversammlung*, West Berlin, May, 1969.
- [118] R. H. Goodenow, *Trans. ASM.*, **59**, 1966, 804.
- [119] I. L. Dillamore and S. F. H. Fletcher, in *Recrystallization, Grain Growth and Textures*, A. S. M. 1966, 448.
- [120] W. Jolley, *J. I. S. I.*, **205**, 1967, 321.
- [121] C. Dasarathy, in *Textures in Research and Practice*, eds. by J. Grewen and G. Wassermann, 1969, 330.
- [122] H. Widmann, *Z. Phys.*, **45**, 1927, 200.
- [123] J. Calvert, *C. R. Acad. Sci.*, (Paris), **200**, 1935, 66.
- [124] R. Chadwick, *J. Inst. Metals*, **51**, 1933, 93.
- [125] A. W. Demmler, *Trans. Met. Soc. AIME*, **206**, 1956, 958.
- [126] P. Albert, O Dimitrov and J. Le Héricy, *Rev. Met.*, (Paris), **54**, 1621.

- [127] J. Talbot, in *Recovery and Recrystallization in Metals*, ed. by L. Himmel, Interscience Publishers Co., New York, 1963, 269.
- [128] E. P. Kostynkova and B. B. Ravinsky, *Izv. Akad. Nauk SSSR, Met. i. Topl.* **1**, 1959, 55.
- [129] C. Messenger and O. Dimitrov, *C. R. Acad. Sci.*, (Paris), **250**, 1960, 1847.
- [130] C. Messenger and O. Dimitrov, *Mem. Sci. Rev. Met.*, **58**, 1961, 357.
- [131] C. Messenger and O. Dimitrov, *C. R. Acad. Sci.*, (Paris), **249**, 1959, 1658.
- [132] H. Hu, in *Recovery and Recrystallization in Metals*, ed. by L. Himmel, Interscience Publishers Co., New York, 1963, 311.
- [133] T. H. Blewitt et al, in *Creep and Recovery*, ( Seminar during 38th Nat. MetalCongress and Exposition, Cleveland, Oct. 6-12, 1956, Seminar Coordinator R. Maddin, 1957, Cleveland, Ohio, ASM, 372.
- [134] J. E. Wilson and L. Thommassen, *ASM Trans.*, **22**, 1934, 769.
- [135] A. S. Tetelman et al, *Acta Met.*, **9**, 1961, 205.
- [136] J. Talbot, in *Recovery and Recrystallization in Metals*, ed. by L. Himmel, Interscience Publishers Co., New York, 1963, 291.
- [137] C. Messenger, *Mem. Sci. Rev. Met.*, **58**, 1961, 357.
- [138] C. Messenger and O. Dimitrov, *Compt. rend.*, **249**, 1959, 1658.
- [139] C. Messenger and O. Dimitrov, *Compt. rend.*, **250**, 1960, 1847.
- [140] W. G. Burgers, *Zeit. Fur. Metallkunde*, **52**, 1961, 19, ( Alcan Translation).
- [141] R. A. Oriani, *Acta Met.*, **8**, 1960, 134.

- [142] E. Orowan, in *Dislocation in Metals*, AIME, New York, 1954, 181.
- [143] R. W. Cahn, *Proc. Phys. Soc.*, ( London), **A63**, 1950, 323.
- [144] T. L. Richards and S. F. Pugh, *J. Inst. Metals*, **88**, 1959-60, 141.
- [145] E. P. Kostynkova and B. B. Ravinsky, *Izv. Akad. Nauk SSSR, Met. i. Topl*, **10**, 1959, 55.
- [146] A. Saulnier and P. Mirand, *Rev. Met.*, ( Paris), **248**, 1959, 2871.
- [147] J. Talbot, *Symp. de Metallurgie Special*, Saclay, 1957, 125.
- [148] E. Votava, *Acta Met.*, **9**, 1961, 870.
- [149] P. Bartuska, *Czech. J. Phys.*, **14**, 1964, 654.
- [150] W. Bollman, *J. Inst. Metals*, **87**, 1958-59, 439.
- [151] A. H. Cottrell, *Prog. Met. Phys.*, **4**, 1953, 255.
- [152] J. P. Nielson, *Trans. Met. Soc. AIME*, **200**, 1954, 1084.
- [153] S. Weissmann, T. Imura and N. Hosokawa, in *Recovery and Recrystallization in Metals*, ed. by L. Himmel, Interscience Publishers Co., New York, 1963, 246.
- [154] C. Rzepski and J. Montuelle, *C. R. Acad. Sci.*, (Paris), **254**, 1962, 1633.
- [155] A. R. Jones in *Grain-Boundary Structure and Kinetics*, Materials Science Seminar, Milwaukee, 1979, 379.
- [156] H. Hu, in *Electron Microscopy and Strength of Crystals*, ed. by G. Thomas and J. Washburn, Interscience, New York, 1963, 546.
- [157] H. Hu, in *Recovery and Recrystallization in Metals*, ed. by L. Himmel, Interscience Publishers Co., New York, 1963, 311.

- [158] H. Hu, *Trans. Met. Soc. AIME*, **230**, 1964, 572.
- [159] Y. S. Avraamov and V. Y. Novikov, *Metalloved Term, Obrab. Metal.*, 1966, 132.
- [160] V. Y. Novikov and V. M. Semenov, *Chern. Met.*, **9**, 1966, 132.
- [161] J. C. M. Li, *J. Appl. Phys.*, **33**, 1962, 2958.
- [162] H. Hu, in *Metallurgical Treatises*, ed. by J. K. Tien and J. F. Elliott, the Metallurgical Society of AIME, 1981, 385.
- [163] H. Hu and R. S. Cline, *Trans. Met. Soc. AIME*, **242**, 1968, 1013.
- [164] C. R. Brinkman and C. H. Pilt, *J. of Less-Common Metals*, **11**, 1963, 323.
- [165] W. Shockley and T. W. Read, *Phys. Rev.*, **78**, 1950, 275.
- [166] C. G. Dunn and F. Lionetti, *Trans. Met. Soc. AIME*, **185**, 1949, 125.
- [167] C. G. Dunn, F. W. Daniels and M. J. Bolton, *Trans. Met. Soc. AIME*, **188**, 1950, 1245.
- [168] K. T. Aust and B. Chalmers, *Proc. Roy. Soc.*, **A201**, 1950, 210.
- [169] K. T. Aust and B. Chalmers, *Proc. Roy. Soc.*, **A204**, 1950, 359.
- [170] K. T. Aust, *Trans. Met. Soc. AIME*, **206**, 1956, 1026.
- [171] K. A. McCarthy and B. Chalmers, *Can. J. Phys.*, **36**, 1956, 1645.
- [172] N. Gjostein and F. N. Rhines, *Acta Met.*, **7**, 1959, 319.
- [173] R. W. Wagner and B. Chalmers, *J. Appl. Phys.*, **31**, 1960, 581.
- [174] C. G. Dunn and F. W. Daniels, *Trans. Met. Soc. AIME*, **191**, 1951, 141.

- [175] R. J. Towner and J. A. Berger, *Trans. Met. Soc. AIME*, **218**, 1960, 611.
- [176] H. Bischel, *Metall.*, **14**, 1960, 196.
- [177] J. J. Gilman, *Acta Met.*, **3**, 1955, 277.
- [178] W. R. Hibbard Jr. and C. G. Dunn, *Acta Met.*, **4**, 1956, 306.
- [179] D. W. Bainbridge, C. H. Li and E. H. Edwards, *Acta Met.*, **2**, 1954, 322.
- [180] W. T. Read, in *Dislocation in Crystals*, McGraw Hill, New York, 1953.
- [181] A. H. Cottrell, in *Dislocations and Plastic Flow in Metals*, Clarendon Press, Oxford, 1953.
- [182] R. W. Cahn, *Proc. Phys. Soc.*, **A63**, 1950, 323.
- [183] P. A. Beck, *J. Appl. Phys.*, **20**, 1949, 633.
- [184] R. E. Smallman, *Modern Physical Metallurgy*, Butterworth, London, 3rd ed., 1970.
- [185] R. W. Cahn, ( editor) *Physical Metallurgy*, North Holland Publ. Co., Amsterdam, 1965 1st ed., 1970 2nd ed..
- [186] J. G. Byrne, (editor), *Recovery, Recrystallization and Grain Growth*, Macmillan, New York, 1965.
- [187] J. P. Nielson, *Trans. AIME*, **200**, 1954, 1084.
- [188] P. A. Beck and P. R. Sperry, *J. Appl. Phys.*, **21**, 1950, 150.
- [189] T. J. Tiedema, *Proc. Kon. Ned. Akad. Wetensch.*, **53**, 1950, 1422.
- [190] C. Crussard, *Metaux*, **28**, 1953, 1.

- [191] K. T. Aust and C. G. Dunn, *Trans. Met. Soc. AIME*, **269**, 1957, 472.
- [192] P. A. Vandermeer and P. Gordon, *Trans. Met. Soc. AIME*, **215**, 1959, 577.
- [193] J. E. Bailey and P.B. Hirsh, *Phil. Mag.*, **5**, 1960, 485.
- [194] W. C. Leslie, J. T. Michalak and F. W. Aul, in *Iron and its Dilute Solid Solutions*, ed. by C. W. Spencer and F. E. Werner, Interscience, New York, 1963, 119.
- [195] E. C. W. Perryman, *Creep and Recovery*, American Society for Metals, Ohio, U. S. A., 1957, 111.
- [196] M. B. Bever, *Creep and Recovery*, American Society for Metals, Ohio, U. S. A., 1957, 14.
- [197] J. C. M. Li, in *Recrystallization, Grain Growth and Textures*, ed. by H. Hargolin, American Society for Metals, Ohio, U. S. A., 1966, 45.
- [198] R. R. Egglestone, *J. Appl. Phys.*, **23**, 1952, 1400.
- [199] R. Drouard, J. Washburn and E. R. Parks, *Trans. Met. Soc. AIME*, **197**, 1953, 1226.
- [200] J. T. Michalak and H. W. Paxton, *Trans. Met. Soc. AIME*, **221**, 1961, 850.
- [201] J. G. Byrne, (editor), *Recovery, Recrystallization and Grain Growth*, MacMillan, New York, 1965.
- [202] D. Kuhlmann-Wilsdorf, *Z. Phys.*, **124**, 1948, 468.
- [203] W. A. Johnson and R. F. Mehl, *Trans. Met. Soc. AIME*, **135**, 1939, 416.
- [204] M. Avrami, *J. Chem. Phys.*, **7**, 1939, 103.

- [205] M. Avrami, *J. Chem. Phys.*, **8**, 1940, 212.
- [206] M. Avrami, *J. Chem. Phys.*, **9**, 1941, 177.
- [207] P. Cotterill and P. Mould, (editors), *Recrystallization and Grain Growth in Metals*, Surrey University Press in association with International Textbook Co. Ltd., 1976, 94.
- [208] E. C. W. Perryman, *Trans. AIME*, **206**, 1956, 1247.
- [209] B. Ancker and E. R. Parker, *Trans. AIME*, **200**, 1954, 1155.
- [210] W. C. Leslie, F. J. Plecity and J. T. Michalak, *Trans. AIME*, **224**, 1962, 614.
- [211] C. E. Lacy and M. Gensamer, *Trans. ASM*, **32**, 1944, 88.
- [212] C. R. Austin, L. A. Luini and R. W. Lindsay, *Trans. ASM.*, **35**, 1945, 446.
- [213] L. A. Niemark and R. A. Swalin, *Trans. AIME*, **218**, 1960, 82.
- [214] H. Kimura, H. Matsui and S. Takaki, in *Mechanical Properties of BBC Metals*, ed. by M. Meshii, The Metallurgical Society of AIME, 1981, 125.
- [215] W. C. Leslie, F. J. Plecity and J. T. Michalak, *Trans. AIME.*, **221**, 1961, 691.
- [216] W. C. Leslie, F. J. Plecity and F. W. Aul, *Trans. AIME.*, **221**, 1961, 982.
- [217] H. Hu and A. Szirmae, *Trans. AIME.*, **221**, 1961, 839.
- [218] S. Weissmann, *Trans. ASM.*, **53**, 1961, 265.
- [219] H. Fujita, *J. Phys. Soc. Japan.*, **16**, 1961, 397.
- [220] N. S. Nakayama, S. Weissmann and T. Imura, in *Direct Observation of Imperfections in Crystals*, ed. by J. B. Newkirk and J. H. Wernick, Interscience, New York, 1962, 573.



- [221] C. G. Dunn and F. W. Daniels, *Trans. AIME.*, **191**, 1951, 147.
- [222] P. A. Beck, *Advances in Phys.*, **3**, 1954, 245.
- [223] S. F. Reiter, *Trans. AIME.*, **194**, 1952, 972.
- [224] E. C. W. Perryman, *Trans. AIME.*, **203**, 1955, 369.
- [225] J. W. Martin, *Metallurgia.*, **55**, 1957, 161.
- [226] W. C. Leslie and N. C. Hicks, *Fund. Research Lab.*, U. S. Steel Corp., unpublished work.
- [227] R. A. Vandermeer and P. Gordon, Report to OOR and ONR, Oct. 1960.
- [228] J. T. Michalak and W. R. Hibbard, Jr., *Trans. ASM*, **53**, 1961, 331.
- [229] T. O. Andrews, *The Production of A Non-quench aging Rimmed Steel by Rapid Annealing*, B.I.S.R.A./I.S.I. Report No.MR/E/5b/3.
- [230] C. Brun, M.Le Gac, F. Moliexe, P. Patou and B. J. Thomas, in *Technology of Continuously Annealed Cold-Rolled Sheet Steel*, ed. by R. Pradham, The Metallurgical Society of AIME, 1985, 223
- [231] J. Garcia and A. Le Bon, *Transformation and Precipitation in Steels after Hot Strip Rolling*, Europ. Coal and Steel Comm., Final Report, Research Project No. 7210-KD/310, April, 1984.
- [232] R. R. Pradham, in *Metallurgy of Continuous-Annealed Sheet Steel*, ed. by B. L. Bramfitt and P. L. Manganon, TMS AIME, Warrendale Penn., U. S. A., 1982, 203.

- [233] S. R. Goodman and A. R. Chaudhry, in *Metallurgy of Continuous-Annealed Sheet Steel*, ed. by B. L. Bramfitt and P. L. Manganon, TMS AIME, Warrendale Penn., U. S. A., 1982, 229.
- [234] R. C. Hudd, A. Jones and M. N. Kale, *J. Iron and Steel Inst.*, **209**, 1971, 121.
- [235] R. C. Sharma, U. K. Lakshmanan and J. S. Kirkaldy, *Met. Trans.*, **15A**, 1984, 545.
- [236] P. N. Richards and K. V. Barratt, *Trans. ASM*, **58**, 1965, 601.
- [237] H. J. Kleemola and E. A. Kunsisto, *Scand. J. Met.*, **5**, 1976, 151.
- [238] P. R. Mould, in *Metallurgy of Continuous-Annealed Sheet Steel*, ed. by B. L. Bramfitt and P. L. Manganon, TMS AIME, Warrendale Penn., U. S. A., 1982, 3.
- [239] P. H. Chang, *Metal. Trans. A*, **15A**, 1984, 73.
- [240] A. S. Keh and W. G. Leslie in *Materials Science Research*, ed. by H. H. Stadelmaier and W. W. Austin, Plenum Press, New York, **1**, 1963, 207.
- [241] W. C. Leslie, *The Physical Metallurgy of Steels*, McGraw-Hill Inc., New York, 1981, 97.
- [242] D. Z. Yang, D. K. Matlock and G. Krauss, in *Technology of Continuously Annealed Cold-Rolled Sheet Steel*, ed. by R. Pradham, The Metallurgical Society of AIME, 1985, 319.
- [243] D. K. Matlock, G. Krauss and F. Zia-Ebrahimi, in *Deformation Processing and Structure*, ed. by G. Krauss, ASM, Metals Park, Ohio, 1984, 47.
- [244] C. A. Wert, *J. of Appl. Phys.*, **20**, 1949, 943.

- [245] C. A. Wert, *Phys. Rev.*, **79**, 1950, 601.
- [246] J. K. Stanley, *Trans. TMS-AIME*, **185**, 1949, 752.
- [247] R. G. Davies, *Metal. Trans. A*, **10A**, 1979, 1549.
- [248] R. P. Krupitzer in *Fundamentals of Dual-Phase Steels*, ed. by R. A. Kot and B. L. Bramfitt, TMS-AIME, Warrendale, Penn., U. S. A., 1981, 315.
- [249] K. Nakaoka, K. Araki and K. Kurihara, in *Formable HSLA and Dual-Phase Steels*, ed. by A. T. Davenport, TMS-AIME, Warrendale, Penn., U. S. A., 1979, 126.
- [250] G. H. Hahn, *Acta Met.*, **10**, 1962, 727.
- [251] H. Katoh, K. Koyama and K. Kawasaki in *Technology of Continuously Annealed Cold-Rolled Sheet Steel*, ed. by R. Pradham, The Metallurgical Society of AIME, 1985, 79.
- [252] J. C. Swartz, *Trans. Met. Soc. of AIME*, **239**, 1967, 68.
- [253] J. Burke, *Phil. Mag.*, **5**, 1960, 176.
- [254] F. E. Fujita, *J. Phys. Soc. Japan*, **19**, (5), 1964, 640.
- [255] K. Kurihara and K. Nakaoka, in *Metallurgy of Continuous-Annealed Sheet Steel*, ed. by B. L. Bramfitt and P. L. Manganon, TMS AIME, Warrendale Penn., U. S. A., 1982, 117.
- [256] K. Kurihara and K. Nakaoka, in *Technology of Continuously Annealed Cold-Rolled Sheet Steel*, ed. by R. Pradham, The Metallurgical Society of AIME, 1985, 95.
- [257] K. Kurihara and K. Nakaoka, *Tetsu-to-Hagane*, **68**, 1982, S1198.

- [258] J. F. Butler, *JISI*, **204**, 1966, 127.
- [259] W. M. Fassell, in *Techniques of Metals Research*, ed. by R. F. Bunshan, Interscience Publ. Co., New York, 1969, 285.
- [260] R. Bakish, *Inter. Conf. Electron Ion Beam Sci. Technol.*, 1st, Toronto, 1964, Wiley, New York, 1965.
- [261] H. W. Mishler and R. E. Monroe, Defense Metals Information Center, Battle Memorial Inst., DM/C Report 174, Sept. 1962.
- [262] L. D. Smullin, *Proc. Symp. Electron Beam Technol.* 3rd, Boston, 1961, 8.
- [263] M. A. Adams and J. R. Beran, *JISI*, **204**, 1966, 586.
- [264] M. Sudo and I. Tsukataui, in *Technology of Continuously Annealed Cold-Rolled Sheet Steel*, ed. by R. Pradham, The Metallurgical Society of AIME, 1985, 203.
- [265] B. Seter, U. Bergstrom and W. B. Hutchinson, in *Technology of Continuously Annealed Cold-Rolled Sheet Steel*, ed. by R. Pradham, The Metallurgical Society of AIME, 1985, 111.
- [266] K. Toda, H. Gondoh, H. Takechi, M. Abe, N. Vehara and K. Komiya, *Trans. ISIJ*, **15**, 1975, 305.
- [267] K. Toda, H. Gondoh, H. Takechi and M. Abe, *Stahl u. Eisen*, **96**, (25/26), 1976, 1320.
- [268] H. Kubotera, K. Nakaoka, K. Araki, K. Watanable, A. Nishimoto and K. Iwase, *Trans. ISIJ*, **17**, 1977, 663.
- [269] P. Paulus and M. Economopoulos, *Stahl u. Eisen*, **98**, (17), 1978, 873.
- [270] H. E. Chandler, *Metal. Progr.*, **124**, (5), 1983, 25.

- [271] K. Matsudo, T. Shimomura and O. Nozoe, *Texture of Crystalline Solids*, **3**, 1978, 53.
- [272] K. Osawa, K. Matsudo, K. Kurihara and T. Susuki, *Tetsu-to-Hagane*, **70**, 1984, S552.
- [273] K. Matsudo, T. Shimomura and M. Kinoshito, *ibid*, **64**, 1978, S756.
- [274] O. Nozoe, K. Matsudo, T. Shimomura and K. Osawa, *ibid*, **66**, 1980, S361.
- [275] A. Nishimoto, Y. Hosoya, and K. Nakaoka, *Trans. ISIJ*, **21**, 1981, 778.
- [276] N. Takahashi, M. Shibata, Y. Furuno, H. Hayakawa, K. Kakuta and K. Yamamoto, in *Metallurgy of Continuous-Annealed Sheet Steel*, ed. by B. L. Bramfitt and P.L. Mangonon Jr., The Metallurgical Society of AIME, 1982, 133.
- [277] K. Toda, H. Gondoh, H. Takechi, M. Abe, N. Vehara and K. Komiya, *ibid*, **61**, 1975, 2363.
- [278] R. E. Hook, A. J. Heckler and J. A. Elias, *Metal. Trans. A*, **6A**, 1975, 1683.
- [279] H. Katoh, H. Takechi, N. Takahashi and M. Abe, in *Technology of Continuously Annealed Cold-Rolled Sheet Steel*, ed. by R. Pradhan, The Metallurgical Society of AIME, 1984, 37.
- [280] S. R. Goodman, P. R. Mould and J. C. Siple, in *Technology of Continuously Annealed Cold-Rolled Sheet Steel*, ed. by R. Pradhan, The Metallurgical Society of AIME, 1984, 167.
- [281] H. Katoh, K. Koyama and K. Kawasaki, in *Technology of Continuously Annealed Cold-Rolled Sheet Steel*, ed. by R. Pradhan, The Metallurgical Society of AIME, 1984, 95.

- [282] S. Miki, Y. Nariai and T. Harada, in *Technology of Continuously Annealed Cold-Rolled Sheet Steel*, ed. by R. Pradhan, The Metallurgical Society of AIME, 1984, 441.
- [283] B. L. Bramfitt and P.L. Mangonon Jr., (editors) *Metallurgy of Continuous-Annealed Sheet Steel*, The Metallurgical Society of AIME, 1982.
- [284] R. Pradhan, (editor), *Technology of Continuously Annealed Cold-Rolled Sheet Steel*, The Metallurgical Society of AIME, 1984.
- [285] T. O. Andrews, *S.C.W. Internal Report*, No. MR/E/5b/2, June, 1968.
- [286] T. O. Andrews, *S.C.W. Internal Report*, No. MR/E/5b/3, Oct, 1968.
- [287] F. Staüb and L. Cieslak, " *Accelerated Recrystallization of Cold-Rolled Low-Carbon Sheet Steels* ", BISIT. Trans. No. 3660.
- [288] R. F. Dewsnap, *An Investigation of the Rapid Annealing of Sheet Gauge Mild Steel*, BISIT Report, No. MW/H/28/60, MW/H/37/60.
- [289] E. W. Williams, *An Investigation into the Rapid Annealing of Blackplate*, BISIT Report, No. MW/H/30/61, MW/H/37/60.
- [290] E. W. Williams, *Temperature Banding during Rapid Annealing of Blackplate*, BISIT Report, No. MW/H/51/62.
- [291] S. Garber, *JISI*, **200**, 1962, 466.
- [292] K. J. Albutt and S. Garber, *JISI*, **204**, 1966, 278.
- [293] K. J. Albutt and S. Garber, *JISI*, **204**, 1966, 1217.
- [294] P. M. Howes, *Temperature Profile of A Short Resistive Heating Element*, B. Met thesis, Univ. of Wollongong, NSW, Australia, 1982.

- [295] P. Kelly, *Investigations into the Rapid Annealing of Aluminium and Ti Stabilized Steel Strip Incorporating Computer Modelling*, B. Met thesis, Univ. of Wollongong, NSW, Australia, 1984.
- [296] J. Conran, *Investigations into the Electrical Behaviour of A Laboratory High Speed Annealing Apparatus*, B. Met thesis, Univ. of Wollongong, NSW, Australia, 1985.
- [297] A. F. Mohri, *Iron & Steel Engineer*, **33**, 1956, 148.
- [298] E. W. Williams, *JISI*, **200**, 1962, 535.
- [299] G. K. L'vov, *Metallovedenie i Term. Obrabotka*, April, 1959, 8.
- [300] F. Staüb and L. Cieslak, *Archiwum Hutnictwa*, **7(4)**, 1962, 333.
- [301] Blanter et al, *Metallovedenie i Term. Obrabotka*, April, 1965, 22.
- [302] H. P. Stüwe, *ISI* Special Report No. 108, 1968, 1.
- [303] V. I. Ivanov and K. A. Osipov, *Izvest A. N. Otdel Tekhn. Met. i Toplivo*, 1962, No. 2, March-April, 84.
- [304] G. Niebch, Proceedings from the International Symposium on Annealing of Low Carbon Steel, Cleveland, Ohio, Oct. 1957.
- [305] A. Cracknell and N. J. Petch, *Acta Met.*, **3**, 1955, 186.
- [306] K. J. Albutt and S. Garber, *ibid*, **205**, 1967, 738.
- [307] R. E. Bentley, *Metals Australasia*, **13(9)**, Oct., 1981, 19.
- [308] R. E. Bentley, *Understanding thermoelectricity*, Aust. Inst. Physics Seminar on Temperature Measurement, Univ. N. S. W., 23 Aug., 1966.

- [309] R. E. Bentley, *Thermocouple Pyrometry*, CSIRO Division of Applied Physics, Sept., 1980,
- [310] T. J. Seebeck, *R. Acad. Sci. Berlin*, 1822-1823, 165.
- [311] J. C. A. Peltier, *Ann. Chim. Phys.*, **56** ( 2nd ser.),1834, 371.
- [312] W. Thomson, *Proc. R. Soc. Edinburgh*, Dec., 1851.
- [313] W. Thomson, *Proc. R. Soc.*, **7**, May, 1854.
- [314] J. P. Joule, *Proc. R. Soc.* , Dec., 1840.
- [315] R. J. E. Clausius, *Ann. Phys. Chem.*, **79** ,1850, 368.
- [316] G. H. Talbot, *Instrument Practice*, **1** ,1847, 265.
- [317] A. C. Becquerel, *Ann. Chim. Phys.*, **31** ,1827, 371.
- [318] C. S. M. Pouillet, *Compt. Rend.*, **iii** ,1836, 786.
- [319] G. Tait, *Trans. Roy. Soc. Edinb*, **27** ,1872, 125.
- [320] H. Le Chatelier, *Compt. Rend.*, **102**,1886, 819.
- [321] H. Le Chatelier, *J. de Phys.*, **6**,1887, 23.
- [322] C. Barus, *Phil. Mag.*, **34**,1892, 376.
- [323] G. K. Burgess, *Bull. Bur. Standards*, **5**,1908, 199.
- [324] W. H. Hatfield, *Trans. Faraday Soc.*, **13**,1917, 289.
- [325] M. Wenzl and F. Morawe, *Metallurgist*, **3**, 1927, 119.
- [326] F. H. Schofield and A. Grace, *Iron Steel Inst.*, Special Report No. **25**,1939, 239.



- [327] C. R. Barber, *J. Iron Steel Inst.*, **147**, 1943, 205.
- [328] B. S. 4937, *British Standards Institution*, 1974.
- [329] R. P. Benedict, (editor), *Fundamentals of Temperature, Pressure and Flow Measurements*, A Wiley-Interscience Publ., John Wiley & Sons, New York, 1984, 103.
- [330] M. Atkinson, private communications.
- [331] E. B. Jones, (editor), *Instrument Technology --- Measurement of Pressure, Level flow and Temperature*, **1**, Newnes-Butterworths, London, 1974, 330.
- [332] C. D. Henning and R. Parker, in *Techniques of Metals Research*, ed. by R. F. Bunshah, Interscience Publ., New York, **1**, 1968, 269.
- [333] D. I. Finch, *General Principles of Thermoelectric Thermometry*, **1161**, Leeds and Northrup Co., Tech. Publ., ENS 2(1), 1962, 7.
- [334] E Jahnke and F. Emde, *Tables of Functions*, Dever, New York, 1945, 24.
- [335] J. P. Holman, (editor) *Heat Transfer*, 6th ed., McGraw-Hill Book Co., New York, 1986, 2.
- [336] G. H. Geiger and D. R. Poirer, (editors) *Transport Phenomenon in Metallurgy*, Addison-Wesley Publ. Co., Reading, Mass., U. S. A., 1973.
- [337] A. S. Foust, et al, *Principles of Unit Operations*, 2nd ed., Wiley and Sons, New York, 1980.
- [338] P. J. Schneider, (editor), *Conduction Heat Transfer*, Addison-Wesley Publ. Co., Reading, Massc., U. S. A., 1957.

- [339] J. Crank and P. Nicholson, A Practical Method for Numerical Evaluations of Partial Differential Equations of the Heat Conduction Type, *Pro. Cambridge, Phil. Soc.*, **43**, 1947, 50.
- [340] J. P. Holman, (editor) *Heat Transfer* , 6th ed., McGraw-Hill Book Co., New York, 1986.
- [341] M. P. Heisler, Temperature Charts for Induction and Constant Heating, *Trans. ASME*, **69**, 1947, 227.
- [342] A. J. Chapman, (editor), *Heat Transfer*, 4th ed., MacMillan Publ. Co., New York, U. S. A., 1984, 23.
- [343] R. C. Weast, (editor), *Handbook of Chemistry and Physics*, 56th ed., CRC Press Inc., Cleveland, Ohio, U. S. A., 1976, F-114.
- [344] V. A. Sandborn, (editor), *Resistance mperature Transducers* , Metrology Press, Fort Collins, Colorado, U. S. A., 1972, 9.
- [345] C. J. Smithells, (editor), *Metals Reference Books* , 5th ed., Butterworth and Co., London, 1978, 942.
- [346] J. P. Holman, (editor) *Heat Transfer* , 6th ed., McGraw-Hill Book Co., New York, 1986, 13.
- [347] W. D. Dewitt, N. C. Gibbon and R. L. Reid, *IEEE Trans. Aerosp. Electron. Syst.*, **4** (5), 1968, 263.
- [348] W. B. Harper and D. R. Brown, *Mathematical Equations for Heat Conduction in the Fins of Air-Cooled Engines* , NACA Rep. 158, 1922.
- [349] K. A. Gardner, *Trans. ASME* , **67**, 1945, 621.
- [350] L. J. Ybarrondo and J. E. Sunderland, *Bull. Mech. Eng. Educ.*, **5**, 1966, 229.

- [351] A. M. Clausing, *Int. J. Heat Mass Transfer*, **9**, 1966, 791.
- [352] D. Q. Kern and A. D. Kraus, (editors), *Extended Surface Heat Transfer*, McGraw-Hill Book Co., New York, 1972.
- [353] C. F. Kayan, *Trans. ASME* , **67**, 1945, 713.
- [354] C. F. Kayan, *Trans. ASME* , **71**, 1949, 9.
- [355] R. Rudenberg, *Elecktrotech. Z.*, **46**, 1925, 1342.
- [356] R. V. Andrews, *Chem. Eng. Prog.* , **52(2)**, 1955, 67.
- [357] H. Z. Barakat and J. A. Clark, *J. Heat Transfer*, Nov., 1966, 421.
- [358] E. Hahne and U. Grigull, *Int. J. Heat Mass Transfer*, **18**, 1975, 751.
- [359] P. J. Schneider, (editor), *Temperature Response Charts* , John Wiley & Sons Inc., New York, 1963.
- [360] E. L. Wilson and R. E. Nicknell, *Nucl. Eng. Des.*, **4**, 1966, 276.
- [361] L. S. Langston, *Int. J. Heat Mass Transfer*, **25**, 1982, 149.
- [362] M. Colakyan, R. Turton and O. Levenspiel, *Heat Transfer Engr.*, **5**, 1984, 82.
- [363] G. M. Dusenberre, (editor), *Heat Transfer Calculations by Finite Difference*, International Textbook Co., Scranton, Pa., U. S. A., 1961.
- [364] A. A. Johnson, *J. Less Common Metals*, **2**, 1960, 241.
- [365] L. A. Niemark and R. A. Swalin, *Trans. AIME*, **218**, 1960, 82.
- [366] W. L. Haworth and J. Gordon Parr, *Trans. ASM*, **58**, 1965, 477-488.
- [367] M. Atkinson, A Linear Short-lever Extensometer ( to be published)

- [368] J. H. Hollomon, *Trans. AIME*, **162**, 1945, 268.
- [369] B. Jaoul, " Etude de la Forme des Courbes de Deformation Plastique", *J. Mech. Phys. Solids.*, **5**, 1957, 95.
- [370] M. Atkinson, " Research Note on A Compliance Approach to Analysis of Plastic Stress-Strain Relationship" *International Journal of Plasticity*, **4**, 1988, 183-194.
- [371] M. T. Shehata and J. D. Boyd, in *Microstructural Science*, **10**, Elsevier Science Pub. Co. Inc., 1982, 229.
- [372] E. Kreysig, ed. *Introductory Mathematical Statistics*, John Wiley and Sons, Inc., New York, 1970, 77.
- [373] J. P. Holman, (editor) *Heat Transfer* , 6th ed., McGraw-Hill Book Co., New York, 1986, 364-384.
- [374] G. J. Huber and M. Hatherly, *Metals Forum*, **1**, 1978, 115.
- [375] Chopra, O. K. and Niessen, P., *J. Mat. Sci.* **8**, 93, 1973.
- [376] Naka, S., Penelle, R., Valle, R. and Lacombe, P., in " *Texture of Materials*" Proc. 5th International Conference on Texture of Materials, Aachen, ed. G. Gottstein and K. Lüke, Springer-Verlag, 405, 1978.
- [377] P. Haasen, (editor), *Physical Metallurgy*, Cambridge University Press, Cambridge, London, 1978, 349.
- [378] M. Atkinson, Ultra-rapid Annealing of Low-Carbon Steel Strip, to be published.
- [379] H. Conrad, Z. Guo, M. Fisher, W. D. Cao and A. F. Sprecher, *Recrystallization'90, International Conference on Recrystallization in Metallic Materials*, January 22-26, 1990, Wollongong, Australia.

- [380] G. E. Dieter, (editor) *Mechanical Metallurgy*, second edition, McGRAW-HILL International book Co., Sydney, 1976.
- [381] J. S. H. Lake, D. J. Willis and H. G. Fleming, *Met. Trans.*, **19A**, 1988, 2085-2117.
- [382] M. Atkinson and I. Maclean, *Sheet Metal Industries*, **42**, 1965, 290-298.